NANYANG TECHNOLOGICAL UNIVERSITY
SINGAPORE

LAND RECLAMATION USING SOFT CLAY FILL AND VACUUM PRELOADING VIA HORIZONTAL DRAINAGE ENHANCED GEOTEXTILE SHEETS

CHEN HAO
SCHOOL OF CIVIL AND ENVIRONMENTAL ENGINEERING

2021

LAND RECLAMATION USING SOFT CLAY FILL AND VACUUM PRELOADING VIA HORIZONTAL DRAINAGE ENHANCED GEOTEXTILE SHEETS

CHEN HAO

School of Civil and Environmental Engineering

A thesis submitted to the Nanyang Technological University
in partial fulfilment of the requirement for the degree of
Doctor of Philosophy

2021

Statement of Originality

I hereby certify that the work embodied in this thesis is the result of original research, is free of plagiarised materials, and has not been submitted for a higher degree to any other University or Institution.

20-AUG-2021

. . . . . .
Date

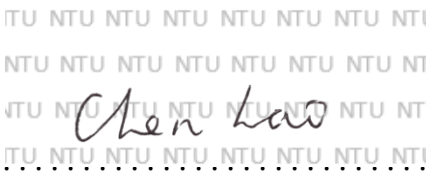

. . . . . .
CHEN HAO

Supervisor Declaration Statement

I have reviewed the content and presentation style of this thesis and declare it is free of plagiarism and of sufficient grammatical clarity to be examined. To the best of my knowledge, the research and writing are those of the candidate except as acknowledged in the Author Attribution Statement. I confirm that the investigations were conducted in accord with the ethics policies and integrity standards of Nanyang Technological University and that the research data are presented honestly and without prejudice.

20-AUG-2021

. . . . . .
Date

. . . . . .
CHU JIAN

Authorship Attribution Statement

This thesis contains material from 1 paper published in the following peer-reviewed journal in which I am listed as an author.

Chapter 3 is published as Chen, H., Chu, J., Guo, W., and Lam, K.P. Modified Broms' method for formation of working platform on very soft soil. *Geotextiles & Geomembranes*, **49(1)**: 57-71 (2020). DOI: 10.1016/j.geotexmem.2020.08.006.

The contributions of the co-authors are as follows:

- Prof Chu Jian provided the initial project direction and edited the manuscript drafts.
- I prepared the manuscript drafts. The manuscript was revised by Prof. Chu and Dr. Guo Wei.
- I co-designed the study with Prof Chu Jian and performed all the laboratory work at the School of Civil and Environmental Engineering. I also analyzed the data under the advice of Prof Chu Jian.
- Dr Guo Wei assisted in rectifying the grammar and content of the manuscript.
- Dr Lam Kok Pang provided the field testing data used in this paper.

20-AUG-2021

. . . . . .
Date

. . . . . .
CHEN HAO

ACKNOWLEDGEMENTS

I would like to first express my deep appreciation to Professor Chu Jian, who gave me kind guidance and valuable suggestions over the last four years. What I have learned most from Prof Chu is the devotion to education, the insight to the essence, and the passion for research. In life, Prof Chu is an approachable person. Every discussion is like an equal exchange of ideas, and with the sparks of thought, my PhD career is fulfilled with challenges and discoveries.

I would also like to extend my appreciation to Dr Wu Shifan, who helped me design the tests and set up lab instruments. It may take much longer for me to configure the test set-up without Dr Wu's kind help.

I would like to express my gratitude to my research team members, Dr Pan Xiaohua, Dr Wang Hao, Dr Lai Hanjiang, Dr Cui Mingjuan, Dr Yu Xiaoniu, Dr Hoang Tung, Mr Wang Lei, Mr Shi Wenjie, Mr Yang Yang and Miss Wang Wenhao, for their support and help in my experimental work and data analysis.

I want to thank Mr. Vincent Heng, Mr. Choi Siew Pheng, Mr. Eugene Tan, Mr. Andy Koh, and Mr. Lim Swee Kuan from Geotechnics Lab for their kind assistance in preparing the experimentations. I would like to thank Professor Guo Wei from Tianjin University, China, who helped rectify my paper and gave suggestions on my research work.

Special thanks are given to Ms. Ng Soo Ching, who helped submit my thesis. Last but not least, I would like to thank my parents who supported and encouraged me from thousands of miles away.

TABLE OF CONTENTS

ABSTRACT

In land-scarce Singapore, land reclamation or other space creation methods are required to cater for future economic development. With the shortage of granular fill materials, other alterative fill materials such as soft marine clay have to be utilized for land reclamation. For the improvement of soft clay, the conventional methods adopted are preloading using either fill surcharge or vacuum pressure with prefabricated vertical drains (PVDs). However, for very soft clay, the preloading using PVDs method is time consuming and technically challenging. The difficulties include the need to form a working platform, the inability to carry out soil improvement during the fill material placement and the construction of containment structures in relatively deep water.

The objective of this study was to develop improved methods for land reclamation using soft soil. The Broms' method of using geotextile sheets and sand berms was modified to facilitate the formation of a working platform on top of very soft clay. An analytical method was developed for the Modified Broms' method to predict the profile of the deformed geotextile and the distribution of tensile strain at the critical condition. Design charts for considering the contact width and the spacing of sand tubes and the property of geotextile were proposed to facilitate the design.

To overcome the difficulties involved in the land reclamation methods using PVDs, a soil improvement method using horizontal drainage enhanced geotextile sheet (HDeG sheet) and vacuum preloading was developed for land reclamation using soft clay fill. Model tests were carried out to study the consolidation behaviour of soft soil around HDeG and the effectiveness of the HDeG method. The results of the model tests indicated that the HDeG method was effective and the effectiveness of the HDeG was much affected by the transmissivity of the geotextile. For the same drain size and spacing, better performance in terms of settlement and pore water pressure dissipation was achieved when non-woven geotextile with better transmissivity was used. A method to measure the transmissivity of non-woven geotextile in clay was also proposed. The testing data indicate that the transmissivity of non-woven geotextile was affected by the type of soil and the applied normal stress.

Both 2D small strain and large strain solutions were proposed for analysing vacuum consolidation of soft clay with the use of HDeG. A horizontal drain element was

developed to model the drainage property of HDeG including the transmittivity of geotextile using the ABAQUS/Standard software. In terms of settlements and excess pore pressure distributions, the results using the proposed consolidation solutions were consistent with those measured in the model tests and those simulated using finite element analysis (FEA). The degree of consolidation computed using the proposed consolidation solutions using either settlements or pore pressure distributions was also consistent with that calculated using the data from the model tests and those from FEA. Theoretically, the degree of consolidation based on pore pressure distribution may lag behind that based on soil surface settlement. The difference was caused by the non-linear compressibility of soft clay. An equation for converting the degree of consolidation based on settlement to that based on pore pressure or verse versa was also proposed.

To improve the performance of HDeG, two new methods were proposed. The first was the use of electro-osmosis with HDeG or electrical HDeG, and second was the use of lime liner with HDeG or lime liner enhanced HDeG. The former incorporated electro-osmosis with HDeG to enhance or accelerate the rate of consolidation using HDeG. The later used a thin layer of lime to improve the permeability along the soil-HDeG interface. Laboratory model tests were carried out. The testing data indicated that the electrical HDeG could improve the consolidation of soft soil particularly for soil that has been consolidated under vacuum pressure, and by using the lime liner enhanced HDeG, the permeability of soil near the HDeG could be improved by 2 to 3 times.

Due to sea level rise and previous land reclamation activities, future land reclamation would have to be carried out in relatively deep water. A method for constructing vertical containment structure for land reclamation using prefabricated concrete cylinders and suction caissons was proposed. Design methods for stability and deformation analyses were proposed. The results from the proposed method agreed well with those from the finite element analysis.

LIST OF TABLES

LIST OF FIGURES

LIST OF SYMBOLS

a	Coefficient of parabolic function
A_1	Area of OAE
A_2	Area of ACDE
A_3	Area of ABC
E	Tensile stiffness
f	Tangential pressure from sand berm at Point $S(x, z)$
k_0	Lateral earth pressure coefficient at rest
L_1	Contact width of sand berm
L_2	Spacing between sand berms/tubes
N_s	Normal pressure from sand berm at Point $S(x, z)$
N_l	Normal pressure from soft soil at Point $S(x, z)$
P_u	Bearing pressure
$P_{u\text{-}t}$	Total bearing pressure
u_0	Excess pore pressure at top of geotextile
T	Tensile force
T_0	Tensile force at Point O
T_1	Tensile force at Point B
ΔT	Increment tensile force between Point O and A
T_{er}	Total error for iteration procedure
S_e	Settlement of sand berms/tubes
s_{OA}	Length of section OA of geotextile
s_{AB}	Length of section AB of geotextile
s	Curve coordinate
x	Horizontal coordinate

z	Vertical coordinate
Δh_1	Penetrated depth of sand berm
Δh_2	Height of the heaved soil
γ_l	Unit weight of soft soil
γ_s	Unit weight of sand
θ	Angle between tangent direction and x axis at Point $S(x, z)$
θ_A	Angle between tangent line and x axis at Point A of geotextile
ε	Tensile strain
ε_0	Tensile strain at Point O
ε_1	Tensile strain at Point B
ε_{avg}	Average tensile strain for section OA of geotextile
ε_u	Ultimate tensile strain
ε_{max}	Maximum tensile strain
c_v	Coefficient of consolidation
e	Void ratio
e_0	Initial void ratio
ω	Water content
h	Consolidation height
k	Permeability
$p(x,t)$	Distribution of excess pore pressure on HDeG sheet
p_{vac}	Absolute vacuum pressure
$p_1(t)$	Equivalent vacuum pressure
T_v	Time factor
t	Time
s_h	Horizontal spacing
s_v	Vertical spacing

u	Excess pore pressure
u_0	Initial excess pore pressure
$U(t)$	Degree of consolidation at time t
v_1	Transient solution for vacuum consolidation
v_2	Transient solution for surcharge consolidation
w	Width of prefabricated drain
θ	Transmissivity of geotextile
σ'_v	Vertical effective stress
I	Current
V	Voltage

CHAPTER 1 INTRODUCTION

1.1 Background

Land reclamation is one of the strategies in many countries to overcome the shortage of land for future economic growth. For countries without sand fill, soft soil or dredged marine clay is also used as fills for land reclamation. How to use soft soil for land reclamation is still a technical challenge.

In the past, preloading using either fill surcharge or vacuum pressure together with prefabricated vertical drains (PVDs) has been adopted as one of the common methods for the treatment of soft cohesive soil. However, the current methods using PVDs have several shortcomings. Firstly, the PVDs can only be installed after all the fill materials have been placed. Secondly, when the fill materials are too soft, a working platform needs to be formed before carrying out any soil improvement works. Although a few methods to form the working platform have been developed (Broms, 1987; Lam et al., 2012), some of these methods are either time consuming or not fully reliable. Therefore, development of new methods is still required such that land reclamation using soft soil can be conducted cost-effectively and efficiently. Furthermore, with the rising sea level and the demand for more nearshore infrastructures, land reclamation may have to be carried out in relatively deep water. The current methods for seawall construction may no longer be applicable or sustainable. New methods for the construction of containment bunds need to be developed.

The use of prefabricated board drains (PBDs) as horizontal drains was applied in the consolidation of a landfill in Japan (Shinsha et al., 2013; Chai et al., 2014). A major problem associated with the use of PBDs is that the positions of PBDs could not be controlled throughout the consolidation process and could be drifted to some positions which are inconsistent with the design assumptions. Some researchers proposed the use of the geo-composite with high discharge capacity as the horizontal drains (Chai et al., 2011; Chai and Nguyen, 2013; de Lillis et al., 2017). Good performance was found using the geo-composites with high discharge capacity. However, the cost for the use of geo-composite for large-scale land reclamation is too expensive. A new form of horizontal drain, the horizontal drainage enhanced geotextile sheet (HDeG sheet), was proposed as an alternative with an intention to improve the performance of the horizontal drain

method (Chu et al., 2016). For HDeG sheet, the discrete drains with a certain spacing were bounded with geotextile sheets. However, further studies on the design methods and construction procedures as well as field verification are required for the use of horizontal drain.

1.2 Research Objectives and Scopes

The key research objectives established for this thesis are as follows:

(1) To develop a more reliable method for the formation of a working platform when the conventional soil improvement methods are adopted.
(2) To study the use of HDeG sheet in vacuum preloading and/or electro-osmosis for the improvement of soft fill materials for land reclamation. These include the evaluation of the performance of the HDeG sheet and the development of design methods for the use of HDeG sheet to accelerate the consolidation of soft soil.
(3) To propose and evaluate the method for vertical concrete containment structures founded on suction caissons.

The scope of work includes:

(1) Develop a modified Broms' method using geotextile sheet and geo-tubes for the design and construction of working platform on top of soft land reclamation fills.
(2) Carry out model tests to study the consolidation behaviour of soft soil using HDeG sheet and vacuum preloading and evaluate the performance of HDeG sheet.
(3) Establish analytical methods for consolidation using HDeG sheet using both small strain and large strain consolidation theories and develop numerical models for the verification of model tests and the design of the HDeG sheet and vacuum preloading methods.
(4) Proposed a design procedure for vertical concrete structure using suction caissons as foundations for containment for land reclamation.

1.3 Outline of Thesis

This thesis is divided into nine chapters. Chapter 2 presents a literature review of the previous studies on the improvement of soft cohesive soil with prefabricated drains, vacuum pressure and electro-osmosis, the methods to form the working platform and the methods for the construction of containment structures for land reclamation. The modified Broms' method for the formation of a working platform using geotextile and sand tubes is proposed in Chapter 3. The vacuum consolidation behaviour of soft soil using HDeG sheet and vacuum preloading was investigated by a series of model tests with different horizontal and vertical spacings. The testing procedure and results are presented in Chapter 4 and 5. A method for measuring the transmissivity of non-woven geotextile in soft cohesive soil was also proposed in Chapter 4. In Chapter 6, consolidation analyses using both small strain and large strain theories as well as numerical analyses for the design of vacuum consolidation using HDeG sheet are presented. Two innovative methods associated with the use of HDeG sheet, the electro-osmosis method and lime liner method are proposed in Chapter 7. Finally, the design of vertical concrete seawalls constructed on suction caissons for land reclamation is studied in Chapter 8. The conclusions and recommendations for future studies are made in Chapter 9.

CHAPTER 2 LITERATURE REVIEW

2.1 Introduction

With the shortage of sand, soft soil or other waste may have to be used as fill materials for land reclamation. Preloading using fill surcharge or vacuum pressure with PVDs becomes a feasible method for the treatment of soft soil. For the installation of PVDs on very soft ground or fill materials, a working platform needs to be constructed first. In this chapter, current literature and practice related to land reclamation using soft soil and associated soil improvement methods are reviewed.

2.2 Vacuum preloading of soft clayey soil using prefabricated vertical drains

2.2.1 Vacuum preloading

The idea of vacuum preloading was proposed by Kjellman (1952). The vacuum preloading method has already evolved into a mature and efficient technique for the treatment of soft clay. This method has been successfully used for many land reclamation projects all over the world (Bergado et al., 1996, 2002; Chen and Bao, 1983; Chu et al., 2000; Chu and Yan, 2005a, 2005b; Cognon, 1991; Holtz, 1975; Indraratna et al., 2005a, 2010, 2012). Varaksin and Yee (2007) and Yan and Chu (2003, 2005) also argued that vacuum preloading is more sustainable as its carbon footprint is much smaller compared with other soil improvement methods.

2.2.1.1 The mechanism of vacuum preloading

The principles and mechanism of vacuum preloading have been well explained in the literature, e.g., Kjellman (1952), Holtz (1975), Qian et al. (1992) and Chu et al. (2000;2006). The consolidation process of saturated soil under surcharge or vacuum loading can be illustrated using the spring analogy as shown in Figure 2.1. The pressures in Figure 2.1 are given in absolute values and p_a is the atmospheric pressure. The initial pore water pressure is same with the atmospheric pressure.

Under a surcharge, Δp, the pore water takes all the load instantly. Therefore, the initial excess pore water pressure, Δu, is the same as the surcharge, Δp. Then, the excess pore water pressure dissipates gradually and tends to the atmospheric pressure. Hence, the

load, Δp, is transferred from pore water to the spring and the effective stress in soil skeleton tends to the surcharge, Δp. It should be noted that the above process is not affected by the atmospheric pressure, p_a.

Under the vacuum pressure instantly, -Δu, the excess pore pressure is same with the vacuum pressure, -Δu, under sealed condition. However, the total stress on the soil is constant and equal to the atmospheric pressure. Therefore, the effective stress increases to the absolute vacuum pressure. Due to the limitation of boiling point under vacuum condition, the maximum increasing of the effective stress in soil skeleton should be equal to the absolute maximum negative water pressure, about 98 kPa.

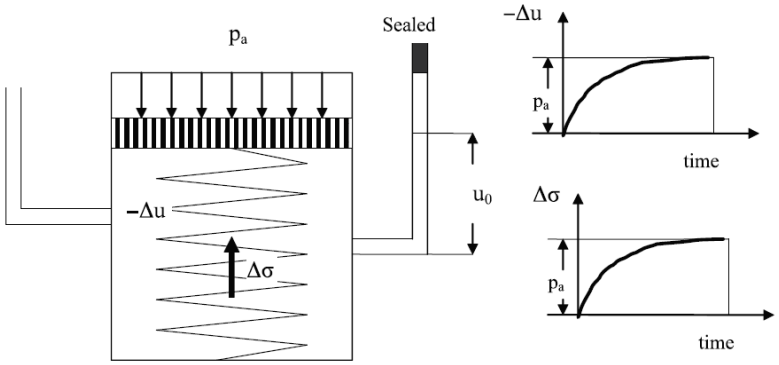

$$u_0 = p_a$$
$$\Delta\sigma' = p_0 - (u_0 - \Delta u) = \Delta u$$

Figure 2.1 Spring analog of consolidation process under vacuum condition (after Yan and Chu, 2005)

For an idealized soil profile with the water table and a single drainage boundary at the ground level, the distribution of pore water pressure and effective stress with depth at a given time during consolidation are plotted in Figure 2.2 for surcharge and vacuum preloading respectively.

Under a surcharge load, the corresponding vertical effective stress at time t, $\sigma'_v(z)$, equals to $\sigma_0 + \Delta\sigma_v - u_t(z)$, where σ'_0 is the initial effective overburden stress, $\Delta\sigma_v$ is the surcharge and $u_t(z)$ is the excess pore water pressure at the same time t. As the drainage surface at ground level, the excess pore water pressure increases with depth and the effective stress decreases with depth.

Under a vacuum load, the effective stress is equal to $\sigma'_0 + u_0(z) - u_t(z)$, where $u_0(z)$ is the hydrostatic pore water pressure, and $u_t(z)$ is the negative pore water pressure. As the vacuum pressure is applied on the drainage surface at ground level, the excess pore pressure, $u_t(z)$, increases with depth. Therefore, the effective stress also decreases with depth and the maximum increment is limited.

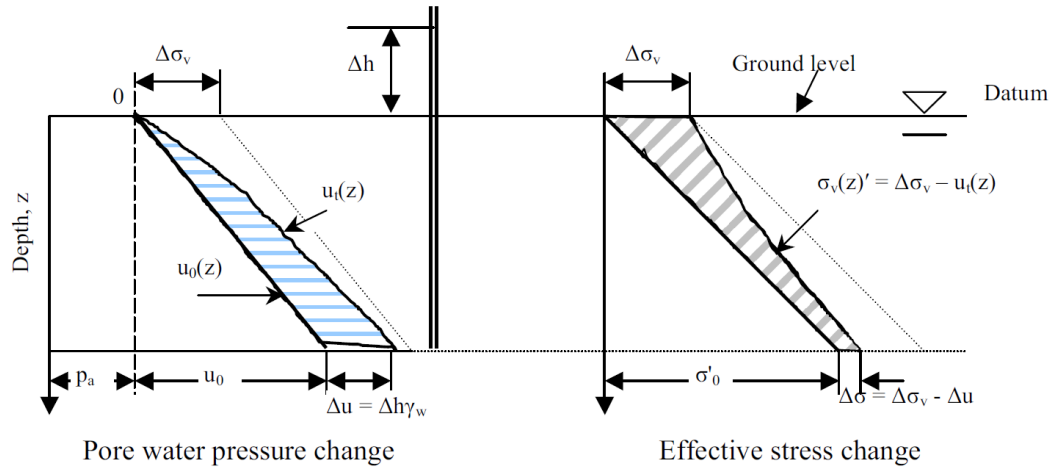

(a) under fill surcharge

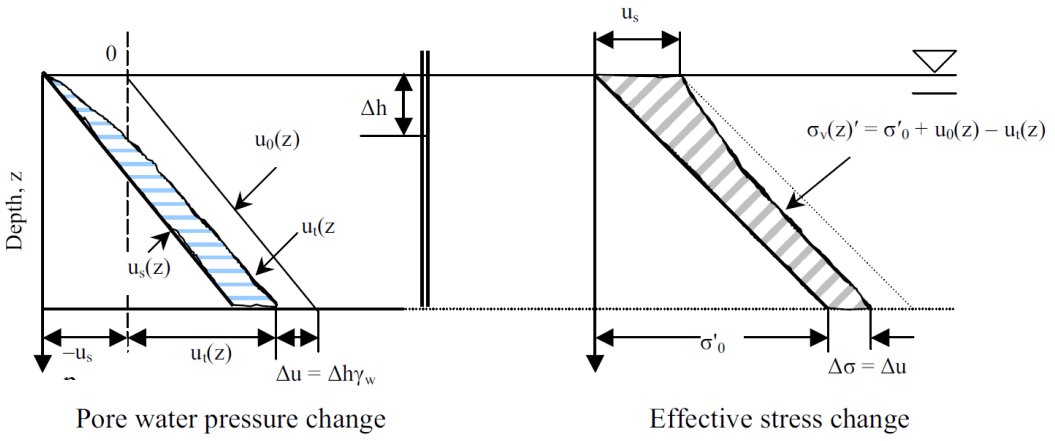

(b) under vacuum loading

$u_0(z)$ = hydrostatic pore water pressure profile; $\sigma_v(z)'$ = effective stress at time t
$u_t(z)$ = excess pore water pressure at time t $u_s(z)$ = suction line
σ_0' = initial effective overburden stress

Figure 2.2 Pore water pressure and effective stress changes (after Yan and Chu, 2005)

2.2.1.2 The vacuum consolidation system

Currently, three main vacuum preloading systems were developed and applied in many land reclamation projects all over the world as shown in Figure 2.3. For the three vacuum

preloading systems, the features for every system are shown in Table 2.1. The Chinese system is similar with Menard system. The differences are the sealing techniques and vacuum pump. For Chinese system, the Jet pump is used, and the membrane is covered with water to sustain high vacuum pressure and prevent the membrane aging. For Menard system, the Menard vacuum station is used, and the primary fill is applied beneath the membrane to increase sealing and stability of system. For Chinese system and Menard system, usually the total area has to be subdivided into a number of sections to facilitate the installation of membrane, the vacuum preloading can only be carried out one section after another. For the BeauDrain system, this system only works when the soil layer is dominantly low permeability soil. The vertical drains are connected directly to the vacuum pump using a tubing system. With the low permeability of soil, the membrane is not required for the surface sealing. It is better to install the PVDs beneath the water level, then the crack of soft clay fill above the water level won't have a great effect on the efficiency of the system. However, the high efficiency may be difficult to be achieved. The vacuum pressure applied can be only 50kPa or lower (Seah, 2006; DAM et al., 2006; Chu et al., 2008).

Because the vacuum pressure cannot be lower than -100kPa, the combined vacuum and surcharge preloading is a common method to accelerate the consolidation of low permeability soil and avoid the unfavorable stability issues under high surcharge as shown in Figure 2.4. This method has been applied in the soil improvement for a storage yard (Yan and Chu, 2005). For vacuum preloading, the lateral deformation of soil is inward. For surcharge preloading, the lateral deformation of soil is outward. Then the vacuum pressure will increase the stability of surcharge fill or the embankment. The maximum height of embankment can be up to 15m with continuous construction. A 12.5m embankment was constructed combined with the vacuum preloading in Japan (Indraratna, 2009; Dam et al., 2006).

However, all this vacuum preloading system are combined with prefabricated vertical drain (PVDs). Hence, before the installation of PVDs, the soft clay fill should be fully filled and the containment bund must be built as the same height of soft clay. For installation of PVDs or the construction of surcharge, a working platform should be formed first. But there are some uncertainties for the construction and design of working platform (Chu et al., 2012).

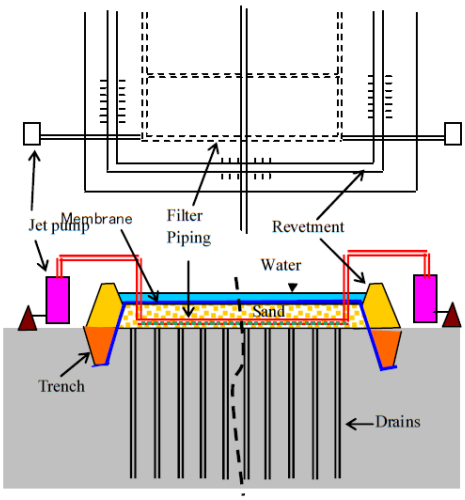

(a) Chinese System

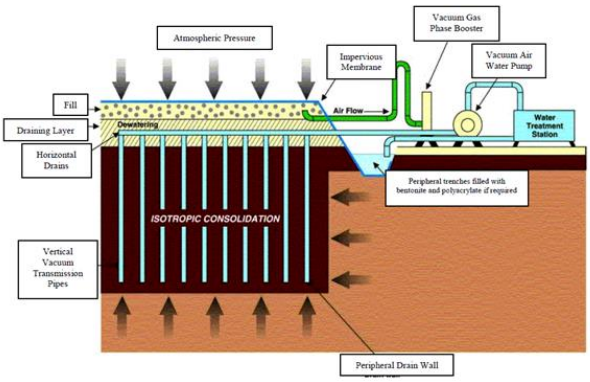

(b) Menard System

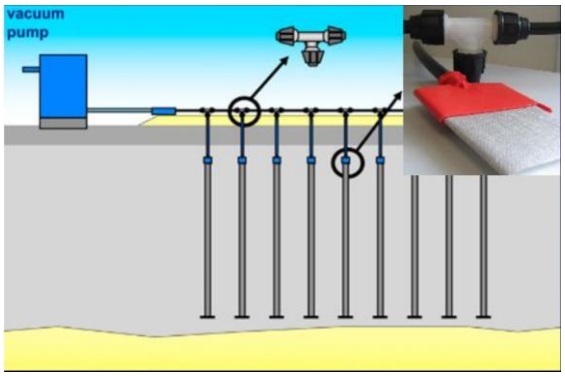

(c) BeauDrain System

Figure 2.3 Vacuum preloading systems (after Dam et al., 2006)

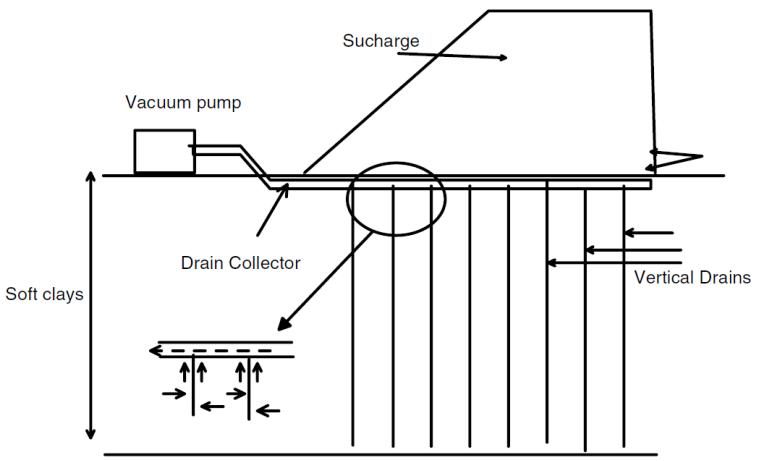

Figure 2.4 Combined vacuum and surcharge preloading system (after Indraratna, 2009)

Table 2.1 Features of different vacuum preloading system (after Dam et al., 2006)

Chinese system	Menard system	BeauDrain system
The membrane is covered with water; Sand mat + manifold from main filter collector pipes with Sand mat + perforated PVC pipes in two perpendicular Bottom natural sand layer. fish-bone branches PVC pipes (China)	Applying primary fill beneath membrane to increase sealing and stability of system; Sand mat + perforated PVC pipes in two perpendicular directions connected to peripheral collector pipe	Vertical PVD (Alidrains) capped at top and buried in the low permeability soil; connect the vacuum channel directly to each individual drain using a tubing system
Individual treatment area: standard 6,000 - 10,000 m^2	Individual treatment area: standard 5,000-7,000 m^2	
Clay mix slurry (China); Clay revetment above the trench for retaining soil fill Primary fill (1.5 m) on top of sand beneath membrane, or extracted water discharged above the membrane; Clay mixed cut-off-wall;	Bentonite aquakeep slurry and backfill water on top; Bentonite slurry wall or sheet piling	Not require trench
φ48Jet pump + 3HA-9 centrifugal water pump of 7.5 kW; 1000-1500 m^2/pump	Menard vacuum pump station MS25 (25 kW); 5,000-7,000 m^2/pump station	Approximately 1500 m^2/pump

2.2.2 Prefabricated vertical drain

For the treatment of soft clayey soil, the preloading is one of the most common methods. The prevalent modern method for the preloading is combined with the PVDs to shorten the drainage path. The preloading with PVDs has been applied successfully in many land reclamation projects (Hansbo, 1979, 1981, 2005; Holtz et al., 1991; Bergado et al., 1993, 1996, 2002; Li and Rowe, 2001b; Chu et al., 2004; 2009a; Choa et al., 2001; Bo et al., 2003; 2005; Indraratna et al., 2005; Yan and Chu, 2005; Seah, 2006; Kitazume, 2007; Varaksin and Yee, 2007; Yan et al., 2009; Chu et al., 2013; Chu and Guo, 2016). The consolidation behavior of soft soil using PVDs has become the core technical issues in the preloading methods.

Some experimental analyses have been conducted to study the mechanism of the consolidation with PVDs (Chu et al., 2006; Deng et al., 2016; Li et al., 2017). The mechanism of consolidation using PVDs is similar with the consolidation behavior using sand drain well. The PVD with high discharge capacity is to shorten the length of the drainage path. After the installation of PVDs, the porewater can seeped horizontally into

the drains and flow out along the drains. Therefore, the effectiveness of PVDs for the soil improvement is affected significantly by the quality of the PVDs, such as the discharge capacity.

2.2.2.1 Prefabricated band drain

In 1937, the prefabricated drain was introduced into the field of geotechnical engineering for soil improvement. The first type of prefabricated drain was developed by Kjellman (1937), which is a band-shaped drain with 35mm by 10mm. Subsequently, several types of prefabricated drains have been applied in land reclamation projects (Hansbo and Torstensson, 1979) as in Figure 2.5. In a word, the band drain is commonly used because of its easy prefabrication, easy quality control, economy and small disturbance to the surrounding soil during installation.

The prefabricated band drain consists of a central core as drainage channels for water, and a non-woven filter which prevents the soil particles from entering and blocking the central core but allows water to flow in. The materials and dimensions of different band drains are shown in Table 2.2.

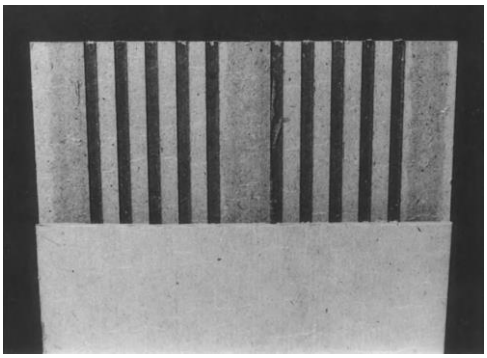

(a)

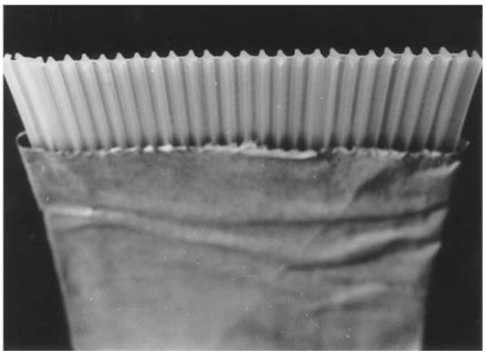

(b)

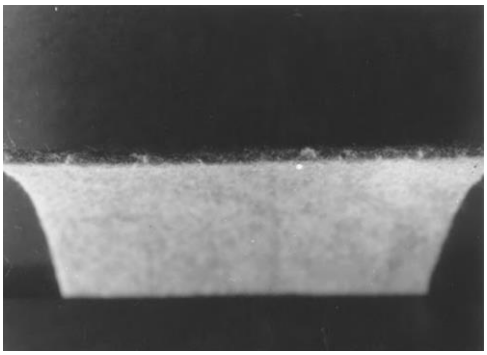

(c)

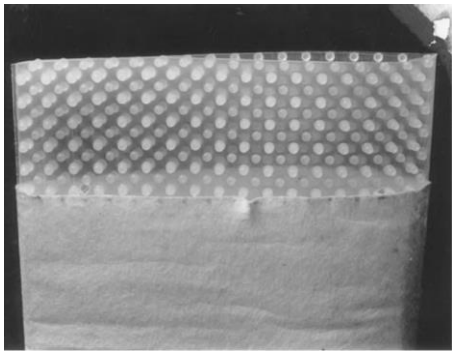

(d)

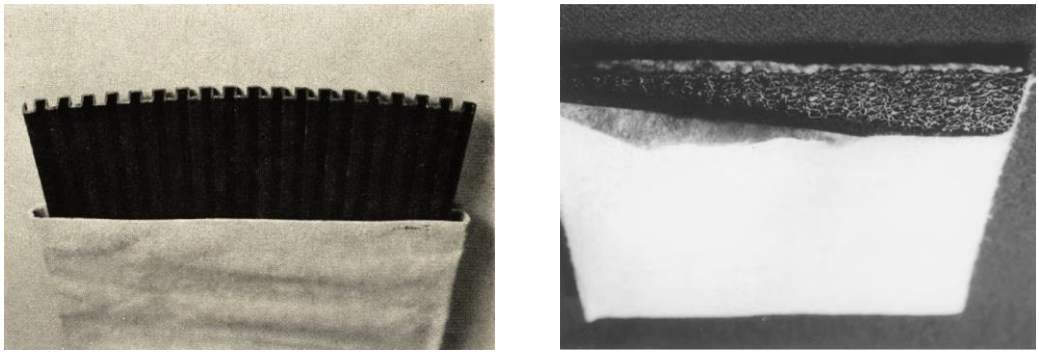

(e) (f)

Figure 2.5 Types of prefabricated drains: (a) Kjellman cardboard wick; (b) Geodrain; (c) Colbond; (d) Alidrain; (e) Mebradrain; (f) (after Hansbo and Torstensson, 1979)

Table 2.2 Material and dimension of different prefabricated drains (after Hansbo and Torstensson, 1979)

Type	Core	Filter	Dimension (mm)
Kjellmann	Paper	Paper	100*3
PVC	PVC	PVC	100*2
Geodrain	PE	Cellulose	95*2
Colbond	Polyester	Polypropylene	100*6

The common prefabricated drain consists of a corrugated plastic core and non-woven filter as shown in Figure 2.6. The permeability of the filter is much large than that of soft clayey soil as shown in Table 2.3. Due to the high permeability of filter and the high discharge capacity, the well resistance can be ignored for the consolidation of soft clayey soil.

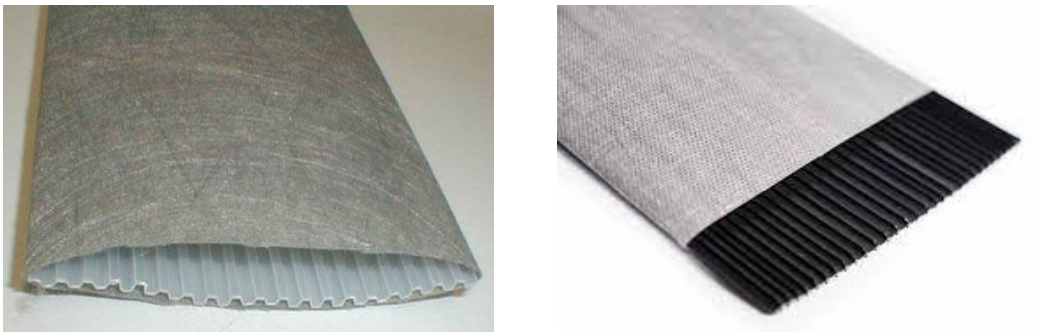

(a) Corrugated shape (b) Fishbone shape

Figure 2.6 Different shapes of core (https://www.tencategeo.asia)

Table 2.3 Properties of prefabricated band drains

PVD	Length (mm)	Width (mm)	Discharge capacity (mL/s)	Permeability (cm/s)
Alidrain	100	2	>70 (Kinked, 250kPa)	0.02
Colbonddrain	100	4	>140 (350kPa)	7

Liu and Chu (2009) developed an integrated PVD with the filter and core adhered together as shown in Figure 2.5. The integrated PVD is with higher tensile strength and greater discharge capacity. More advantages have been discussed in the paper by Liu and Chu (2009).

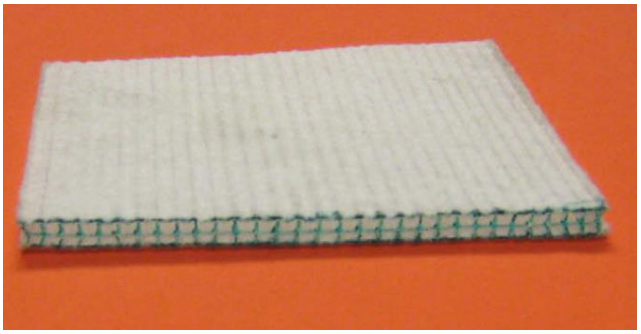

Figure 2.7 Integrated prefabricated drain (after Liu and Chu, 2009)

2.2.2.2 Installation of prefabricated vertical drains

The installation sequence of PVDs is shown in Figure 2.8. First, prepare the equipment and anchor plate for the installation of PVDs. Second, drive the rig with PVDs into soil, and stop the driving when the PVDs reach the desired depth. Third, pull out the rig, then the PVDs can stay in soil. Fourth, cut down the drain after the rig is fully pulled out. In terms of in-situ soil, the soil around the PVDs will be disturbed during the installation. Then the soil properties of smear zone should be considered. For the land reclamation of soft soil, the soft soil is under slurry condition, then the smear zone can be ignored.

A type of mini-PVD rig as shown in Figure 2.9 was developed to be applied on soft ground. For underwater soil improvement using PVDs, the installation barge as shown in Figure 2.10 can be used to support the PVD rig.

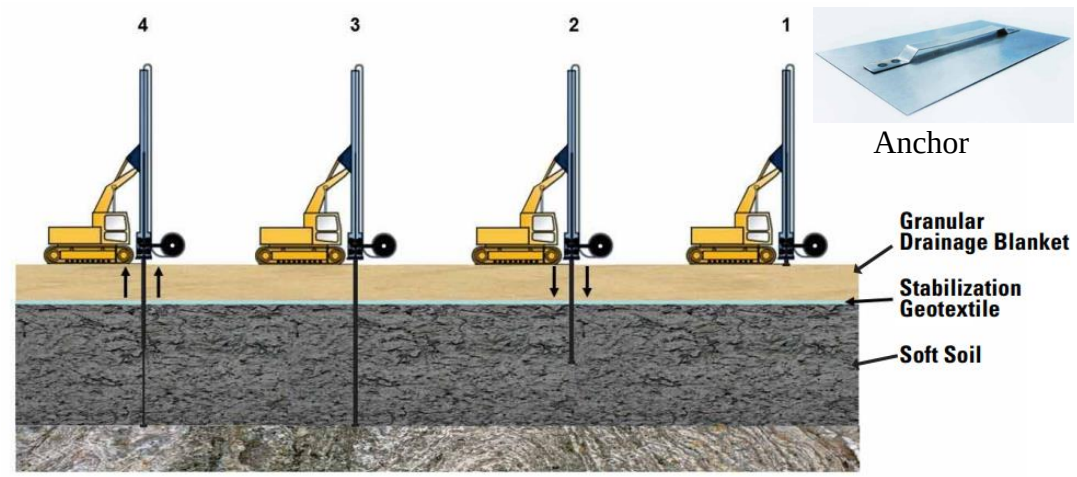

Figure 2.8 Installation sequence of PVDs (https://www.tencategeo.asia)

Figure 2.9 Mini-PVD rig

Figure 2.10 Offshore barge for PVD installation (after Yan et al., 2009)

2.2.3 Construction of working platform

For very soft or slurry types of fill materials, a combined vacuum preloading and fill surcharge with PVDs is commonly used in land reclamation projects (Chu et al., 2000; Varaksin and Yee, 2007; Yan and Chu, 2005). However, the installation of PVDs and the placement of surcharge on the soft soil ground are difficult. Hence, a working platform should be formed to support the working machines for the installation of PVDs and the placement of sand layer. Various methods summarized by Chu et al (2012) are to treat the top few meters of soft soil as working platform for the installation of PVDs or carrying out other types of soil improvement. The summary of those methods is in Table 2.4. The use of geotextile and the dewatering method is more suitable for the formation of working platform due to the relatively low cost and tropical weather in Singapore.

Table 2.4 Methods for creating a working platform on top of a layer very soft or high-water content slurry (after Chu et al., 2012)

No.	Method	Description/mechanisms	Advantages	Limitations
1	Sun drying	Form a desiccation soil layer due to evaporation	Simple and economical	Time-consuming
2	Capping with sand or competent soil	Place a thin layer of sand or good earth	Relatively cheap	Slow and difficult to implement
3	Use of geotextile	Place a layer of geotextile on soft soil ground	Relatively expensive	Relatively quick and reliable
4	Cement mixing	Use cement mixing to strengthen topsoil	Expensive	Difficult to control the properties of cement treated soil
5	Dewatering	Consolidate topsoil via special drainage system	Relatively cheap	Special equipment and procedure required

2.2.3.1 Broms' method

When the soil in the ground is soft, but still has a little bit of undrained shear strength (1 to 5 kPa), it may be possible to place geosynthetics such as geotextile directly over the soft ground. With the aid of geotextile, the sand or good soil can be placed using mechanical method by workers. This type of method has been used for reclamation of

lagoons, waste mining sites or construction of embankment (Rowe and Li, 2005; Espinoza and Sabatini, 2008; Yee, 2016).

Broms (1987) proposed a method for using geotextile or geogrid to form a working platform over soft clay. The sketch illustration of the Broms method is shown in Figure 2.11. To increase the stability of the sand berms, a layer of geotextile is laid on the surface of the soft soil. The sand berms are laid onto the geotextile layer in finger shape from one end to the other. To prevent the geotextile from sliding into the soft soil, the boundaries of the geotextile has to be fixed using sand berms. After the sand berms placed, the geotextile is stretched and settles down into the soft soil till the whole system is balanced. Then the "mud wave" is generated on the surface of the soft soil as shown in Figure 2.11. By spreading the sand berms over, the working platform can be formed. The technology is commonly referred to the "finger fill soil placement technique". In this method, the form of finger fill soil is the critical stage.

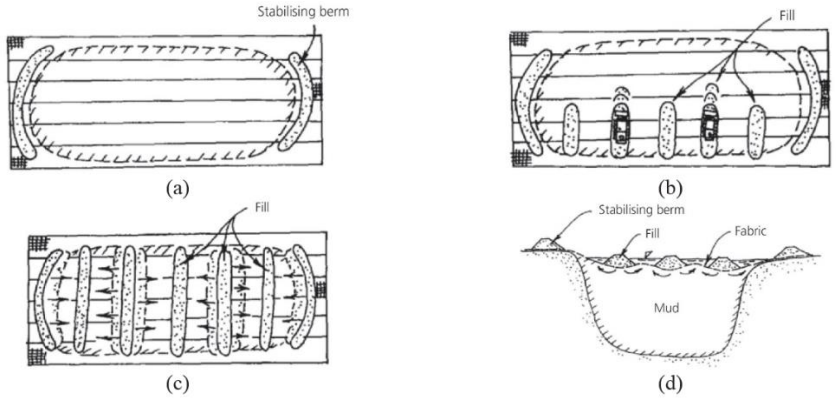

Figure 2.11 Broms Method: (a) placement of stabilitising berms; (b) placement of fill; (c) widening of berms; (d) elevation view. (After Broms, 1987 and Chu et al., 2012)

For the Broms method, the analytical model is shown Figure 2.12.

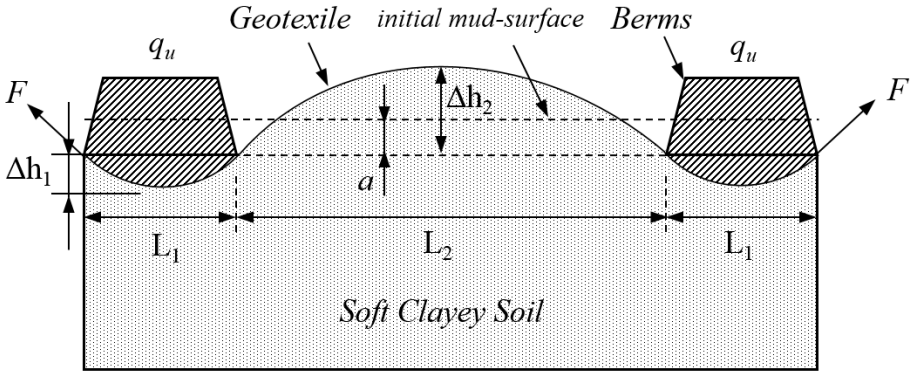

Figure 2.12 The analysis model of Broms method

The bearing capacity (q_u) of soft soil reinforced with geotextile can be obtain based on the Terzaghi's theory. The analytical solutions are:

$$a = \frac{2}{3}\Delta h_1(\alpha - 1) \tag{2.1}$$

$$q_u = N_c c_u + (1+\alpha)\frac{F}{R_1} + \frac{2(1+\alpha)}{3}\Delta h_1 \gamma'_{soil} \tag{2.2}$$

where, a is the settlement of geotextile under sand berms; $\alpha = L_2/L_1$; q_u is referred to the total weight of the berm material; N_c is the normalized bearing capacity, here equal to 5.7; c_u is the undrained strength of soft clayey soil; F is the tensile force of geotextile; R_1 is the radius of the deformed geotextile under berms; γ'soil is the buoyant unit weight of soft clayey soil.

The Broms' method has been applied in land reclamation projects using soft soil at the Cherry Island in USA (Guglielmetti et al., 1996). Similar methods were also adopted for soil improvement projects in Malaysia and China (Yee et al., 2012; Yee, 2016). The height and width of the sand berms are the key design parameters for creating the stability and providing the required bearing capacity. However, there are construction uncertainties in the formation of the sand berms or to control the height and width of the sand berms. Mud waves are sometimes created before the sand berms were formed as described by Toh et al. (1994) and Lam (2018) in real constructions. This causes uncertainties in both design and construction for the use of Broms' method. Even when the sand berms have been formed, the spreading of the sand in the berms is not an easy task either.

2.2.3.2 Short PVD +vacuum preloading

For the dewatering method, the short PVDs are more efficiently used to consolidate the top few meters soft soil as working platform in some reclamation projects (Sun et al., 2017)). The short PVDs is installed manually. This is not difficult as the ground was soft. The horizontal pipes and sand blanket for distributing vacuum pressures and providing drainage as well as membranes for sealing the ground for vacuum pressure are used. However, the placement of sand blanket is difficult. Hence, an alternative method using sealed flexible pipes is applied to distribute the vacuum pressure.

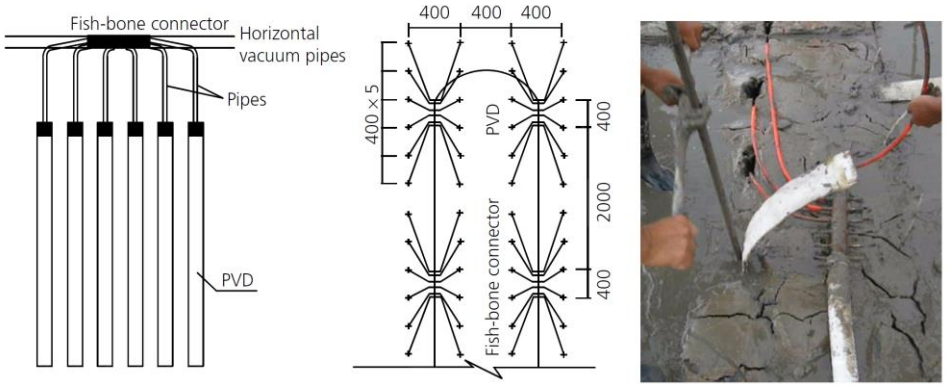

Figure 2.13 Method to use vacuum preloading combined with short PVD method to form the working platform (after Sun et al., 2017)

A pilot tests were conducted in Tianjin, China. The results before and after vacuum preloading are shown in Table 2.1 After vacuum consolidation, the water content was reduced significantly. The undrained shear strength was from 2.7 kPa at ground surface to 20.5 kPa.

Table 2.5 Soil properties and the degree of consolidation in the test site (Sun et al., 2017)

(a) Soil properties before and after vacuum preloading

γ (kN/m^3)	e	w_L (%)	w_P (%)	w_0 (%)	w_f (%)	s_{u0} (kPa)	s_{uf} (kPa)
15.2	2.32	45	22	83.8	48.0	2.7	20.5

(b) Degree of consolidation using settlement data

Method	$S_{t=60d}$ (mm)	S_∞ (mm)	U (%)
Asoka	729.9	873.7	83.5
Hyperbolic		816.8	89.4

By using the short PVDs and vacuum preloading method to form the working platform, the amount of settlement and degree of consolidation are not the controlling factor. The main targeting parameter should be the undrained shear strength or water content. Therefore, the water content and field vane shear data could be used to evaluate the performance of this method. To achieve an enough undrained shear strength, the water

content of soft soil should be lower than the liquid limit. One shortcoming of this method is that the top 1 m of soil could not be treated properly as the vacuum pressure was not applied to this layer due to the use of sealed tube.

2.3 Theoretical analysis of consolidation

2.3.1 Sedimentation and self-weight consolidation

In many offshore reclamation projects, the slurry or ultra-soft marine clay was used as the fill material. Because of the high-water content, the slurry will be into sedimentation phase after pumped into the reclamation pond. It will take a long time for slurry into self-weight consolidation dominated phase from sedimentation dominated phase. Many researchers have studied on the sedimentation and self-weight consolidation (Kycn, 1951; Imai, 1981; Been and Sills, 1981; Schiffman and Cargill, 1981; Lee and Sills, 1981; Lee, 1981; Fitch, 1983; Concha and Vustos, 1987; Tan et al., 1988; Tan et al., 1990; Kim et al., 1991; Katagiri and Imai, 1994; Bo, 2008; Zhang and Zhu, 2014; He et al., 2017; Zhang et al., 2017).

The sedimentation process can be divided into three stages as shown in Figure 2.14. at the beginning, the soil particles are suspended. Then the particles are settling on the bottom, the suspension surface are moving down. At the same time, the consolidation zone at the bottom after settling are into self-weight consolidation. The sedimentation curves are shown in Figure 2.15.

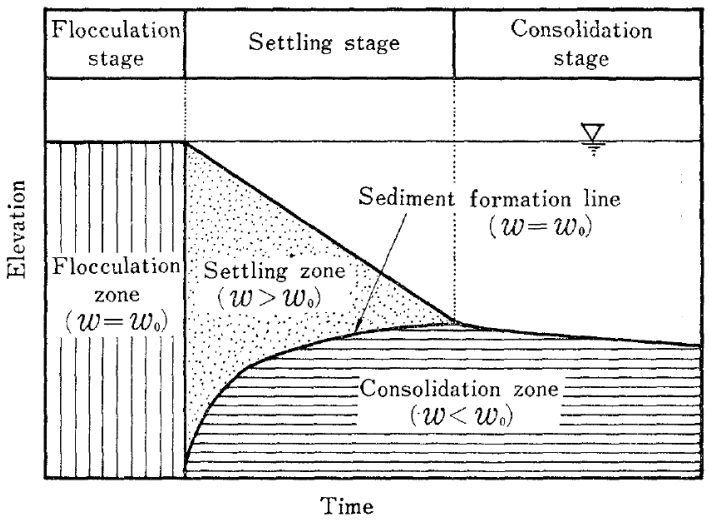

Figure 2.14 General characteristics of sedimentation curve of soil slurry (after Imai, 1981)

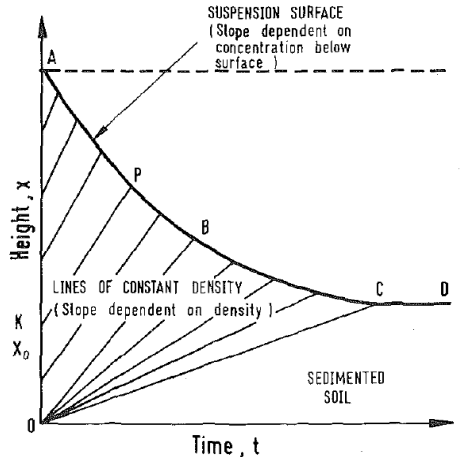

Figure 2.15 Typical Kynch's plot of constant concentration lines (after Tan, 1990)

The self-weight consolidation process is shown in Figure 2.16. The excess pore water pressure is shown in Figure 2.17. The self-weight consolidation usually is the one-dimensional consolidation. The drainage boundary is at the surface.

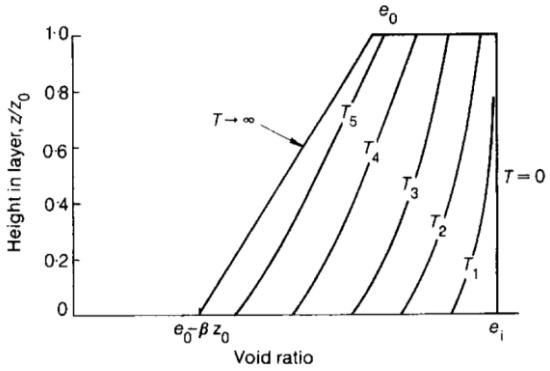

Figure 2.16 Isochrones of void ratio: expected form from experiments (after Been and Sills, 1981)

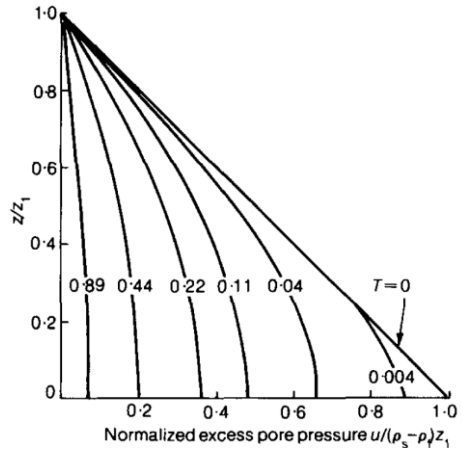

Figure 2.17 Isochrones of excess pore water pressure when $z_1 = 1.5z_0$ (after Been and Sills, 1981)

2.3.2 Non-linear consolidation theory

From the self-weight consolidation to primary consolidation, the effective stress is low, and the soil is very soft. The deformation of soil is large, and the large consolidation theory should be applied.

Gibson et al. (1967 and 1981) developed a non-linear consolidation theory in which the large settlement is in vertical direction. The Lagrange coordinate (a) and the Euler coordinate (ξ) are used in the analytical model as shown in Figure 2.18. Assuming uniform soil and constant water density and particle density, the relationship between two coordinates is shown in Eq. (2.26). For one-dimensional and two-dimensional non-linear consolidation theory, the governing equations are shown in Eq. (2.27) and (2.28). The surcharge can be combined into the initial pore pressure conditions and the vacuum pressure can be considered as the boundary condition.

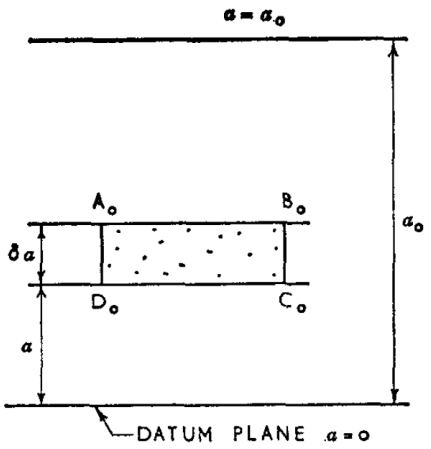

(a) initial configuration at t=0

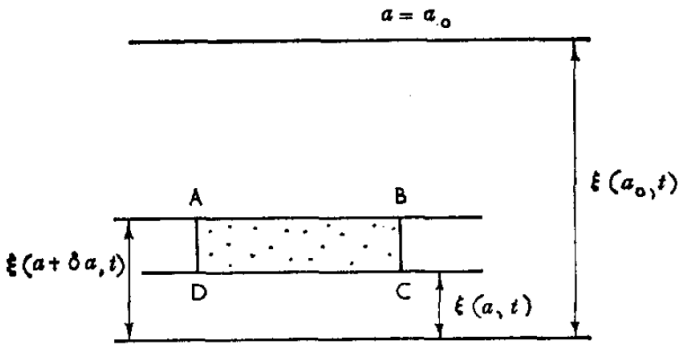

(b) current configuration at time t

Figure 2.18 Analytical model foe one-dimensional large-strain consolidation (after Gibson, 1967)

$$\frac{\partial \xi}{\partial a} = \frac{1+e}{1+e_0} \qquad 2.26$$

$$\frac{\partial \Delta u}{\partial t} = -\frac{(1+e_0)^2}{\gamma_w}\frac{d\sigma'}{de}\frac{\partial}{\partial a}\left(\frac{k_z}{(1+e)}\frac{\partial \Delta u}{\partial \mathrm{a}}\right) \qquad 2.27$$

$$\frac{\partial \Delta u}{\partial t} = \frac{(1+e_0)^2}{\gamma_w}\left(-\frac{d\sigma'}{de}\right)\frac{\partial}{\partial a}\left(\frac{k}{1+e}\frac{\partial \Delta u}{\partial a}\right) - \frac{1+e}{\gamma_w}\left(-\frac{d\sigma'}{de}\right)\frac{\partial}{\partial x}\left(k\frac{\partial \Delta u}{\partial x}\right)] \qquad 2.28$$

Few researchers proposed the non-linear relationships of void ratio-effective stress and void ratio-permeability for finite strain consolidation theory (Gibson et al., 1981; Tan et al., 1990; Kim 1991). The exponent relationship was proposed by Gibson et al. (1981) as shown in Figure 2.19. the Log-log relationship was proposed by Kim et al. (1991). Tan (1988) conducted few experiments to study the void ratio-effective stress relationship and void ratio-permeability relationship of marine clay in Singapore as shown in Figure 2.20.

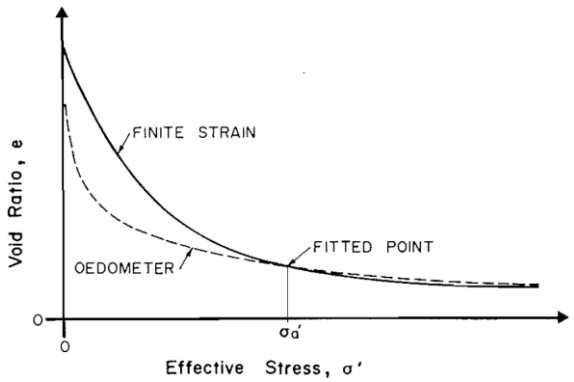

Figure 2.19 Void ratio - effective stress relationships for finite strain consolidation theory (after Gibson et al., 1983)

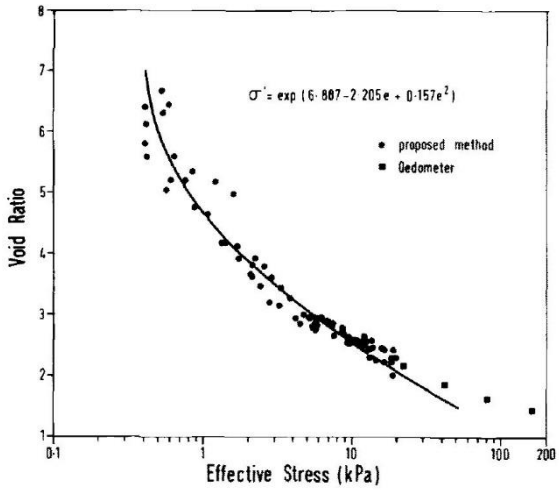

(a) void ratio-effective stress relationship

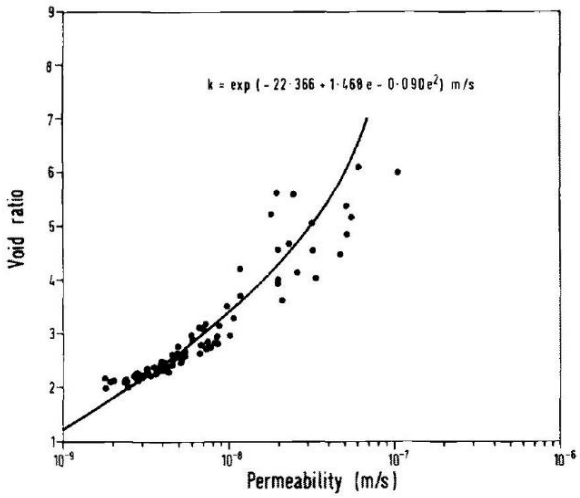

(b) void ratio – permeability relationship

Figure 2.20 Experimental results from large strain consolidation of marine clay in Singapore (after Tan et al., 1988)

2.3.3 One-dimensional consolidation theory

The one-dimensional consolidation theory was developed by Terzaghi (1925). The water flow and soil deformation is assumed only in the vertical direction. The one-dimensional consolidation solution under surcharge is in Eq. (2.1) and (2.2) under single drainage condition.

$$u(z,t) = \sum_{m=1}^{\infty} (\frac{2}{H}\int_0^H u_0 sin\frac{Mz}{H}dz) sin\frac{Mz}{H} e^{-M^2 T_v} \tag{2.1}$$

$$U = 1 - \sum_{m=1}^{\infty} \frac{2}{M^2} e^{-M^2 T_v} \tag{2.2}$$

where, $u(z, t)$ is the excess pore pressure; H is the length of drainage path; u_0 is the initial excess pore pressure; $M = (2m\text{-}1)\pi/2$; $T_v = c_v t/H^2$.

The vacuum preloading has been applied in land reclamation of soft soil. The one-dimensional consolidation theory with vacuum boundary condition has been proposed by Chai and Carter (2011). The vacuum pressure is added on the consolidation boundary. The one-dimensional vacuum consolidation solutions are in Eq. (2.3) under single drainage condition and in Eq. (2.4) under double drainage condition. The degree of consolidation for vacuum preloading under single and double drainage condition is the same as in Eq. (2.2).

$$u = -p_{vac}[1 - \sum_{m=1}^{\infty} \frac{2}{M} sin(\frac{Mz}{H}) e^{-M^2 T_v}] \quad (2.3)$$

$$u = -p_{vac}[(1\frac{z}{H}) - \sum_{n=1}^{\infty} \frac{2}{N} sin(\frac{Nz}{H}) e^{-N^2 T_v}] \quad (2.4)$$

where, p_{vac} is the absolute vacuum pressure at vacuum drainage boundary; $N = n\pi$.

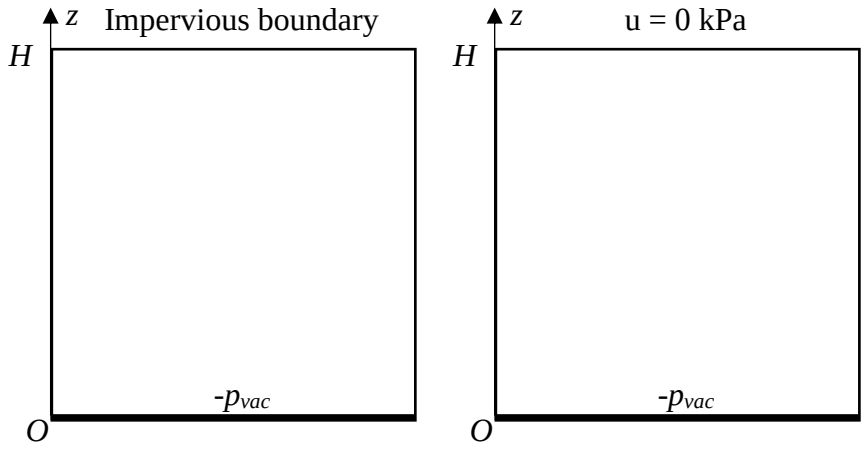

(a) Single drainage condition (b) Double drainage condition

Figure 2.21 Analytical model for one-dimensional vacuum consolidation theory

2.3.4 Two-dimensional consolidation theory

With the use of PVDs, the pore water flow is in two directions. The two-dimensional consolidation theory should be considered. The vacuum behaviour of a unit cell is considered in Cartesian coordinate system or cylindrical coordinate system. The PVDs can be simplified as sand drain using Eq. (2.8). The pattern of PVDs is in either a rectangular or a triangular distribution with uniform spacing, s_p. The simplified unit cell is in Figure 2.22.

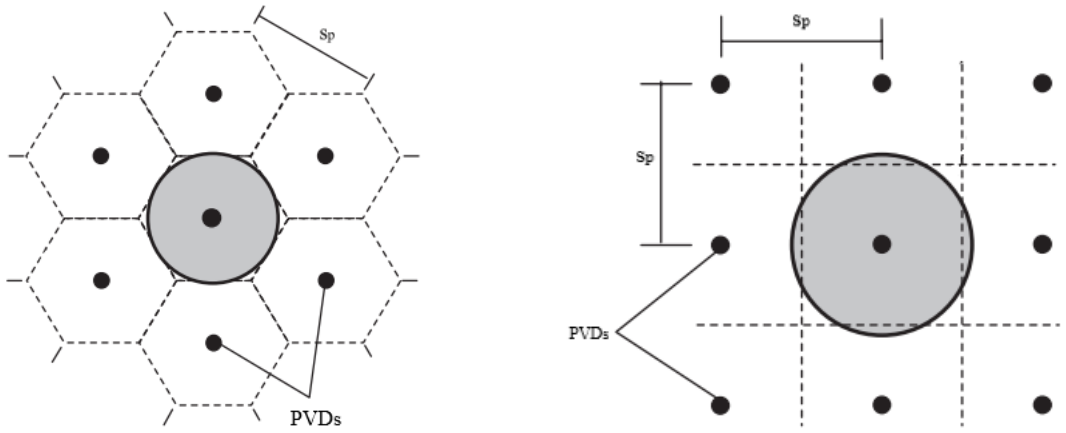

(a) Triangular arrangement (b) Rectangular arrangement

Figure 2.22 Installation pattern of PVDs (after Basu et al., 2010a)

Consolidation with PVDs

The mechanism of consolidation with PVDs is similar with the consolidation theory for sand drain well (Chu et al., 2006; Deng et al., 2016; Li et al., 2017). So far, the theories related to the consolidation with PVDs have been reviewed very recently elsewhere by Chu et al. (2012) and Chu and Raju (2013). Many analytical solutions were proposed for the design of the consolidation with PVDs (Barron, 1948; Carillo, 1942; Hansbo, 1981; Onoue et al., 1991; Walker et al., 2012; and Yoshikuni and Nakanodo, 1974; Zeng and Xie, 1989; Indraratna et al., 2005a).

The analytical model for the consolidation with sand well established by Hansbo (1981) is shown in Figure 2.23. The analytical solution is as following.

$$U_h = 1 - e^{-\frac{8T_h}{F(n)}} \tag{2.5}$$

$$F(n) = Ln(n) - 0.75 + Ln(s)(\frac{k_h}{k_s} - 1) + \pi z(2l - z)\frac{k_h}{q_w} \tag{2.6}$$

$$T_h = \frac{c_h t}{d_w^2},\ n = \frac{d_e}{d_w},\ s = \frac{d_s}{d_w} \tag{2.7}$$

$$d_w = \frac{2(w + a)}{\pi} \tag{2.8}$$

where, c_h is the horizontal coefficient of consolidation of soil; t is time; d_e is the diameter of soil cylinder; $F(n)$ is a function of d_e; d_s is the diameter of the smear zone; k_h is the horizontal permeability of the soil; k_s is the horizontal permeability of the smeared zone. q_w is the discharge capacity of PVDs; L is the length of sand drain; z is the depth. w is the width of PVDs; a is the thickness of PVDs; $d_e = 1.128 s_p$ for a square grid and $d_e = 1.05\ s_p$ for a triangle grid.

Due to the installation of PVDs, the soil around the PVDs was disturbed. A lot of studies about the disturbed soil (smear zone) have been conducted (Hansbo 1979; 1981; Bergado et al. 1991, Onoue 1991; Madhav et al. 1993; Almeida et al. 1993; Indraratna and Redana 1998; Chai and Miura 1999; Hird and Moseley 2000; Bo et al. 2003; Basu and Prezzi 2007; Chai and Carter 2011).

For simplicity in design, the 2D plane strain analytical solution for the consolidation with PVDs was proposed (Basu et al., 2010; Hird et al., 1992; Indraratna and Redana, 1997; Rujikiat- kamjorn et al., 2008). The PVDs is simplified as vertical drain walls as in Figure 2.24. The conversion equation of the soil permeability under axisymmetric condition into the simplified permeability under plane strain condition is in Eq. (2.9).

$$k_{hp} = \frac{k_h[\alpha + \beta(k_{hp}/k_{sp}) + \theta(2lz - z^2)}{Ln\frac{n}{s} + \frac{k_h}{k_s}Ln(s) - 0.75 + \pi(2lz - z^2)\frac{k_h}{q_w}} \tag{2.9}$$

$$\alpha = \frac{2}{3}\frac{(n-s)^3}{3(n-1)n^2} \tag{2.10}$$

$$\beta = \frac{2}{3}\frac{(s-1)}{(n-1)n^2}[3n(n-s-1) + (s^2+s+1)] \tag{2.11}$$

$$\theta = \frac{2k_{hp}}{Bq_z}(1 - \frac{1}{n}) \tag{2.12}$$

where, k_{hp} is the soil permeability under plane strain condition; k_{sp} is the equivalent permeability under plane strain condition in the smeared zone; $q_z = 2q_w/\pi B$ is the equivalent discharge capacity under plane strain condition; B is the equivalent width of soil based on same cross-section area.

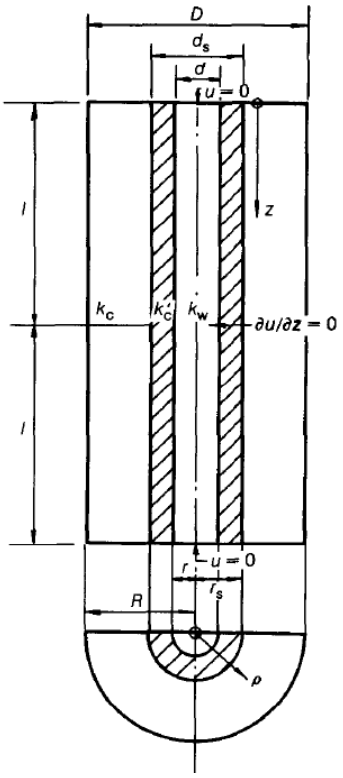

Figure 2.23 Schematic picture of soil cylinder dewatered by vertical drain (after Hansbo, 1981)

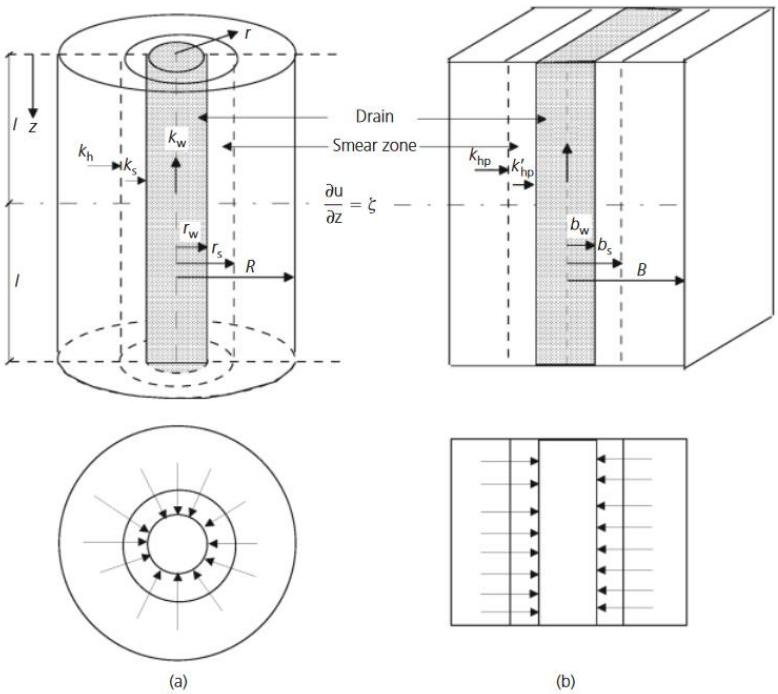

Figure 2.24 Conversion of (a) an axisymmetric unit cell into (b) plane strain condition (after Indraratna et al., 1997)

Vacuum Preloading with PVDs

In vacuum preloading system, PVDs are used to distribute the vacuum pressure. Several analytical solutions are proposed through combining the vacuum boundary condition with the analytical solution for the consolidation with PVDs (Chai and Carter, 2011; Indraratna et al., 2012). The analytical model for vacuum consolidation is shown in Figure 2.25. The analytical solution is as following. The horizontal average degree of consolidation (U_h) is:

$$u(r,z,t) = -p_{vac}[1 - v(r,z,t)], r_s < r \leq r_e \tag{2.13}$$

$$u(r,z,t) = -p_{vac}[1 - v'(r,z,t)], r_w < r \leq r_s \tag{2.14}$$

$$v(r,z,t) = \frac{1}{r_e^2 \mu}[r_e^2 Ln\frac{r}{r_s} - \frac{r^2 - r_s^2}{2} + \frac{k_s}{k_w}(r_e^2 Lns - \frac{r_s^2 - r_w^2}{2}) + \frac{k_h}{k_w}(n^2-1)(2lz - z^2)]e^{-\frac{8T_h}{\mu}},\ r_s < r \leq r_e \tag{2.15}$$

$$v'(r,z,t) = \frac{k_h}{k_s r_e^2 \mu}[r_e^2 Ln\frac{r}{r_w} + \frac{r^2 - r_w^2}{2} + \frac{k_s}{k_w}(n^2-1)(2lz - z^2)]e^{-\frac{8T_h}{\mu}},\ r_w < r \leq r_s \tag{2.16}$$

$$\mu = Ln\frac{n}{s} + \frac{k_h}{k_s}Lns - \frac{3}{4} + \pi z(2l - z)\frac{k_h}{q_w} \tag{2.17}$$

where, $s = r_s/r_w$, $n = r_e/r_w$, and l = the drainage length of a PVD, k_h is the horizontal permeability of soil, k_s is the permeability in smear zone, k_w is the permeability of PVD filter.

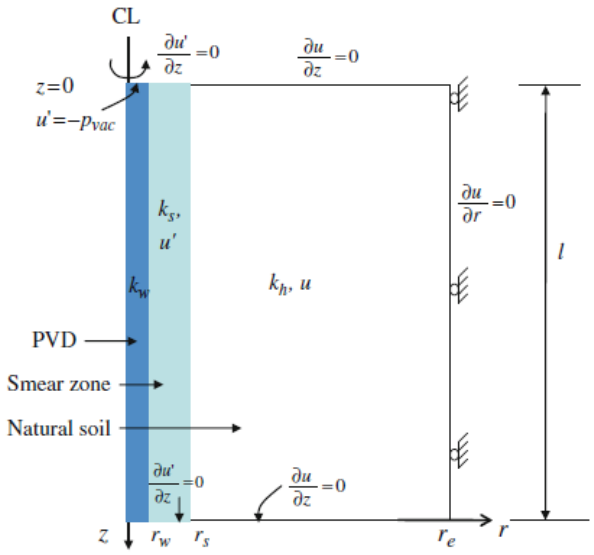

Figure 2.25 Unit cell model and boundary conditions (after Chai and Carter, 2011)

With the use of sand blanket to distribute the vacuum pressure, the vacuum boundary is on ground surface. Based on Carrillo's method (1942), the degree of consolidation of unit cell for vacuum consolidation with sand blanket and PVDs are in Eq. (2.18). the vertical degree of consolation is in Eq. (2.2).

$$U = 1 - (1 - U_v)(1 - U_h) \tag{2.18}$$

2.4 Vacuum preloading with horizontal drains

In recent years, some researchers have proposed a new method for soil improvement. In this method, the installation of the horizontal drains was followed by the placement of soft soil layer by layer. By using the horizontal drains, the vacuum pressure can be applied through the horizontal drains to accelerate the consolidation of soft soil as early as the first few meters of soft soil was laid. Therefore, a working platform to support the soil improvement works later is not necessary since the soft soil has already been consolidated and solidified to a certain degree during the infilling stage, and the containment bund does not have to be built as high as the maximum height of the reclaimed soft soil. By using this method, the overall vacuum preloading duration will be cut down and the cost will be saved for land reclamation projects.

2.4.1 Soil improvement using horizontal drains

Shin and Oh (2007) conducted a field test using prefabricated drains as horizontal drains for vacuum preloading of soft dredged marine clay. It took a few months for the vacuum consolidation to achieve the 70 % of average water content. In Japan, two landfill sites on shore were used to dispose the soft dredged soil. The soil improvement of soft dredged soil was conducted using vacuum preloading with horizontal drains. The horizontal drains consisted of the prefabricated drains only with 0.8 m horizontal spacing and about 2.5 m vertical spacing (Shinsha et al., 2013; Shinsha and Kumagai, 2014). For this field test, it took 294 days for the infilling and consolidation of soft dredged soil to achieve the 110 % of average water content from 200 % of initial average water content. Therefore, by using prefabricated drains only as the horizontal drains, the duration of vacuum consolidation is still relatively long to achieve a certain degree of consolidation. As the vertical and horizontal spacings are different for the vacuum preloading using horizontal drains, Chai et al. (2014) developed a modified Hansbo's solution by using the modified coefficient of consolidation from the finite element analyses. Moreover, few researchers proposed the use of the geo-composite with high discharge capacity as horizontal drains (Chai et al., 2011; de Lillis et al., 2017). Few lab tests have been conducted for the performance of geo-composites used as horizontal drains by Chai and Nguyen (2013). The good performance can be obtained by using geo-composites with high discharge capacity for long term condition. However, the cost for the use of geo-composite for large-scale land reclamation is expensive. A new form of horizontal drains, the horizontal drainage enhanced geotextile sheet (HDeG), was proposed by Chu et al. (2012; 2016) as in Figure 2.26b. For HDeG, the drains with a certain spacing are bounded with geotextile sheets. With the transmissivity of geotextile sheets, the vacuum pressure in drains can be transmitted through the geotextile sheets.

By using the geotextile for the proposed horizontal drains, the transmissivity of geotextile has an effect on the distribution of negative pore pressure on the proposed horizontal drains. Some laboratory tests to measure the transmissivity of non-woven geotextile in soft clayey soil were conducted (Durst et al., 1981; Koerner and Sankey, 1982; Chai and Miura, 2002). Because of the different effective stress and the clogging due to fine-grain particles, the transmissivity of non-woven geotextile in soft clayey soil will decrease significantly (Chai and Miura, 2002). The clogging phenomena of non-woven geotextile in soft soil was observed by using SEM a shown in Figure 2.27.

Koerner et al. (1982) reported the transmissivity of non-woven geotextile is reduced exponentially in soft clayey soil and tend to constant with the increasing of normal stress. Moreover, when the non-woven geotextile in soft soil with high clay contents (>30%), the transmissivity is reduced largely, almost tend to 1/100 of the original value as in Figure 2.28.

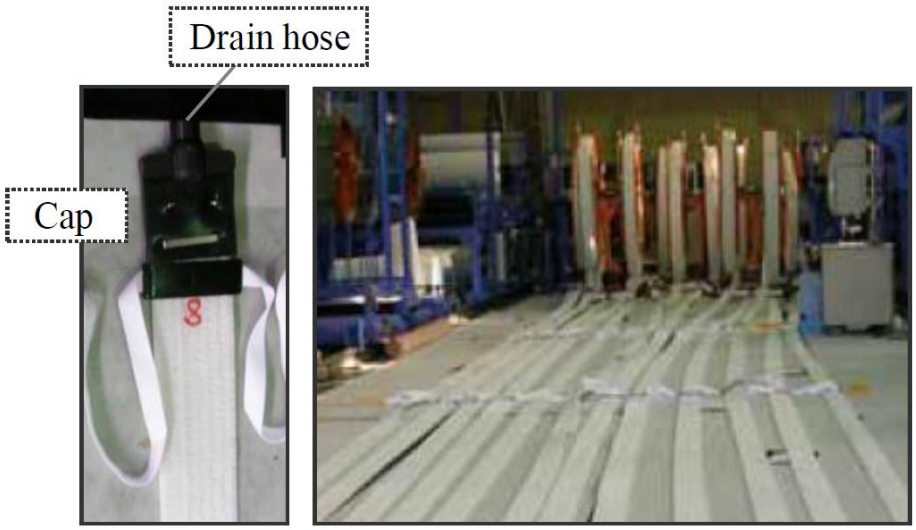

(a) Prefabricated board drains

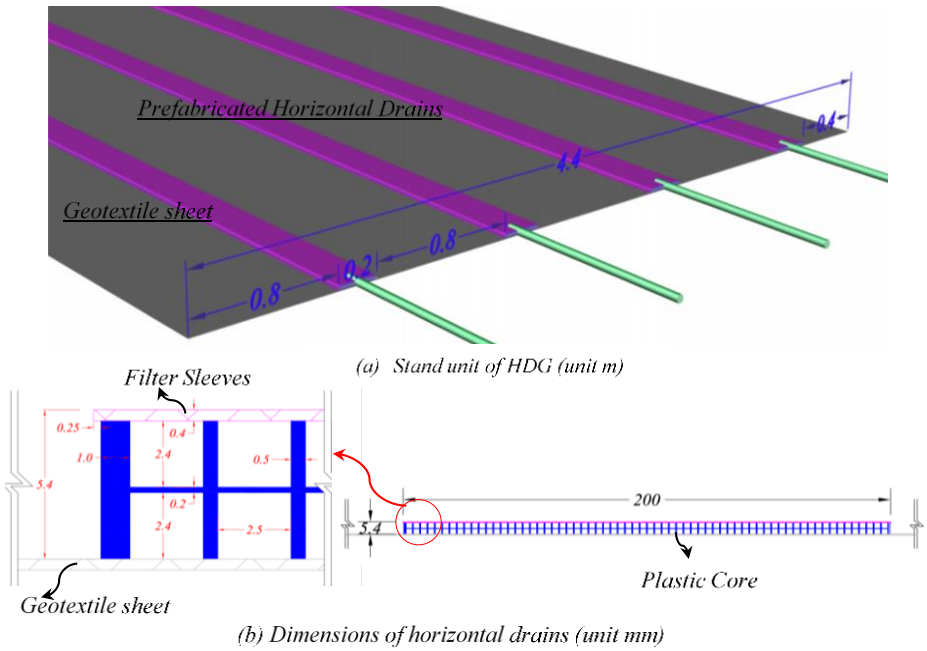

(b) Horizontal drainage enhanced geotextile

Figure 2.26 Horizontal drains for vacuum consolidation (after Shinsha et al., 2013; Chu et al., 2016)

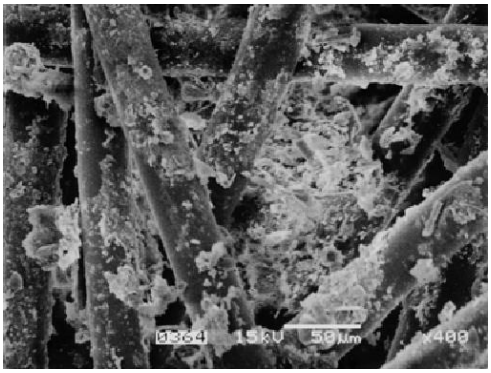

Figure 2.27 SEM for the clogging of non-woven geotextile due to the clay particles (after Chai and Miura, 2002)

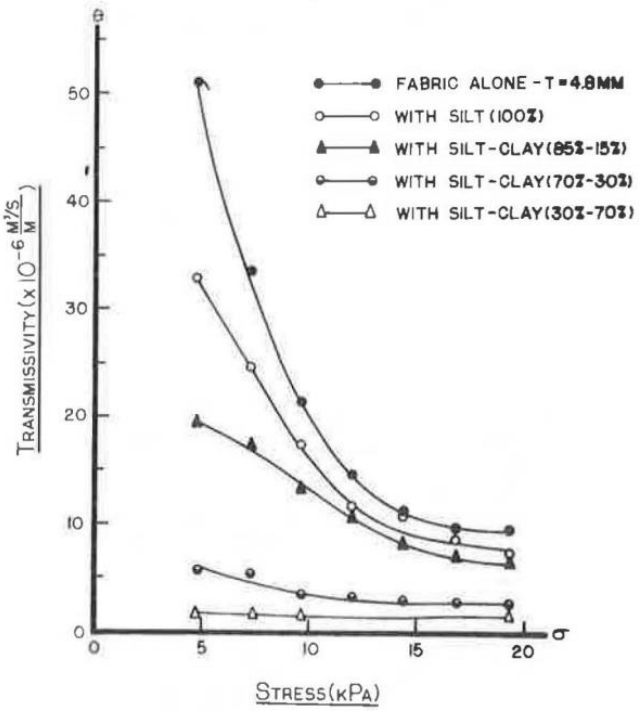

Figure 2.28 Transmissivity versus allied stress for soil/fabric/soil system (after Koerner et al. 1982)

2.4.2 Theoretical analysis

With the use of prefabricated drains as horizontal drains, a modified consolidation theory using horizontal drains was developed by Chai (2012) based on the Hansbo's solution. The analytical model is shown in Figure 2.29. In that theory, the different distance of drains in vertical and horizontal was considered and the reduction of the coefficient of consolidation was determined using finite element analyses. A design chart of the reduction of coefficient of consolidation was illustrated as in Figure 2.30.

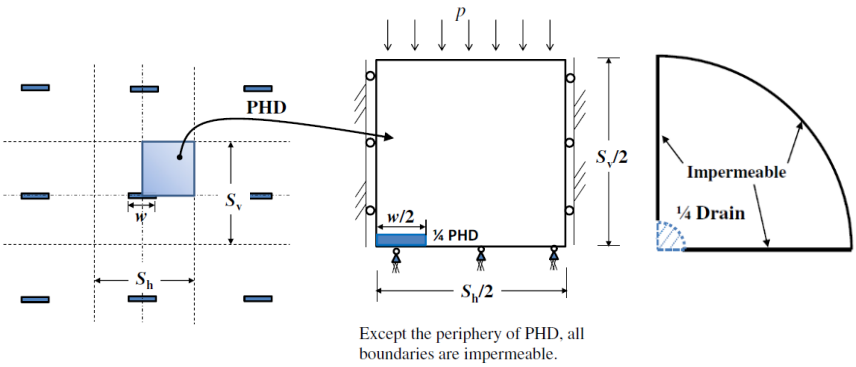

Figure 2.29 Analytical model for the consolidation using horizontal drains (after Chai et al., 2014)

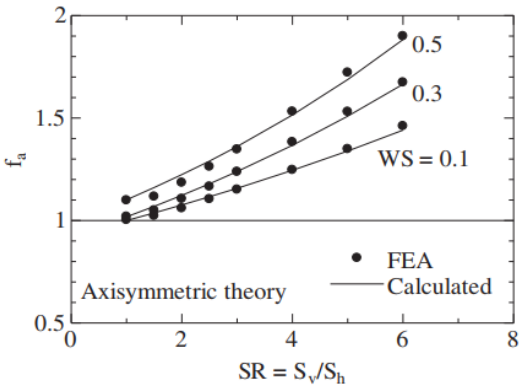

Figure 2.30 Reduction of coefficient of consolidation for different geometry (after Chai et al., 2014)

However, for the consolidation of soft soil using horizontal drains, the strain in soil is mainly in vertical direction. Due to the gravity and different vertical and horizontal spacings, the pore pressure distribution around the prefabricated drain is not really axisymmetric, especially for the use of horizontal drainage enhanced non-woven geotextile.

2.5 Improvement methods of soft soil

2.5.1 Electro-osmosis

In 1939, Casagrande demonstrated that applying an electro-kinetic force to fine grained soils with high water contents resulted in an increasing of effective stress in soil through the generation of negative pore water pressures (Casagrande, 1949, 1952, 1983). The application of electro-osmosis in the soil improvement have been studied by Casagrande

(1948, 1983), Bjerrum et al. (1967), Esrig & Gemeinhardt (1967), Fetzer (1967), Lo et al. (1991a&1991b), Shang (1998), Su & Wang (2003), Hu et al. (2012), Wu & Hu (2011), Lee (2015), Lamont-Black et al. (2016) and Shen et al. (2017). The electroosmotic consolidation as a soil improvement technique has been applied in projects such as stabilization of earth dams, railways embankment, slopes and pile foundation. The electroosmotic consolidation has also been applied in the land reclamation projects combined with surcharge, vacuum pressure and prefabricated drains. With the low permeability of soft clayey fill, the electro-osmosis can accelerate consolidation in the land reclamation projects using soft dredged marine clay or soft clayey soil.

2.5.1.1 Mechanism of electro-osmosis

The electro-kinetic dewatering process consists of the electro-osmosis, electrophoresis and electrochemical. In soil, the soil particle usually exhibits a negative surface charge (Mitchell and Soga, 2005; Pusch, 1976). The cations in pore water are surrounded by water molecules, see Figure 2.31. When a direct current is applied to the soil, the cations move towards the cathode. Then the water molecules will move together with the cations towards the cathode as shown in Figure 2.31. With a drain at cathode, the water can flow out, then the water content of soil will be reduced and the soil is consolidated.

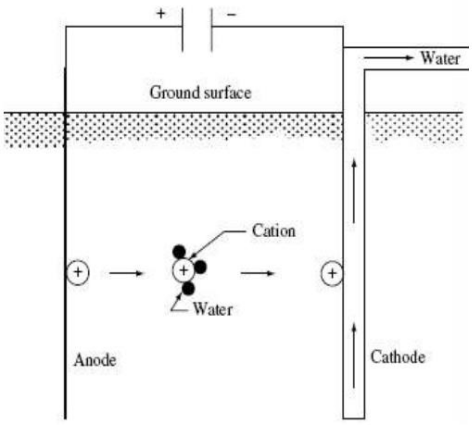

Figure 2.31 Electro-osmosis glow (after Asadi et al., 2013)

The electrode reactions at anode can be summarized as follow. At the anode

$$H_2O \rightarrow O_2\uparrow + H^+ \tag{2.18}$$

$$M_a \rightarrow M_a^{n+} + ne^- \tag{2.19}$$

where, M_a the anode metal. The metal at anode will be corroded.

At the cathode

$$H_2O \rightarrow H_2\uparrow + OH^- \tag{2.20}$$

$$M_i^{n+} + ne^- \rightarrow M_i \downarrow \tag{2.21}$$

$$M_i^{n+} + OH^- \rightarrow M_i(OH)_n \downarrow \tag{2.22}$$

where, $M^{n+}{}_i$ the dissolved cation species i in solution.

The efficiency of electro-osmosis is affected by the current. Hence, that is affected by the cation valence as in Eq. (2.19) and (2.21). The electro-osmosis is the more useful for the consolidation of soft clayey soil because the electro-osmosis permeability is effectively independent of grain size as shown in Figure 2.32. The electro-kinetic flow rate is 100 to 10,00 times greater than the hydraulic flow rate in fine-grained materials (Jones et al., 2008).

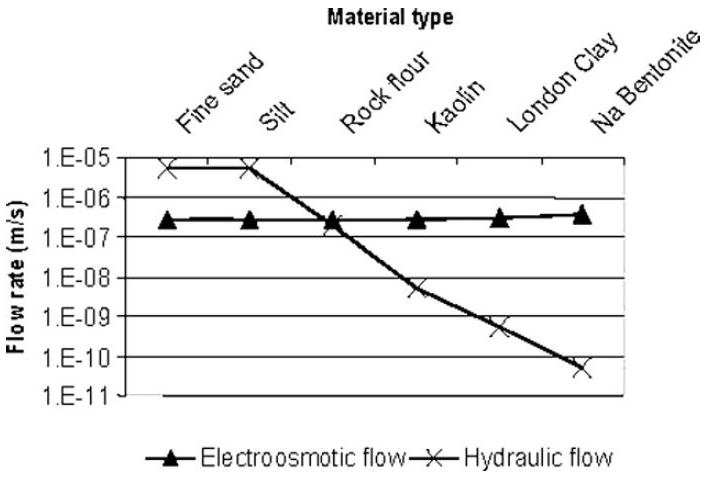

Figure 2.32 Comparison of hydraulic and electrokinetic flow rates (after Jones et al, 2008)

2.5.1.2 Application of electroosmosis

Because the efficiency of electro-kinetic treatment is affected by the electrode material used, so the selection of electrode material is important. Lokhart (1983) use steel, copper and carbon electrodes to study the electro-osmotic dewatering of kaolinite. The author reported that the copper electrode proved best for dewatering of Cu-kaolinite. Segall and Bruell (1992) reported that the flow rate generated by iron electrodes was twice the flow rate generated by graphite electrodes. Zhou et al. (2015) reported the graphite electrodes have a better electroosmosis effect over the iron and copper electrodes under high

potential gradient. The copper electrodes showed the rapid decreases in current and effective potential which is due to the anode passivation. However, Mohamedelhassan and Shang (2001) reported that the carbon electrodes cause significant voltage drops at the anode. The voltage drop at the electrodes reduces the voltage gradient in the soil and hence decreases the efficiency of the treatment as shown in Figure 2.33.

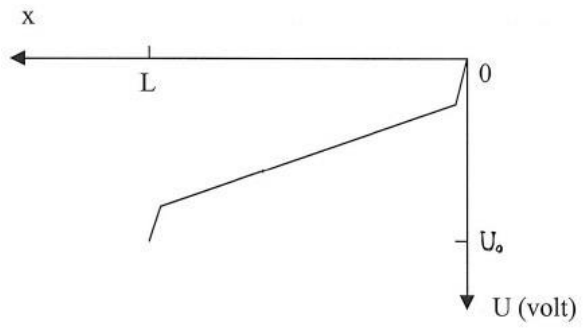

Figure 2.33 Distribution of electrical potential (after Mohamedelhassan and Shang, 2001)

Some consolidation tests combining the vacuum preloading with electro-osmosis have been conducted (Lo et al., 1991b; Shang, 1997; Wang & Vu, 2010; Jeyakanthan et al., 2010; Shen et al., 2012; Shen et al., 2017; Sun et al., 2017; Wang et al., 2016). Liu (2014) studied the consolidation process combining the electro-osmosis, vacuum pressure and surcharge. The electroosmosis can accelerate the consolidation of fine grain soil due to the high electrical permeability in soil. After the application of Electro-osmosis, the pore-water pressure has a slight drop, and the undrained strength is increasing. The technique of polarity reversal (reversing the polarity of the applied voltage periodically) can increase the average current flowing through the soil.

The electro-kinetic geosynthetics (EKG) has been proposed by many researchers (Jones, 1996; Jones et al., 1997; Nettleton et al., 1998; Shang, 1998; Abiera et al., 1999; Rowe and Jones, 2000; Pugh et al., 2000; Jones, 2001; Hamir et al., 2001; Jones and Pugh, 2001; Pavlakis et al., 2001; Lamont- Black et al., 2001; Pugh, 2002; Chew et al., 2004; Lorenzo et al., 2004; Glendinning et al., 2005; Jones et al., 2005, 2008; Ritterong et al., 2008; Lamont-Black et al., 2010; Jones et al., 2011; Karunaratne, 2011; Zhuang et al., 2014; Bourges-Gastand et al., 2015; Lamont-Black et al., 2015; Lamont-Black and Jones, 2015; Zhaung, 2015). The EKG combines the electro-kinetic phenomena of electro-osmosis, electrophoresis and associated electro-kinetic with the traditional

geosynthetics functions of drainage, filtration, containment and reinforcement. The electrically conductive PVDs was developed by using copper electrodes in the electrically conductive polymer cores of PVDs as shown in Figure 2.34(a) and (b) (Lee, 2015; Shen et al., 2017). The conductive polymer is made of the polymer and carbon powder.

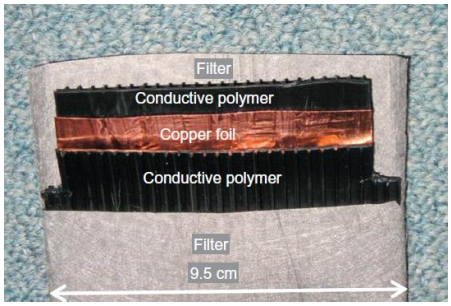

(a)

(b)

Figure 2.34 Electrically conductive PVD (after Lee, 2015; Shen et al., 2017)

2.5.2 Lime treatment

Lime has been used as a binder to treat soft soil for many years (Broms, 1981??, McCallister and Petry, 1992; Locat et al., 1996; Yamadera, 1999; Chew et al., 2004; Al-Mukhtar et al., 2012).

2.5.2.1 Mechanism of lime treatment

Both quick lime and hydrated lime have been used for soil treatment. For hydrated lime, there are two reactions during the treatment of soft clayey fill using hydrated lime (Clare et al., 1957; Ormsby et al., 1973; Locat et al., 1990; Broms, 1999; Le Runigo et al., 2009; Salehi and Sivakugan, 2009; Mukhtar et al., 2010; Vitale et al., 2016). One is the calcium ion exchange with the clay minerals to reduce the thickness of double layer surrounding the clay particles. The other is the pozzolanic reaction for the long-term increase of shear strength. For the former, the calcium ion exchange results in the flocculation of clay

particles and the formation of large particles (Sherwood er al., 1993; Broderick et al., 1990; Rogers et al., 1996; Leroueil et al., 1996; Nalbantoglu and Tuncer, 2001; Rajasekaran and Narasimha Rao, 2002). Hence, the lime treated soft clayey soil has a grainy, crumbly or blocky structure which is more porous and laminated as in Figure 2.35 (Kavak and Tuyluce, 2012). For the later, the pozzolanic reaction forms calcium silicate hydrate, calcium aluminate hydrate, and calcium alumino silicate hydrate gels to bond clay particles together and result in a long-term increase in the shear strength of soil (Mitchell et al., 1986; Croft, 1964; Ingles et al., 1972; Bell, 1996; Little, 1996; James et al., 2008).

Due to the porous and laminated soil structure, the permeability of lime treated soil can increase by several times as reported by many researchers (Broms, 1999; Brandl, 1981; Rajasekaran and Narasimha Rao, 2002; Alhassan, 2008). The permeability of lime treated soil depends on the lime concentration and the curing period. After a certain lime concentration, the permeability of lime treated soil decreases due to the formation of cementitious compounds among the soil particles and the blocking of flow channels (Onitsuka et al., 2001; Milburn and Parsons, 2004; Alhassan, 2008; Quang and Chai, 2015)

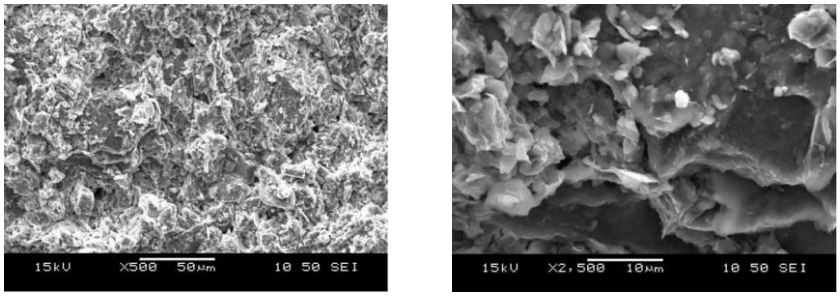

(a) Lime treated clay (b) Original marine clay

Figure 2.35 SEM of lime treated soil (after Kavak and Tuyluce, 2012)

2.5.2.2 Applications of lime treatment

The lime treatment has been applied in stabilisation of embankment, slope, column, foundation, excavated and dredged material (Hansbo and Torstensson, 1978; Endo, 1976; Broms, 1983, 1984b; Holm, 1986; Axelsson and Larsson, 1994; Edstam, 1996). The good performance was obtained in these projects due to the high shear strength of lime treated clay. The combination of vacuum preloading and lime treatment was also

applied in the land reclamation of soft dredged marine clay (Salehi and Sivakugan, 2009; Zhang et al., 2015; Wang et al., 2017). Due to the increase of permeability, the vacuum preloading of lime treated soil was more efficient. the optimum lime content is 2%. And the use of lime reduced the clogging of PVDs

2.6 Numerical Analysis

2.6.1 Finite differential method (FDM)

The FDM method has been used to predict the consolidation behavior of soil by many researchers as the high-quality computer doesn't require. This method has the advantage that any pattern of initial excess pore water pressure can be adopted, and it is possible to consider problems in which the load is applied gradually over a period of time. The errors associated with the method are negligible and the solution is easily programmed for the computer (Craig, 2004). This method is based on a depth–time grid as shown in Figure 2.36. The non-linear soil consolidation behavior can be simulated using FDM method in one-dimension or two-dimension condition by using the non-linear compression and permeability properties. To simplify the calculation, the plan strain and axisymmetric model were applied.

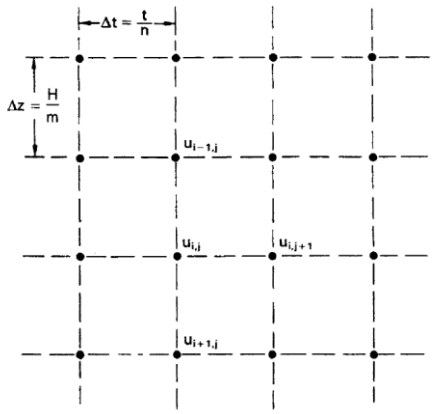

Figure 2.36 The depth-time grid of 2D calculation model (after Craig, 2004)

The rate of excess pore pressure to time is approximated using the first forward difference equation and the second partial derivatives of excess pore pressure in vertical and horizontal directions are approximated using the second central difference equation (Mitchell and Griffiths, 1980).

2.6.2 Finite element analysis (FEA)

The finite element simulation has been conducted by many researchers in either 2D model (Small and Zhang, 1991) or 3D model. The non-linear consolidation behaviour is usually adopted by inputting the non-linear compression and permeability parameters and using non-linear geometry. To consider the change of pore water pressure and effective stress, the modified cam-clay was applied. For the in-situ soil, the different permeability in horizontal and vertical direction are more reasonable for the simulation of consolidation process. The permeability of smear zone was considered in some models.

To simulate the consolidation using PVD, the PVD is considered as sand well or negative excess pore pressure boundary. In land reclamation, the detailed simulation of PVDs is difficult. A PVD element is developed by Peng and Liu (2005). For 2D model, to simulate the consolidation using PVD, the rows of drains are simplified as drainage wall as shown in Figure 2.37(a) and the simplified permeability under plane strain condition is used (Indraratna et al., 1997; 2005; 2005b).

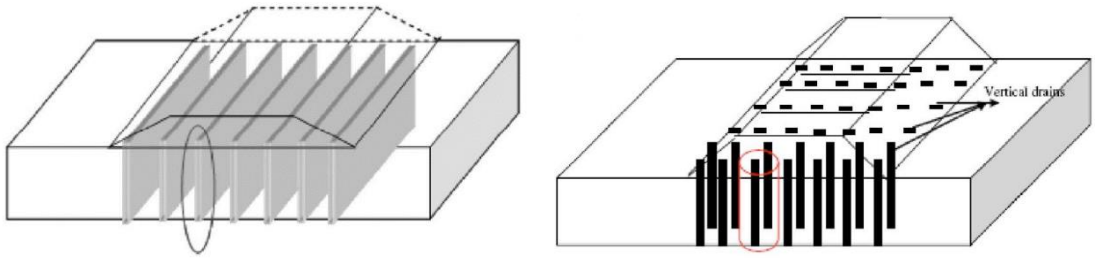

(a) 2D model (b) 3D model

Figure 2.37 Simulation model in 2D and 3D (after Indraratna et al., 2005)

2.7 Containment dike

As land reclamation is usually carried out in the onshore area, a containment dike is required to set the boundary for land reclamation. Several types of containment dikes have been used in the past which can be divided into three categories, earth-fill dike, geosynthetic dike and prefabricated concrete/steel dike. (Leung et al., 2006; Chu et al., 2009). When the seabed soil is also very soft, soil improvement should be conducted for the seabed soil too. Some soil improvement techniques that have been adopted to improve the seabed soil include soil replacement, stone columns, sand compaction piles,

deep soil mixing, and underwater consolidation. Different types of containment dikes and soil improvement methods are reviewed as follows.

2.7.1 Earth-fill dike

The common type of earth-fill dike is the sand bund, which has been applied in many land reclamation projects in Singapore in the past (Chu et al., 2009b). A schematic cross-section of a sand bund is shown in Figure 2.38. In relatively shallow water, sand bunds are easier and more economical to be constructed. In deep water, too much sand is required to build a sand bund and this option will no longer be feasible for sand scarce Singapore.

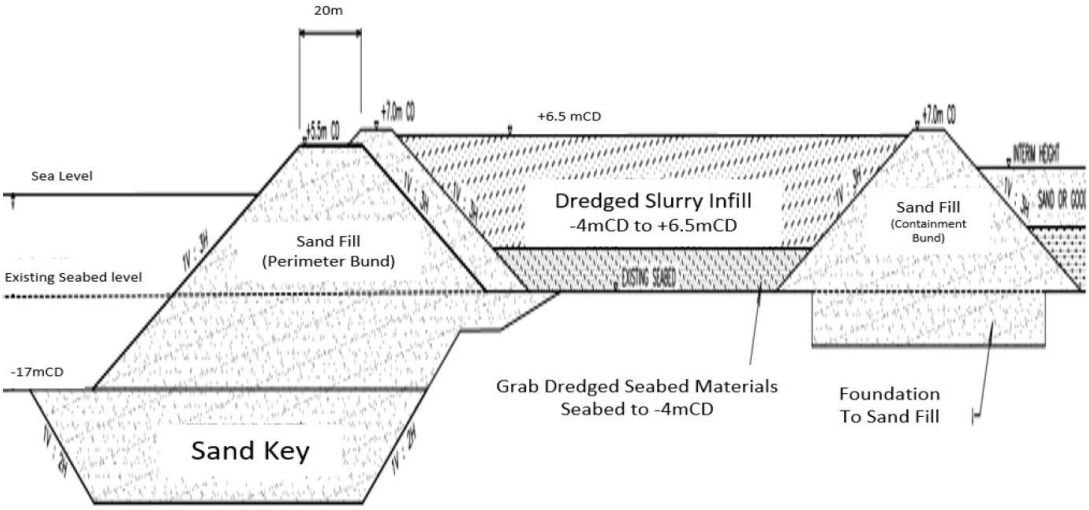

Figure 2.38 Schematic cross-section of sand dike in offshore land reclamation (after Lam, 2018)

Another form of earth-fill dike is the so-called PM-clay dike used in Japan (Taku, 2013). The PM-clay dike is constructed using solidified disposed soil by mixing and stirring solidification material such as cement and soft dredged cohesive soil as back-filling material. The construction method of the PM-clay dike is shown in Figure 2.39. In this method, the construction period can be shortened. The schematic cross-section of PM-clay dike is shown in Figure 2.40. However, this type of dike may also be only suitable for projects in relatively shallow water.

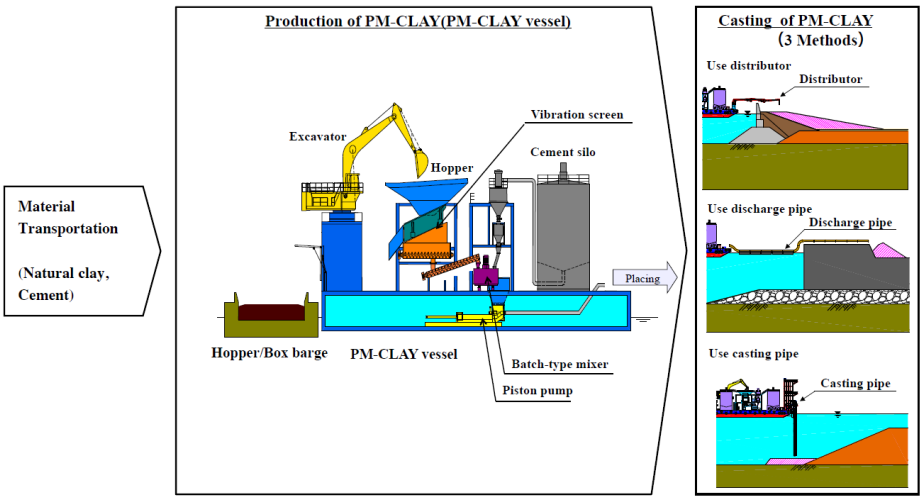

Figure 2.39 Construction method of PM-clay dike (after Take, 2013)

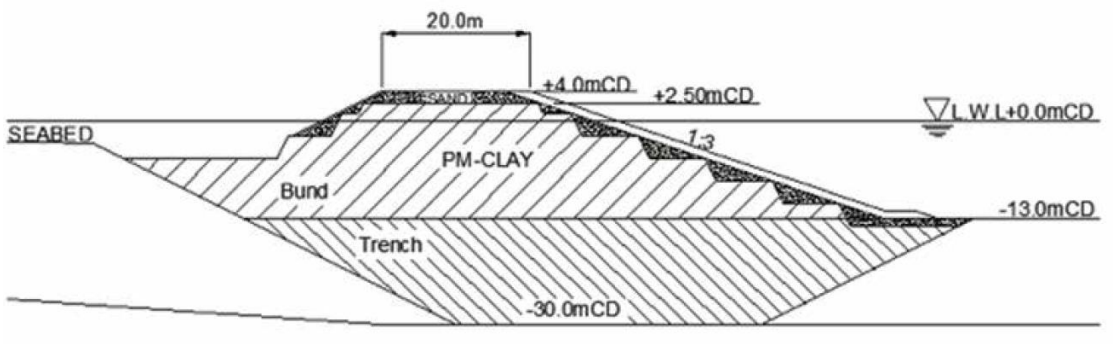

Figure 2.40 Schematic cross-section of PM-clay dike (after Taku, 2013)

2.7.2 Prefabricated concrete/steel dike

The containment bund can also be constructed using prefabricated concrete/steel caisson such as those showing in Figure 2.4 (Chu et al., 2012). As shown in Figure 2.4a, the segments are towed to the required location and sunk by filling seawater or soil. This construction method is suitable for quick installation of containment structures.

One example is the use of semi-circular prefabricated caissons for a breakwater in Tianjin, China (Yan et al., 2009; Yan and Chu, 2012). Seawalls made of steel cylinders were applied for land reclamation for the artificial islands in the Hong Kong-Zhuhai-Macau Bridge project (Yeung, 2016). The construction of the artificial island is show in Figure 2.42.

For the structures shown in Figure 2.41 (a) and (b), the foundation soil needs to be improved first. Suction caissons can be used as a type of foundation to support the super structures used for seawalls. One example is shown in Figure 2.41 (d). The suction caisson foundation consists of 4 identical concrete suction caissons connected together by a top slab and vertical webs. Part of the reasons for using 4 suction caissons is to facilitate installation. The use of 4 suction caissons as a group enables the vertical settlement of the caissons to be uniform to avoid titling by controlling the suction applied to each cylinder. The seawall comprises a series of single cylinders and vertical webs sitting on top of the suction caisson foundation. The assembly is towed to the required position and penetrated into the required depth under the hydrostatic pressure outside and the suction inside the chambers of caissons which are sealed at the bottom by the seabed clay.

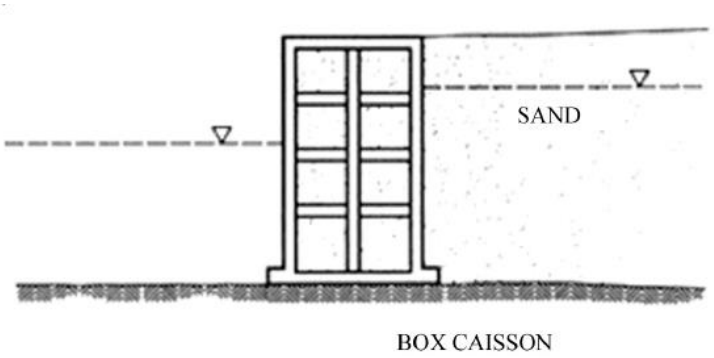

(a) box caisson (after Bo and Choa 2004)

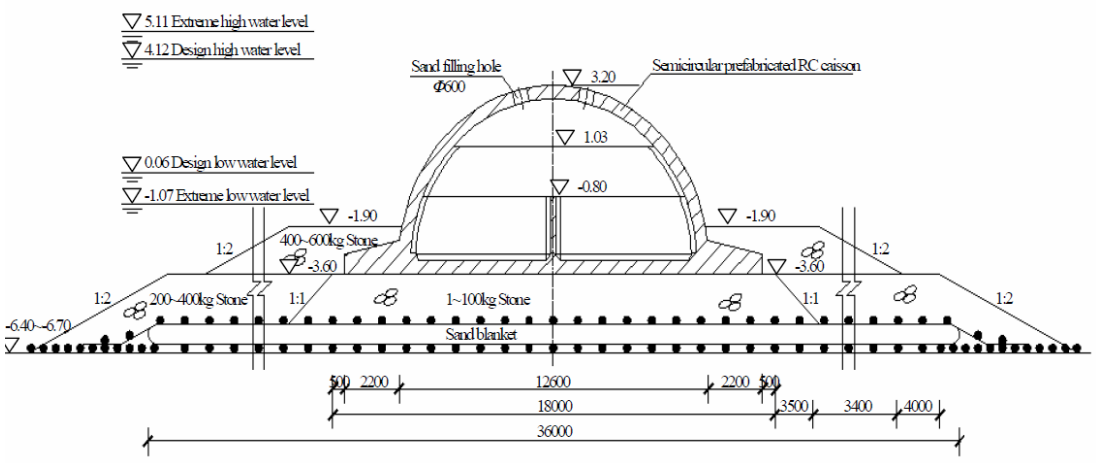

(b) semi-circular concrete caisson (after Yan et al., 2009)

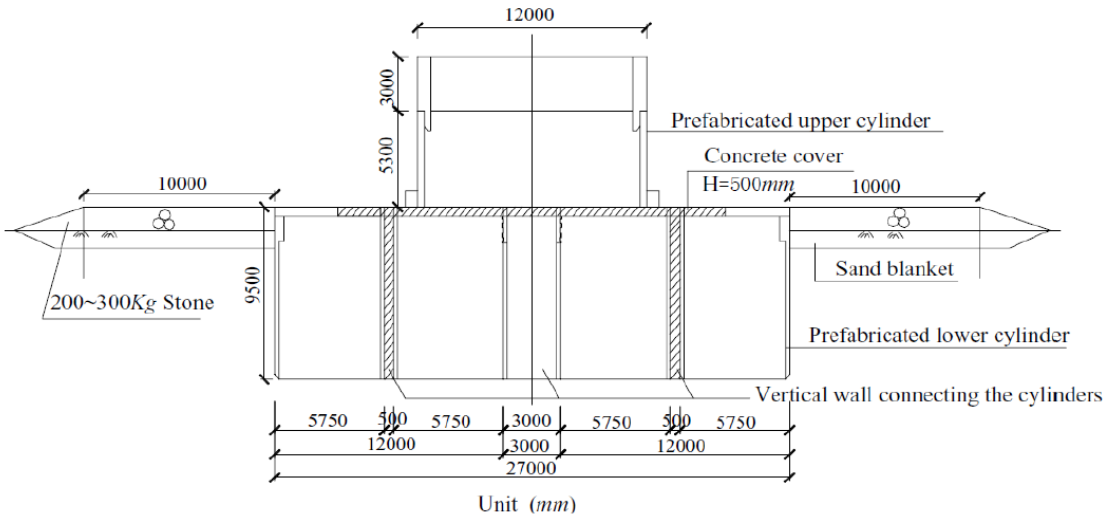

(d) concrete caissons (after Yan and Chu, 2012)

Figure 2.41 Few types of prefabricated concrete/steel dike

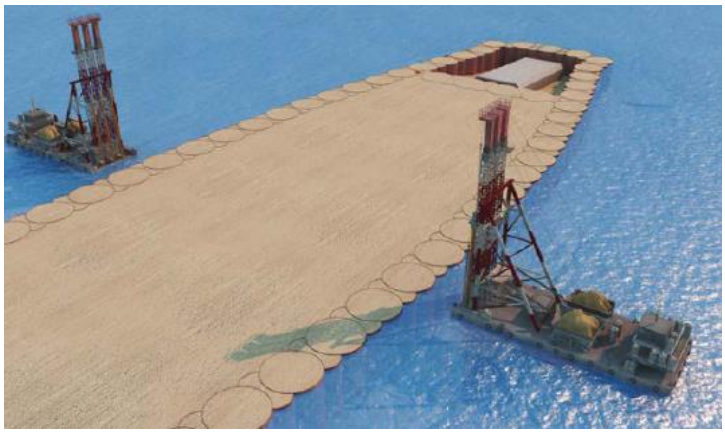

Figure 2.42 Construction of steel cylinder dike (after Yeung, 2016)

2.7.3 Geosythetic dike

The Geosythetic dike has been applied in many offshore projects since 1990s (Silvester and Hsu, 1993; Jongeling and Rövekamp, 1999). The common forms are the geo-tube, geo-bags, geo-container and the rubber bag filled with sandy soil or soft clay (Kazimierowicz, 1994; Miki et al., 1996; Leshchinsky et al., 1996; Pilarczyk, 2000; Cantre, 2002; Moo-Young and Tucker, 2002; Restall et al., 2002; Kim et al., 2004; Koerner and Koerner, 2006; Alvarez et al., 2007; Shin and Oh, 2007; Recio and Oumeraci, 2007). To form a geosynthetic dike, the geo-tubes or geotextile bags are placed layer by layer as shown in Figure 2.43.

Figure 2.43 A picture showing the formation of a dike using clay slurry filled geo-tubes (after Yan and Chu, 2010)

Either sandy soil or soft clay can be used to pump into the geo-tubes or bags. For near shore or offshore projects, a suction dredger can be used to pump sand from the seabed or a sand pit directly into the geo tubes or bags. (Chu and Yan, 2007; Guo et al., 2009; Yan and Chu, 2010). For soft clay, it has to be in a slurry state in order to be pumped into the geo-tube or bag. Then the slurry has to be consolidated in a permeable geo-tube or bag under an ambient pressure. Soft clay filled geo-tubes or bags was used as the containment dike for a land reclamation project in Tianjin, China. The schematic cross-section of geo-tubes or bags formed dike is shown in Figure 2.44.

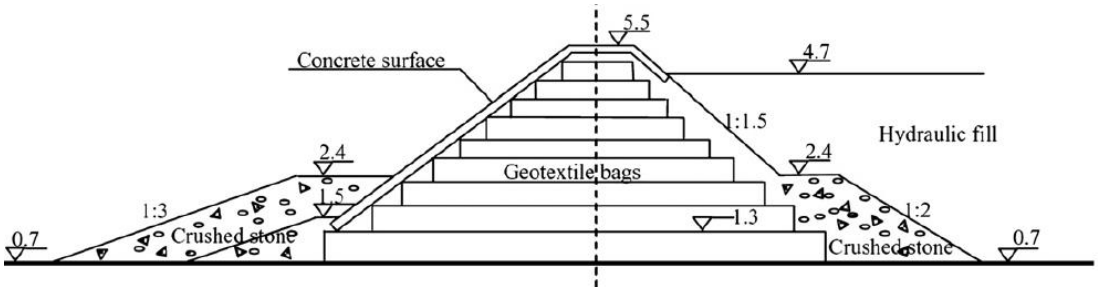

Figure 2.44 Schematic cross-section of geo-tubes or bags dike (after Chu and Yan, 2007)

2.8 Conclusion

In this Chapter, some research background and progresses related to land reclamation and soil improvement were reviewed. Existing methods on the formation of working platforms, preloading methods using fill surcharge or vacuum pressure together with

PVDs, electro-osmosis-induced consolidation, and construction of containment structures for land reclamation were presented and reviewed.

When high-water content soft clay is used as fill material, there are still technical challenges to be studied. How to create a working platform is one of them. Few methods to create the platform were reviewed. As land reclamation has to be carried out in deep water gradually, methods on the construction of containment bund were also reviewed.

CHAPTER 3 DESIGN AND CONSTRUCTION OF WORKING PLATFORM USING MODIFIED BROMS' METHOD

3.1 Introduction

One difficulty to improve the properties of very soft land reclamation fill is that its top surface is too soft for machines to go on top to install PVDs. One of the solutions for this problem is the use of dewatering and geotextile (Chu et al., 2012; Sun et al., 2017). In this Chapter, the use of geotextile was proposed to form the working platform over soft clay ground. This method is referred to as Broms' method as it was proposed by Broms (1987). However, there are difficulties in using Broms' method when the fill material is too soft (Toh et al., 1994; Lam, 2018). To overcome the uncertainties in design and construction of Broms method, a modified Broms' method was proposed to use geotextile tubes to form berms for better construction control. A new analytical solution was also developed to analyse the stabilization of sand tubes and the working platform using the modified Broms' method. A simplified method was also established to calculate the dimension of geotextile tube and the contact length.

3.2 Modified Broms' method

One construction difficulty in applying the Broms' method is that it is hard to form the sand berms and keep them in shape when the fill materials are too soft such as clay slurry. In the modified Broms' method, geotextile tubes are used to confine the sand forming the berms. Such an approach allows better control during berms placement and the confining effect of the geotextile tubes keeps the sand berms in shape without collapsing even when the underlying geotextile deforms. As illustrated in Figure 3.1, after the geotextile sheet is placed in the same way as in the Broms' method, geotextile tubes are placed on top (Figure 3.1(a)) and sand is pumped in the tubes to form the geotextile-tube confined sand berms (or sand tubes) as shown in Figure 3.1(b) and Figure 3.1(c). To form a working platform, sand fill in thin layers are then placed layer by layer in between the tubes and on top of the sand tubes as shown in Figure 3.1(d).

It should be pointed out that the cross-sections of the geotextile and sand berms/tubes are changing all the time irrespective of whether the Broms' or the modified Broms' method is adopted. Any analysis can only be carried out for the most critical condition, that is, when the full loads from the sand berms or tubes are applied. During the placement of sand in between the sand berms/tubes, the geotextile was slack. Then the tensile force and strain were reduced. Therefore, the condition illustrated in Figure 3.1c is considered as the most critical state. As the soft soil fill contributes very little to bearing capacity, the tensile strength mobilized from the geotextile deformation is the key factor that controls the bearing pressure of the system.

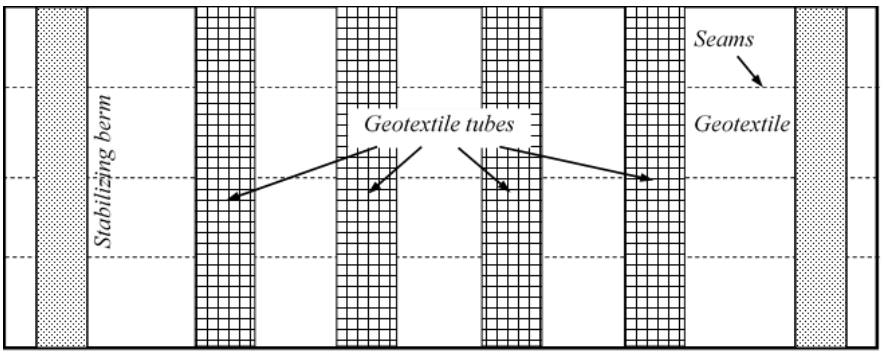

(a) Placement of geotextile tubes

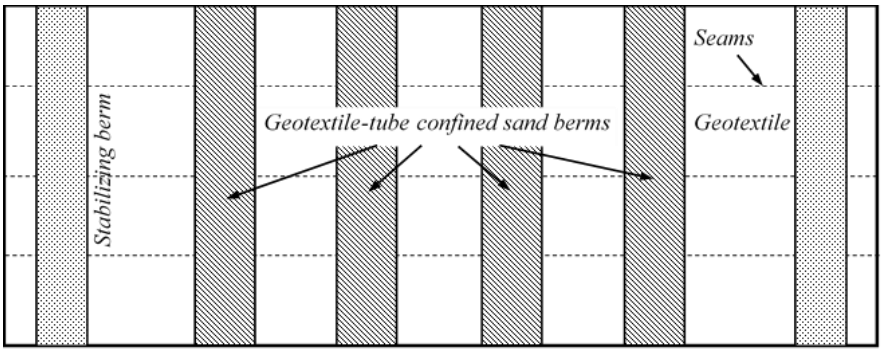

(b) Pumping sand into geotextile tubes

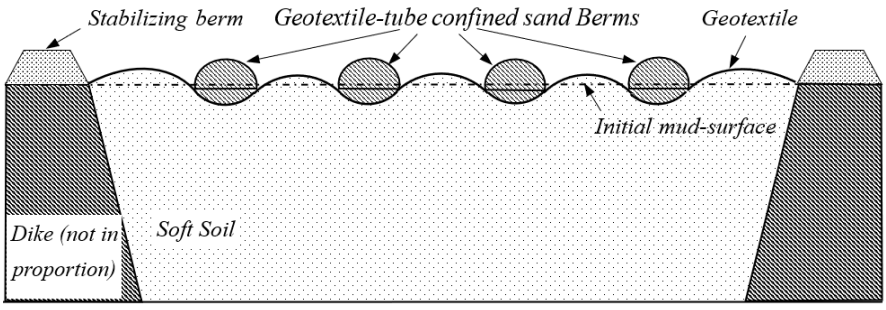

(c) Elevation view after the placement of geotextile-tube confined sand berms (sand tubes)

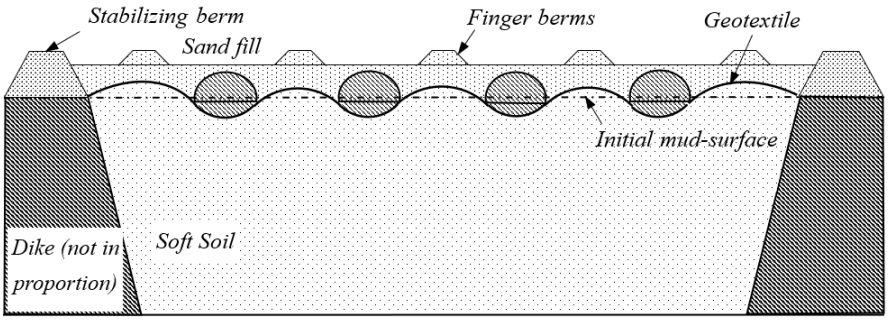

(d) Placement of sand fill

Figure 3.1 Fill placement over soft soil using modified Broms' method

3.3 Theoretical and numerical analyses for geotextile sheet

3.3.1 Theoretical analysis for geotextile sheet

An analytical solution was developed based on either force equilibrium or membrane effect for the simplified cross-section of geotextile supported sand berms/tubes on soft soil as shown in Figure 3.2a. Compared with the dimension of reclamation area, the dimension of the sand berms/tubes was small. Hence the sand berms/tubes with the same contact width should be placed on the geotextile at a specific and periodic spacing in the modified Broms' method or the Broms' method. Then the cross-section of geotextile and sand berms/tubes could be considered as symmetric. So only half of the cross-section was used as the analytical model as shown in Figure 3.2(b) due to symmetry and the part of sand berms/tubes above the datum surface is simplified as uniform pressure.

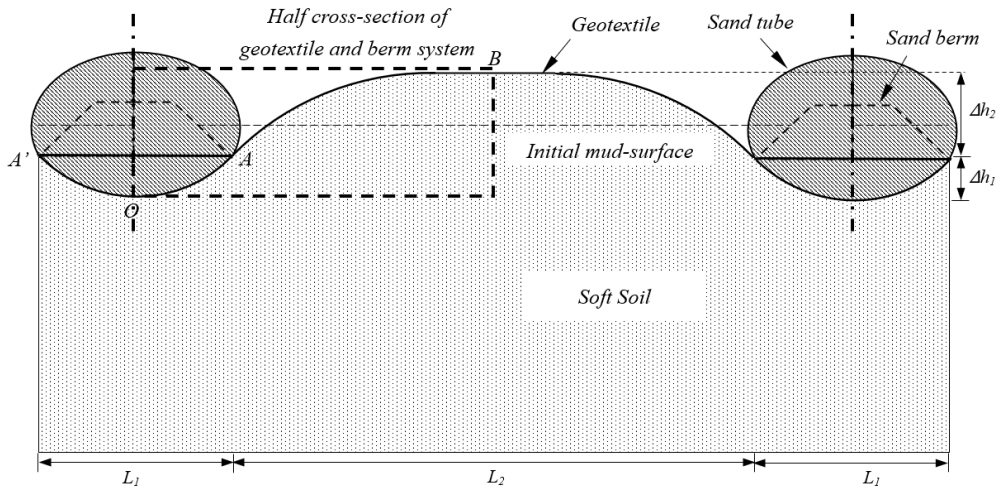

(a) Idealised elevation view for Broms's method with sand berms and modified Broms' method with sand tubes and the deformed geotextile and soft soil

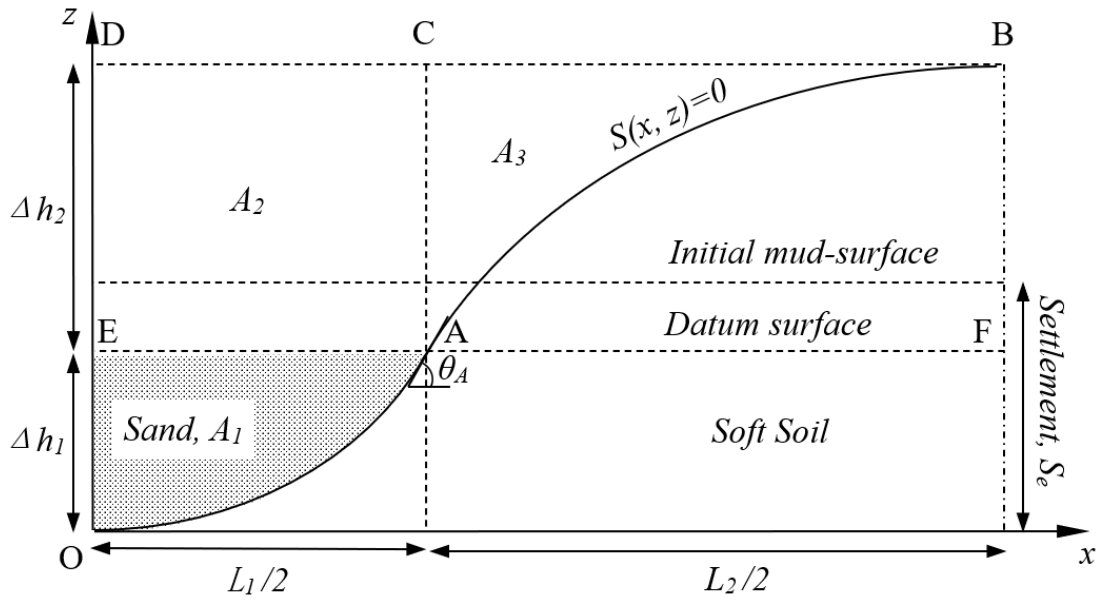

(b) Geometry and symbols used for the selected section as shown in Fig. 3.2(a)

Figure 3.2 A section of the cross-section of the geotextile and berms/tubes system used for the theoretical analysis (L_1: contact width of sand tube; L_2: spacing of sand tubes)

3.3.1.1 Basic assumptions

The following assumptions are adopted in this solution:

(1) The geotextile and sand berms/tubes are sufficiently long to be assumed at a plane strain condition.
(2) The profile of the geotextile in the soil (Section OA in Figure 3.2b) can be fitted into a parabolic curve. This assumption has also been used by Giroud and Noirey (1981), Raumann (1982) and Pham (2020).
(3) The soft soil is under an undrained condition.
(4) The density of soft soil and sand is uniform.
(5) The weight of geotextile is ignored.
(6) The cross-section at the time when all the sand berms/tubes have been placed is considered the most critical state. At this time, it is assumed that the dissipation of excess pore pressure in soft soil through the geotextile as well as consolidation of the soft soil have not taken place.
(7) The geotextile-tube confined sand berm is considered only as a load acting on geotextile supported soft soil.

3.3.1.2 Theoretical derivation

The cross-section shown in Figure 3.2(b) is used for analysis. The coordinates are set-up with x in the horizontal direction and z in the vertical direction. The origin is taken as the centre of the geotextile underneath the sand berms/tubes. The contact width and the penetrated depth of sand berms/tubes below the datum surface (at the line going through point A), are denoted as L_1 and Δh_1, respectively. The height of the heaved soil between the sand berms/tubes is denoted as Δh_2 above the datum surface and the spacing between the sand berms/tubes is L_2. The distance between the initial mud-surface and the x axis is the settlement of sand berms/tubes, S_e. The areas of *OAE*, *ACDE* and *ABC* are denoted as A_1, A_2 and A_3, respectively. The angle between the tangent line and x axis at point A is θ_A.

3.3.1.3 Boundary condition

For section OB of geotextile in Figure 3.2(b), the following geometrical boundary conditions can be adopted:

(1) $\theta = 0$ at point O ($x = 0$, $z = 0$) and;

(2) $\theta = \theta_A$ at point A ($x = L_1/2$, $z = \Delta h_1$) and;

(3) $\theta = 0$ at point B [$x = (L_1+L_2)/2$, $z = (\Delta h_1+\Delta h_2)$] and;

(4) $(L_1+L_2)/2 = s_{OA}/(1+\varepsilon_{avg}) + s_{AB}/(1+\varepsilon_1)$.

where, s_{OA} is the length of section OA of geotextile; ε_{avg} is the average tensile strain of section OA of geotextile; s_{AB} is the length of section AB of geotextile; ε_1 is tensile strain of section AB of geotextile. After the placement of sand berms/tubes, the geotextile is stretched from initial length as expressed by boundary condition (4).

3.3.1.4 Parabolic section of deformed geotextile

Based on Assumption (2) and Boundary conditions (1) and (2), the parabolic curve as expressed by Eq. (3.1) is chosen to fit the section OA of geotextile in Figure 3.2(b).

$$z = ax^2 \tag{3.1}$$

where, a is equal to $4\Delta h_1/L_1^2$. So θ_A (rad) is equal to $ArcTan(4\Delta h_1/L_1)$. And the length of section OA of geotextile can be expressed by Eq. (3.2).

$$s_{OA} = \frac{L_1\sqrt{1+a^2L_1^2}}{4} + \frac{ArcSinh(aL_1)}{4a} \tag{3.2}$$

3.3.1.5 Force equilibrium of geotextile and berm system

The free body diagram for the cross-section shown in Figure 3.2(b) is given in Figure 3.3. P_u is bearing pressure; T_1 and T_0 is tensile force; γ_s and γ_l is unit weight; u_0 is excess pore pressure; k_0 is the coefficient of lateral earth pressure at rest.

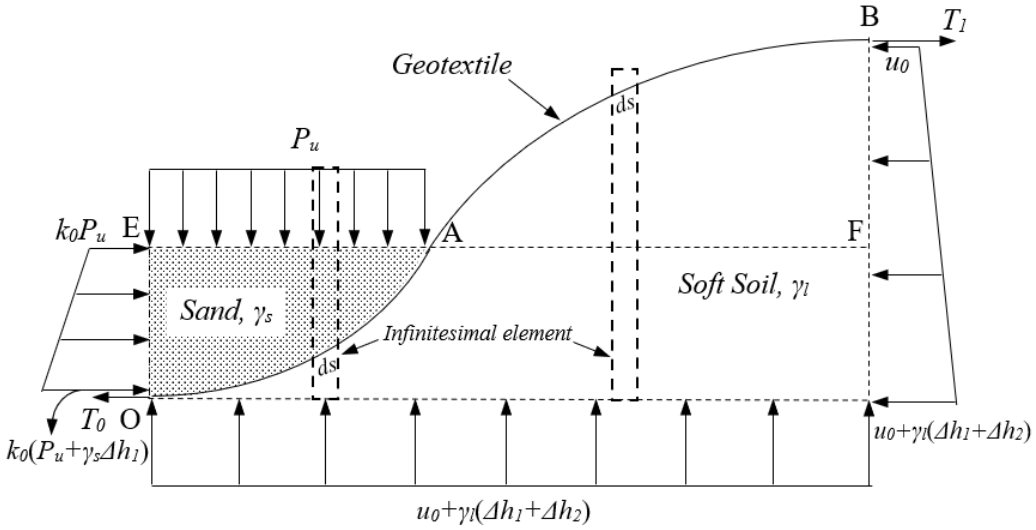

Figure 3.3 Free body diagram for the selected section

The strain-stress relationship of the geotextile is assumed to be linearly elastic-perfectly plastic:

$$T = E\varepsilon \tag{3.3}$$

where, T (kN/m) is tensile force; ε is tensile strain; E (kN/m) is tensile stiffness of geotextile. The rupture of geotextile is at the ultimate tensile strain, ε_u.

The unit weight of soft soil and sand are constant and denoted as γ_l and γ_s, respectively. The bearing pressure, P_u, above line AE in Figure 3.3 is assumed to be uniform. Due to the symmetry, there is no lateral movement for the sand berms/tubes. Hence the lateral earth pressure coefficient of sand is denoted as k_0. Then the lateral earth pressure at rest is k_0P_u at point E and increases linearly with depth. The tensile force and strain are T_0 and ε_0 at point O, and T_1 and ε_1 at point B.

The excess pore pressure u_0 at top of geotextile is built up gradually as the increasing of the weight of sand berms/tubes. The lateral earth pressure acting on the right side of the

free body increases linearly with depth. Because of the undrained condition, the coefficient of lateral earth pressure of soft soil can be set as 1.0. Therefore the lateral earth pressure acting on the geotextile from soft soil is same with that on right side, which depends on the elevation. Then the vertical earth pressure acting on the bottom is $u_0+\gamma_l(\Delta h_1+\Delta h_2)$. Using the free-body diagram in Figure 3.3, the force equilibriums in the vertical and horizontal directions yield the following two equations:

$$P_u \frac{L_1}{2} = u_0 \frac{L_1+L_2}{2} + \gamma_l(A_1+A_2+A_3) - \gamma_s A_1 \tag{3.4}$$

$$T_1 - T_0 = u_0(\Delta h_1+\Delta h_2) + \frac{1}{2}\gamma_l(\Delta h_1+\Delta h_2)^2 - k_0 P_u \Delta h_1 - \frac{1}{2}k_0\gamma_s \Delta h_1^2 \tag{3.5}$$

3.3.1.6 Membrane effect

For an infinitesimal element *ds* around an arbitrary point *S*(*x*, *z*) shown in Figure 3.3, the free body diagram can also be established as shown in either Figure 3.4(a) or Figure 3.4(c), depending on the location. The infinitesimal small curve *ds* can be treated as a straight line. The angle between the tangential direction at point *S*(*x*, *z*) and the *x* axis is denoted as θ. Then two geometrical equations relating the angle between the tangential direction along the cross-section and the *x* and *z* coordinates can be written as Equations (3.6) and (3.7).

$$\frac{dx}{ds} = cos\theta \tag{3.6}$$

$$\frac{dz}{ds} = sin\theta \tag{3.7}$$

Using the free-body diagram of the infinitesimal element as shown in Figure 3.4(a), the force equilibriums along the tangential and normal directions give:

$$\frac{dT}{ds} = f \tag{3.8}$$

$$\frac{d\theta}{ds} = \frac{N_s - N_l}{T} \tag{3.9}$$

where, *f* is the tangential pressure from sand berm/tubes acting on the geotextile at point *S*(*x*, *z*); N_s is the normal pressure from sand berms/tubes acting at point *S*(*x*, *z*); N_l is normal pressure from soft soil acting at point *S*(*x*, *z*). Because of the balanced geotextile and sand berms/tubes system, the change of tensile force is only related to the tangential force. Then the tensile force *T* in the geotextile changes with *z*.

The vertical and lateral earth pressure from sand berms/tubes acting at point $S(x, z)$ are $[P_u + \gamma_s(\Delta h_1\text{-}z)]$ and $k_0[P_u + \gamma_s(\Delta h_1\text{-}z)]$, respectively. Then based on the free-body diagram in Figure 3.4(b), the normal pressure, N_s, and tangential pressure, f, from sand berms/tubes acting at point $S(x, z)$ can be expressed by Eq. (3.10) and (3.11).

$$N_s = \left[P_u+\gamma_s(\Delta h_1\text{-}z)\right](\cos^2\theta+k_0\sin^2\theta) \tag{3.10}$$

$$f = (1\text{-}k_0)[P_u + \gamma_s(\Delta h_1\text{-}z)]\cos\theta\sin\theta \tag{3.11}$$

When point $S(x, z)$ is along section AB of geotextile in Figure 3.3, only the normal pressure N_l from the soft soil is acting on the geotextile.

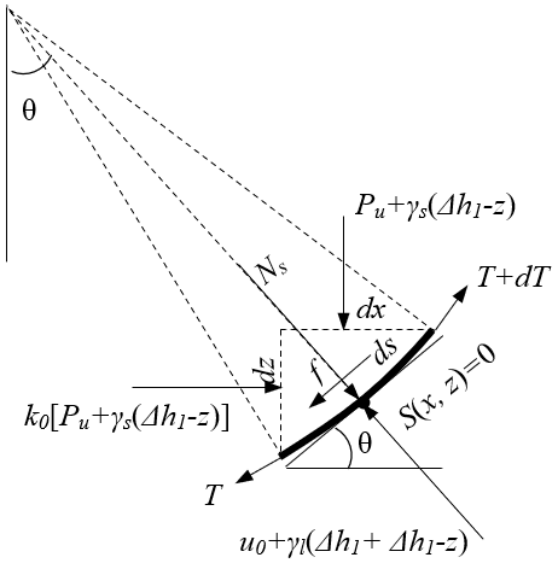

(a) Section OA of geotextile

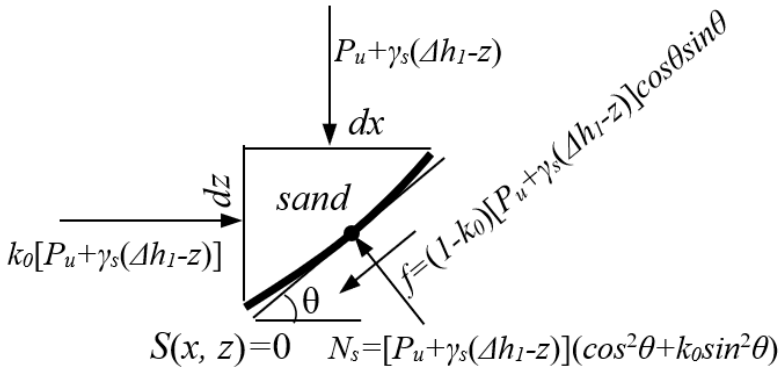

(b) Sand right next to section OA of geotextile

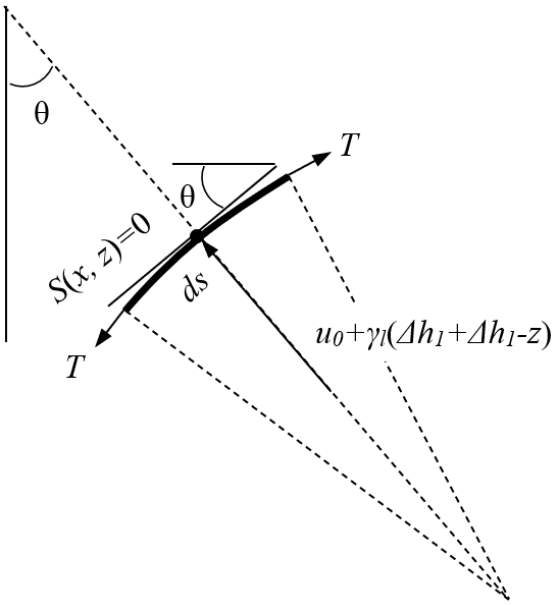

(c) Section AB of geotextile

Figure 3.4 Free body diagrams for an infinitesimal element along the geotextile

Then the tensile force along section AB of the geotextile is constant. Using the free-body diagram shown in Figure 3.4(c), the force equilibriums along the normal and the tangential directions yield:

$$\frac{dT}{ds} = 0 \tag{3.12}$$

$$\frac{d\theta}{ds} = -\frac{N_l}{T} \tag{3.13}$$

where

$$N_l = u_0 + \gamma_l(\Delta h_1 + \Delta h_2 - z) \tag{3.14}$$

By integrating Eq. (3.8) for section OA of the geotextile, the increment of tensile force, ΔT, between point O and point A and the tensile strain, ε_x, along the section OA of geotextile can be obtained as expressed by Eq. (3.15) and (3.16), respectively.

$$\Delta T = \frac{(1-k_0)}{2a}(P_u + \gamma_s \Delta h_1 + \frac{\gamma_s}{6a})(\sqrt{1+4a^2L_1^2}-1) - \frac{(1-k_0)\gamma_s L_1^2}{24}\sqrt{1+4a^2L_1^2} \tag{3.15}$$

$$\varepsilon_x = \varepsilon_1 - \frac{(1-k_0)}{2aE}(P_u + \gamma_s \Delta h_1 + \frac{\gamma_s}{6a})(\sqrt{1+4a^2x^2}-1) + \frac{(1-k_0)\gamma_s}{6E}x^2\sqrt{1+4a^2x^2} \tag{3.16}$$

The increment of tensile force as expressed by Eq. (3.15) should be equal to the difference of tensile force as expressed by Eq. (3.5). Then the average tensile strain for section OA of geotextile can be obtained by integrating Eq. (3.16) over the half contact width of sand berms/tubes as expressed by Eq. (3.17).

$$\varepsilon_{avg} = \varepsilon_1 - \frac{(1-k_0)}{2a}(P_u+\gamma_s\Delta h_1+\frac{\gamma_s}{6a})[\frac{\sqrt{1+a^2L_1^2}}{2}+\frac{ArcSinh(aL_1)}{2aL_1}-1]+\frac{(1-k_0)\gamma_s}{384a^2E}[2(1+2a^2L_1^2)\sqrt{1+a^2L_1^2}-\frac{2ArcSinh(aL_1)}{L_1}] \quad (3.17)$$

By integrating Eq. (3.11) for section AB of the geotextile, the vertical force equilibrium for area ABF can be obtained as expressed by Eq. (3.18).

$$E\varepsilon_1 sin\theta_A = \frac{u_0 L_2}{2} + \gamma_l A_3 \quad (3.18)$$

Because of the balanced whole system, the horizontal force equilibrium for area ABF is expressed by Eq. (3.19).

$$E\varepsilon_1(1-cos\theta_A) = u_0\Delta h_2 + \frac{1}{2}\gamma_l\Delta h_2^2 \quad (3.19)$$

3.3.1.7 Solution

By transforming the Eq. (3.18) and Eq. (3.19), the formulas of A_3 and u_0 was determined. By substituting the formulas of A_3 and u_0 into Eq. (3.4), Eq. (3.5) and Eq. (3.13) and combining the Eq. (3.2), Eq. (3.4), Eq. (3.5), Eq. (3.13), Eq. (3.15), Eq. (3.17) and Boundary condition (4), we can get four equations which are the function of P_u, Δh_1, Δh_2 and ε_1. By solving the four equations, the profile of deformed geotextile, the bearing pressure and the tensile strain in the geotextile can be obtained. As the tensile force increases from point O to A and keeps constant along section AB of geotextile, then the tensile strain, ε_1, at point B is the maximum tensile strain, ε_{max}.

Based on assumption (3), the volume strain of soft soil is zero. Then the areas of OAHIE and BHG in Figure 3.5 are same as shown in Eq. (3.20).

$$A_1+(S_e-\Delta h_1)\frac{L_1}{2}+A_3-A_z-(\Delta h_1+\Delta h_1-S_e)(\frac{L_2}{2}-l)=(\Delta h_1+\Delta h_1-S_e)l-A_z \quad (3.20)$$

where, A_z is the area of BJH; S_e is the settlement; l is the length of distance BJ. In Eq. (3.20), the left part is the area of OHI and the right part is the area of BHG. By simplifying the Eq. (3.20), we can obtain the settlement S_e as shown in Eq. (3.21).

$$S_e = \Delta h_1 + \Delta h_2 - \frac{2(A_1 + A_3) + \Delta h_2 L_1}{L_1 + L_2} \tag{3.21}$$

When the undrained shear strength is not zero, the total bearing pressure can be calculated by Eq. (3.22) (Broms, 1987; Espinoza, 2008).

$$P_{u\text{-}t} = P_u + 5.14 c_u + \frac{2}{3}\gamma_s \Delta h_1 \tag{3.22}$$

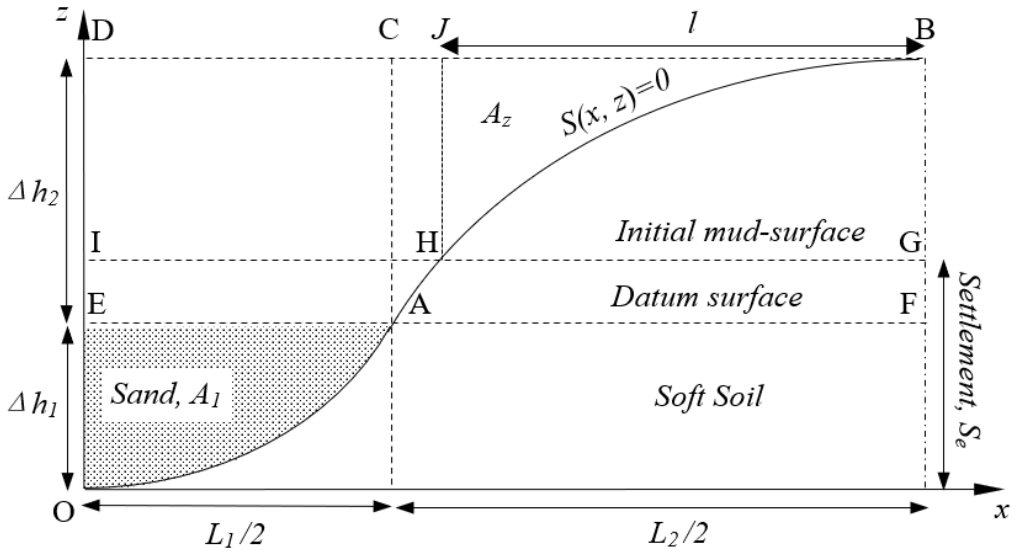

Figure 3.5 Geometry for the derivation of settlement S_e

3.3.1.8 Iteration method

As there is no closed-form solution for the four equations, the linear programming method was applied to obtain the optimum solution for the profile of deformed geotextile, the bearing pressure and the tensile strain in the geotextile.

The parameters related to the soil and geotextile properties were taken as inputs, such as the unit weight of soft soil and sand, γ_l and γ_s, the undrained shear strength of soft soil, c_u, the ultimate tensile strain, ε_u, the tensile stiffness of geotextile, E, and the lateral earth pressure coefficient at rest of sand, k_0. By minimizing the total error, T_{er}, for the iteration of Δh_2 and ε_{max} and using solver add-in on excel, the profile of deformed geotextile, the bearing pressure, P_u, the excess pore pressure at top of geotextile, u_0, and the maximum tensile strain, ε_{max}, were solved.

By setting the initial values of Δh_2 and ε_1 for the specific Δh_1, L_1 and L_2, the A_3, P_u, u_0, T_1-T_0, ΔT, ε_{avg} and s_{OA} were calculated by using Eqs. (3.2), (3.4), (3.5), (3.15), (3.17), (3.18) and (3.19). The profile and length s_{AB} of section AB of geotextile and the calculated $\theta_{A\text{-}C}$ and $\Delta h_{2\text{-}C}$ were computed using Eq. (3.13) and Boundary conditions (2) and (3) based on finite difference formula. The increment, Δx, for forward difference formula was set as 1 mm. So, based on the boundary conditions, the control conditions and total error, T_{er} were as following:

$$e_1 = ABS\left(\frac{T_1 - T_2 - \Delta T}{E}\right) \tag{3.23}$$

$$e_2 = ABS(\Delta h_2 - \Delta h_{2\text{-}C}) \tag{3.24}$$

$$e_3 = ABS(\theta_A - \theta_{A\text{-}C}) \tag{3.25}$$

$$e_4 = ABS\left[\frac{L_1 + L_2}{2} - \frac{s_{OA}}{1+\varepsilon_{avg}} - \frac{s_{AB}}{1+\varepsilon_1}\right] \tag{3.26}$$

$$T_{er} = e_1 + e_2 + e_3 + e_4 \tag{3.27}$$

3.3.2 Numerical analysis for geotextile sheet

Finite element analysis (FEA) was also carried out to verify the deformation of geotextile and soft soil under a plane strain condition in ABAQUS/Standard. The soil and geotextile properties are shown in Table 3.1 and Table 3.2. The Mohr-Coulomb model was used to simulate the soft soil under an undrained condition with c_u = 0.5 kPa, γ_l = 13.5 kN/m and Poisson ratio μ = 0.495. The undrained stiffness of soft soil, E_u, was taken as 300 c_u. The geotextile was modelled as a beam element. The linearly elastic-perfectly plastic model with E = 800 kN/m, ε_u = 6% and thickness t = 2 mm was applied (Guo et al., 2014). The cross-section of beam element was rectangular with 2 mm in thickness and one unit in width which was the same as that of soft soil in numerical model. The weight of geotextile and the friction between geotextile and soft soil were neglected in the analysis, which is same as the assumptions of the proposed solution. The penalty method was applied for the normal contact property between geotextile and soft soil. Due to symmetry, two symmetric units of the balanced geotextile and berms/tubes system were considered as shown in Figure 3.6. Using the basic assumption (7) (section 3.3), the vertical line load with contact width L_1 = 2 m acting on the

geotextile was considered as sand berms/tubes. The line load increased gradually until the FEA simulation was finished. The spacing, L_2, was set to 2 m, 6 m and 10 m as shown in Table 3.3. The normal displacement for lateral and bottom boundaries was set to zero.

Table 3.1 Soil properties for the proposed analytical method and FE Analyses

γ_l (kN/m^3)	c_u (kPa)	E_u (kPa)	Poisson's ratio μ	γ_s (kN/m^3)	Sand friction angle (°)
13.5	0.5	150	0.495	19.0	30

Table 3.2 Geotextile properties for the proposed analytical method and FE Analyses

Thickness, t (mm)	Tensile stiffness, E (kN/m)	Ultimate tensile stress (kPa)	Ultimate tensile strain, ε_u (%)
2	800	48	6

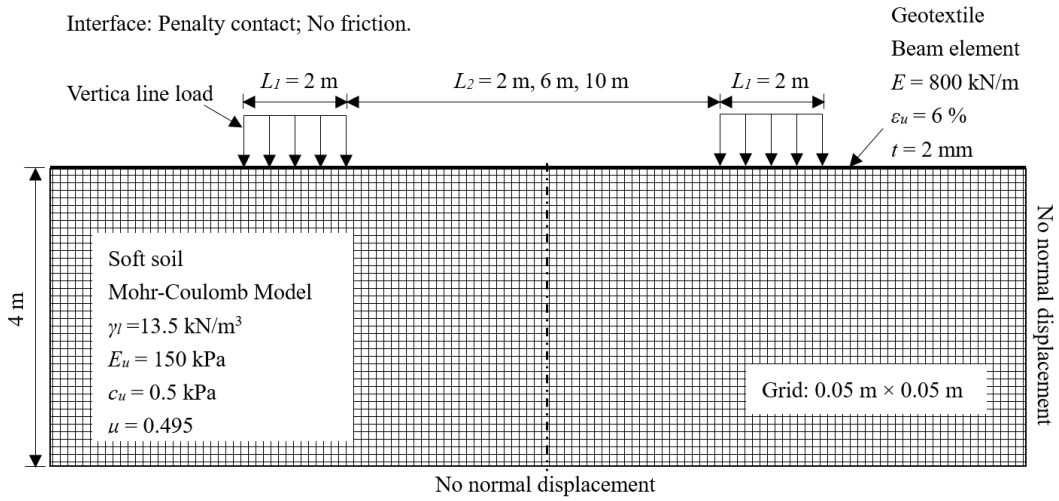

Figure 3.6 Numerical model for FE Analyses

Table 3.3 Contact widths and spacings of sand berms/tubes adopted in FE analyses

Model	Contact width, L_1 (m)	Spacing, L_2 (m)
1	2.0	2.0
2	2.0	6.0
3	2.0	10.0

3.3.3 Results and discussion

3.3.3.1 Comparison between the analytical solution and FEA

The profile of the deformed geotextile is shown in Figure 3.7 together with tensile strain values. For the selected section, the profiles of the deformed geotextile obtained from the FEA and the proposed solution are shown in Figure 3.8.

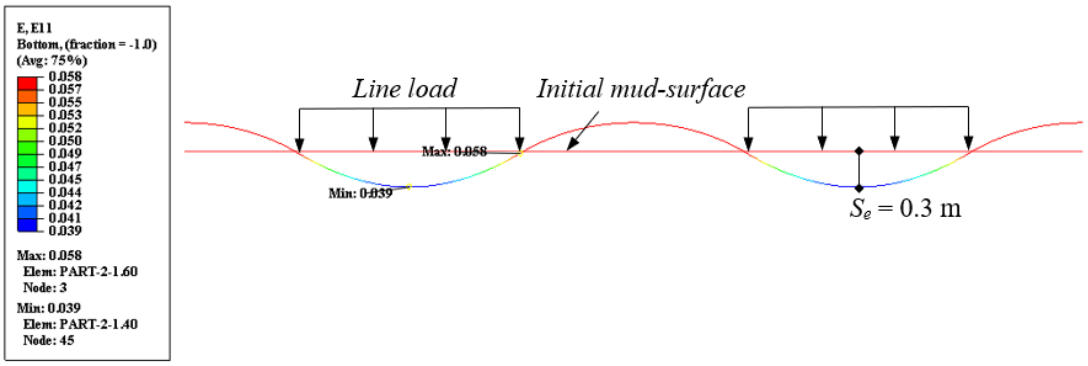

(a) Model 1: ε_{max} = 5.8 %

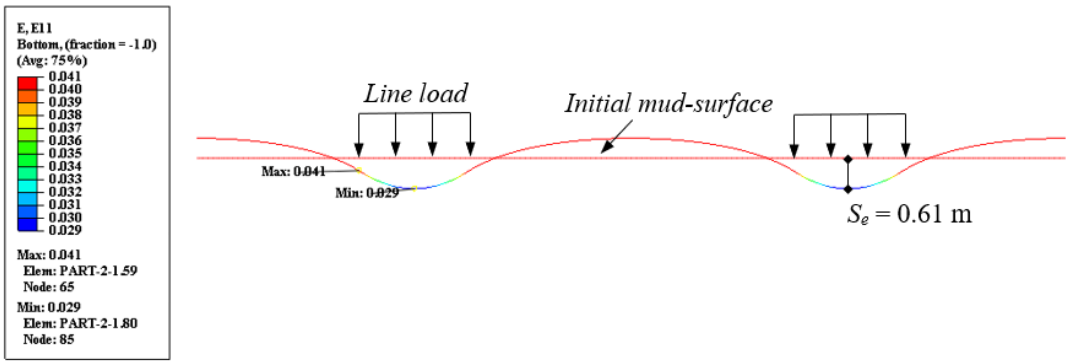

(b) Model 2: ε_{max} = 4.1 %

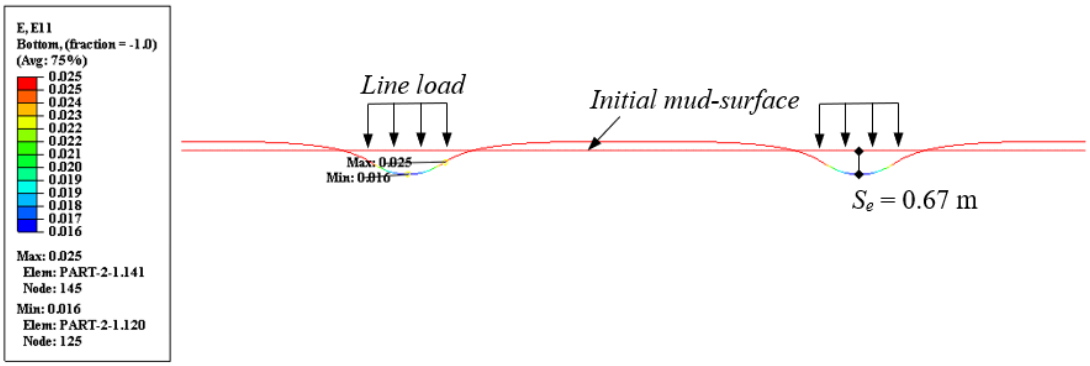

(c) Model 3: ε_{max} = 2.5 %

Figure 3.7 Tensile strain in the geotextile for the three models

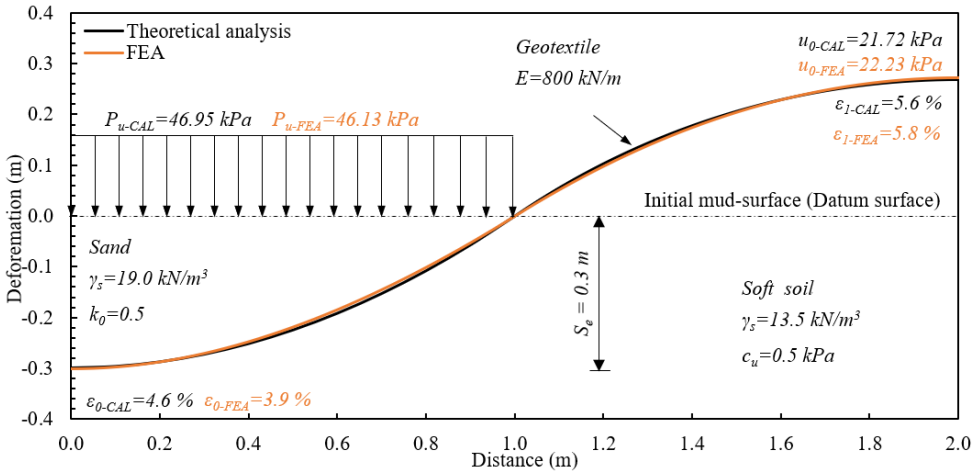

(a) L_2/L_1 = 1

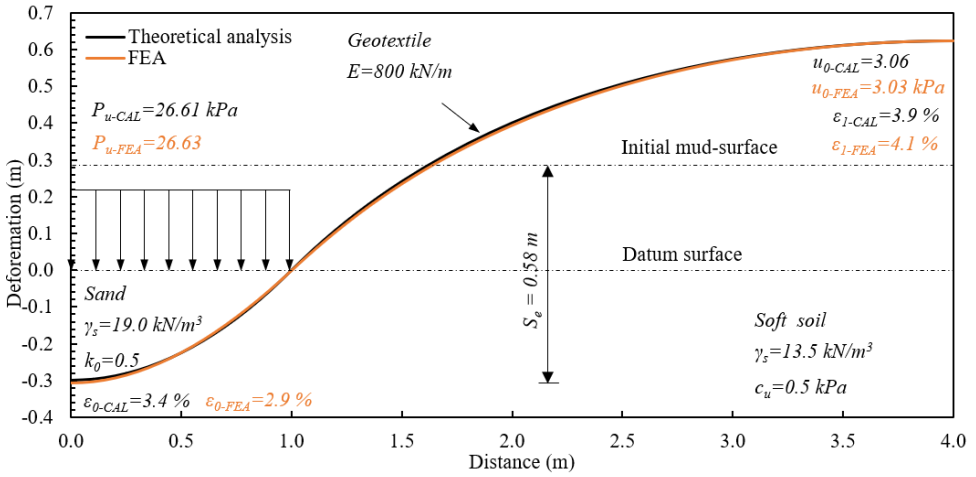

(b) L_2/L_1 = 3

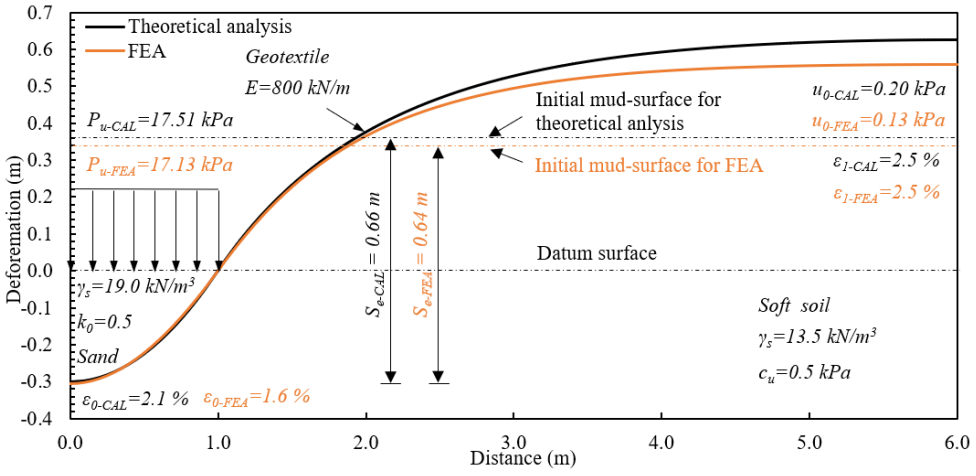

(c) L_2/L_1 = 5

Figure 3.8 Computed cross-section for the examples with given parameters of E = 800 kN/m, Δh_1 = 0.3 m and L_1 = 2 m.

The profile of deformed geotextile for section OA from the FEA was close to parabolic curve as assumed for the proposed solution. The bearing pressure and maximum tensile strain based on two methods were also close. For example, those for L_2 = 2 m are 46.95 kPa and 5.6% for proposed solution and 46.13 kPa and 5.8% for FEA. The difference of the tensile strain in section OA of geotextile from two methods was caused without the lateral earth pressure acting on the geotextile. However, the vertical earth pressure was the main factor that affect the deformation of geotextile. For FEA, the contact pressure between geotextile and soft soil at top of geotextile was considered as the excess pore pressure, u_0, at top of geotextile. Comparing the three cases from the analytical solution with those of FEA, the trendline was consistent. The bearing pressure, P_u, excess pore pressure, u_0, and maximum tensile strain, ε_{max}, for spacing L_2 = 2 m were larger. As the spacing increases, the bearing pressure, the excess pore pressure or the maximum tensile strain reduced. The ratio of $\Delta h_2/L_2$ was about 0.14 for L_2 = 2 m and 0.06 for L_2 = 10 m. That indicated that the cross-section of geotextile between sand berms/tubes is flatter for larger spacing. The settlement for L_2 = 10 m, about 0.66 m for proposed solution and 0.64 m for FEA, was much greater than that for L_2 = 2 m, about 0.30 m, or L_2 = 6 m, about 0.58 m.

3.3.3.2 Design charts and parametric studies for geotextile sheet in Broms' method

Given the soil properties as shown in Table 3.1, the main variables controlling the geometry of the berms/tubes are L_1, $\alpha = L_2/L_1$ and geotextile properties. By knowing those design values, we can obtain the bearing pressure, the excess pore pressure and the maximum tensile strain in the geotextile under different deformations.

For the convenience of preliminary design and parametric studies, we have developed a few design charts to determine the bearing pressure, P_u, and the maximum tensile strain, ε_{max}, in the geotextile for different normalized tensile stiffnesses $J = 4E/\gamma_l L^2_1$ of 25, 50, 75, 100, 200 and 400 and different $\alpha = L_2/L_1$ values of 1 to 5 as shown in Figure 3.9. In the charts, the relationships between the normalized bearing pressure ($2P_u/\gamma_l L_1$) and the normalized deformation ($2\Delta h_1/L_1$) in solid lines as well as between the maximum tensile strain and the normalized deformation ($2\Delta h_1/L_1$) in dash lines are given. With the 30 degrees of reposed angle of sand, the maximum dimension of sand berms in Broms' method is limited for a specific contact width of berms. When the normalized bearing pressure, $2P_u/\gamma_l L_1$, is less than 0.4, the design charts are also suitable to be used for the Broms' method.

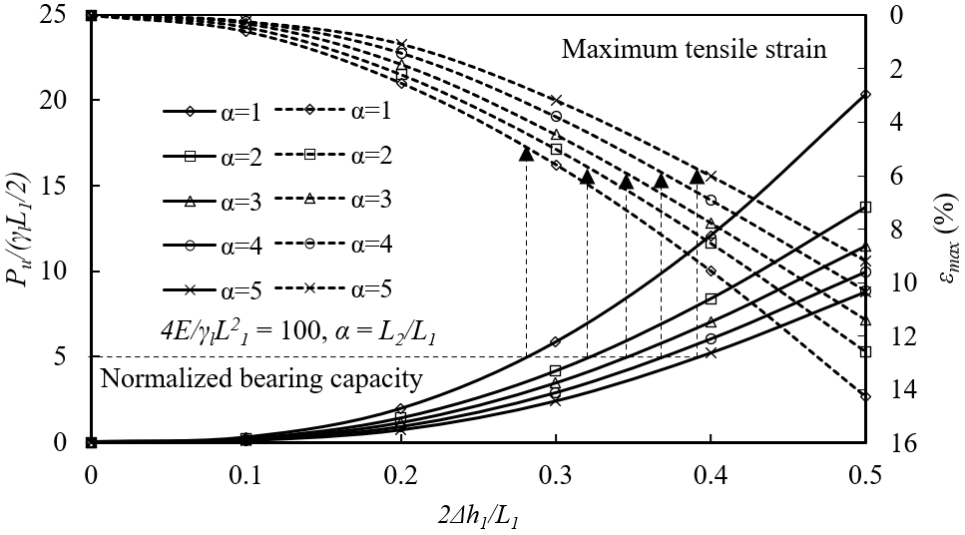

(a) $4E/\gamma_l L^2_1 = 100$

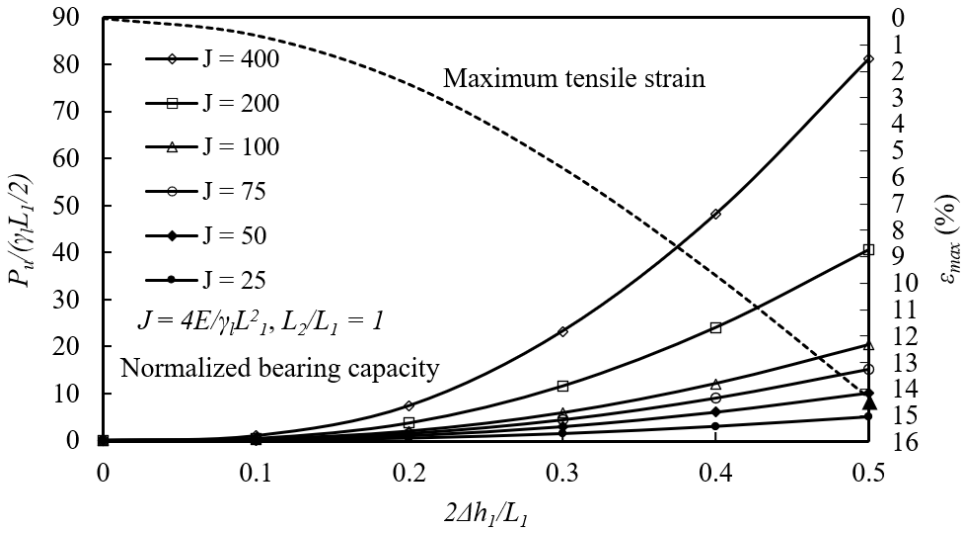

(*b*) L_2/L_1 =1

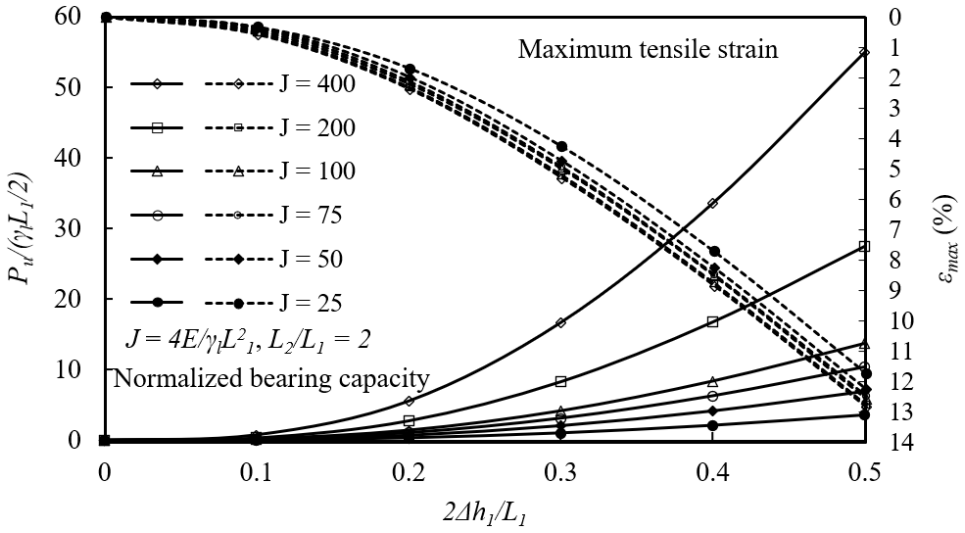

(c) L_2/L_1 =2

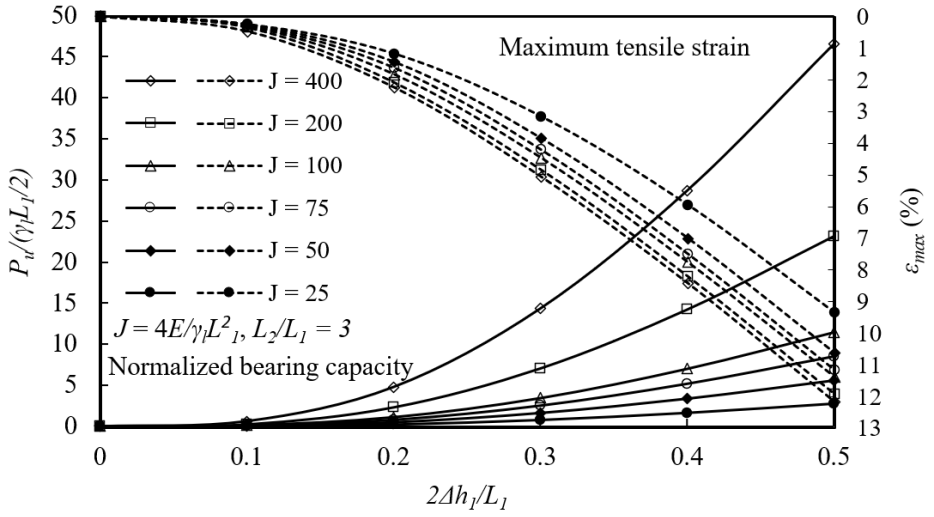

(d) L_2/L_1 =3

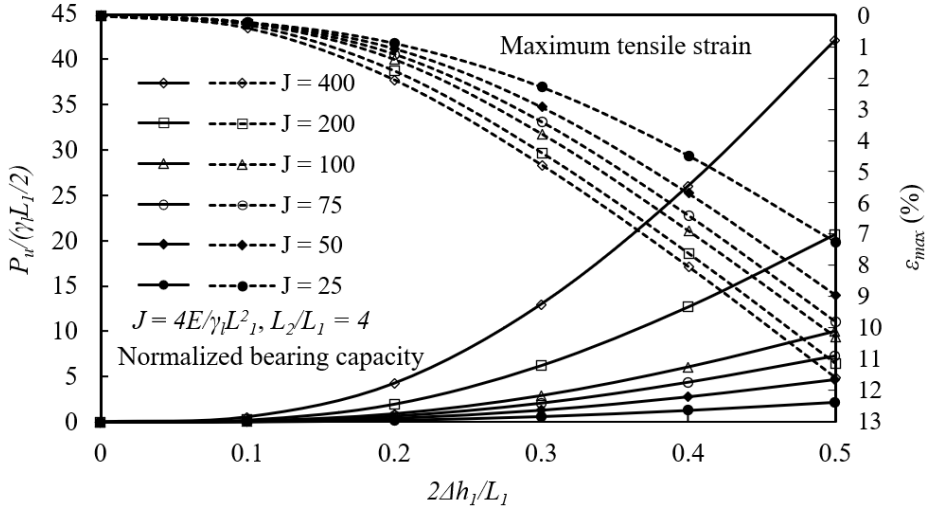

(e) L_2/L_1 =4

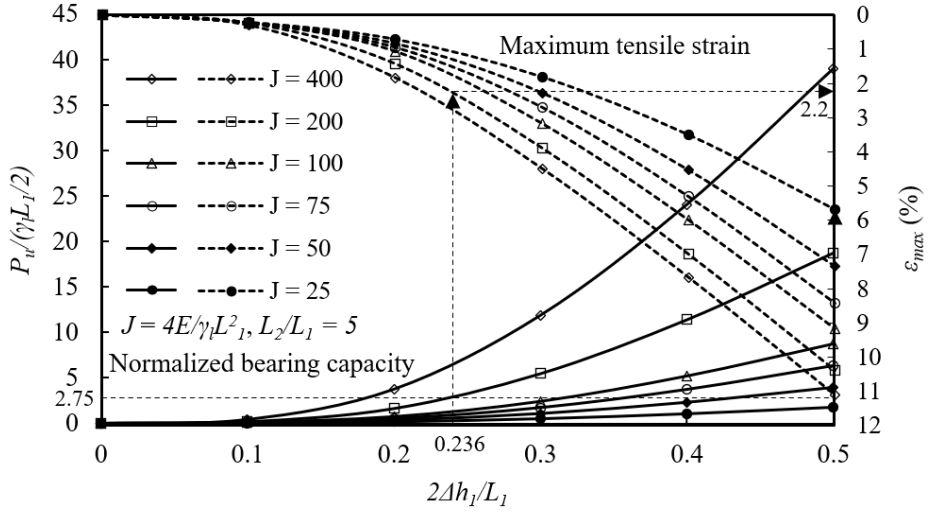

(f) L_2/L_1 =5

Figure 3.9 Design charts developed for different contact widths and spacings of sand berms/tubes and tensile stiffnesses

It can be seen from Figure 3.9a that for the same normalized deformation $2\Delta h_1/L_1$, both the normalized bearing pressure and the maximum tensile strain reduced as α or the spacing of sand berms/tubes L_2 with respect to L_1 increased. In Figure 3.9b, the maximum tensile strain was given in the same curve for different normalized tensile stiffnesses. From Figure 3.9b to Figure 3.9f, for the same normalized deformation, both the normalized bearing pressure and the maximum tensile strain increased as the normalized tensile stiffness increased, and the ratio of different normalized bearing pressures was around the ratio of the corresponding normalized tensile stiffnesses. For example, with the normalized deformation $2\Delta h_1/L_1$ of 0.4 in Figure 3.9b, the normalized bearing pressure for J = 400 was about 48 which was twice of that for J = 200 about 24.

To support a specific weight of a sand berm/tube with a given contact width at the critical state, L_1, the smaller the spacing of the sand berms/tubes, L_2, the smaller the penetrated depth of the sand berms/tubes, Δh_1, and the local maximum tensile strain was found for a specific L_2 as shown in Figure 3.9a. For a specific spacing L_2, the higher the tensile stiffness, the smaller the penetrated depth, and the smaller the maximum tensile strain as an example in Figure 3.9e. However, a smaller L_2 also means more berms/tubes to be placed and it may not be the most economical design. In terms of the maximum tensile strain, ε_{max}, it does not seem to be affected too much by α as shown in Figure 3.9a. With a better tensile stiffness of geotextile, the sand berms/tubes are more stable.

In practice, it is difficult to control the width and height of the sand berms to be consistent when using the Broms' method. This increases the uncertainties in the design and construction. The width of the sand berms cannot be too small, unless confined laterally. The use of geotextile tubes can overcome the above difficulties and thus the modified Broms' method is proposed.

3.4 Application of Modified Broms' method

3.4.1 Field trial

Due to a lack of granular fill materials, clayey fill materials including slurry has been used for land reclamation in Singapore in recent years. A field trial to use soft marine clay slurry dredged from seabed as fill materials for land reclamation was carried out. The field trial site covered an area of 3,600 m^2. The clay slurry layer had a thickness of up to 12.5 m. To improve the engineering properties of the clay slurry, a working platform had to be formed on the clay slurry using the modified Broms' method.

(a) Placement of geotextile and geotextile tube

(b) Installation of sand berms using geotextile tubes

Figure 3.10 Construction process of a working platform for the field trial: (a) Placement of geotextile and geotextile tube and (b) Installation of sand berms using geotextile tubes

The construction process is described briefly as follows. Before the placement of geotextile, the surface water was drained out. The mud surface was maintained at wet condition to reduce the pulling friction. The geotextile was seamed together with double stitches at a 150 mm overlap. A few steel pipes were wrapped one by one in the geotextile to help spread out the pulling stress as shown in Figure 3.10(a) and connected to the bulldozers or excavators. After the fully placement of geotextile, the geotextile was stretched as far as possible mechanically. Then the geotextile tubes with the required spacing were placed by workers in the direction perpendicular to the seams of geotextile. Once the geotextile tubes were in position, the fluidized sand was hydraulically pumped into the tubes to form the geotextile-tube confined sand berms as shown in Figure 3.10b.

In field trial, a woven geotextile layer (Tencate HPa380) with an elongation of 12% at break and the tensile stiffness of 700 kN/m was used (see Figure 3.10a). The properties of the geotextile and soft soil are given in Table 3.4 and Table 3.5. The unit weight and undrained shear strength were about 13.5 kN/m^3 and 0.0 kPa respectively for the high-water content clay slurry. Based on the field observation as shown in Table 3.6, the cross-section of sand tubes was nearly elliptic with about 1.5 m width and 0.8 m height and not all the bottom part of the sand tubes were in contact with geotextile. The centre to centre spacing of the sand tubes, L_1+L_2, was 6 m. The total deformation of geotextile, $\Delta h_1+\Delta h_2$, in-situ was about 0.5 m and the maximum settlement was about 0.4 m. The circumference of geotextile tubes was about 4 m and the pumping pressure was about 4.5kPa.

Table 3.4 Materials Specifications of Mirafi HPa380 used for field trial

S/N	Geotextiles properties	Direction	Value	Unit
1	Tensile modulus @ 2% strain	MD	700	kN/m
2	Tensile modulus @ 2% strain	CD	800	kN/m
3	Wide width tensile strength	MD	65	kN/m
4	Wide width tensile strength	CD	45	kN/m
5	Elongation at break	MD	12	%
6	Elongation at break	CD	10	%

MD: Machine direction; CD: Cross direction

Table 3.5 Properties of clay slurry and sand fills used in field trial

$\gamma_{sat\text{-}clay}$ (kN/m^3)	$\gamma_{sat\text{-}sand}$ (kN/m^3)	Water Content (%)	Liquid Limit (%)	Plastic Limit (%)	Plasticity Index (%)	c_u (kPa)
13.5	19.0	185	59	35	34	0.0

Table 3.6 In-situ observation and calculated results of field trial

Parameters	Observation					Calculation		
	Height (m)	Width (m)	Total deformation (m)	Maximum settlement (m)	L_1+L_2 (m)	$P_{u\text{-}t}$ (kPa)	L_1 (m)	L_2 (m)
In-situ	0.8	1.5	0.5	0.4	6.0	19.8	1.2	4.8

* L_1: contact width of sand tubes; L_2: spacing between the sand berms/tubes; $P_{u\text{-}t}$: total bearing pressure.

The cross-section of the sand tubes is calculated using a solution provided by Guo et. al. (2011; 2014). The calculated geometry of sand tubes is about 1 m contact width, 1.53 m width, 0.85 m height and 1.05 m^2 area, which is close to the in-situ observation. Then the spacing of sand tubes, L_2, is 5 m and the calculated total bearing pressure, $P_{u\text{-}t}$, is about 20.0 kPa. The cross-section of geotextile tube, the profile of geotextile sheet and the distribution of tensile strain are shown in Figure 3.11. The calculated bearing capacity was a bit larger than that of in-situ as shown in Table 3.6.

The FEA was also used to verify the results of proposed solution. The cross-section of the deformed geotextile under the sand tubes of proposed solution and FEA are shown in Figure 3.11. The results of proposed solution and FEA as shown in Table 3.7 were close to the field observation. To support the required load, the settlement, the total deformation of geotextile, the excess pore pressure and the maximum tensile strain for the proposed solution were 0.339 m, 0.542 m, 1.60 kPa and 2.48%, respectively. The closest results using FEA were 0.337 m, 0.500 m, 1.12 kPa and 2.26 %, respectively. The maximum tensile strain based on two methods was much less than the elongation at break of geotextile. Based on the results, the proposed solution was valid to predict the stabilization of berms.

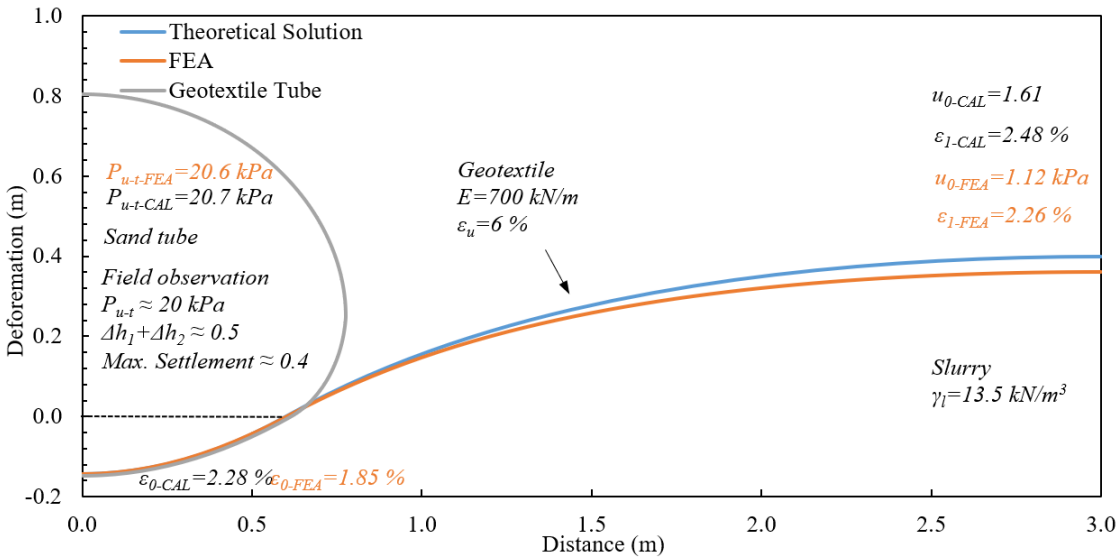

Figure 3.11 Calculation results for the geotextile tube and the geotextile sheet

Table 3.7 Results of the proposed solution and FE Analysis for field trial

Solution	$P_{u\text{-}t}$ (kPa)	Settlement (m)	Penetration depth (m)	Heave (m)	Total deformation (m)	Max. tensile strain ε_{max} (%)
FEA	20.6	0.337	0.141	0.359	0.500	2.26
Proposed	20.7	0.339	0.144	0.398	0.542	2.48

3.4.2 Comparison between proposed and Broms' method

As a comparison, the proposed solution as well as Broms' solution were applied to the case in the field trial to predict the bearing pressure, the deformation of geotextile and the tensile strain. The calculated results for the three solutions are compared with the results from FEA in Table 3.8. The parameters of soft soil and geotextile used are the same as those shown in Table 3.4 and Table 3.5.

Table 3.8 Results using analytical solutions and FE Analysis for field trial

Solution	$P_{u\text{-}t}$ (kPa)	Settlement (m)	Penetration depth (m)	Heave (m)	Total deformation (m)	Max. tensile strain ε_{max} (%)
FEA	20.6	0.329	0.124	0.348	0.472	2.2
Proposed	20.7	0.339	0.118	0.387	0.505	2.2
Broms	20.6	0.381	0.104	0.520	0.624	2.9

*$P_{u\text{-}t}$; total bearing pressure

It can be seen from Table 3.8 that the maximum tensile strain, the settlement and the total deformation obtained from the proposed solution (2.2%, 0.339 m and 0.505 m) agree well with those from FEA (2.2%, 0.329 m and 0.472 m). The Broms' solution overestimates the maximum tensile strain (2.9%), the settlement (0.381 m) and the total deformation (0.624 m). In the Broms' solution (1987), the deformed geotextile is assumed to be a circular. The proposed solution is thus more general than the Broms' solution in theory. The proposed solutions also agree well with the monitoring data from

the field trial. Furthermore, using the proposed solution, the profile of deformed geotextile can also be obtained. Compared with the Broms' solution, the predicted profile of deformed geotextile using the proposed solution is more realistic as compared with the deformation of geotextile observed in the field trial. Using the distribution of tensile strain, the potential rupture position of geotextile can also be estimated.

3.4.3 Design procedure

Based on the proposed solution, the following steps were proposed to design the geotextile supported sand tubes on soft soil.

(1) Select the values for the contact width, L_1, and the spacing, L_2, of sand berms/tubes. And calculate the expected loading as bearing pressure, P_u. for Broms' method or modified Broms' method and get the normalized bearing pressure.
(2) Select the ultimate tensile strain, e.g., the elongation of geotextile at break. Calculate the allowed tensile strain with a factor of safety against rupture equal to 2.
(3) Estimate the minimum value of the normalized tensile stiffness, *J*, corresponding to the allowed tensile strain using Figure 3.9. The linear interpolation can be used between the curves of the maximum tensile strain to estimate the *J* value.
(4) Calculate the minimum tensile stiffness, $E_{min} = J\gamma_l L^2_1/4$.

An example to use the design procedure is described briefly as follows. Assuming that the soft soil has γ_l = 13.5 kN/m^3 and c_u = 0 kPa. The design contact width and spacing of sand tubes are 2 m and 8 m. The modified Broms' method is applied to form the working platform and the sand tubes with 6 m circumference of geotextile tube is formed under 6 kPa pumping pressure. Then the design bearing pressure is 40.5 kPa and the normalized bearing pressure is 3.0 as shown in Figure 3.12. A specific geotextile should be selected from a series of geotextiles with an elongation at break equal to or greater than 12%. Then the allowed tensile strain is 6% with the factor of safety equal to 2.

As the normalized bearing pressure is 3.0, the corresponding minimum normalized tensile stiffness *J* is about 50 at 6% of tensile strain as shown at point A in Figure 3.12. Then the minimum tensile stiffness is about 675 kN/m. So the geotextile with the tensile stiffness more than 675 kN/m can be used in the construction of working platform.

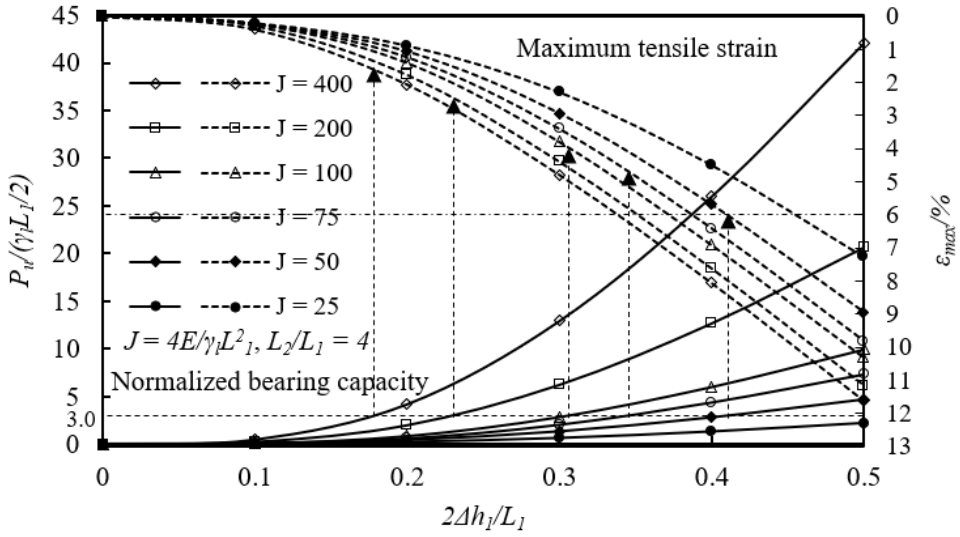

Figure 3.12 Design chart for current case

3.5 Conclusions

In this chapter, a modified Broms' method for the formation of a working platform on top of soft ground was proposed. A new analytical solution was also established to analyse the stress and strain in the geotextile under sand berms/tubes for either the Borms' method or the modified Broms' method. Based on the parametric studies and observations from the field trial, the following conclusions can be obtained:

(1) A modified Broms' method was proposed to use geotextile tubes to form sand berms on top of the geotextile sheet placed on soft ground. A field trial on the use of the modified Broms' method was also carried out. The results obtained from the field trial confirmed that the proposed method was easier to implement and could reduce uncertainties involved in both design and construction as the dimension and stability of the sand berms could be better maintained.

(2) An analytical solution for the modified Broms' method was proposed to calculate the tensile stresses and tensile strains in the geotextile and the deformed profile of the geotextile sheet. The design procedure based on the proposed methods for modified Broms' method was developed.

(3) The proposed analytical solution was also validated using finite element analyses. The analytical predictions agreed well with FE analyses and reasonably well with the field monitoring data.

CHAPTER 4 MODEL TESTS FOR USING HORIZONTAL DRAINAGE ENHANCED GEOTEXTILE SHEET

4.1 Introduction

As discussed in Chapter 2, soft clay and other waste materials may have to be used as fill material for land reclamation when there is a lack of granular fill materials. However, soft clay is normally low in shear strength and high compressibility, and thus needs to be treated. Preloading using PVDs via either fill surcharge or vacuum preloading is the common method for the improvement of soft clay. However, there are disadvantages for the use of PVDs, as discussed in Chapter 2. Therefore, vacuum preloading or combined vacuum preloading with horizontal drains approaches were proposed (Shin et al., 2013; Chai et al., 2014; Chu et al., 2016). To assess the effectiveness of the proposed approaches, a series of model tests were set up to study the vacuum consolidation behaviour of soft marine clay. The performance of the horizontal drainage enhanced geotextile sheet (HDeG sheet) as horizontal drains was investigated as well. The test data suggested that the performance of the HDeG sheet could be affected by the transmissivity of geotextile. Since the reduction of transmissivity of geotextile in soft clay being pointed by Koerner et. al. (1982), a study on the measurement of the transmissivity of geotextile in soft clay under different normal stresses was also carried out.

4.2 Model tests set-up

The whole vacuum consolidation system for model tests consisted of the consolidation tank, prefabricated drain, vacuum chamber, vacuum pump and recording system as in Figure 4.1.

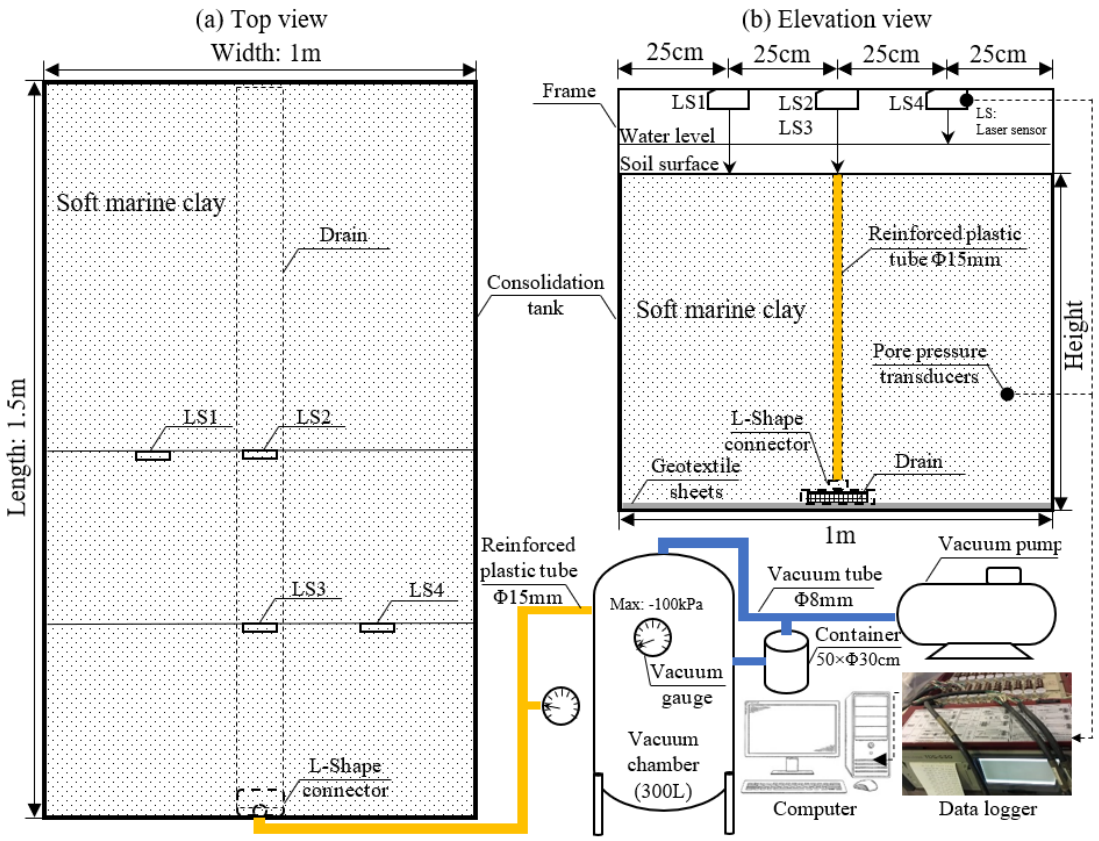

Figure 4.1 Model tank used for model tests: (a) Top view and (b) Elevation view

4.2.1 Consolidation tank, vacuum pump and vacuum chamber

The consolidation tank was 1.5 m long and 1.0 m wide. It was made of fibre glass with smooth vertical boundary to reduce friction between the soil and the sides of the tank. The vacuum pump was the core machine and was used to apply a negative air pressure in the horizontal drains. The vacuum pump and vacuum chamber were connected by vacuum tube of 8 mm in diameter. The 300 L vacuum chamber was used to store the water discharge from horizontal drains. To avoid insufficient storage capacity, a small acrylic container of 30 cm in diameter and 50 cm in height was used to measure the volume of the water discharge and draw out water from the vacuum chamber by siphoning whenever necessary. The vacuum pressure in vacuum chamber was measured using a vacuum gauge as shown in Figure 4.2.

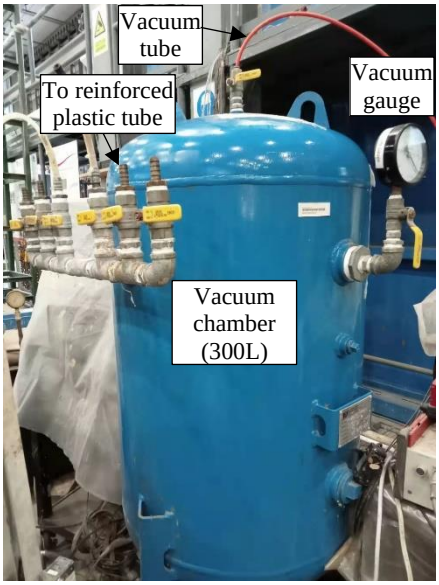

Figure 4.2 Vacuum chamber used to apply vacuum pressure for the model tests

4.2.2 Horizontal drainage enhanced geotextile sheet

The horizontal drainage enhanced geotextile sheet was proposed to use as the horizontal drains for the model tests. The drain used was 100 mm in width and 3 mm in thickness. Tencate TS10 non-woven geotextile with about 1 mm in thickness was used for the horizontal drainage enhanced geotextile sheet as shown in Figure 4.3. The drain was connected with the vacuum chamber via a reinforced plastic tube of 15 mm in diameter and L-Shape connector.

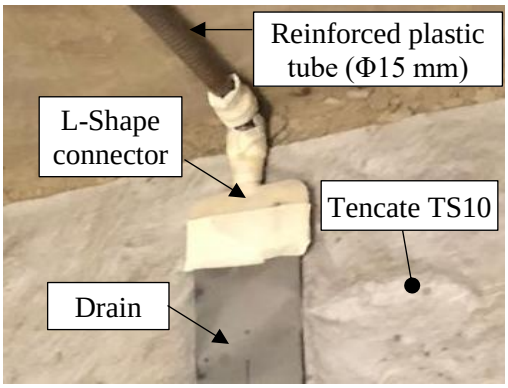

Figure 4.3 Drain, non-woven geotextile and L-shape connector

4.2.3 Measurement Instruments

The data logger and converter system were used to record the data every 5 minutes as in Figure 4.1. The pore-water pressure transducers (PPTs), model KPD-200KPA, were

used to measure the change of pore-water pressure in soil as in Figure 4.4. Before installation, the transducers were soaked in water for 24 hours to ensure a high degree of saturation. The PPTs were calibrated using a strain gauge indicator cum data logger. A layer of non-woven geotextile was used to wrap the transducers to avoid the clogging of the porous stone on the PPTs. The IL serial laser sensors of Keyence were used to measure the soil surface settlement or the water level. The laser sensors were fixed on the consolidation tank using angle bars shown as in Figure 4.5.

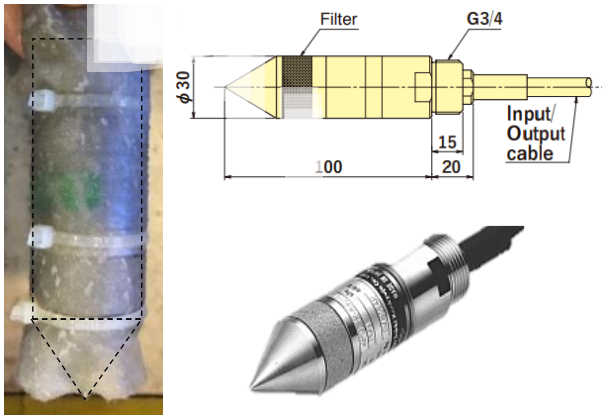

Figure 4.4 Pore-water pressure transducers

Figure 4.5 IL serial laser sensors of Keyence

4.2.4 Soil preparation

The basic properties of soft marine clay used were characterised. The grain size distribution of the marine clay is shown in Figure 4.6. The fines content was 93%. The liquid limit and plastic limit were 72% and 32%, respectively. The plastic index was 44% and the organic content was 2.23%. The soil was classified as high plasticity organic

clay based on USCS. The specific gravity was measured to be 2.69. Three consolidated drained (CD) triaxial tests with a shearing strain rate of 0.005% per minute were conducted under different confining pressures of 100, 200 and 300 kPa, respectively. The failure stresses of the CD tests are given in Table 1 and the failure points are also plotted in Figure 4.7. The effective internal friction angle obtained was 22.6°. The soil properties are summarized in Table 4.2.

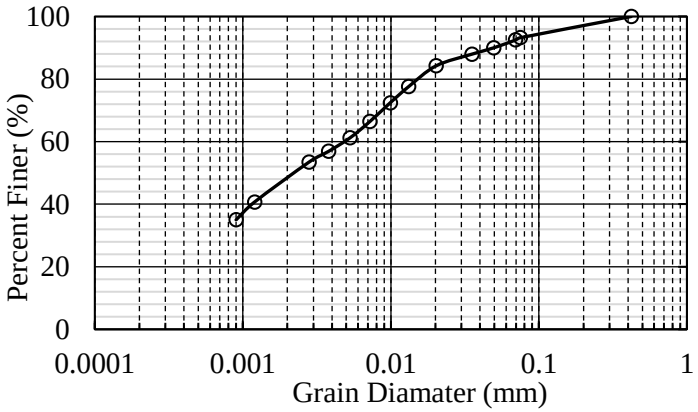

Figure 4.6 Grain size distribution of marine clay

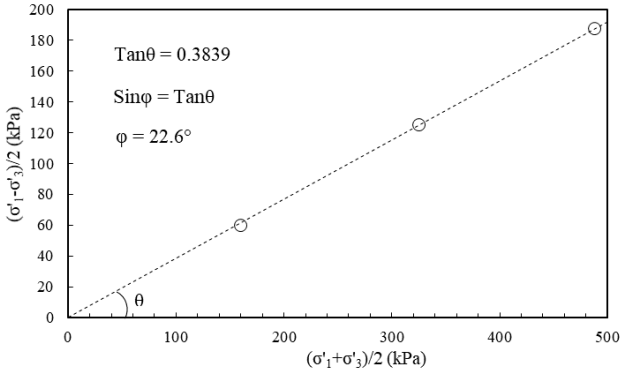

Figure 4.7 Failure condition for CD tests and effective friction angle

Table 4.1 Results of CD tests

CD Test	1	2	3
Failure σ'_1 (kPa)	220	450	675
Failure σ'_3 (kPa)	100	200	300
Void ratio after consolidation	1.05	0.96	0.87

Table 4.2 Properties of remould marine clay

Properties	Value
Specific Gravity	2.69
Liquid Limit (W_L/%)	72
Plastic Limit (W_P/%)	32
Friction Angle (φ'/˚)	22.6˚
Organic Content (‰)	2.23

Six standard Oedometer tests were also conducted. The samples were consolidated under 40 kPa or were collected from model tests. Another seven small-scale consolidation tests for remoulded marine clay with high-water contents were conducted under vertical drainage condition and radial drainage condition using the NTU Consolidometer device (Chu et al., 1997) are shown in Figure 4.8. The initial high-water contents were 71.0, 94.5, 110.5 and 131.0 % for vertical drainage condition and 72.9, 110.0 and 127.0 % for radial drainage condition. The sample of high-water content soft marine clay was first placed in a vacuum cell to remove the trapped air. The initial resistance of device was measured to be about 3.0 kPa for vertical drainage tests and 4.6 kPa for radial drainage tests. Under vertical drainage condition, two porous plastic discs were placed at top and bottom of samples as drainage boundaries, see in Figure 4.8b. Under radial drainage condition, two rubber discs were placed at top and bottom of samples as impermeable boundaries and a porous plastic was placed around the ring inside as drainage boundary, see in Figure 4.8c. The test results are shown in Figure 4.9.

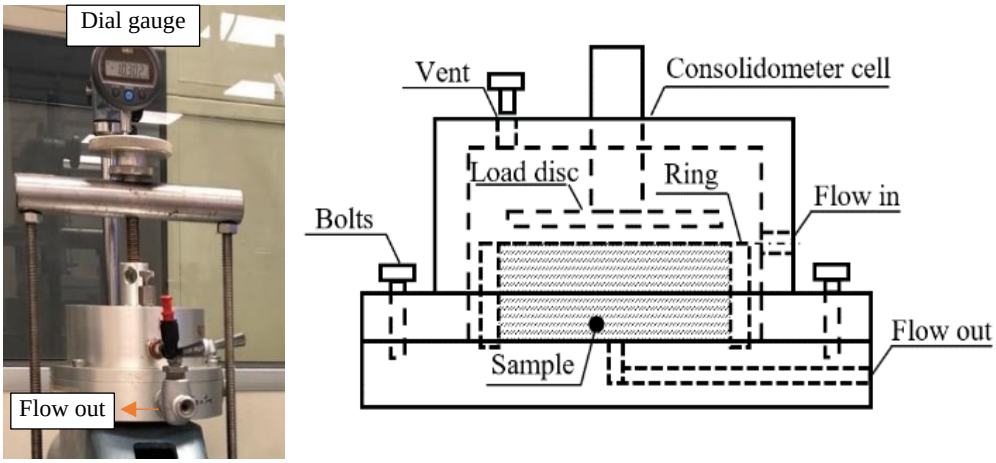

(a) Consolidometer cell

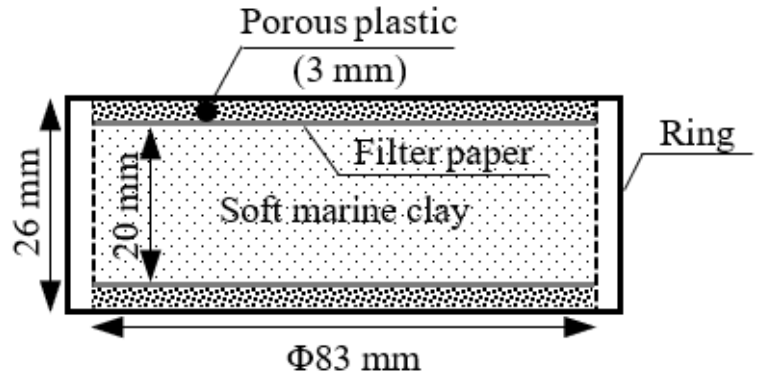

(b) Vertical drainage condition

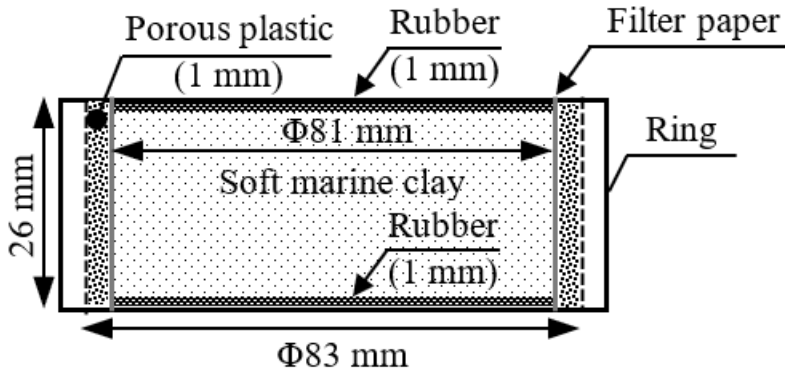

(c) Radial drainage condition

Figure 4.8 Consolidation tests of soft soil with high-water content: (a) Consolidometer cell; (b) Vertical drainage condition and (c) Radial drainage condition

There were some differences for the compression curves of the soft marine clay under vertical and radial drainage conditions. After a certain effective stress, the compression curves tended to close. The coefficient of consolidation, c_v, at normal consolidation range, see in Figure 4.10, based on the high-water content consolidation tests and oedometer tests was calculated using the U-$\sqrt{t}$ method (Taylor, 1948; Head, 2006). As the increase of effective stress, the coefficient of consolidation increased. The average coefficient of consolidation below 100 kPa was about 0.4 m^2/yr. By using the data at normal consolidation range from the compression curves, the fitting curves of the data as the normal consolidation lines of soft marine clay are shown in Figure 4.11. The transition void ratio at 6 kPa is 1.94, which is the void ratio at liquid limit, e_L. The transition void ratio is 1.05 at 100 kPa and is 0.65 at 1000 kPa.

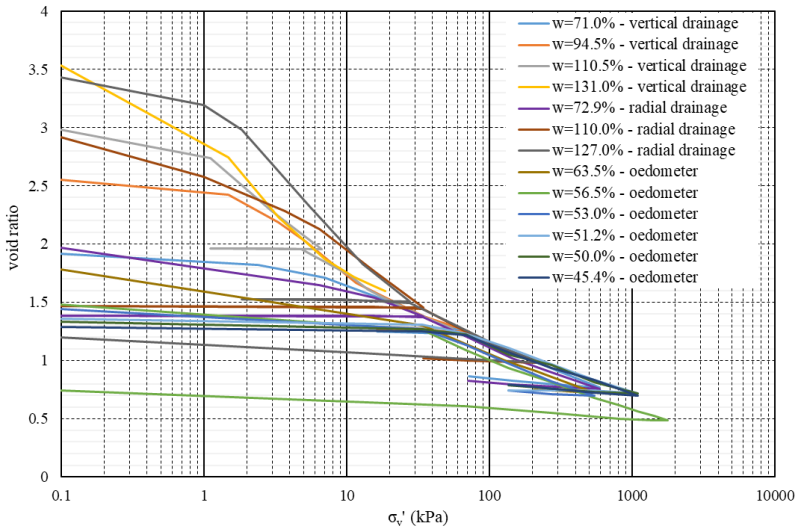

Figure 4.9 Compressibility of remoulded Singapore marine clay

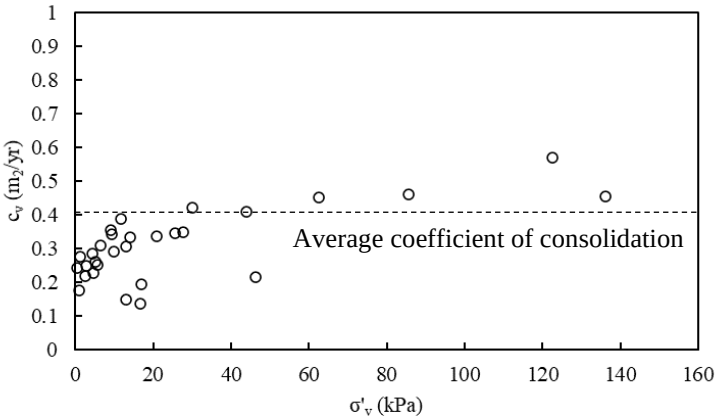

Figure 4.10 Coefficient of consolidation of remoulded Singapore marine clay

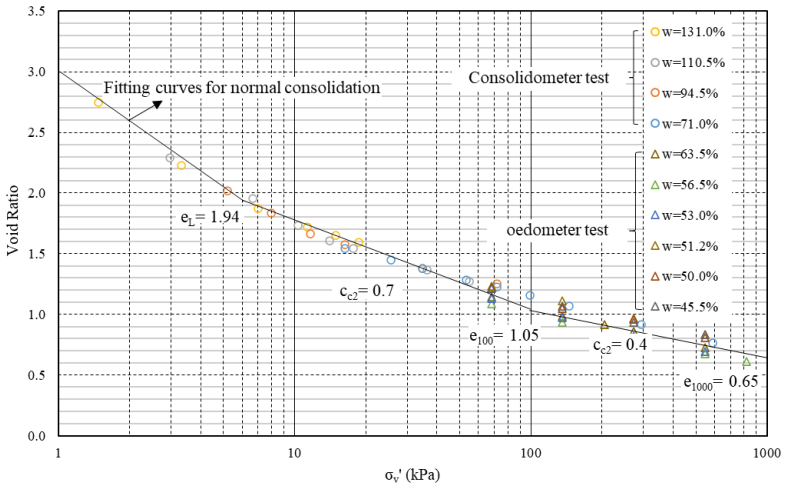

Figure 4.11 Fitting curve as normal consolidation lines for soft marine clay

The permeability was calculated based on c_v obtained from Oedometer tests and Consolidometer tests. The Permeability tests using falling head method was also conducted for the consolidated soil under vertical drainage condition using a set up shown in Figure 4.12. The initial water contents of the soil samples were 46, 100, and 125 %. The calculated permeability under vertical and radial drainage conditions was close as shown in Figure 4.13. The average void ratio was used for the calculated permeability. The fitting line of the calculated permeability was consistent with the measured permeability using falling head method as in Figure 4.13.

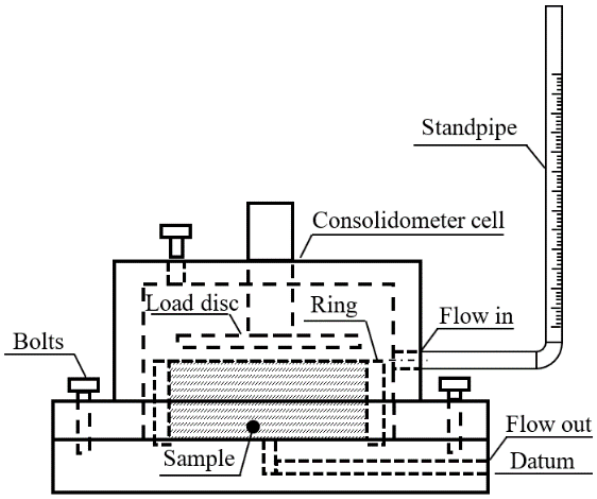

Figure 4.12 Permeability tests using falling head method for the consolidated soil under vertical drainage condition

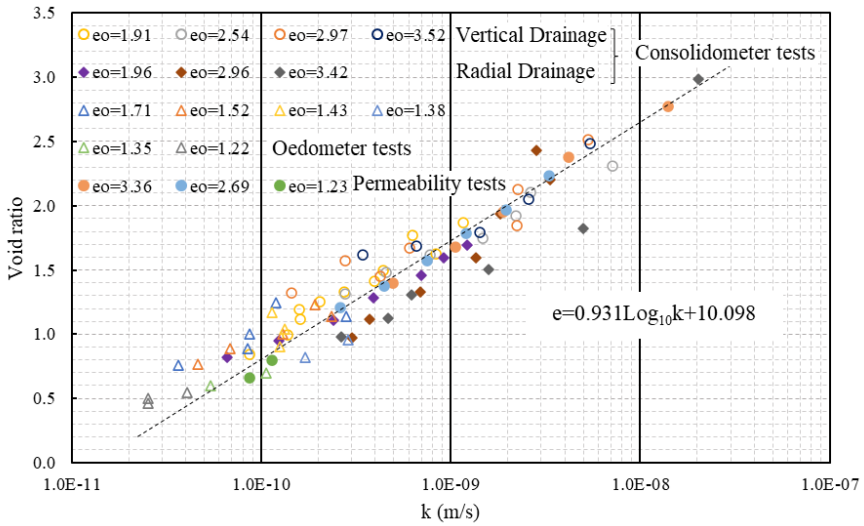

Figure 4.13 Permeability of remoulded Singapore marine clay

4.3 Model test procedure

Three large-scale unit-cell model tests of soft marine clay using HDeG sheet and prefabricated horizontal drains were carried out. In Model test 1, the horizontal drain formed by a single prefabricated drain was placed at the centre of the bottom of model tank as shown in Figure 4.14. In Model test 2, HDeG sheet with double non-woven geotextile sheets was used as shown in Figure 4.15. In Model test 3, two layers of HDeG sheet with single non-woven geotextile sheet were used at the bottom and top of soft marine clay, respectively, as shown in Figure 4.16. A layer of plastic membrane covered the top surface of the clay for seal.

The initial thicknesses of slurry in the three model tests were 0.85, 0.77 and 0.79 m, respectively. The average initial water contents were 126, 110 and 117 %, respectively. After about two weeks of the sedimentation and self-weight consolidation, the thickness of soft marine clay was reduced to 0.80, 0.74 and 0.74 m, respectively. The average water contents were 115, 105 and 106 %, respectively at the start of vacuum consolidation.

During vacuum consolidation, the settlements of the soil in the three model tests were measured using laser sensors. In Model test 1 and 2, the top boundary was not sealed using plastic. The vacuum pressure in vacuum chamber fluctuated between -90 to -96 kPa due to the long-term stability of the vacuum pump. The vacuum pressure in the reinforced plastic tube was about -85 kPa for Model tests 1 and 3 and up to -95 kPa for Model test 2. The pore water pressure transducers (PPTs) were installed at different distances from drain as shown in Figure 4.14 to Figure 4.16. The lateral porous stone as shown in Figure 4.4 allows the pore pressure transducers to measure the pore pressure on non-woven geotextile sheets.

For all the three model tests, the tests were terminated at similar settlement after 103 days, 31 days and 21 days, respectively. The laboratory vane shear tests with 50 mm by 33 mm of vane was conducted at different depths and different cross-sections in the clay. The water contents were measured at the corresponding positions and the values are shown in Figure 4.17. Samples around the HDeG sheet or drain were also collected for unconfined compression tests.

Table 4.3 Summary of three model tests for vacuum consolidation

Model test	Model 1	Model 2	Model 3
Initial Thickness (m)	0.80	0.74	0.74
Initial Water content (%)	115	105	106
Initial Void ratio	3.09	2.82	2.85
Duration (day)	103	34	21
Vacuum (kPa)	-85	-85 to -95	-85

*Terminated condition: 20 cm of settlement

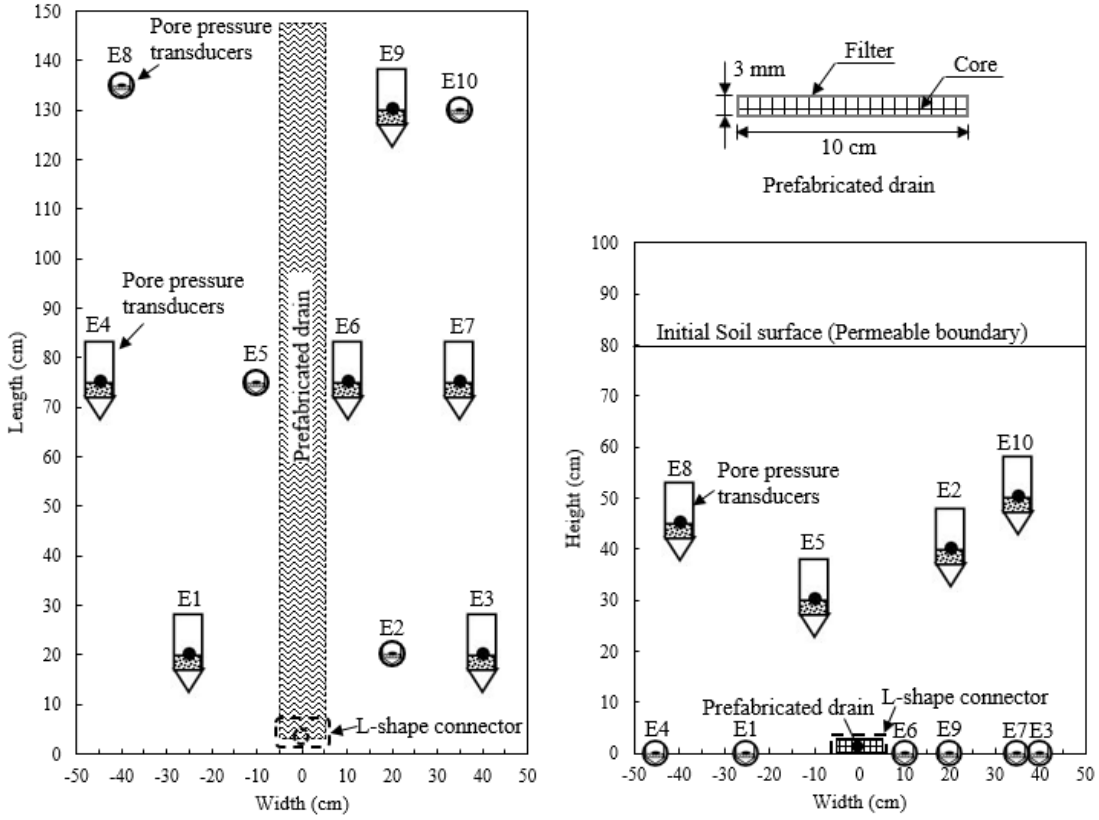

(a) Top view (b) Elevation view

Figure 4.14 Model test 1 using single drain only: (a) Top view and (b) Elevation view

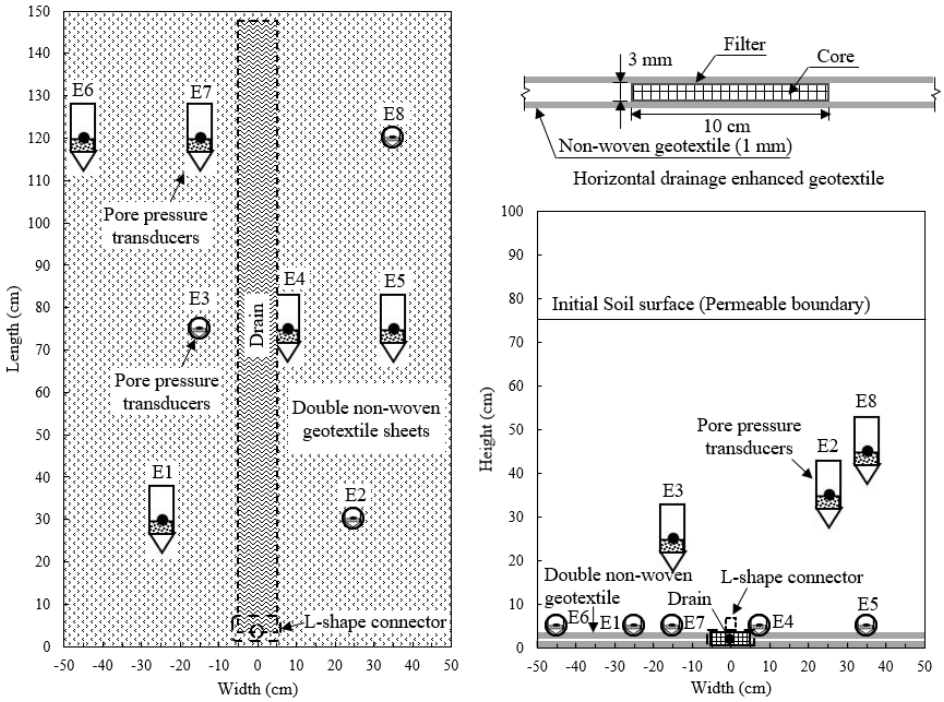

(a) Top view (b) Elevation view

Figure 4.15 Model test 2 using HDeG with double non-woven geotextile sheets: (a) Top view and (b) Elevation view

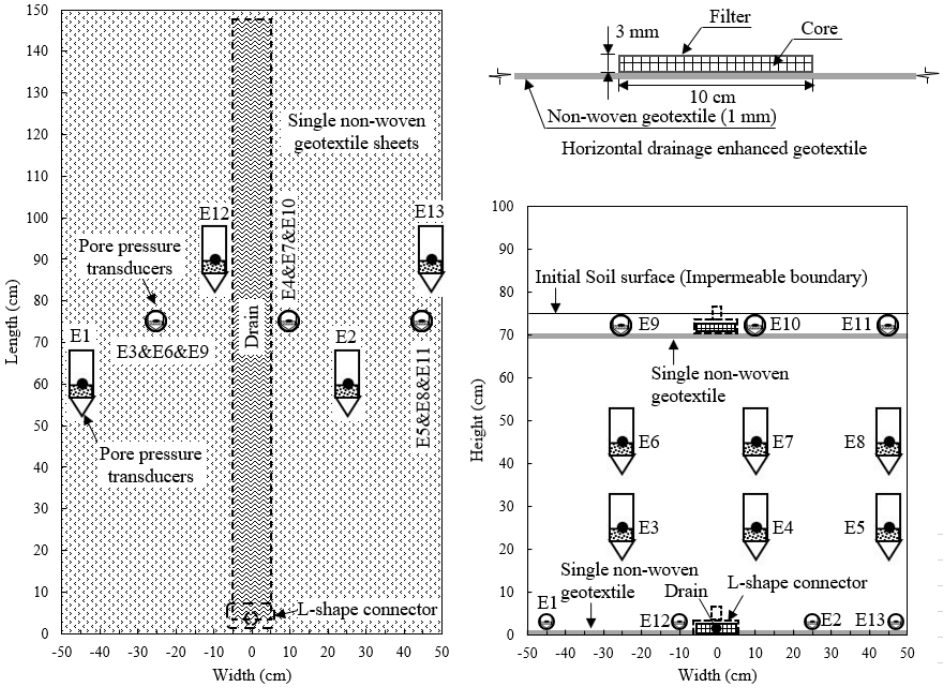

(a) Top view (b) Elevation view

Figure 4.16 Model test 3 using HDeG with single non-woven geotextile sheet: (a) Top view and (b) Elevation view

(a) Vane shear device

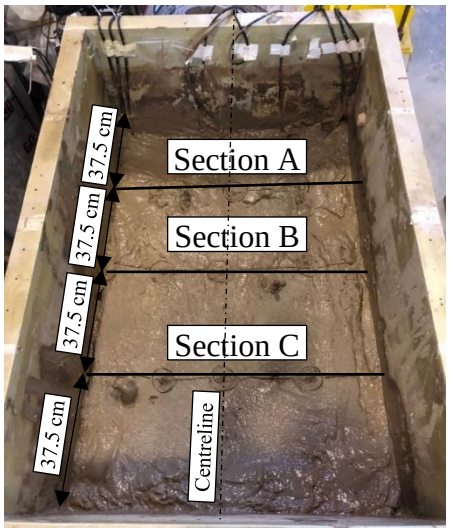

(b) Three sections for testing

Figure 4.17 Vane shear test and testing sections: (a) Vane shear device and (b) Three sections for testing

4.4 Model Testing Results

4.4.1 Sedimentation

During the sedimentation, the distributions of initial pore-water pressure are shown in Figure 4.18. The initial pore water pressure was linear and reduced a bit at the bottom after about two weeks. The theoretical distribution was calculated using the saturated unit weight, γ_{sat}, of soft marine clay and depth. The difference between the measured and the calculated pore water pressure distributions may because the reduction of pore water pressure and the small zero drift of PPTs after installation.

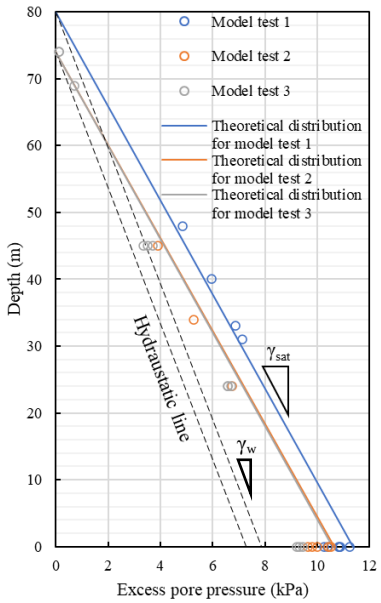

Figure 4.18 Initial pore-water pressure for vacuum consolidation after sedimentation

4.4.2 Pore pressure and settlement

- Model test 1

The surface settlement and pore water pressure obtained from Model test 1 are shown in Figure 4.19. The vacuum consolidation in Model Test 1 took the longest time, about 103 days, to reach the similar final settlement among the three model tests. As shown in Figure 4.19, the change of water level was much lower than the settlement of soil surface. But the change of water level was consistent with the water discharge. Here the water discharge was calculated using the collected water volume over the area of consolidation tank on top view. The difference of water level and soil surface kept increasing until after 75 days. Thus, the water was seeping out from the soil surface before 75 days due to the sedimentation and self-consolidation. The observed soil surface was unform. Thus the difference of the measured settlement was small.

The maximum negative pore water pressure, at transducer E6 (about 5 cm from the drain), was about -20 kPa. That is because the soil around drain was consolidated firstly and the permeability reduced largely referred to Figure 4.13. Therefore, the gradient of pore water pressure around drain was large and the reductions of pore water pressure apart from the drain were small.

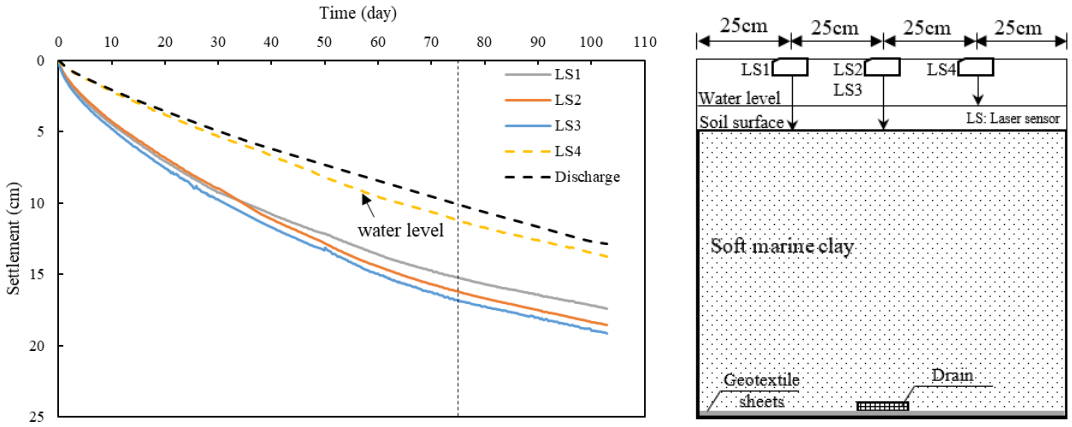

(a) Settlement

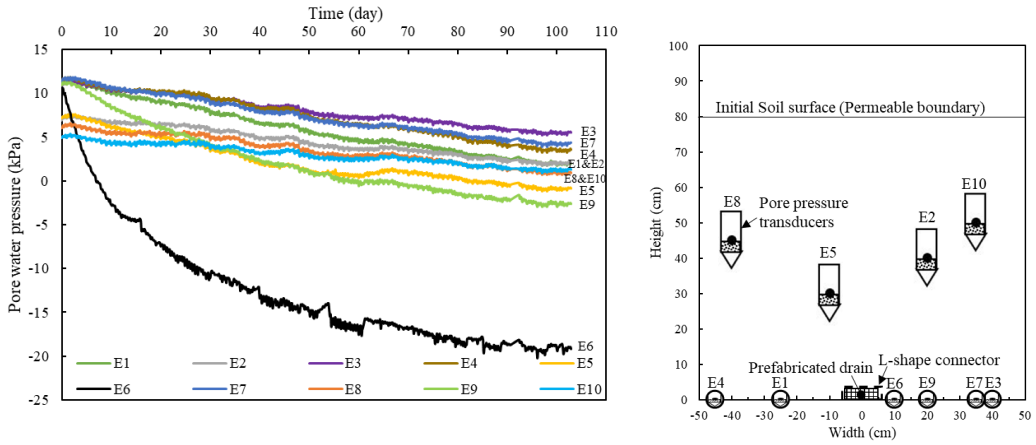

(b) Pore water pressure

Figure 4.19 Monitoring data of Model test 1: (a) Settlement and (b) Pore water pressure

- Model test 2

The settlement and pore water pressure in Model test 2 are shown in Figure 4.20. The drop of pore water pressure on 24th day was due to the power maintenance for 8 hours. In Model test 2, it took 34 days to reach the similar final settlement of Model test 1. The difference of water level and soil surface kept constant after 10 days and reduced to zero gradually after 24 days. However, the difference was lower than that in Model test 1. The change of water level was also same with the water discharge. Same with Model test 1, the water also could seep out through soil surface due to the sedimentation and self-consolidation. Therefore, the soil surface of Model test 1 and 2 could be considered as the permeable boundary with zero pore water pressure.

Based on the observation in Model test 2, there was no water in reinforced plastic tube at the end of testing. Therefore, the negative pore water pressure in drain was close to the vacuum pressure in the vacuum chamber, up to -96 kPa. The pore water pressures on the HDeG sheet with double non-woven geotextile sheets, at transducers E1, E4, E5, E6 and E7, were reduced quickly up to -95 kPa which was close to the vacuum pressure in vacuum chamber due to the large transmissivity of double non-woven geotextile sheets.

Because of the nearly uniform pore water pressure on HDeG sheet with double non-woven geotextile as vacuum drainage boundary, the vacuum consolidation behaviour in Model test 2 was close to the 1D consolidation behaviour. Thus, the settlement of LS1 and LS2 was almost same and the soil surface was uniform based on observation.

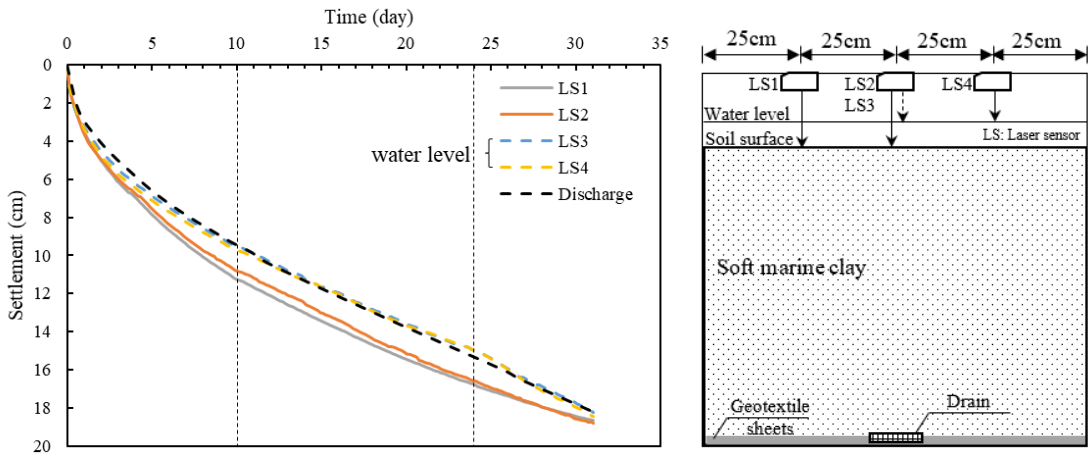

(a) Settlement

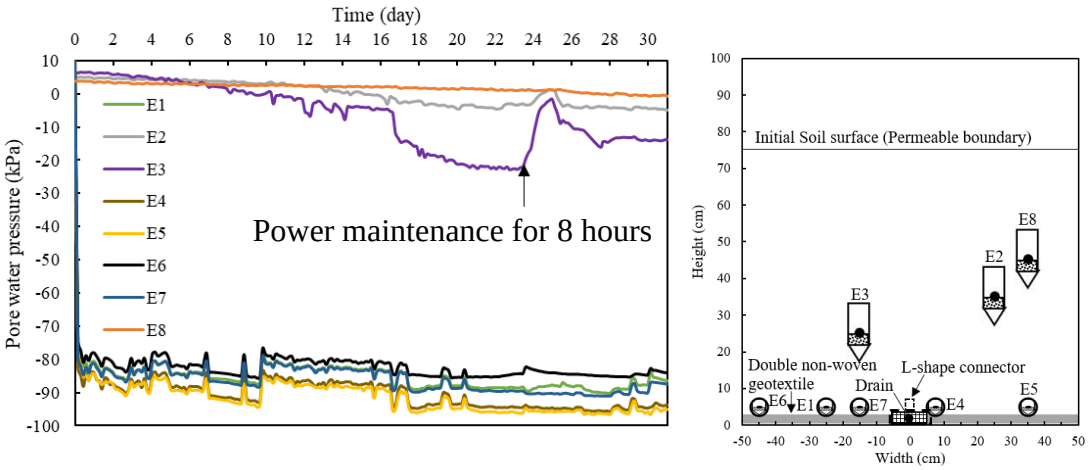

(b) Pore water pressure

Figure 4.20 Monitoring data for Model test 2: (a) Settlement and (b) Pore water pressure

- Model test 3

In Model test 3, because the two HDeG sheet with single non-woven geotextile were at the top and bottom of soil, respectively, and were covered by plastic membrane, the vacuum consolidation was relatively fast. The pore water pressure on the HDeG sheet, at transducers E2, E9, E10, E11, E12 and E13, were also reduced relatively quickly and the final values were below -30 kPa due to the transmissivity of non-woven geotextile sheet in soft marine clay. However, the reductions of pore water pressure on HDeG sheet in Model test 3 were lower than those in Model test 2 due to the lower transmissivity of single non-woven geotextile. As the pore water pressure on top and bottom HDeG sheet were different, the pore water pressure distributions on HDeG sheet should be affected by the surrounding soil or the effective stress.

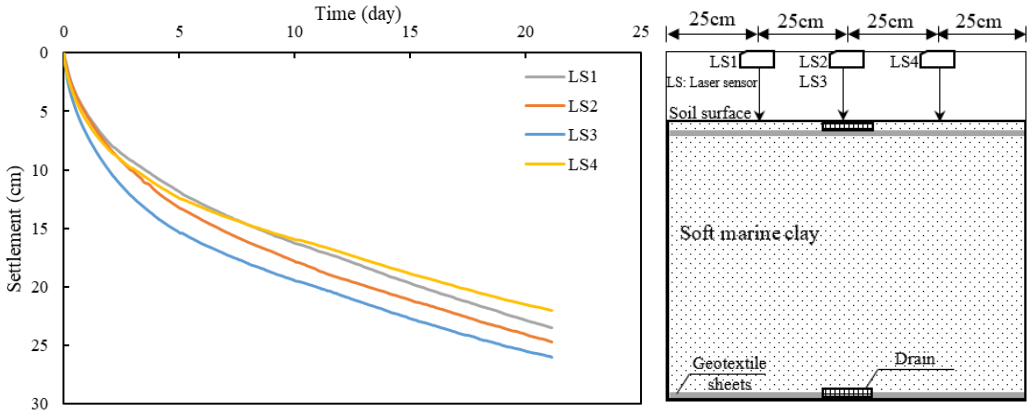

(a) Settlement

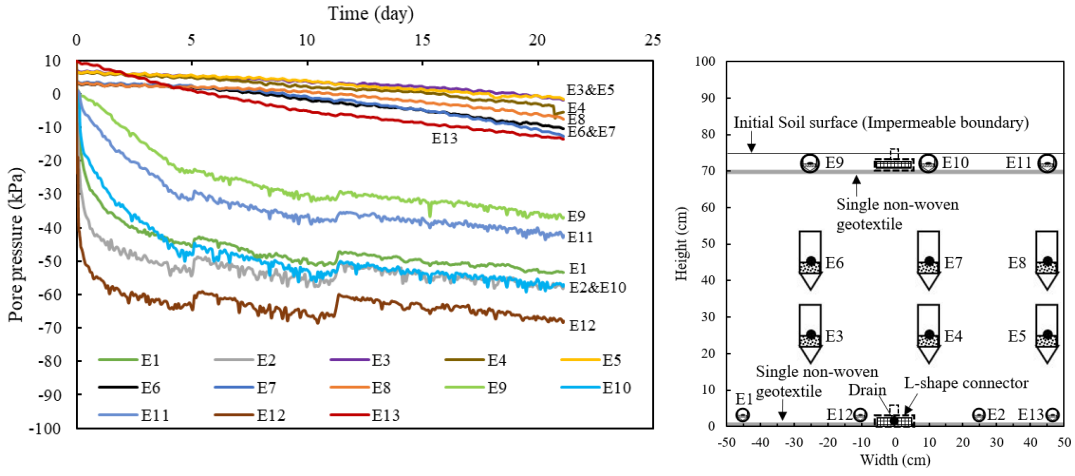

(b) Pore water pressure

Figure 4.21 Monitoring data for model test 3: (a) Settlement and (b) Pore water pressure

4.4.3 Distributions of excess pore water pressure

From the distributions of excess pore water pressure in Model tests 1 and 2, at early stage, the gradient of excess pore pressure was upward to soil surface, then pore-water was sept out at soil surface. In Model test 2, the gradient of excess pore water pressure toward to the HDeG sheet was much larger than that toward to soil surface, so that the excess pore water pressure induced by self-weight of soft clay was mainly dissipated through HDeG sheet. Compared with Model test 1, the distributions of excess pore pressure in Model tests 2 and 3 were closer to the suction line due to the transmissivity of non-woven geotextile and the sealed condition.

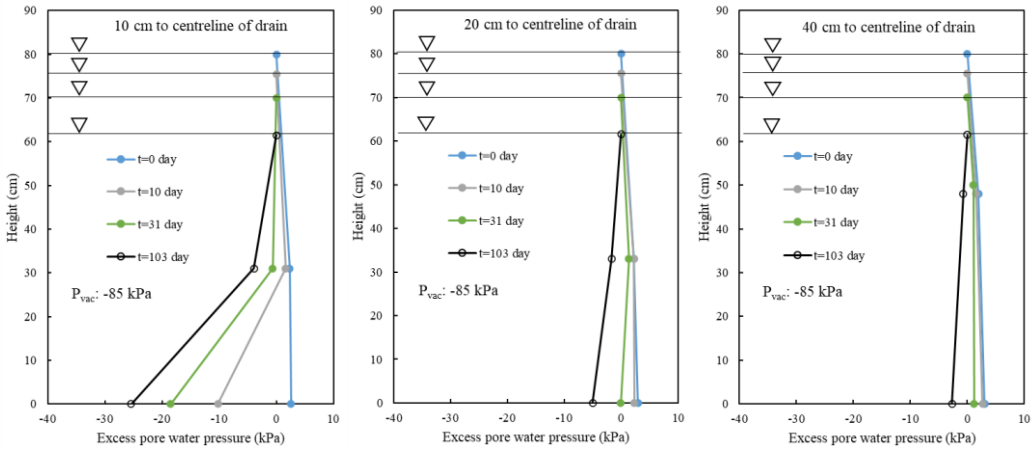

Figure 4.22 Distributions of excess pore pressure for Model test 1 (P_{vac}: Vacuum pressure)

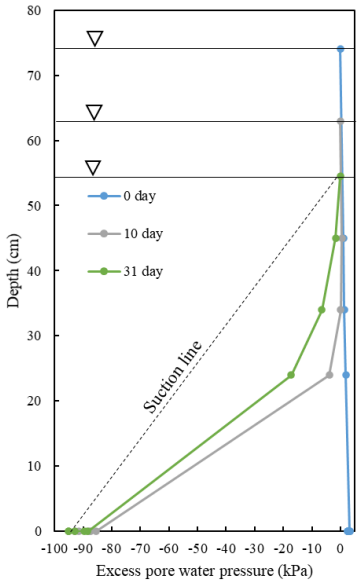

Figure 4.23 Distributions of excess pore pressure for Model test 2

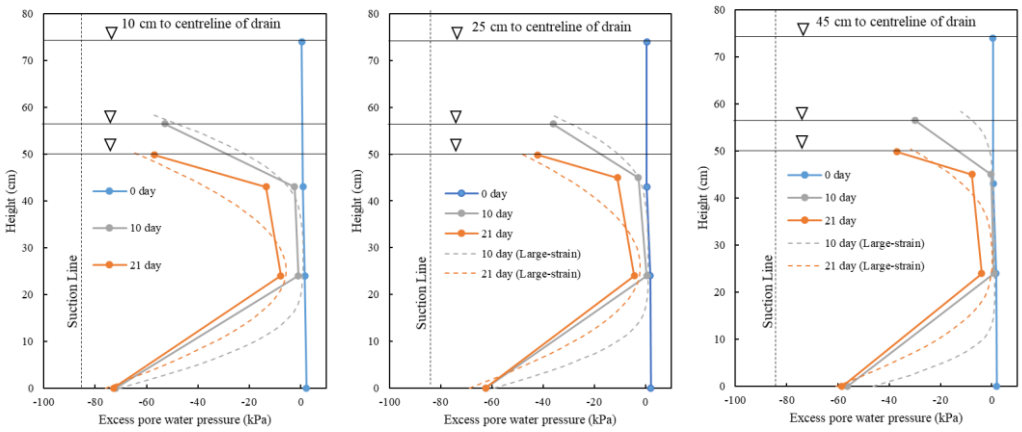

Figure 4.24 Distributions of excess pore pressure for Model test 3

4.4.4 Undrained shear strength and water content

Due to unloading after the vacuum was turned off, the soil was over-consolidation. Hence, theoretically, in terms of the treated soil with same pre-consolidation pressure, the undrained shear strength of treated soil under a normally consolidated condition should be larger than that under an over-consolidated condition. Based on the interpolation method on Mathematica, a software package (Wolfram Research, Inc., 2021), the contours of the measured undrained shear strength and water content are shown in Figure 4.25 to Figure 4.30.

In Model test 1, the maximum undrained shear strength and the minimum water content were 10.4 kPa and 52.5% around the drain. In Model test 2, because of the good transmissivity of the double non-woven geotextile sheets used in the HDeG sheet, the distributions of undrained shear strength and water content were rather uniform horizontally. The maximum undrained shear strength and the minimum water content were 13.5 kPa and 44.2% around the drain. For soil adjacent to the HDeG sheet in Model test 2, the undrained shear strength decreased slightly and the water content increased slightly in the soil away from the drain. Therefore, compared with Model test 1, a better performance in Model tests 2 and 3 was achieved due to the transmissivity. However, the average water contents of Model tests 1 and 2 at soil surface were still high, about 110% for Model test 1 and 105% for Model test 2.

In Model test 3, the maximum undrained shear strength and the minimum water content around the bottom drain were 7.9 kPa and 48.1%. And those around the top drain were about 9.45 kPa and 43.3%. Because of the single non-woven geotextile sheet, the

undrain shear strength was reduced a bit from drain for the adjacent soil of HDeG sheet, and the water content was increased from the drain. The average water content at HDeG sheet level was about 50%. That at the middle of soil was about 67% which was lower than the liquid limit, about 72%.

At the end of vacuum consolidation in three model tests, the influence zone where the undrained shear strength is non-zero and the water content is lower than the liquid limit was about 20 cm to 30 cm around the drain or HDeG sheet.

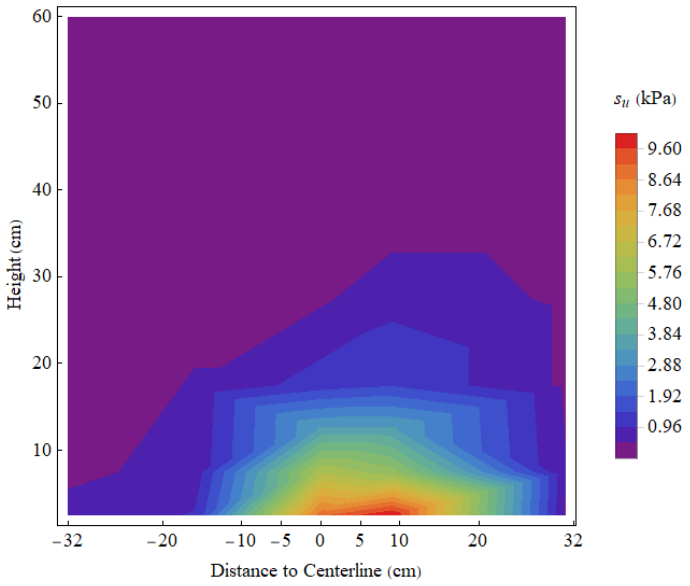

(a) Section A (Maximum undrained shear strength: 10.13 kPa)

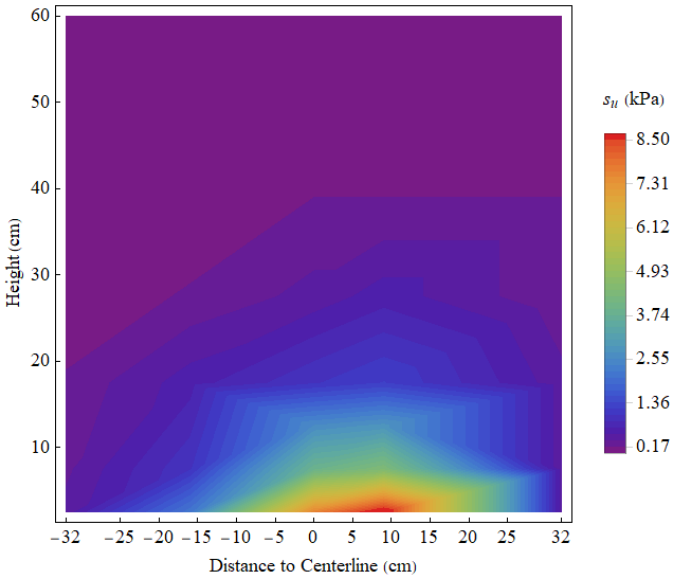

(b) Section B (Maximum undrained shear strength: 9.00 kPa)

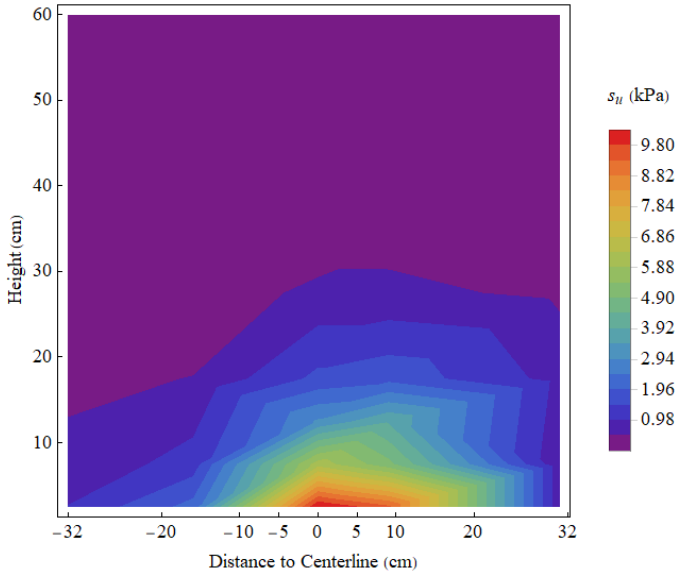

(c) Section C (Maximum undrained shear strength: 10.35 kPa)

Figure 4.25 Undrained shear strength for Model test 1 after testing: (a) Section A; (b) Section B and (c) Section C

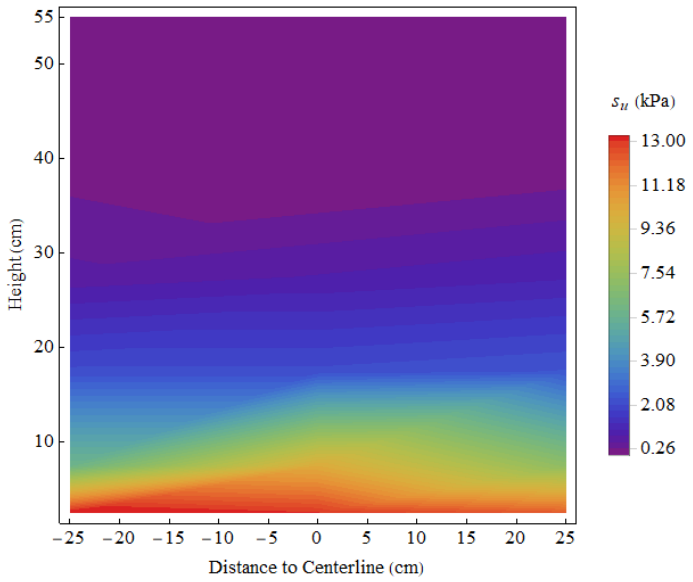

(a) Section A (Maximum undrained shear strength: 13.50 kPa)

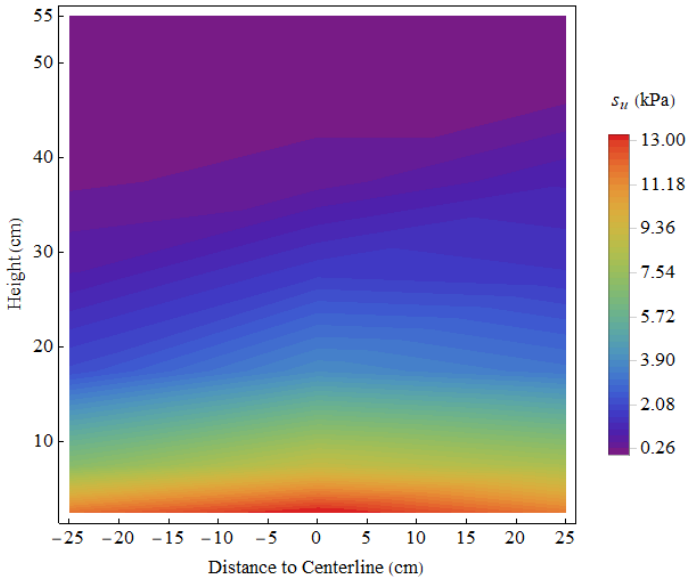

(b) Section B (Maximum undrained shear strength: 13.50 kPa)

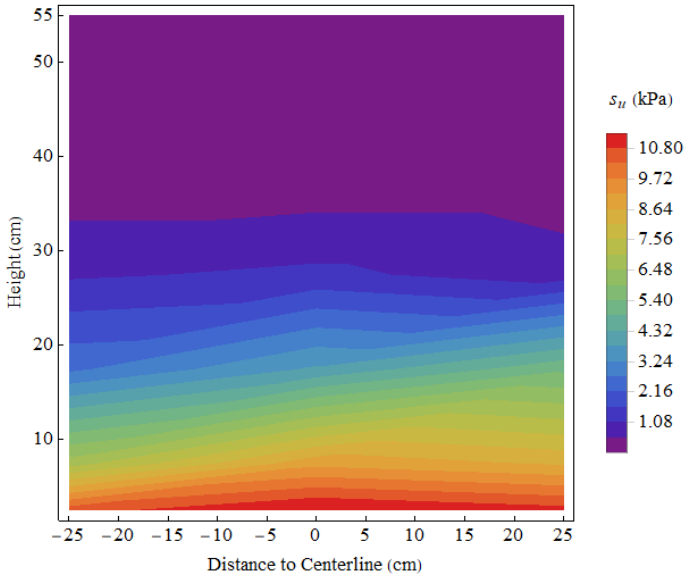

(c) Section C (Maximum undrained shear strength: 11.48 kPa)

Figure 4.26 Undrained shear strength for Model test 2 after testing: (a) Section A; (b) Section B and (c) Section C

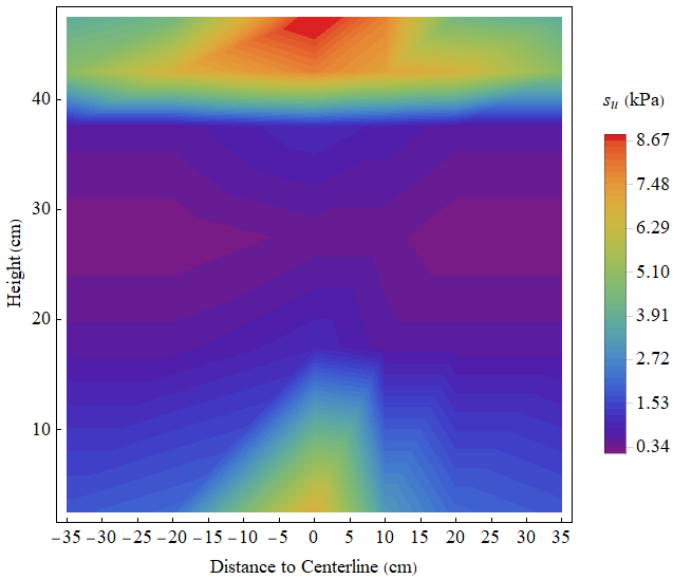

(a) Section A (Maximum undrained shear strength: 9.23 kPa)

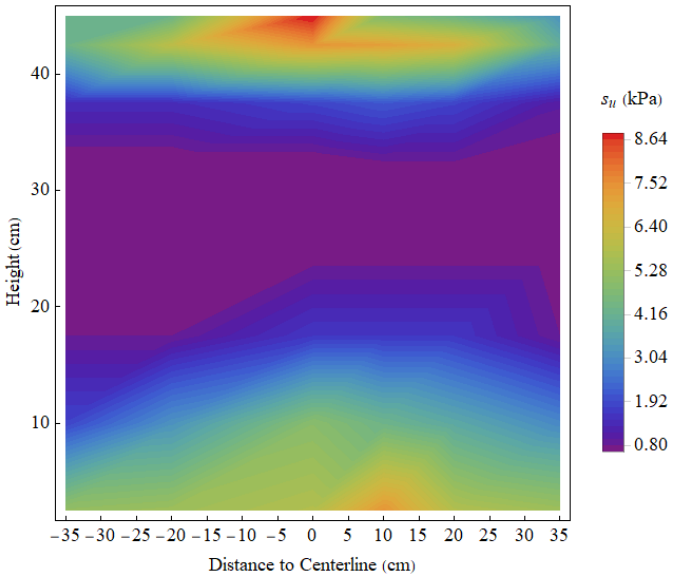

(b) Section B (Maximum undrained shear strength: 9.00 kPa)

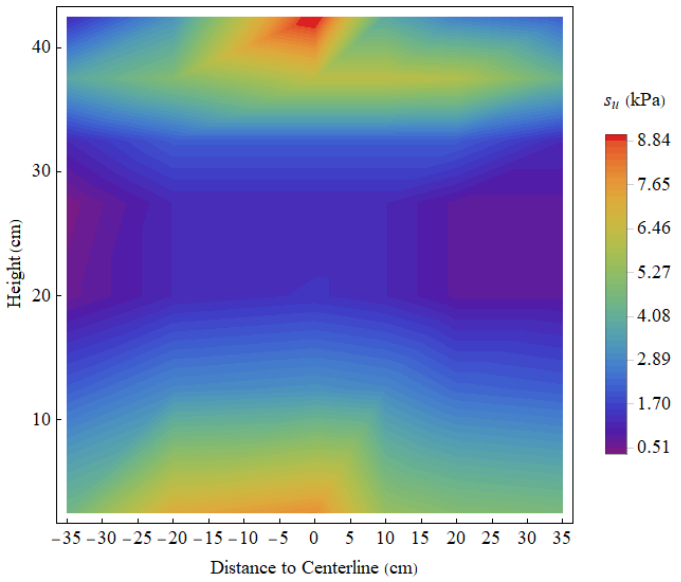

(c) Section C (Maximum undrained shear strength: 9.45 kPa)

Figure 4.27 Undrained shear strength for Model test 3 after testing: (a) Section A; (b) Section B and (c) Section C

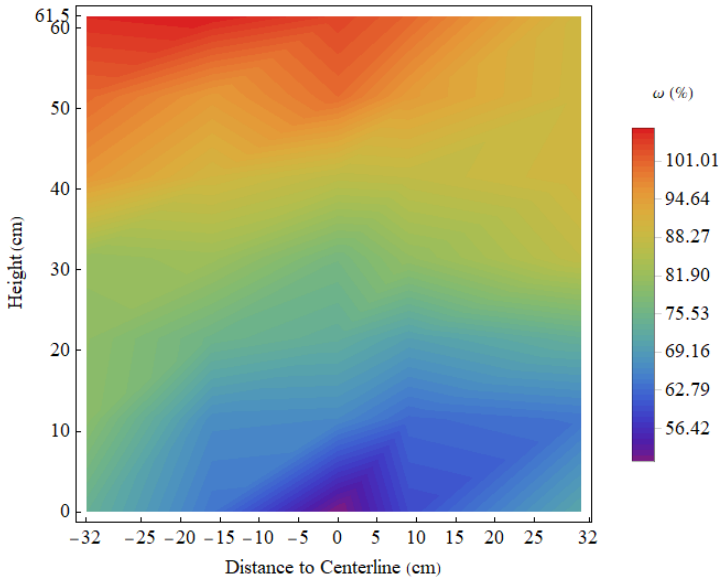

(a) Section A (Minimum water content: 49.2%)

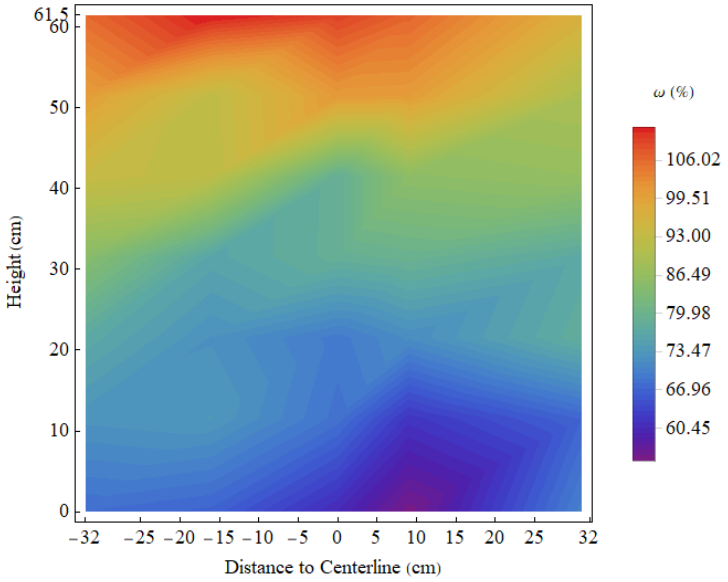

(b) Section B (Minimum water content: 55.2%)

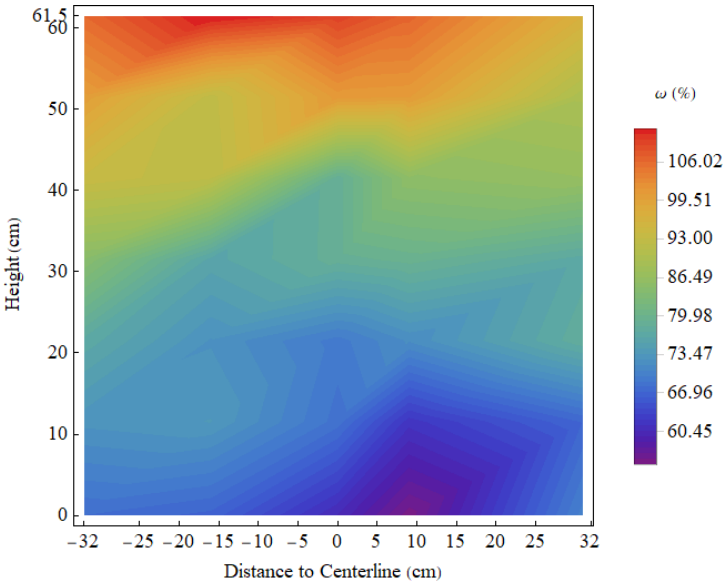

(c) Section C (Minimum water content: 52.5%)

Figure 4.28 Water content for Model test 1 after testing: (a) Section A; (b) Section B and (c) Section C

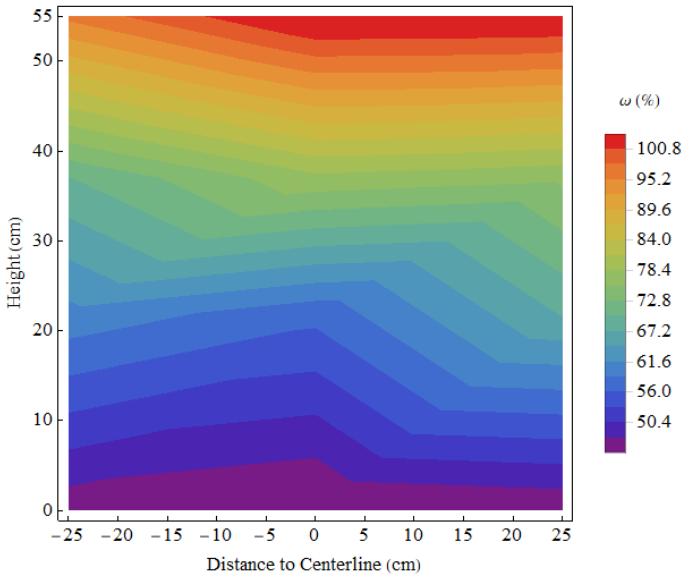

(a) Section A (Minimum water content: 44.2%)

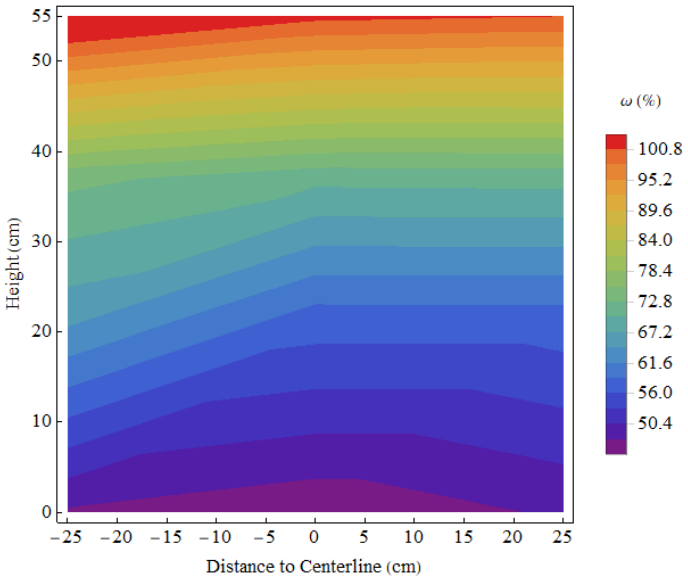

(b) Section B (Minimum water content: 45.5%)

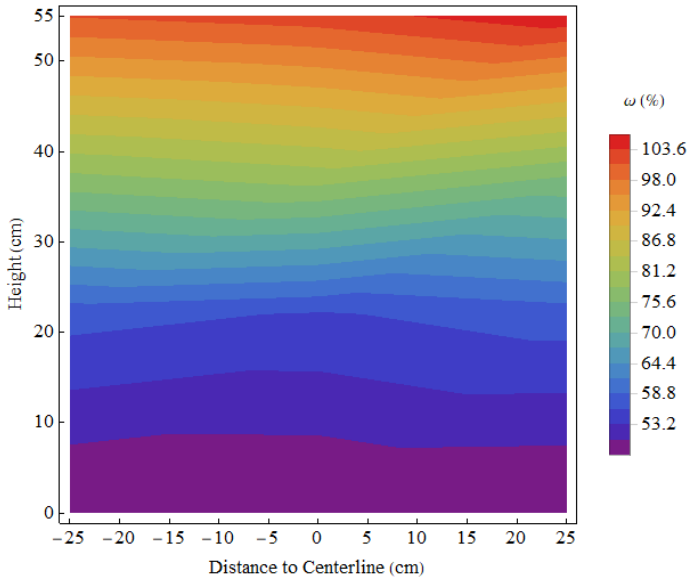

(c) Section C (Minimum water content: 46.8%)

Figure 4.29 Water content for Model test 2 after testing: (a) Section A; (b) Section B and (c) Section C

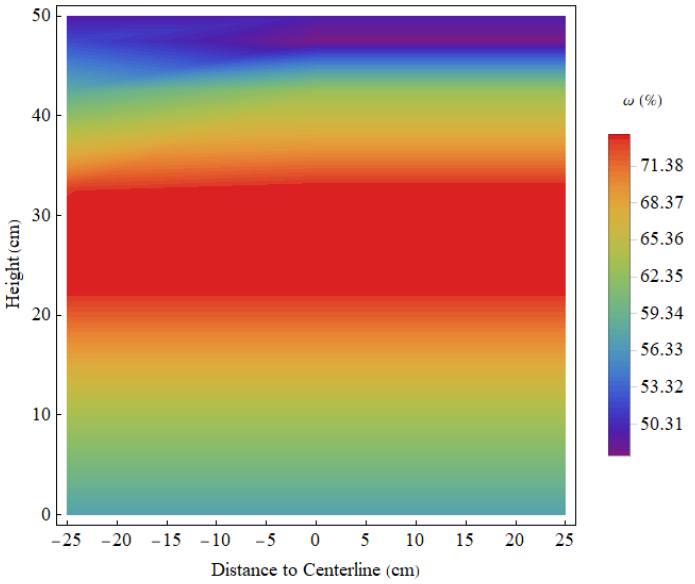

(a) Section A (Minimum water content: 45.3%)

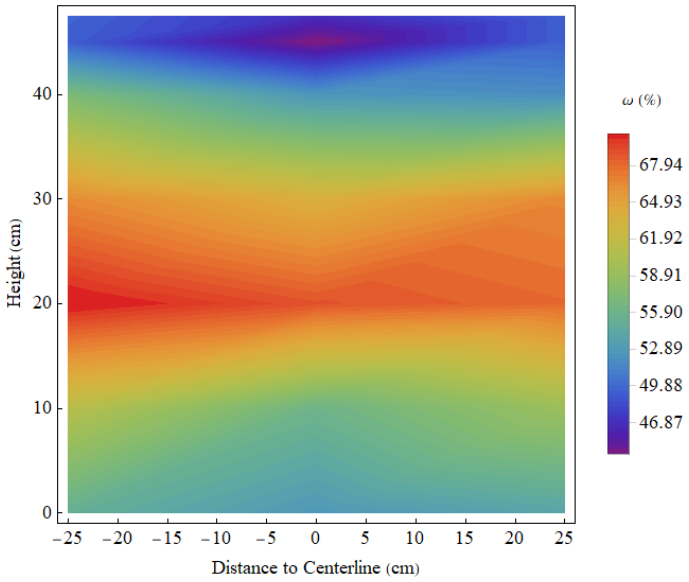

(b) Section B (Minimum water content: 46.7%)

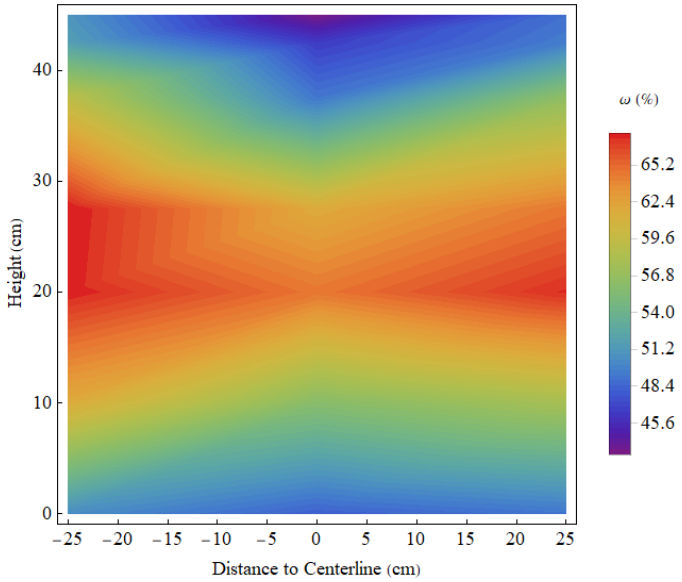

(c) Section C (Minimum water content: 43.3%)

Figure 4.30 Water content for Model test 3 after testing: (a) Section A; (b) Section B and (c) Section C

4.5 Relationships of effective stress, void ratio and undrained shear strength

For fully saturated soft marine clay, the reductions in the average void ratio were 0.94, 1.03 and 1.33, respectively, as calculated using the measured water content. These change in void ratios can be converted into average settlements of 18.1, 19.4 and 24.6

cm, respectively, for Model tests 1 to 3. These values are consistent with the measured average settlements of 18.4, 18.7 and 24.2 cm for Model tests 1 to 3, respectively.

Table 4.4 Comparison of the measured and calculated average settlement

Model test	Reduction of void ratio, Δe_{avg}	Average settlement measured, s_m (cm)	Calculated settlement using water content, s_ω (cm)
1	0.94	18.4	18.1
2	1.03	18.7	19.4
3	1.33	24.6	24.2

The plot of water content versus undrained shear strength obtained from lab vane shear tests is shown in Figure 4.31. The soil was over-consolidated as the vane shear tests were carried out after the removal of vacuum. The data points can be fitted into a curve. The point where the undrained shear strength reduced to almost zero was at the liquid limit. Some unconfined compression (UC) tests were also carried out on samples collected near the drain or HDeG sheet as shown in Figure 4.32. The UC strength data agreed well with the vane shar data although the UC data are slightly lower than that of vane shear data, which should be due to the unloading and slightly disturbance of soil during collecting and sampling. In terms of saturated soil, the water content and void ratio are equivalent. Therefore, a unique relationship between the void ratio and undrained shear strength was obtained.

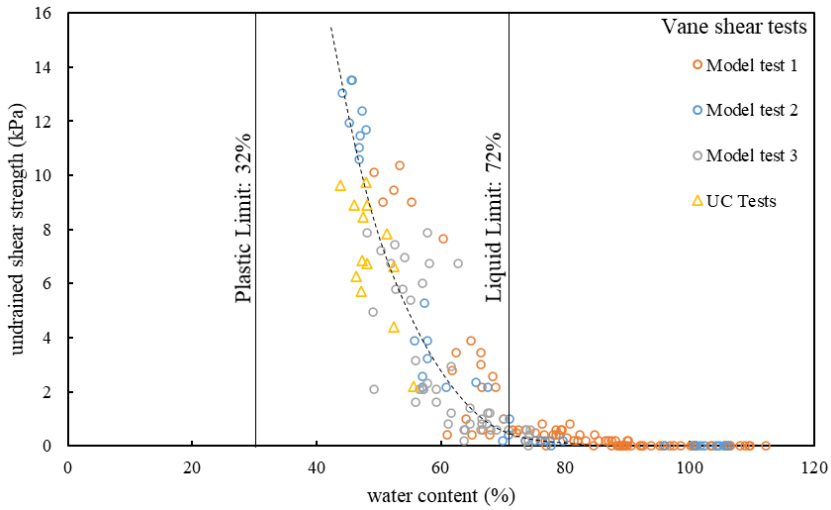

Figure 4.31 Relationship of water content and undrained shear strength for soil after consolidation

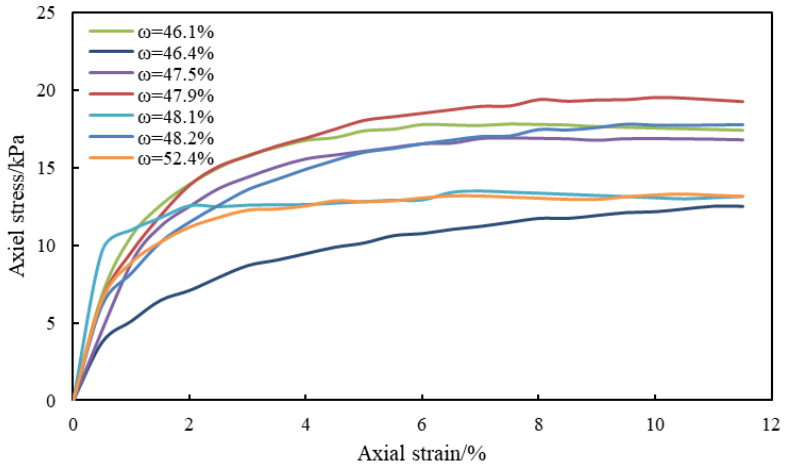

Figure 4.32 unconfined compression tests

The void ratio calculated using the measured water content and the corresponding effective stress calculated using the measured pore pressure are plotted in Figure 4.33 with the compression curves from Oedometer and Consolidometer tests. Good agreement is achieved although the void ratio data are slightly above the compression curves which could be due to unloading.

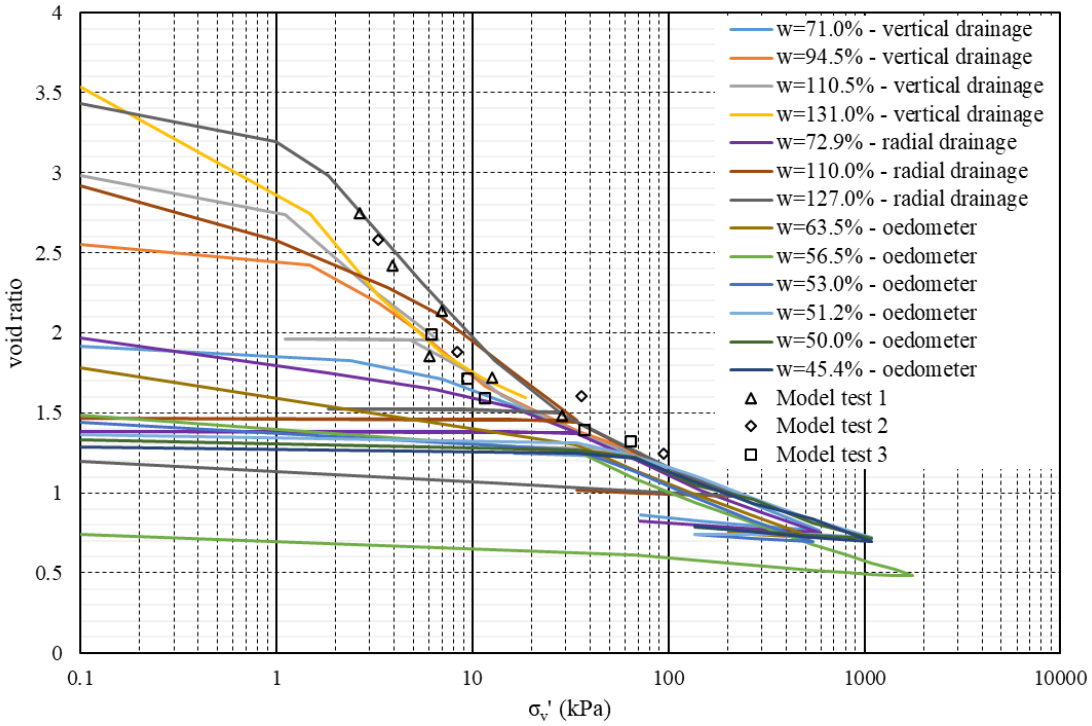

Figure 4.33 Calculated void ratio and effective stress of model tests

4.6 Degree of consolidation

As the horizontal drain sheet was placed at bottom of model tank only for Model tests 1 and 2. So these two models were comparable. And as the top and bottom boundary were both the pervious boundary for Model tests 2 and 3. So the Model tests 2 and 3 were also comparable (Craig, 2004).

Based on Asoka's method (1978), the ultimate settlements of three model tests are 29.0, 26.8 and 33.2 cm as shown in Figure 4.34. The degree of consolidation based on settlement was calculated using the average settlement and the ultimate settlements of three model tests. The degree of consolidation based on excess pore water pressure was calculated using the distributions of excess pore water pressure and linear interpolation method as in Figure 4.22 to Figure 4.24. Due to the limit measurement data of pore water pressure, the degree of consolidation based on pore water pressure was overestimated.

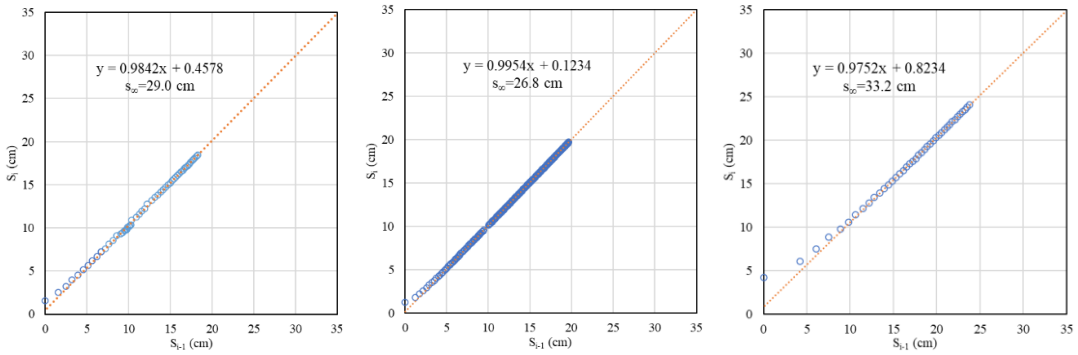

(a) Model test 1 (b) Model test 2 (c) Model test 3

Figure 4.34 Ultimate settlement using Asoka's method

The values of degree of consolidation calculated based on both settlements and pore water pressure distributions for the three model tests are shown in Figure 4.35 and Table 4.5. For the same duration, the degree of consolidation of Model tests 2 and 3 are larger than that of Model test 1 and the degree of consolidation of Model test 2 is larger than that of Model test 3. Therefore, the HDeG sheet with good transmissivity is more feasible to be used as horizontal drain for vacuum consolidation of soft clay. The degree of consolidation based on the excess pore water pressure was lower than that based on settlement in Model tests 1 and 3. That may because the non-linear compressibility and the calculation using few data points of measured pore water pressure. However, for Model test 2, the degree of consolidation based on two methods were close. That may

because the uniform vacuum drainage boundary and double drainage condition. Further discussion about the difference of degree of consolidation based on pore water pressure and settlement will presented in Chapter 6.

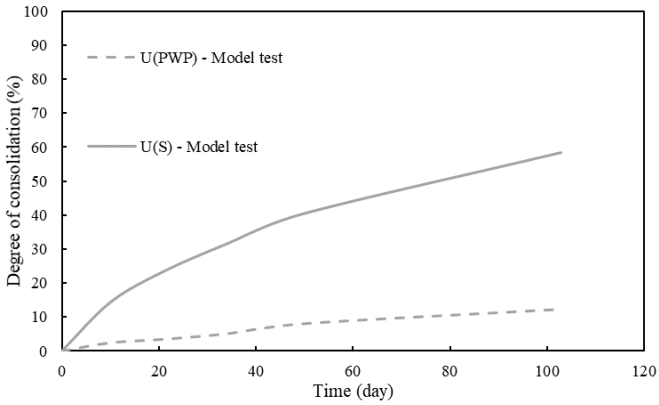

(a) Model test 1

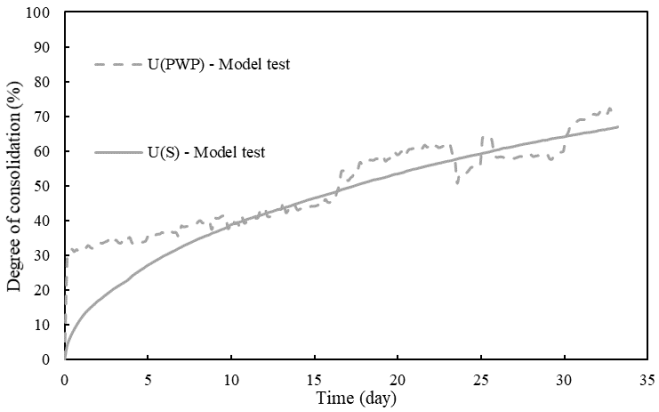

(b) Model test 2

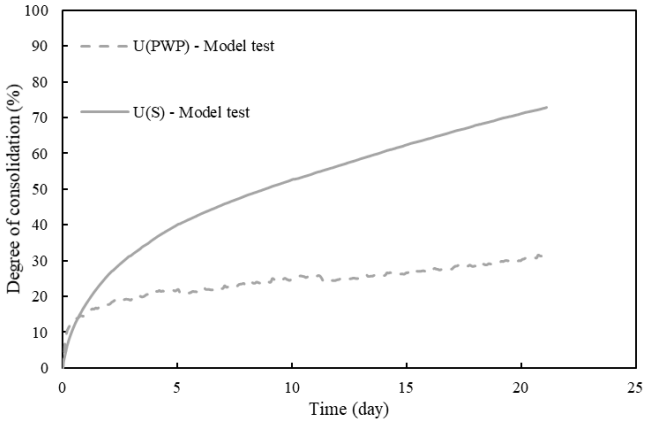

(c) Model test 3

Figure 4.35 Degree of consolidation: (a) Model test 1; (b) Model test 2 and (c) Model test 3

Table 4.5 Degree of consolidation of three model tests at some days

Model test	Day / Method	10th	21st	31st	50th	103rd
1	Settlement	15.2%	24.7%	33.3%	42.8%	61.7%
	Pore water pressure	2.4%	3.5%	5.1%	8.0%	12.2%
2	Settlement	40.9%	58.1%	70.3%	---	---
	Pore water pressure	41.0%	59.6%	69.0%	---	---
3	Settlement	52.6%	72.4%	---	---	---
	Pore water pressure	22.5%	28.0%	---	---	---

4.7 Performance of HDeG sheet

To compare the performance of different horizontal drains, the distribution of excess pore water pressure at horizontal drain level after 21 days are shown in Figure 4.36. The excess pore water pressure at drain was set as -85 kPa for Model tests 1 and 3 and -95 kPa for Model test 2.

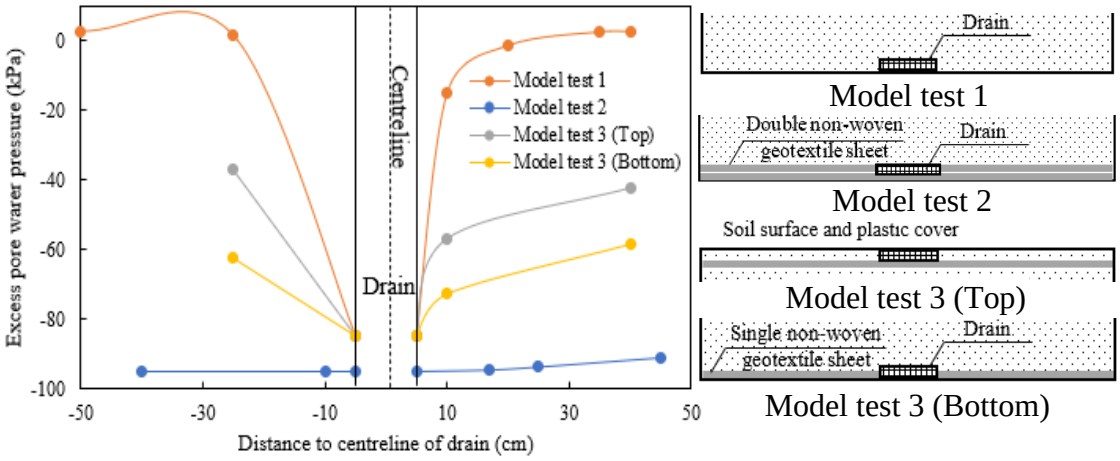

Figure 4.36 Distribution of excess pore pressure at horizontal drain level

In Model test 1 and 3, the excess pore water pressure was reduced largely from the single drain (Model test 1) or double drains (Model test 3) in the HDeG sheet. In Model test 3, the negative excess pore-water pressure at the bottom HDeG was larger than that on the top HDeG (Figure 4.36). This was because 5 cm of soft marine clay was placed on top of the HDeG to cover the transducers on the non-woven geotextile. Because of the use

of double non-woven geotextile sheets, the excess pore pressure on HDeG in Model Test 2 was almost uniform with values from -91 kPa to -95 kPa.

At the end of testing, the water content and undrained shear strength of treated soil near the bottom horizontal drains in Section C (See Figure 4.17) are shown in Figure 4.37 and Figure 4.38 for all three model tests. It can be seen that the water content of treated soil near the bottom horizontal drains in Model test 1 varied from 50 to 70%. In Model tests 2 and 3 with the use of non-woven geotextile, the water contents were more uniform ranging from 44 to 46 % for Model test 2 and from 48 to 51 % for Model test 3.

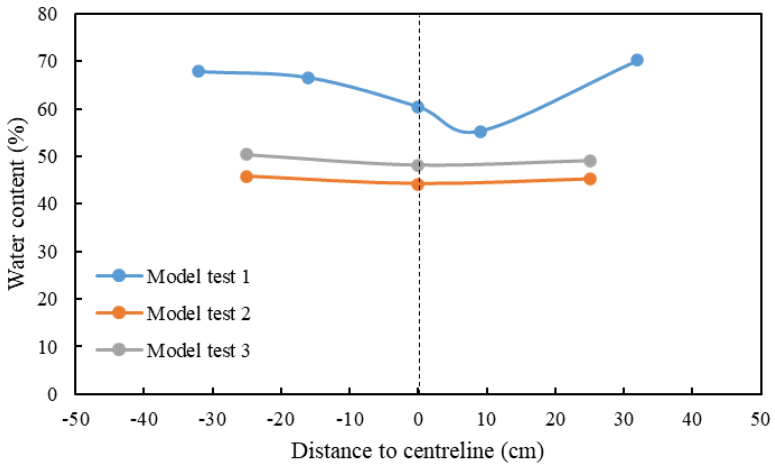

Figure 4.37 Water content for the treated soil at the bottom

Compared with Model test 1, the undrained shear strength of Model test 2 and 3 near the bottom HDeG sheet was larger and more uniform as shown in Figure 4.38. The formula as in Figure 4.38 (Bo et al., 2003b; Chang et al., 2001) to calculate the undrained shear strength, s_u, was also used to predict the undrained shear strength of the soil using vertical effective stress, σ'_v, and the over-consolidation ratio, OCR. After the testing, the average unit weight of treated clay was calculated using the measured water content in terms of fully saturated clay. The vertical effective stress was calculated using the average unit weight of treated soil and the depth. The treated soil was over-consolidated after the removal of vacuum. The pre-consolidation pressure of treated soil was calculated using initial stress and the measured pore water pressure in soil near the bottom horizontal drain. The predicted undrained shear strength values agree rather well with those measured by the lab vane shear tests.

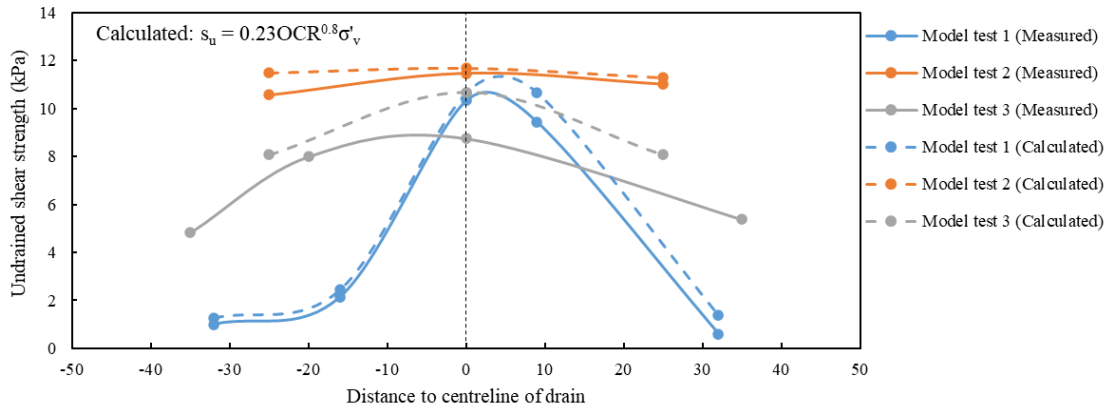

Figure 4.38 Measured and calculated undrained shear strength for the adjacent soil near the bottom horizontal drain

To conclude, the performance of HDeG can be considerably affected by the transmissivity of geotextile. Therefore, geotextile is an important component in the HDeG and its function is as important as the drains and the properties of the geotextile need to be properly selected. As shown by the model tests so far, transmissivity of geotextile is an important factor and a geotextile with a high transmissivity should be used. For this reason, non-woven geotextile is better to be used for HDeG sheet. As transmissivity of geotextile is an important property, how to measure transmissivity reliably became a topic studied in this project.

4.8 Transmissivity of non-woven geotextile in soft marine clay

The function of the non-woven geotextile on HDeG sheet is to provide a drainage boundary. Due to the clogging of non-woven geotextile in soft clay with a large amount of fine-grained particles, the transmissivity of non-woven geotextile in soft clay should be much lower than the transmissivity of geotextile without clay (Koerner and Sankey, 1982; Chai and Miura, 2002). A method was proposed in this study to measure the transmissivity of non-woven geotextile in soft clay under different consolidation pressures. This method is introduced in the following.

4.8.1 Test procedure

The device to measure the transmissivity of non-woven geotextile in soft marine clay is shown in Figure 4.39. This device was modified from a device for discharge capacity measurement (Chu et al. 2004). Tencate TS10 non-woven geotextile was used for the

tests. The transmissivity of a non-woven geotextile sheet was measured first without soil. The effective dimension of the non-woven geotextile was 8 cm in width and 8 cm in length. The non-woven geotextile was saturated in distilled water and placed in vacuum chamber under a vacuum of -85 kPa for three days. Two rubbers were placed above and below the non-woven geotextile sample without air bubble. To compare with the parameters from supplier, three normal stress, 20, 50 and 100 kPa were applied on the sample. A constant head method with a hydraulic gradient of 1.0 and a falling head method were used to measure the transmissivity of the non-woven geotextile.

The transmissivity of the same non-woven geotextile sheets in soft marine clay was also measured. The soft marine clay was placed below and above the non-woven geotextile. As the dimension of the container for soft marine clay below the non-woven geotextile is 8 cm in width, 8cm in length, and 8 mm in depth. The effective dimension of the non-woven geotextile in soft marine clay was also 8 cm in width and 8 cm in length. Before the test, the internal friction of loading plate in the device was measured to be 1.0 kPa which was negligible. Four different loads, 6, 20, 50, and 100 kPa, were applied to the soft marine clay for consolidation. For the first sets of tests, double non-woven geotextile sheets were tests. The initial water content, ω_o, of the soft marine clay was 108.6 %. For the second sets of tests, only a single non-woven geotextile sheet was used. Three different initial water contents, ω_o, of soft marine clay were used 87.2, 108.6 and 128.4 % were used.

The soft marine clay was placed in vacuum chamber under a vacuum of -85 kPa for 8 hours to remove the air bubbles. The soft marine clay was placed in the device with effort to avoid trapping of air bubbles. Two steel plates wrapped with rubber membrane was placed on the outflow and inflow to support the top soft marine clay. The top soft marine clay was up to 15 mm in thickness and wrapped with plastic film. The loading plate was placed on the plastic film and the top soft marine clay below. With the presence of the plastic film, the top and bottom boundaries of the bottom and top of soft marine clay was impermeable. The pore water only was able to be drained out through the non-woven geotextile.

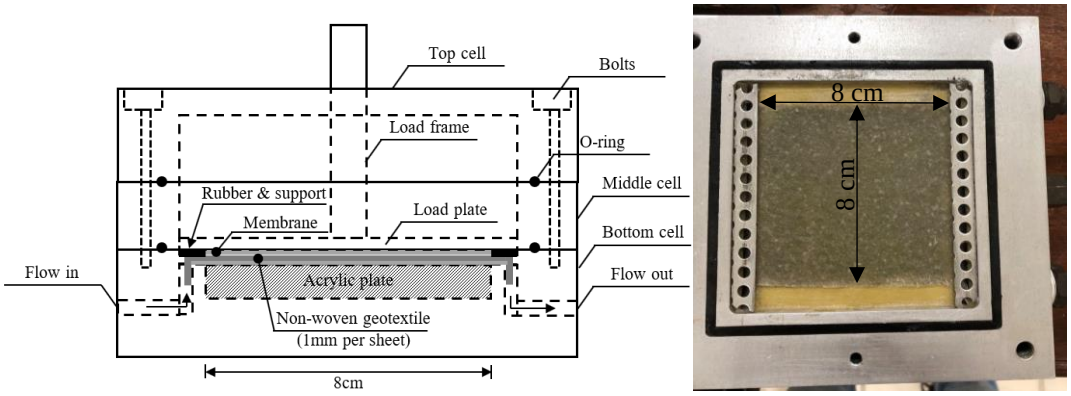

(a) Measuring the transmissivity of non-woven geotextile without soil

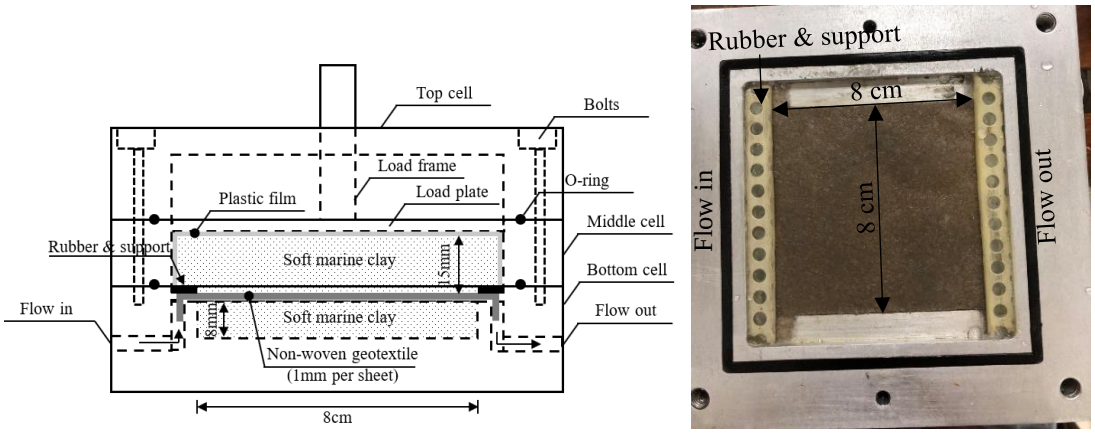

(b) Measuring the transmissivity of non-woven geotextile in soft marine clay

Figure 4.39 Test device for (a) Measuring the transmissivity of non-woven geotextile without soil and (b) Measuring the transmissivity of non-woven geotextile in soft marine clay

After more than 24 hours of consolidation, the falling head or constant head tests using distilled water were conducted to measure the transmissivity of non-woven geotextile in soft marine clay. Both constant head tests were used to measure the transmissivity for the first sets of tests with double non-woven geotextile sheets. For tests for the single non-woven geotextile sheet in soft marine clay, only falling head tests were used as the transmissivity was low. For each test, the transmissivity was measured for three times and the error of different data was less than 5%. After the tests, the true drainage length of non-woven geotextile samples in soil was measured to amend the transmissivity.

4.8.2 Test results

The measured transmissivity of non-woven geotextile without soil are shown in Figure 4.40 and compared with the values given by the supplier. The agreement is rather good although there were some differences in the measurement at 20 kPa which could be affected by other factors.

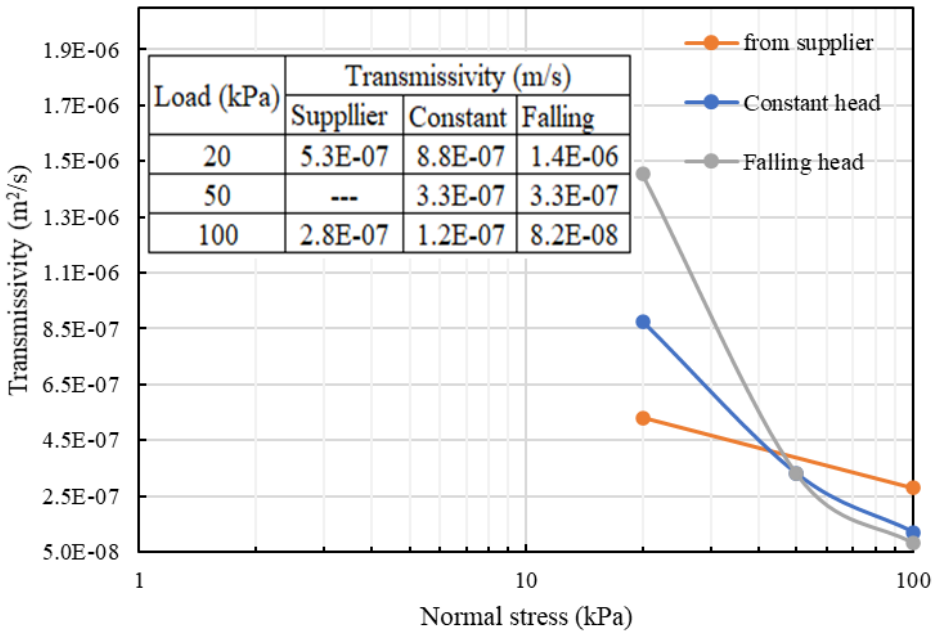

Figure 4.40 Original transmissivity of Tencate TS10 non-woven geotextile

The test results for a single non-woven geotextile sheet in soft marine clay with an initial water content of 108.6% are shown in Figure 4.41. For a transmissivity test at a given initial load, the trendline of the measured transmissivity was close to linear in a semi-log plot shown in Figure 4.41. For the data sets at different initial loads shown in Figure 4.42, the trendline was close to power function. The testing data show that the transmissivity of geotextile is affected by the soil in which the geotextile is embedded. As the transmissivity is also affected by the loads applied, the transmissivity of non-woven geotextile should be measured or specified for different soils and at different loads when the values are to be used for the design for consolidation using HDeG sheet.

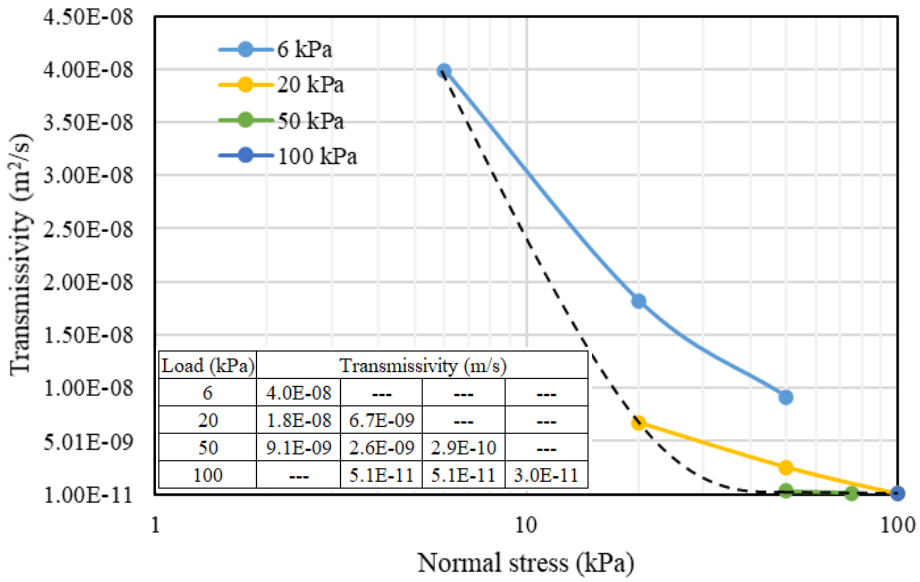

Load (kPa)	Transmissivity (m/s)			
6	4.0E-08	---	---	---
20	1.8E-08	6.7E-09	---	---
50	9.1E-09	2.6E-09	2.9E-10	---
100	---	5.1E-11	5.1E-11	3.0E-11

Figure 4.41 Transmissivity in soft soil with 108.6% of initial water content at different initial normal stress

The testing results of two sets of tests at different initial loads are shown in Figure 4.42. With decreasing in the initial water content, the transmissivity of non-woven geotextile in soft marine clay at a specific initial load was increased. But for initial water contents of 108.6 and 128.4%, the transmissivity in soft marine clay was close. Thus, when the initial void ratio was larger than 3.0, the transmissivity of non-woven geotextile in soft marine clay was close and the same fitting curve or formula could be used. As the thickness of a single sheet was less than 1 mm, the in-plane permeability of single non-woven geotextile in soft marine clay was close to that of fine sand.

The transmissivity of double non-woven geotextile sheets at different initial loads was also measured using constant head and falling head tests. The transmissivity measured using either constant head or falling head tests were close. Similar to the results of a single non-woven geotextile sheet, the trendline was close to power function. The transmissivity of double non-woven geotextile sheets in soft marine clay was much larger than that of a single sheet. As the thickness of double sheet is less than 2 mm under loading, the in-plane permeability of double non-woven geotextile sheets in soft marine clay is close to that of medium sand.

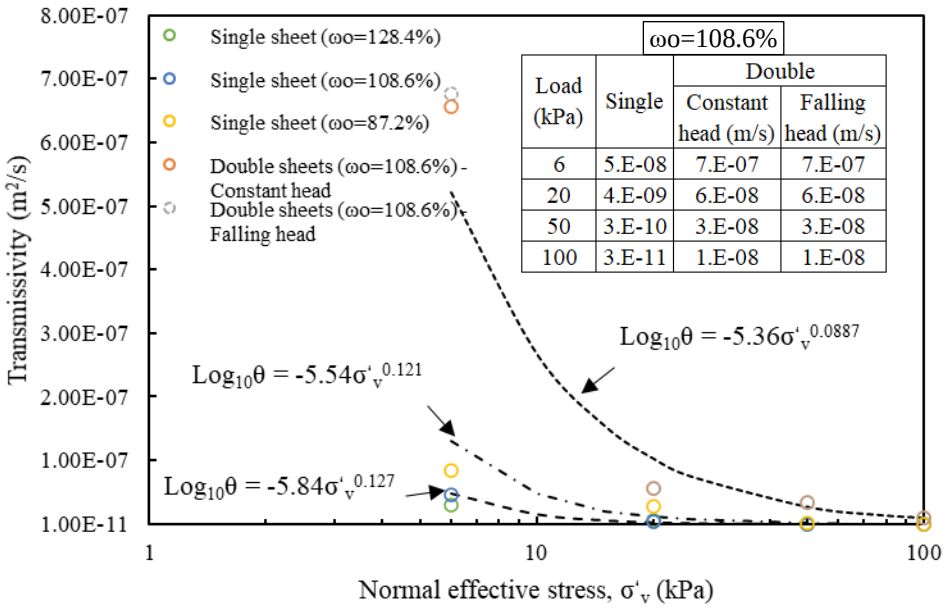

ωo=108.6%

Load (kPa)	Single	Double	
		Constant head (m/s)	Falling head (m/s)
6	5.E-08	7.E-07	7.E-07
20	4.E-09	6.E-08	6.E-08
50	3.E-10	3.E-08	3.E-08
100	3.E-11	1.E-08	1.E-08

Figure 4.42 Transmissivity of non-woven geotextile in soft marine clay (ω_o: Initial water content)

4.9 Enhancement of vacuum consolidation using HDeG sheet

To investigate the effect of the transmissivity of geotextile on the distribution of pore water pressure along the HDeG, some more laboratory tests were conducted using HDeG sheet with non-woven geotextile sheets.

4.9.1 Test procedure

Four trial tests were conducted using HDeG sheet with single or double non-woven geotextile. The drain was modified into 3 cm in width and bonded with single or double non-woven geotextile sheets as shown in Figure 4.43. A small plastic box, 30 cm in width, 20 cm in depth and 50 cm in length, was used as the testing tank. Two pore-water pressure transducers (PPTs) were placed on the HDeG sheet. A high-water content slurry with an initial water conte nt of 120% was used. The thickness of the slurry in the box was 25 mm.

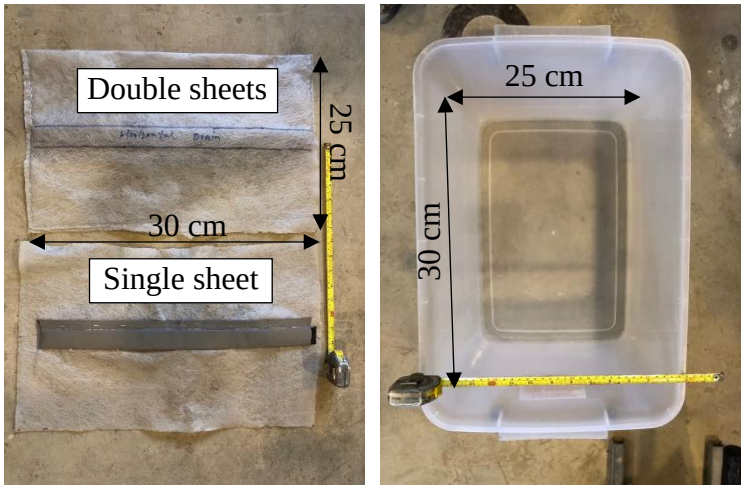

Figure 4.43 Horizontal drainage enhanced geotextile sheets and test tank

The configuration of the Trial tests is shown in Figure 4.44. In Trial test 1, the HDeG sheet with double non-woven geotextile sheets was used and placed at the middle of slurry. In Trial test 2, 3 and 4, the HDeG sheet with single non-woven geotextile sheet was used. In Trial test 2, the HDeG sheet was at the middle of slurry. In Trial test 3, the HDeG sheet was at the bottom of tank. In Trial test 4, a part of non-woven geotextile was cut off as shown in Figure 4.44(d). The four tests were operating in a few hours. The vacuum pressure in drain was read about -85 kPa.

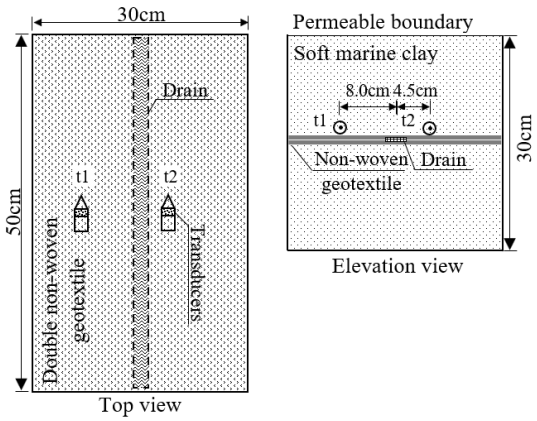

(a) Trial test 1

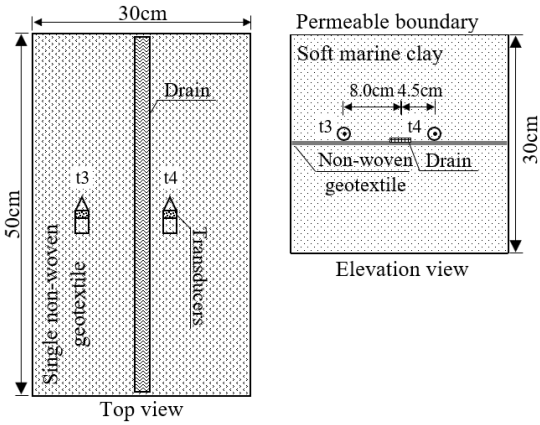

(b) Trial test 2

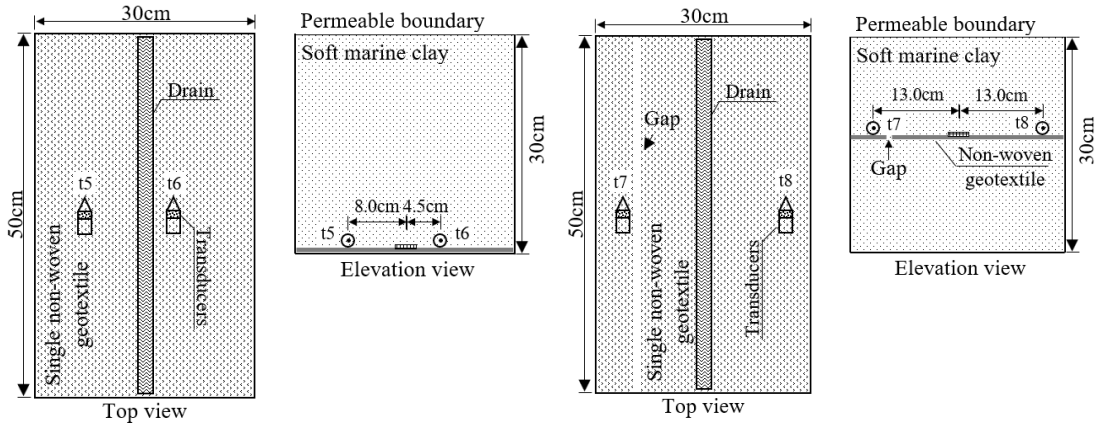

(c) Trial test 3 (d) Trial test 4

Figure 4.44 Schematic illustration of trial tests: (a) Trial test 1; (b) Trial test 2; (c) Trial test 3 and (d) Trial test 4

4.9.2 Test results

The pore water pressures of transducers are shown in Figure 4.45. By using HDeG sheet with double non-woven geotextile in Trial test 1, the pore water pressure at different locations on non-woven geotextile sheets were almost same and reduced quickly to about -50 kPa after the vacuum added due to the large transmissivity. When the HDeG sheet with single non-woven geotextile was at the bottom of tank as in Trial test 3, the pore water pressures from two transducers reduced quickly and were almost the same as that from test 1. That may because there was no slurry below the non-woven geotextile in Trial test 3 and the non-woven geotextile was partly clogged. In Trial test 2, the reduction of pore water pressure depended on the distance to drain. As the increase of distance to drain, the reduction of pore water pressure decreased. In Trial test 4, two transducers were at same distance to drain. But there was one gap on non-woven geotextile sheet between one of transducers and drain. The pore water pressure at gap side didn't change. Thus, the non-woven geotextile bonded with prefabricated drain was able to transmit the pore water pressure induced by vacuum pressure. Moreover, the transmissivity of non-woven geotextile has a great effect on the performance of horizontal drainage enhanced geotextile sheet. With larger transmissivity, the reduction of pore water pressure on HDeG sheet was larger.

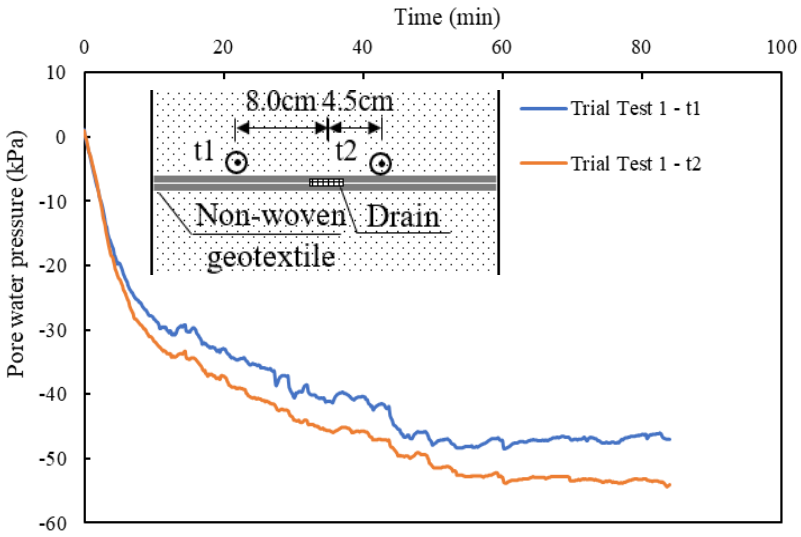

(a) HDeG sheet with double non-woven geotextile sheets

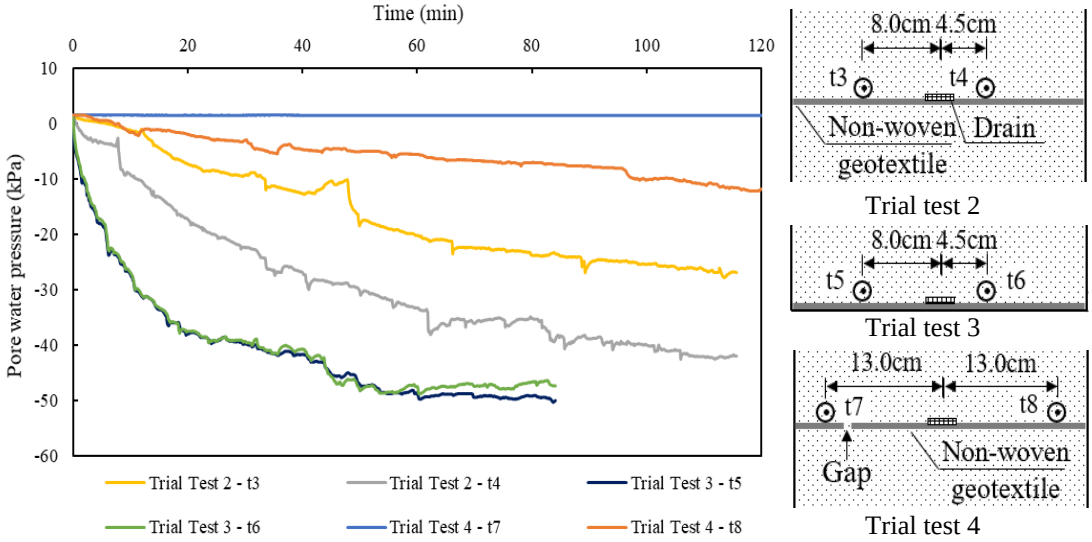

(b) HDeG sheet with single non-woven geotextile sheet

Figure 4.45 Pore water pressure of trial tests

The pore water pressure on HDeG sheet at different normalized distances in Trial tests 2 and 4 are shown in Figure 4.46. The normalized distance was the ratio of real distance to drain over the half width of drain. From Figure 4.46, the pore water pressure on HDeG sheet was reduced exponentially as the increase of normalized distance due to the relatively low transmissivity of single non-woven geotextile. As time elapsing, the reduction of excess pore water pressure on HDeG sheet increased.

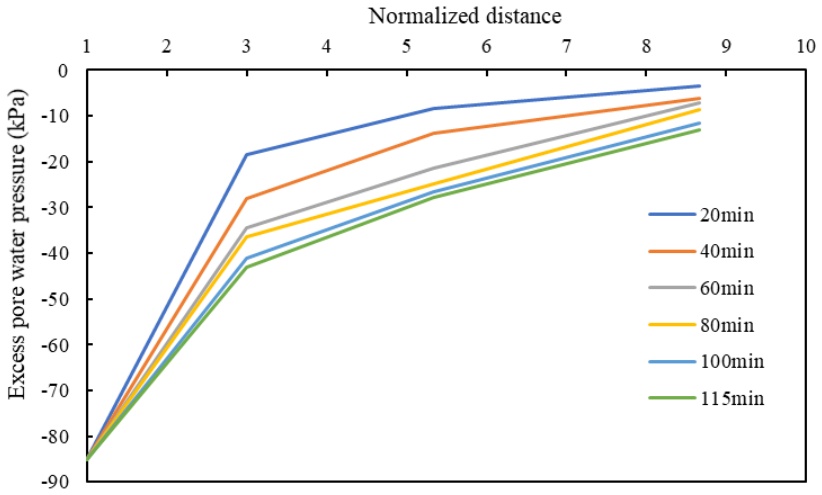

Figure 4.46 Variation of pore water pressure along with the single non-woven geotextile sheet in HDeG (Normal distance: the ratio of real distance to drain over the half width of drain)

4.10 Conclusion

In this chapter, model tests were carried out to study the consolidation behaviour of soil with the use of HDeG and vacuum pressure and to evaluate the effectiveness of HDeG for soft soil improvement. The following conclusions can be made from the study:

(1) The consolidation of soft soil using HDeG and vacuum was more effective than the use of a horizontal drain and vacuum alone. The vacuum pressure could be distributed almost uniformly across the entire HDeG with double non-woven geotextile sheets. With HDeG using a single non-woven geotextile sheet, the pore water pressure distribution along the geotextile was not uniform, but within -60 to -80 kPa and the value is reducing with time.

(2) High degree of consolidation in terms of settlement was obtained when HDeG was used with vacuum for the consolidation of soft marine clay in the model tests. One layer of HDeG with double non-woven geotextile sheets performed better than that using two layers of HDeG with single layer of non-woven geotextile. Whether one layer or two layers of non-woven geotextile is more effective in terms of both performance and cost needs further study.

(3) The transmissivity of geotextile had a significant effect on the transmission of vacuum pressure in the soil. The transmissivity of non-woven geotextile was

affected by the type of soil it embedded and the normal stress. For this reason, a method to measure the transmissivity of geotextile in soil was proposed and used in this study.

CHAPTER 5 VACUUM CONSOLIDATION OF SOFT CLAY USING HORIZONTAL DRAINAGE ENHANCED GEOTEXTILE SHEET

5.1 Introduction

As mentioned in Chapter 4, the proposed HDeG sheet could be used to consolidate the soft marine clay. For the land reclamation using horizontal drains only or HDeG sheet, the vertical spacing of the horizontal drains or HDeG sheet becomes a key design parameter. To investigate the consolidation behaviour of soft clay fill using HDeG sheet, four model tests were conducted. Different horizontal and vertical spacings of HDeG sheet were used in the model tests. The efficiency of vacuum consolidation using HDeG sheet for soft marine clay was evaluated in terms of settlement, distributions of excess pore pressure, undrained shear strength and degree of consolidation. Attempts were also made to establish relationships between effective stress, void ratio and undrained shear strength of consolidated clay.

5.2 Model tests with soft clay fill

5.2.1 Test arrangement

Much of the setup such as the vacuum pump, the vacuum chamber and the data logging system were the same as those used for the model tests described in Chapter 4. The test box used for the model tests were 0.6 m in width, 0.6 m in length and 1.5 m in height. It was made of timber plates and aluminium frame as shown in Figure 5.1. The testing arrangement for the model tests is shown in Figure 5.2. The vacuum tubes with 8 mm in diameter were used to connect the drain of 100 mm in width with the vacuum chamber. Three steel rods of 1 m in length were used to install pore pressure transducers (PPTs) at different depths. The PPTs were wrapped with non-woven geotextile and saturated in water for 24 hours before calibration or usage. Laser sensors were also used to measure the surface settlement of the soil. Double layers of plastic bags of 0.3 mm in thickness, 0.6 m in width, 0.6 m in length and 2 m in height were fitted into the test box to prevent

water leakage. The soft marine clay was prepared by mixing the wet marine clay with tap water using a large pan mixer with 0.5 L capacity as shown in Figure 5.3.

Figure 5.1 Test box

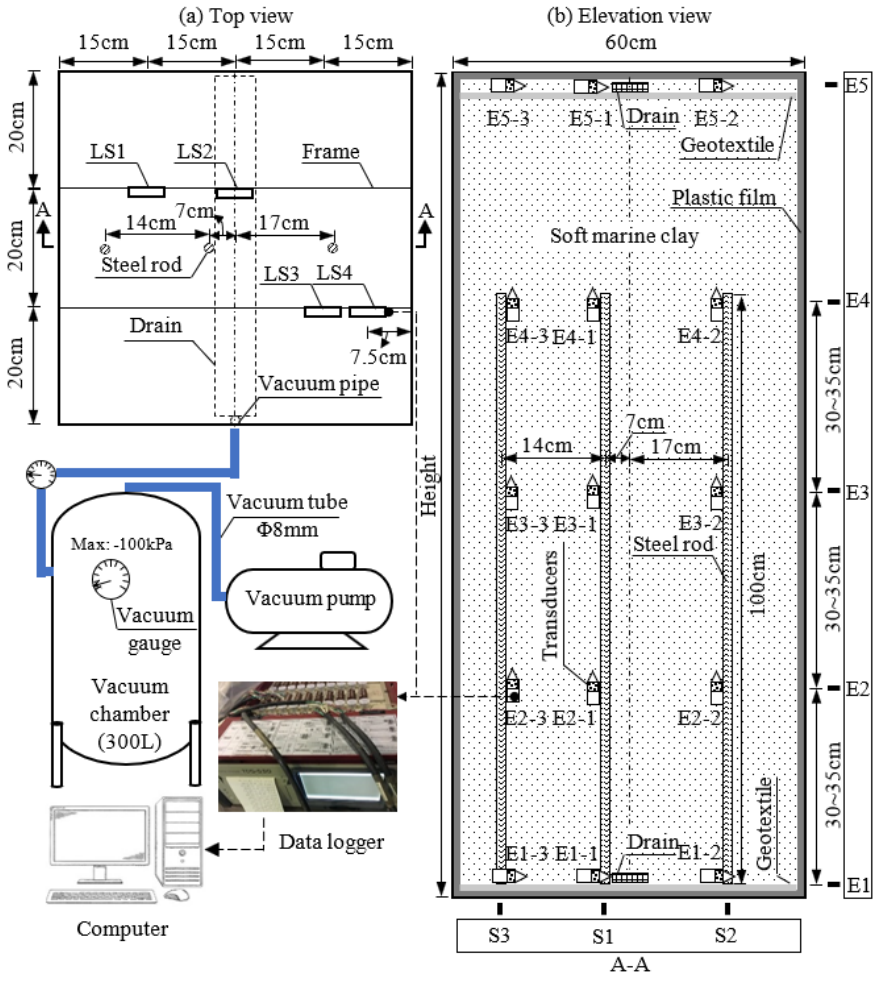

Figure 5.2 Model test arrangement: (a) Top view and (b) Elevation view

Figure 5.3 Mixed marine clay slurry used for the model tests

5.2.2 Test procedure

Four unit-cell model tests were conducted to analyse the vacuum consolidation behaviour of soft marine clay using horizontal drains. The summary of the four model tests is shown in Table 5.1. The different drains and HDeG sheet were used for model tests as shown in Figure 5.4. w is the width of drain. s_h is the horizontal spacing of the drains. s_v is the vertical spacing of the drains or HDeG sheet. The drain only was used in Model tests 4 and 5. The HDeG sheet with single non-woven geotextile was used in Model tests 6 and 7. The vacuum pressure in the vacuum chamber was controlled to -90 to -96 kPa. The vacuum degree in drain was about -85 kPa.

The PPTs were fixed on the three steel rods. The PPTs were placed at five elevations (E1, E2, E3, E4, E5) with a 0.30 m to 0.35 m of vertical interval and three steel rods with different distances to centreline, 0.07 m, 0.17 m, and 0.21 m were marked using S1 (0.07 m), S2 (0.17 m) and S3 (0.21 m) as shown in Figure 5.2. When using the drain only, the PPTs at top elevation (E5) were not available. When using HDeG sheet with non-woven geotextile, three PPTs were placed on the top non-woven geotextile sheet (at E5) and covered by a thin, soft marine clay. The initial water content of the mixed soft marine clay in all the four model tests was 120%. The soft marine clay slurry was poured into the test box along the side walls to reduce air trapped. A plastic membrane was used to cover the soil surface of the clay for sealing.

Table 5.1 Summary of four model tests

Test	Horizontal drain	Height (cm)	Water content (%)	Void Ratio	Unit weight (kN/m^3)	w/s_h	w/s_v	s_v/s_h	P_{vac} (kPa)	Duration (day)
M1	Drain only	135	120	3.23	14.1	0.083	0.037	2.25	-85	47
M2	Drain only	143	127	3.42	14.0	0.333	0.070	4.77	-85	21
M3	HDeG	145	115	3.09	14.2	0.333	0.069	4.83	-85	32
M4	HDeG	145	122	3.28	14.1	0.167	0.069	2.42	-85	52

*w: Width of prefabricated drain; s_h: Horizontal spacing of prefabricated drain; s_v: vertical spacing of HDeG sheet; P_{vac}: Vacuum pressure

*Terminated condition: 1 m of final height of consolidated soil

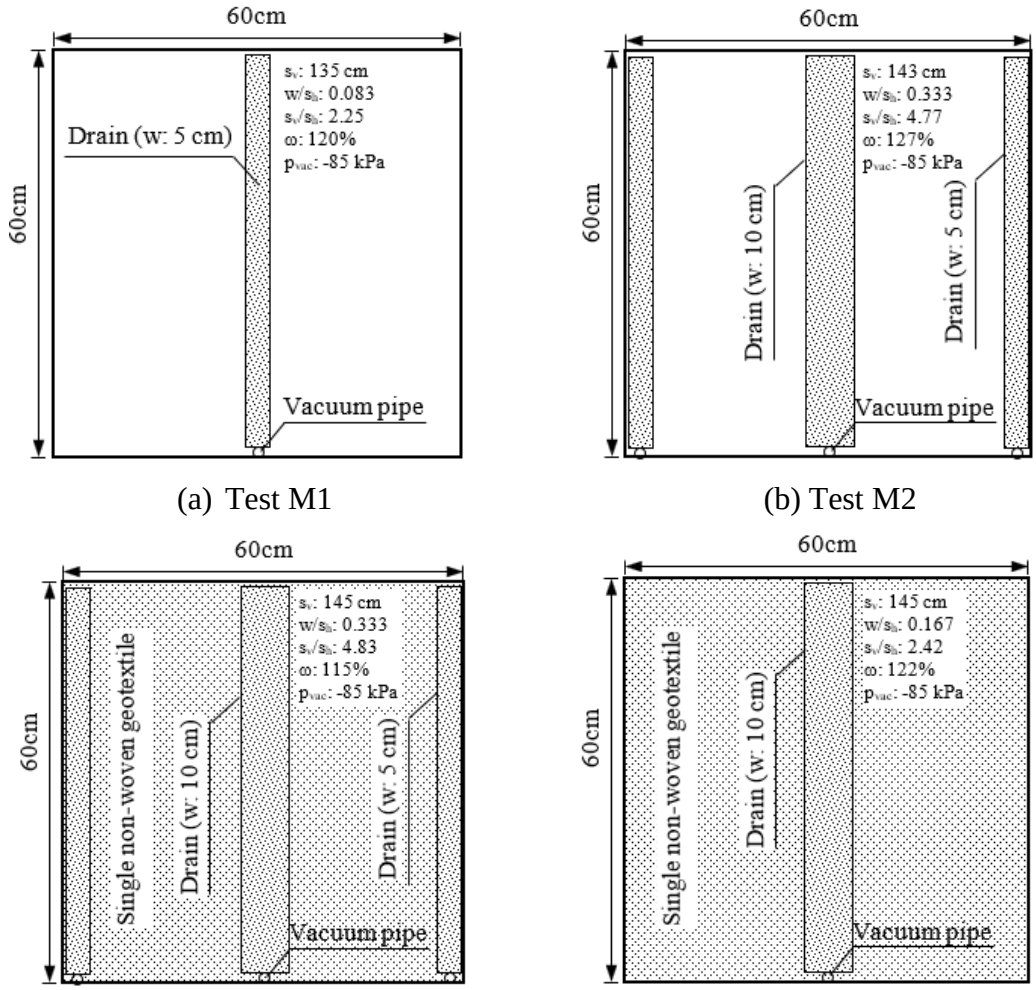

Figure 5.4 Configurations of horizontal drains in different model tests: (a) Test M1; (b) Test M2; (c) Test M3; (d) Test M4

As the steel rods was 1 m length, the maximum settlement achieved was limited by the steel rods. In order to investigate the vacuum consolidation behaviour under long-term condition, the steel rod was cut to 0.7 m in Model test 7.

After the tests, lab vane shear tests were conducted at five locations on top view as in Figure 5.5 and every 0.1 m along the height of consolidated soil. The consolidated soil was dig out every 0.1 m along the height, then the water content was measured for the soil near the five locations for vane shear tests.

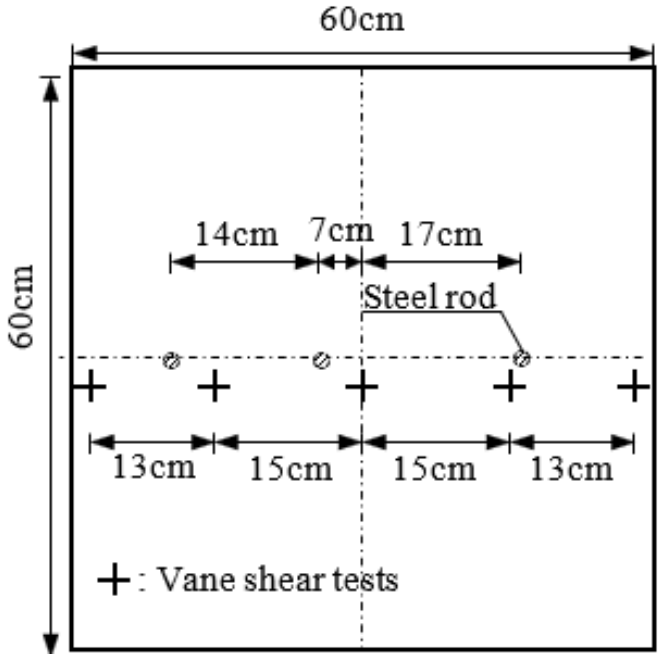

Figure 5.5 Locations of sampling for vane shear tests and water content after testing

5.3 Model tests results

5.3.1 Pore water pressure and settlement

- Test M1

Test M1 was carried out using the drain (5 cm) only, which was placed on the bottom and top of soil. The initial and final height were 1.35 m and 1.02 m, respectively. The pore pressure transducers were fixed on the steel rods at four elevations, E1, E2, E3 and E4 as in Figure 5.6.

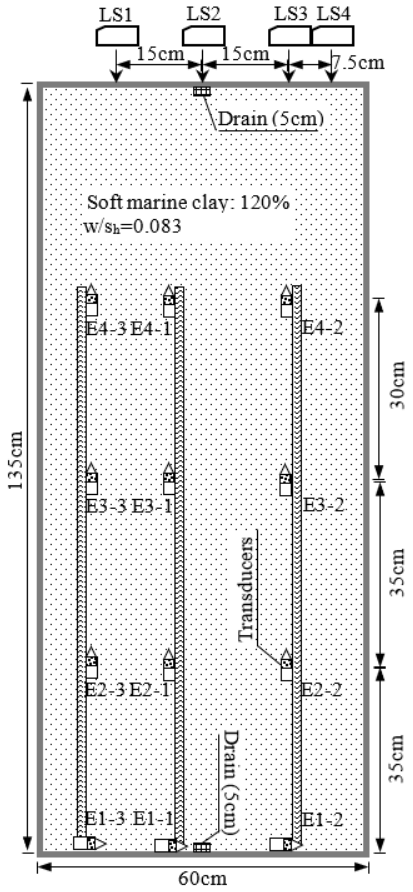

Figure 5.6 Elevation view of the pore water pressure transducers and laser sensors in Test M1

The monitoring data from Test M1 are shown in Figure 5.7. It can be seen from Figure 5.7a to 5.7d, the maximum reductions of pore water pressure were at the bottom level (E1). However, the pore water pressure acquired from transducer E1-1 was not accurate as the transducer was not functioning properly. The measured maximum reduction of pore water pressure was about 20 kPa at E1-2. As the vacuum pressure in drain was about -85 kPa, the gradient of pore water pressure from drain to E1-3 was large, which was consistent with the results of Model test 1 in Chapter 4. At 0.35 m level (E2), the final difference of pore water pressures was small, about 2 kPa, due to the large pore water pressure gradient. As the settlement increased, the distance between the E4 level and the drain reduced. Therefore, the final reduction of pore water pressure at E4-1 was larger than that of E4-2 or E4-3. At level E3 in the middle of soil, the three pore pressures changed synchronously.

To summary, the further the distance to the drain was, the more uniform the changes of the pore water pressures at same elevation were. Then the flow lines, perpendicular to the equipotential lines, were vertical at level E3.

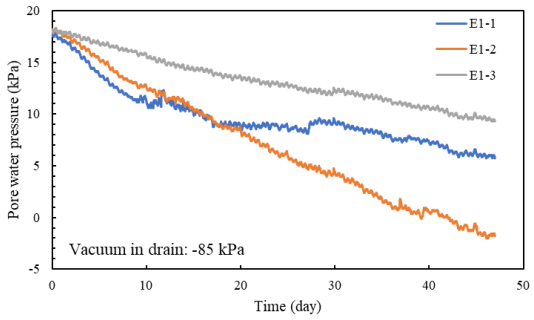

(a) Level E1 (0 m)

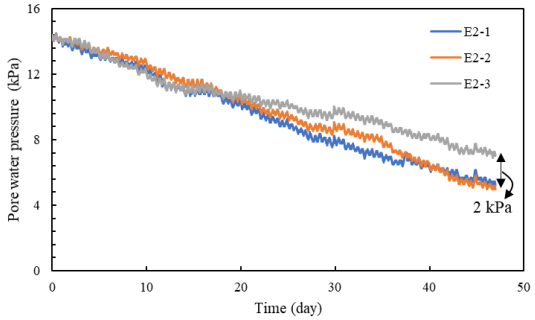

(b) Level E2 (0.35 m)

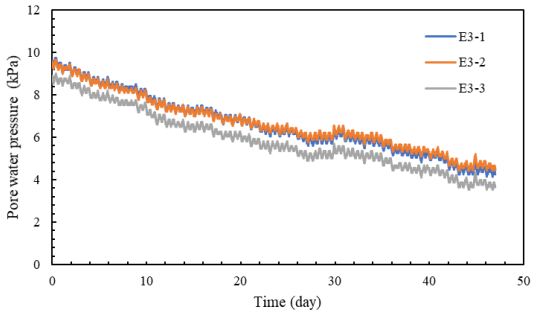

(c) Level E3 (0.70 m)

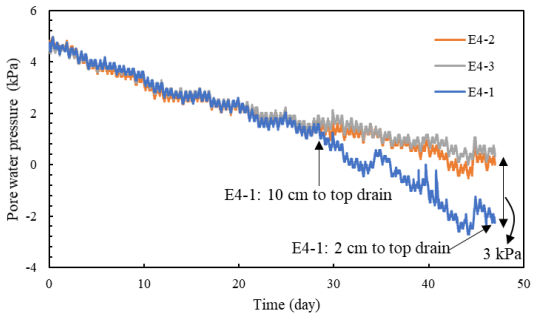

(d) Level E4 (1.00 m)

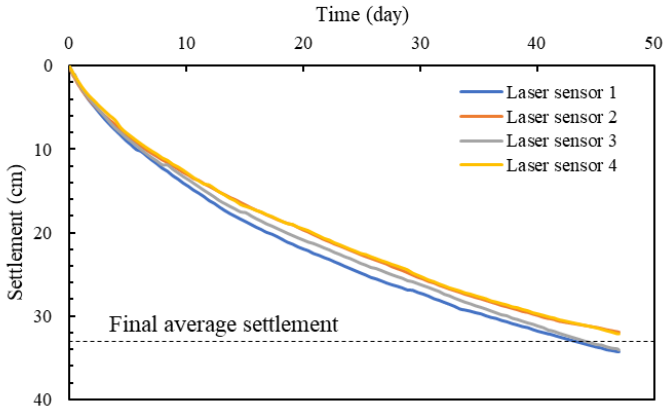

(d) Settlement

Figure 5.7 Monitoring data of Test M1: (a) Level E1 (0 m); (b) Level E2 (0.35 m); (c) Level E3 (0.70 m); (d) Level E4 (1.00 m) and (e) Settlement

- Test M2

Test M2 was also carried out using the drain only. The initial and final height were 1.43 m and 1.03 m, respectively. The pore pressure transducers were also fixed on the steel rods at four elevations, E1, E2, E3 and E4 as in Figure 5.8.

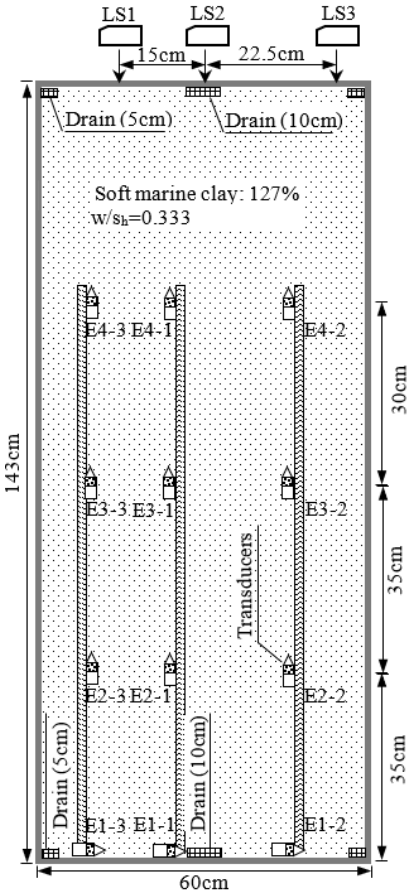

Figure 5.8 Elevation view of the pore water pressure transducers and laser sensors in Test M2

The monitoring data from Test M2 are shown in Figure 5.9. The power supply was turned off from the 9th to 10th day due to power interruption. As the drain with 5 cm in width was placed near the side of test box as in Figure 5.8, the pore water pressure at E1-3 was larger than that at E1-2 located between the prefabricated drains. The maximum reduction of pore water pressure was about 40 kPa at E1-1. The final average reductions of pore water pressure at level E2 and E4 were about 10 kPa and larger than those of Test M1 which were about 3 kPa at 21st day. This was resulted by the larger ratio of width, w, to horizontal spacing, s_h, of drains. The difference between the pore water pressures at E2 or E4 was about 1.5 kPa, which was smaller than that in Test M1.

The pore water pressure at level E3 also changed synchronously. The final average reduction of pore water pressure at level E3 was about 6 kPa which was larger than that at level E3 in Test M1 which was about 3 kPa at 21st day.

With larger ratio of width to horizontal spacing of the drain, w/s_h, of 0.333 for Test M2, the pore water pressure turned to be more uniform at the same level and the reductions of pore water pressure were larger at the same time. The flow lines were close to be vertical at E2, E3 and E4.

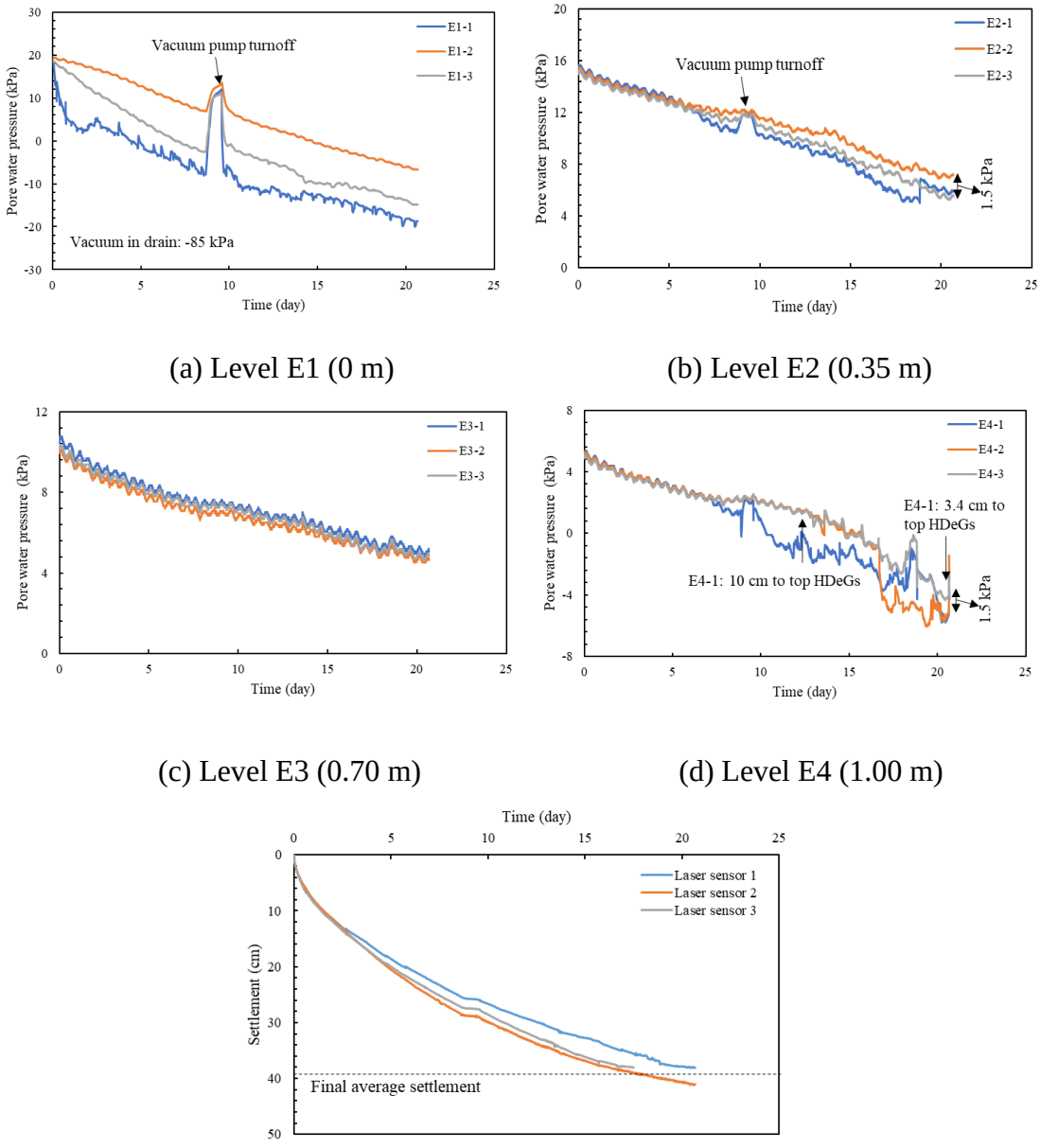

(a) Level E1 (0 m)

(b) Level E2 (0.35 m)

(c) Level E3 (0.70 m)

(d) Level E4 (1.00 m)

(e) Settlement

Figure 5.9 Monitoring data of Test M2: (a) Level E1 (0 m); (b) Level E2 (0.35 m); (c) Level E3 (0.70 m); (d) Level E4 (1.00 m) and (e) Settlement

- Test M3

Test M3 was carried out using the HDeG sheet with non-woven geotextile. The initial and final height were 1.45 m and 1.03 m, respectively. The pore pressure transducers were fixed on the steel rods at five elevations, E1, E2, E3, E4 and E5 as in Figure 5.10.

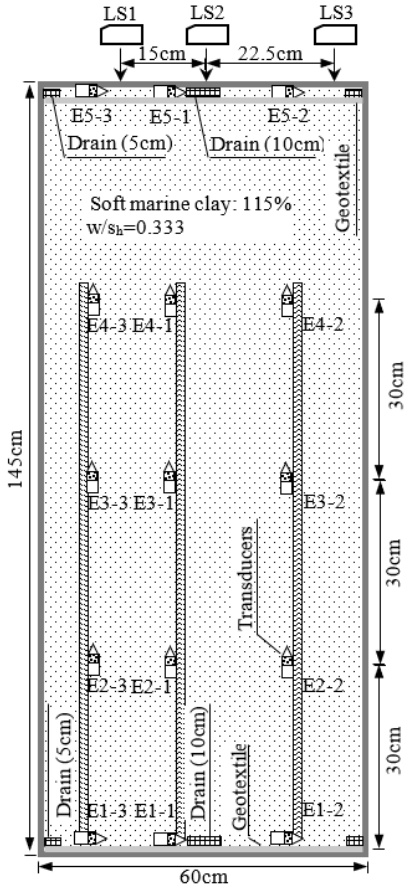

Figure 5.10 Elevation view of the pore water pressure transducers and laser sensors in Test M3

The monitoring data of Test M3 are shown in Figure 5.11. The reductions of pore water pressure at E1 and E5 level were fast and close to the vacuum pressure in drain due to the use of single non-woven geotextile sheet for HDeG sheet. The reductions of pore water pressure at level E2, E3 or E4 were synchronous, especially for level E3 and E4. From 13th day, as the HDeG sheet close to E4 level, the reductions of pore pressure at E4 level became faster. The maximum reductions of pore water pressure at level E2, E3 and E4 were about 16 kPa, 8.5 kPa and 12 kPa, respectively.

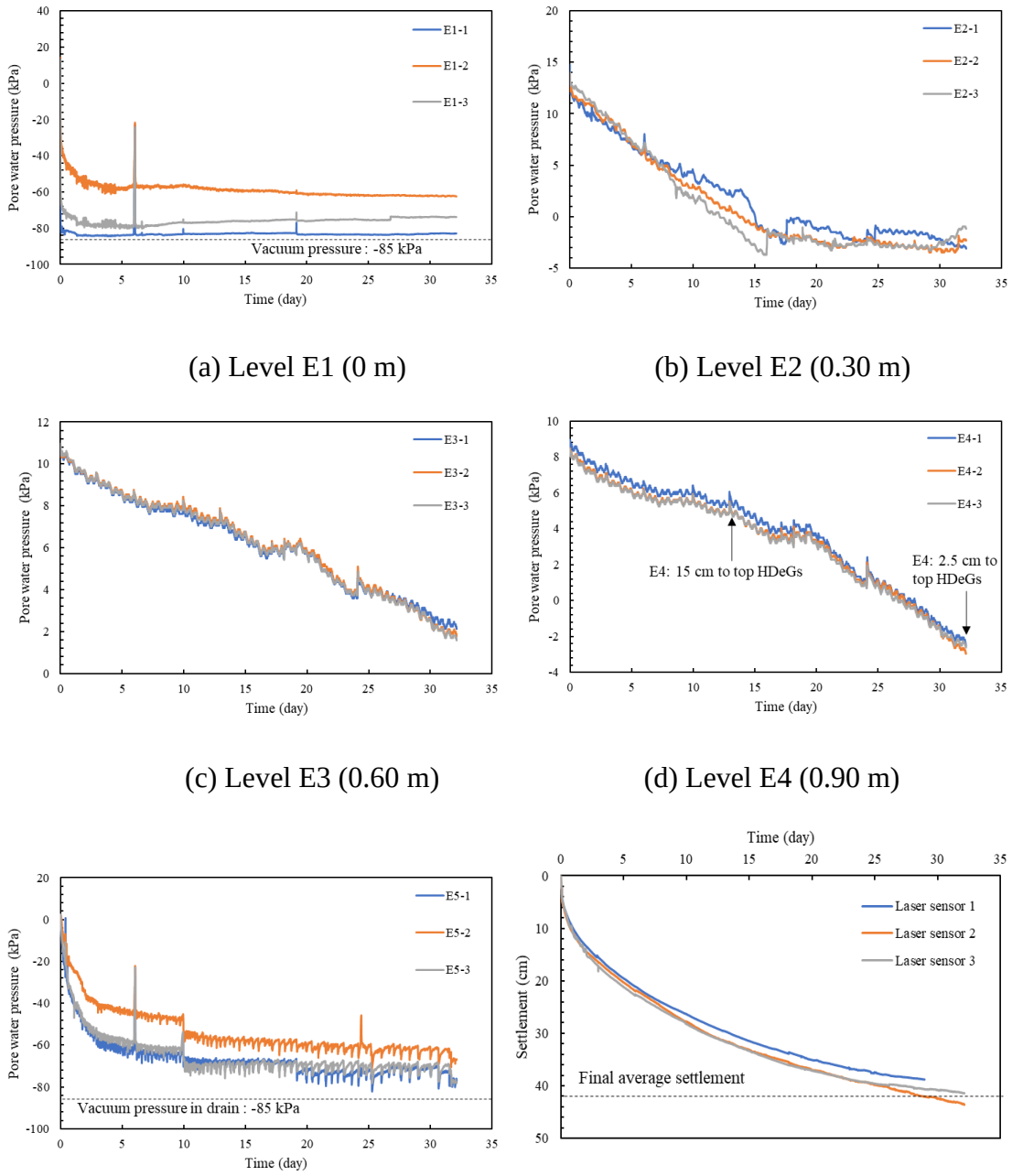

(a) Level E1 (0 m)

(b) Level E2 (0.30 m)

(c) Level E3 (0.60 m)

(d) Level E4 (0.90 m)

(e) Level E5

(f) Settlement

Figure 5.11 Monitoring data of Test M3: (a) Level E1 (0 m); (b) Level E2 (0.30 m); (c) Level E3 (0.60 m); (d) Level E4 (0.90 m); (e) Level E5 and (f) Settlement

Compared with Test M2, the reductions of pore water pressure at level E2, E3 and E4 were larger and more uniform in Test M3 using HDeG sheet with non-woven geotextile. Therefore, the flow lines were also close to be vertical at E2, E3 and E4.

Due to two months of circuit breaker in Singapore, the consolidation under the self-weight of soil almost finished, especially for the soil at bottom, and the average

settlement was 11 cm. Before the vacuum consolidation, the soft marine clay with same initial water content of about 120% was filled into test box to the height of 145 cm. Although the average settlement was about 37 cm at 21st day in Test M3, the total average settlement of Test M3 with the consideration of self-weight consolidation should be much larger than that of Test M2.

- Test M4

Test M4 was also carried out using the HDeG sheet with non-woven geotextile. The initial and final height were 1.45 m and 0.84 m, respectively. The pore pressure transducers were also fixed on the steel rods at four elevations, E1, E2, E3 and E5 as in Figure 5.12.

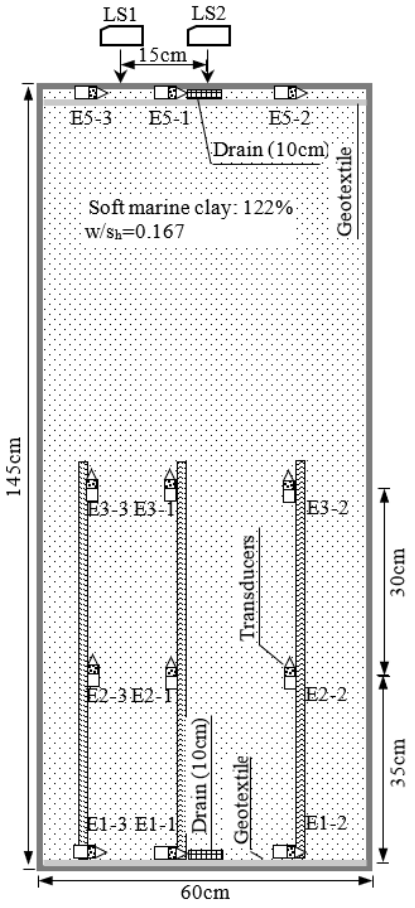

Figure 5.12 Elevation view of the pore water pressure transducers and laser sensors in Test M4

The monitoring data of Test M4 are shown in Figure 5.13. Due to power interruption, the vacuum pump was turned off for one day. The pore water pressure was fluctuated at

the final stage because of the vacuum leakage. Only two laser sensors were used to measure the settlement as the measuring range of the other two laser sensors were limited.

In this model test, the pore water pressure transducers at E4 were not used. The reductions of pore water pressures were less than those in Test M3 due to the lower ratio of width to horizontal spacing of prefabricated drain, w/s_h =0.167. The reductions of pore water pressure at level E1 and E5 were still significant. However, the reductions of pore pressure at E1 were less than those at E5, which was because the uneven non-woven geotextile at E5 under the weight of transducers as in Figure 5.14. Therefore, the transducers at E5 level were much closer to the drain than those at E1.

The reductions of pore water pressures at E2 or E3 were almost synchronously and about 12.5 kPa and 9 kPa at the 32nd day, which were a bit smaller than those of Test M3 which were about 18 kPa and 11 kPa. Therefore, as the distance to HDeG sheet increasing, the flow lines were almost vertical.

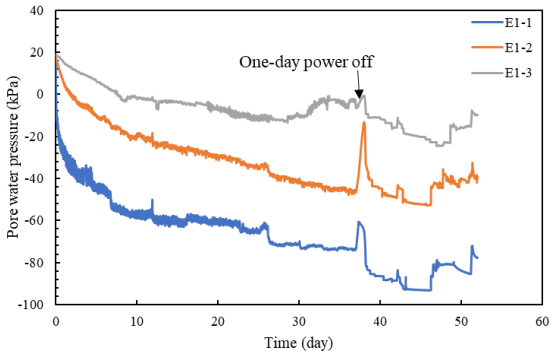

(a) Level E1 (0 m)

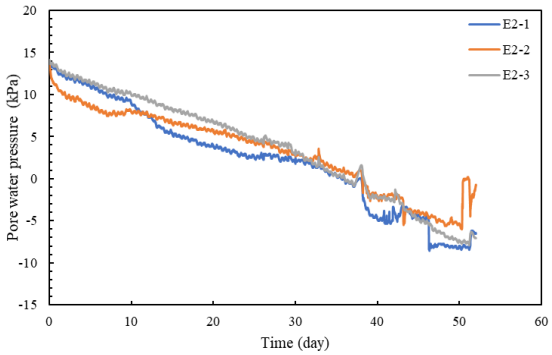

(b) Level E2 (0.35 m)

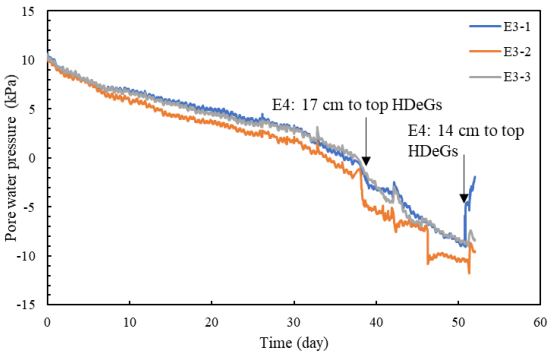

(c) Level E3 (0.65 m)

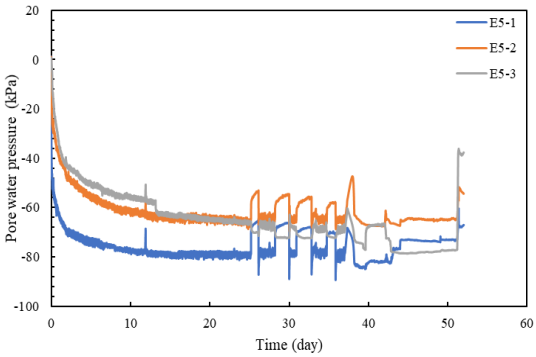

(d) Level E5

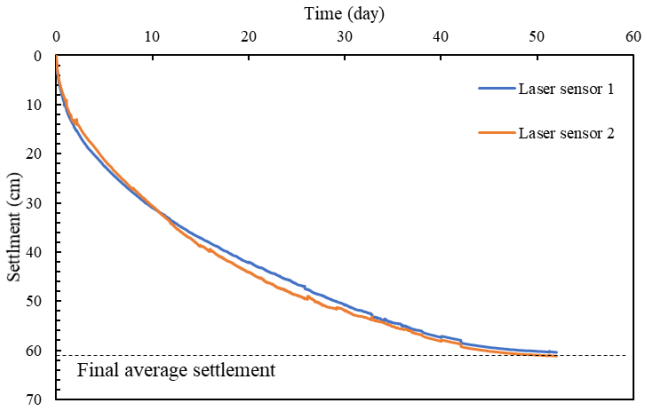

(e) Settlement

Figure 5.13 Monitoring data of Test M4: (a) Level E1 (0 m); (b) Level E2 (0.30 m); (c) Level E3 (0.65 m); (d) Level E5 and (e) Settlement

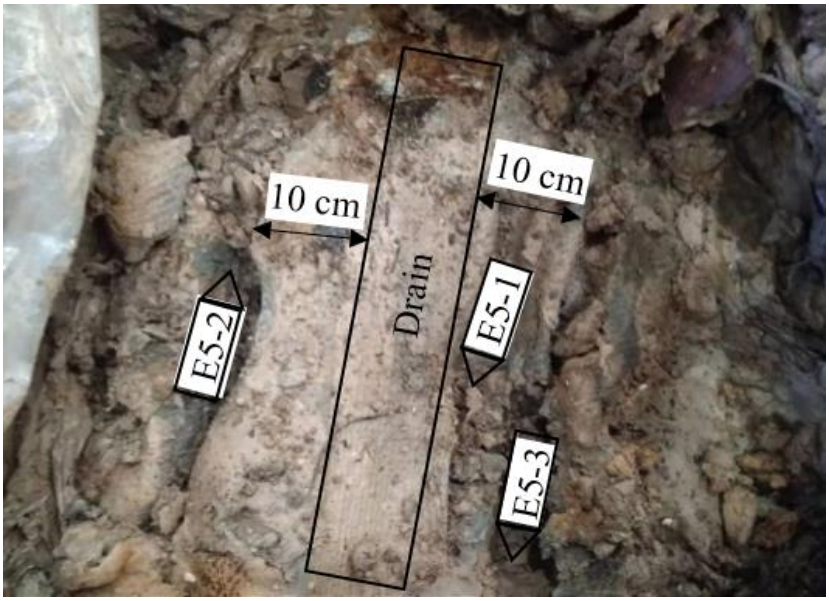

Figure 5.14 Deviation of pore pressure transducers at E5 level

5.3.2 Vane shear tests and water content

When the vacuum pressure was turned off, the consolidated soil turned into over-consolidation condition. The distributions of undrained shear strength, s_u, obtained from vane shear tests are shown in Figure 5.15. The distributions of water content, ω, are shown in Figure 5.16.

From Figure 5.15 and Figure 5.16, the relatively high undrained shear strength and low water content were around the HDeG sheet in Tests M1 and M2. As the HDeG sheet

with non-woven geotextile were used in Tests M3 and M4, the undrained shear strength and water content were almost uniform at the same elevation. Because of two months vacuum consolidation in Test M4, the water contents of soil were about 38 to 60 % on the whole cross-section, which were much lower than the liquid limit of 72%. Therefore, the average undrained shear strength was about 5 kPa.

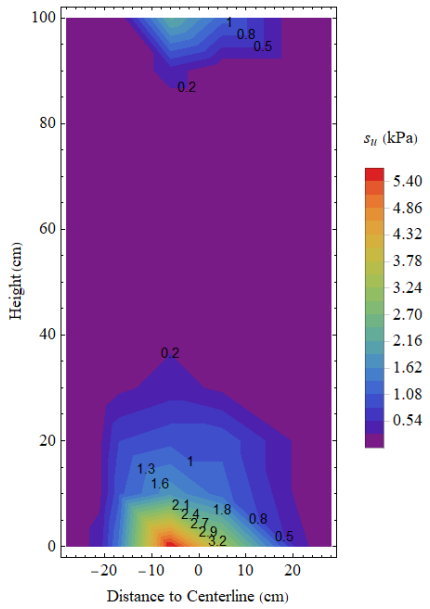

(a) Test M1 (maximum: 9.2 kPa)

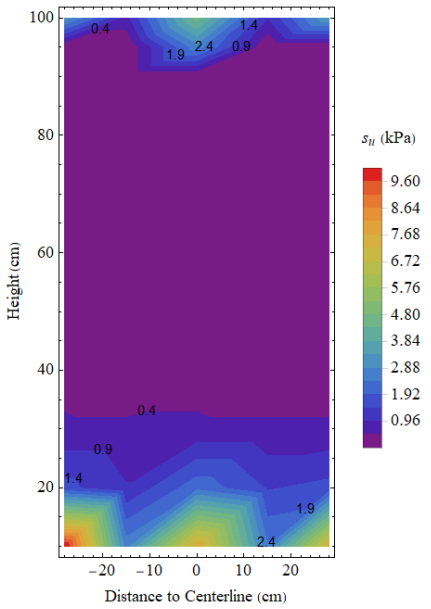

(b) Test M2 (maximum: 10.3 kPa)

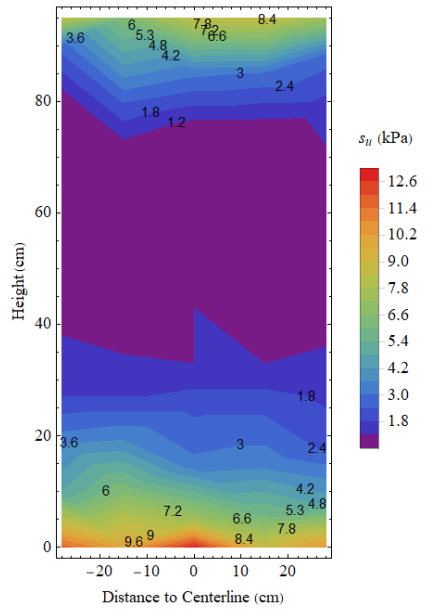

(c) Test M3 (maximum: 13.0 kPa)

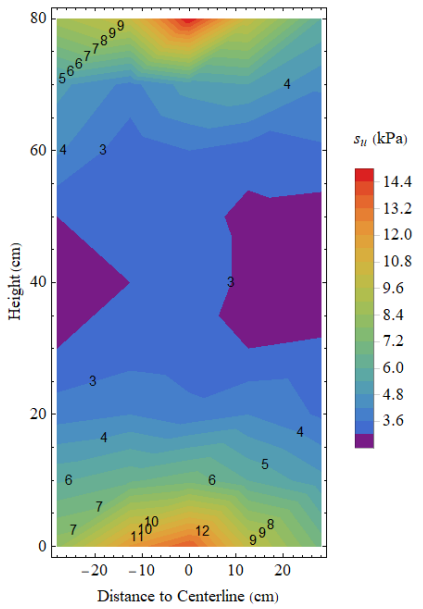

(e) Test M4 (maximum: 15.1 kPa)

Figure 5.15 Undrained shear strength using laboratory vane shear tests after testing: (a) Test M1; (b) Test M2; (c) Test M3 and (d) Test M4 (s_u: undrained shear strength)

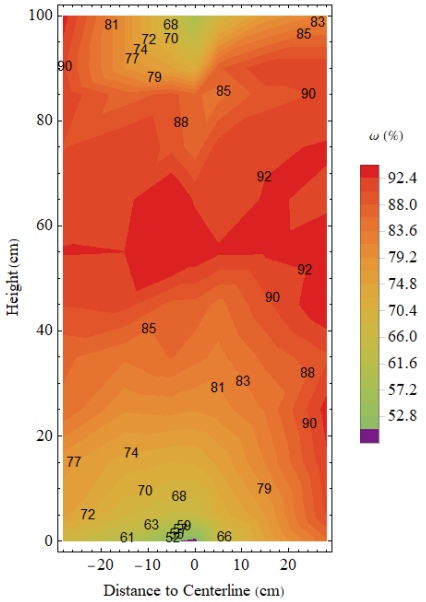

(a) Test M1 (minimum: 49.2%)

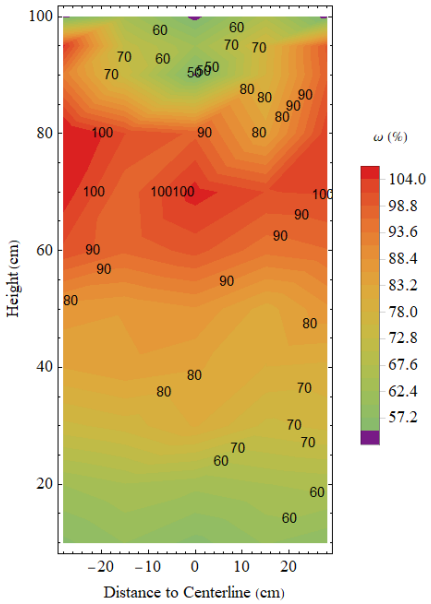

(b) Test M2 (minimum: 46.6%)

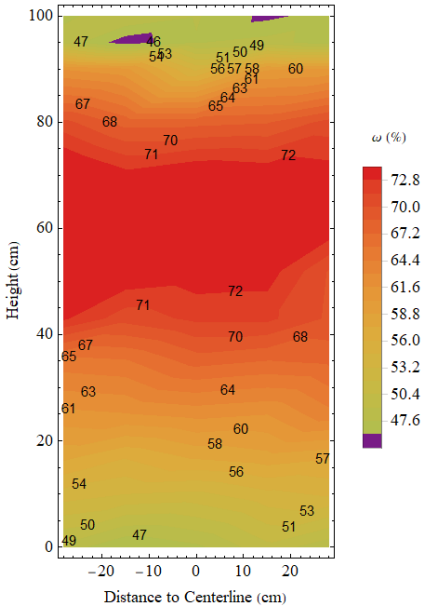

(c) Test M3 (minimum: 45.8%)

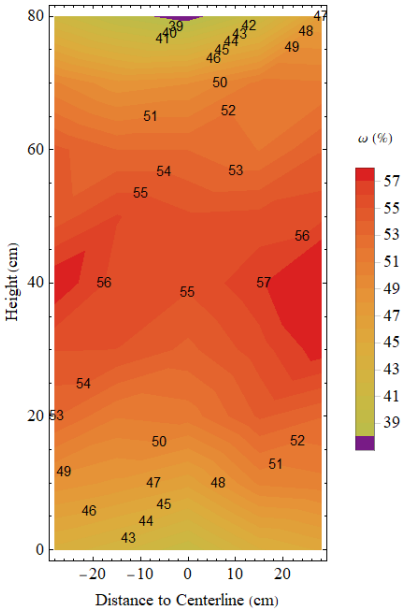

(d) Test M4 (minimum: 37.2%)

Figure 5.16 Distributions of water content after testing: (a) Test M1; (b) Test M2; (c) Test M3 and (d) Test M4 (ω: water content; Liquid limit: 72%; Plastic limit: 32%)

5.3.3 Distributions of excess pore pressures

Based on the monitoring data, the distributions of excess pore water pressure at the distances to centreline, 0.07 m (S1), 0.17 m (S2) and 0.21 m (S3), were obtained.

- Test M1 and M2

The distributions of excess pore water pressure in Tests M1 and M2 are shown in Figure 5.17 and Figure 5.18. The reductions of excess pore water pressure were relatively large at the bottom of the soil. For the distributions at 7 cm to centreline, as the deformation of soil, the reduction of excess pore pressure at E4-1 increased, but it was still not significant. Therefore, by using drain only, the reduction of excess pore water pressure in soil was still small when compared with the vacuum pressure in drain which was about -85 kPa. Therefore, based on the results of Tests M1 and M2, the performance of drain only for vacuum consolidation of soft marine clay was not very effective.

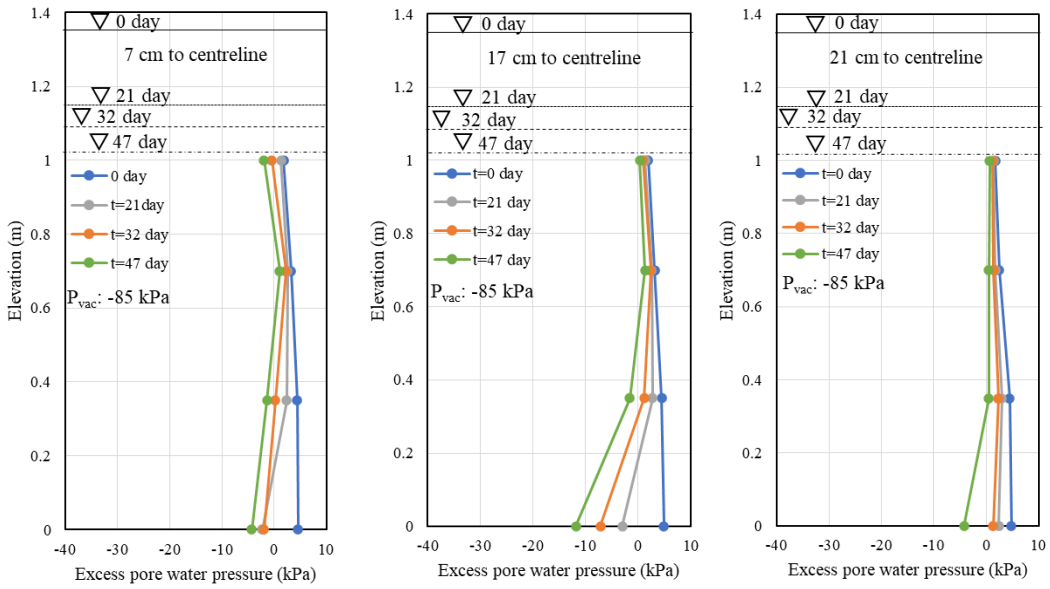

(a) S1 (7cm) (b) S2 (17cm) (c) S3 (21cm)

Figure 5.17 Distributions of excess pore water water pressure in Test M1: (a) S1 (7cm); (b) S2 (17cm); (c) S3 (21cm) (P_{vac}: Vacuum pressure)

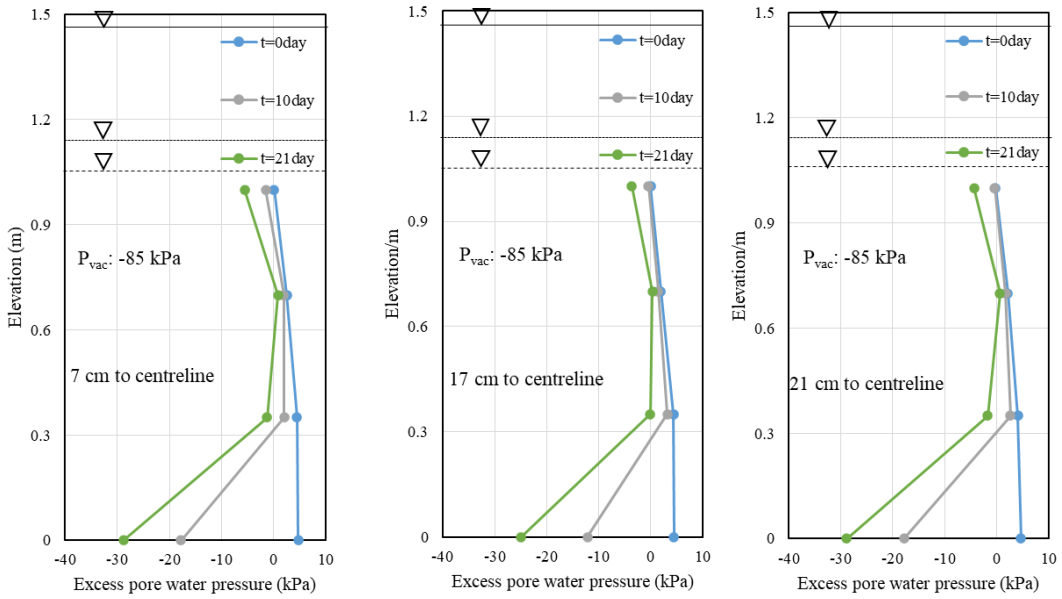

(a) S1 (7cm) (b) S2 (17cm) (c) S3 (21cm)

Figure 5.18 Distributions of excess pore water water pressure in Test M2: (a) S1 (7cm); (b) S2 (17cm); (c) S3 (21cm) (P_{vac}: Vacuum pressure)

- Test M3 and M4

The distributions of excess pore water pressure of Tests M3 and M4 are shown in Figure 5.19 and Figure 5.20. Due to the two months of self-weight consolidation in Test M3, the initial excess pore water pressure was close to zero. Because of the vacuum leakage in last 5 days, the change of the excess pore water pressure was small in Test M4.

Compared with Tests M1 and M2, the distributions of excess pore water pressure in Tests M3 and M4 were closer to suction line because of the use of HDeG sheet with non-woven geotextile. With the lower ratio, w/s_h, of the width to the horizontal spacing of drain, 0.167 for Test M4, the reductions of excess pore water pressure in Test M4 were a bit lower than those of Test M3 at the same day. Therefore, with the use of non-woven geotextile, the vacuum consolidation of soft marine clay using HDeG sheet with good transmissivity becomes more effective. However, due to the low permeability of the adjacent soil around HDeG sheet, the excess pore water pressures at E2, E3 and E4 level were still relatively small compared with those at E1 and E5.

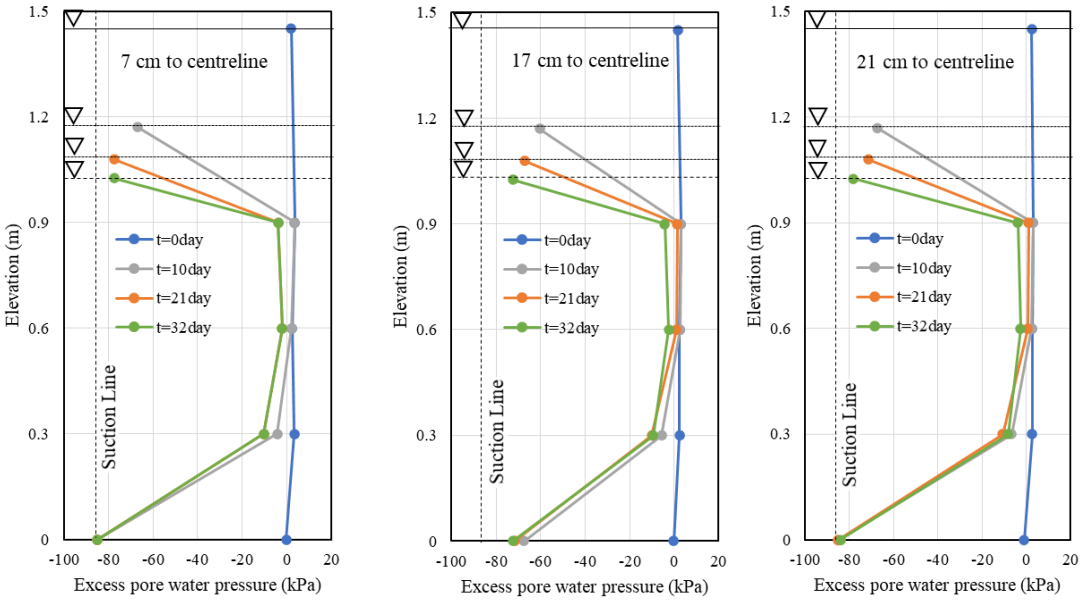

(a) S1 (7cm) (b) S2 (17cm) (c) S3 (21cm)

Figure 5.19 Distributions of excess pore water pressure for Test M3: (a) S1 (7cm); (b) S2 (17cm); (c) S3 (21cm)

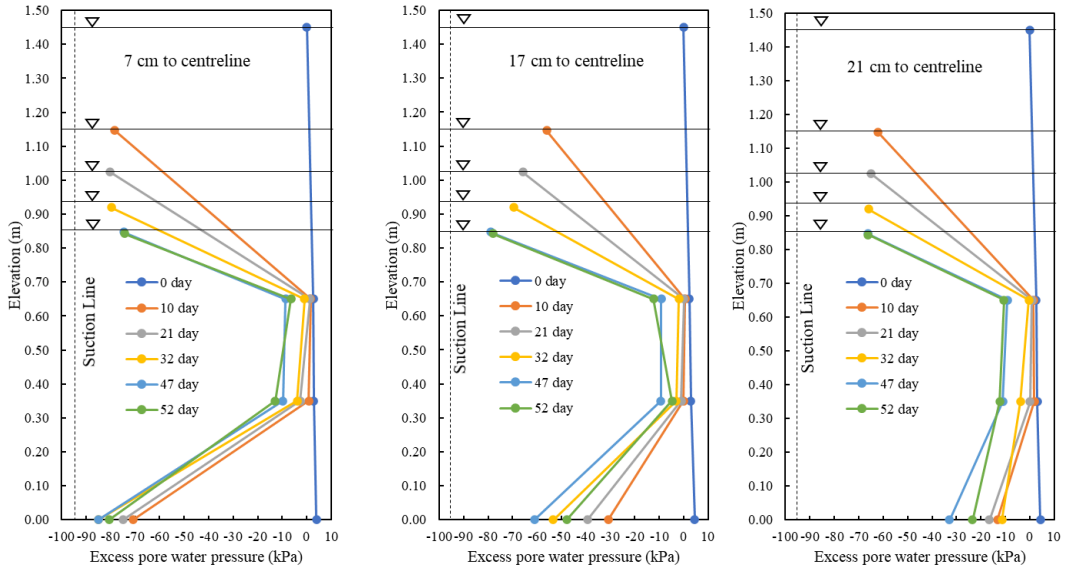

(a) S1 (7cm) (b) S2 (17cm) (c) S3 (21cm)

Figure 5.20 Distributions of excess pore water pressure for Test M4: (a) S1 (7cm); (b) S2 (17cm); (c) S3 (21cm)

5.4 Flow fields

The relationship between undrained shear strength and water content as obtained from all the model tests is shown in Figure 5.21. The results were consistent with those of large-scale tests and unconfined compression tests. Most of the data points were located on the same curve. When the water content was lower than the liquid limit, the undrained shear strength increased exponentially.

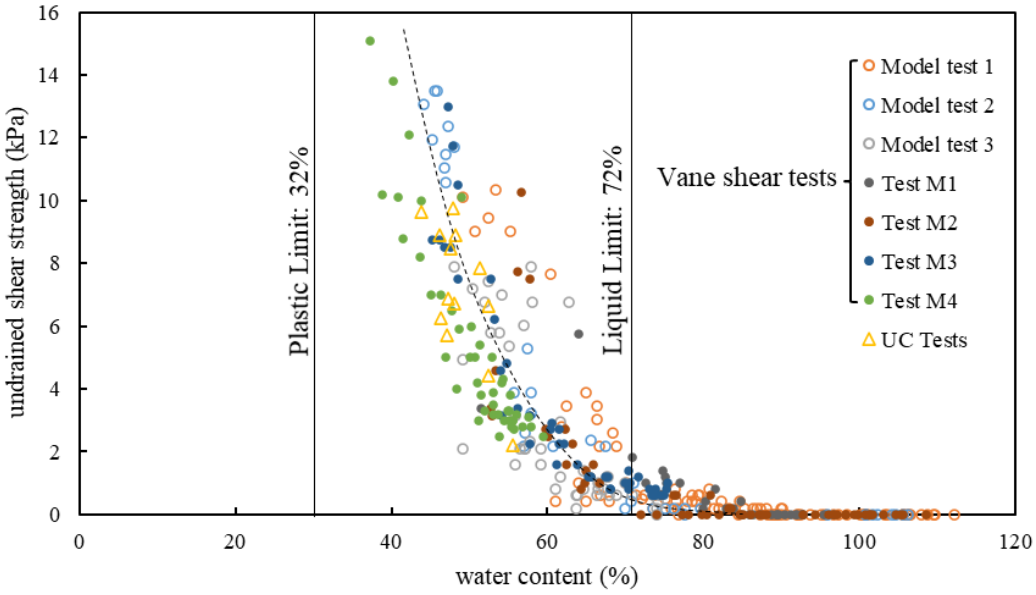

Figure 5.21 Relationship between undrained shear strength and water content

The calculated effective stress and void ratio are plotted in Figure 5.22 with the normal consolidation lines obtained from the consolidation tests of soft marine clay. The effective stress was calculated using the measured pore water pressure. The corresponding void ratio was calculated using the measured water content and specific gravity. The calculated effective stress and void ratio in Test M1 to M4 were also consistent with the normal consolidation lines. The difference of the data point and the normal consolidation lines was mainly due to the unloading. According with the studies by Kim et al. (1995), Lee and Sills (1981), Katagiri and Imai (1994) and Bo et al. (2003), the compression index at slurry stage (below 6 kPa) is affected by the initial void ratio to consider the deformation of self-weight consolidation of soft marine clay.

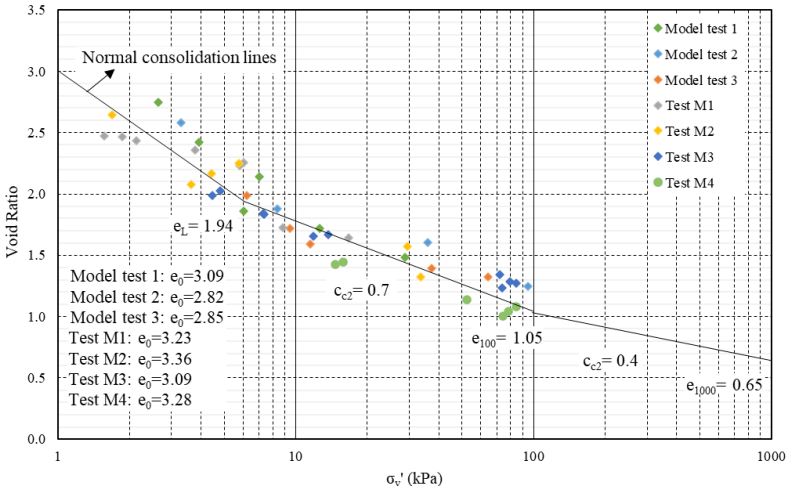

Figure 5.22 Calculated void ratio and effective stress of model tests

Therefore, the unique relationships of effective stress, void ratio and undrained shear strength were obtained with fully saturated soft marine clay. As the change of initial excess pore water pressure on the whole cross-section of unit cell is small, the relationships of excess pore water pressure, void ratio and undrained shear strength are also unique. Hence, the contours of water content and undrained shear strength can represent the contours of excess pore water pressure. The excess pore water pressure distributions on whole cross-section can be calculated using the undrained shear strength and average unit weight of treated soil as in Eq. (5.1) to Eq. (5.6).

$$e=\omega G_s \tag{5.1}$$

$$\gamma_{sat}=\frac{(e+G_s)}{(1+e)}\gamma_w \tag{5.2}$$

$$\sigma_v'=(\gamma_{t,sat}-\gamma_w)d \tag{5.3}$$

$$\sigma_p'=u_0-u \tag{5.4}$$

$$u_0=(\gamma_{i,sat}-\gamma_w)D \tag{5.5}$$

$$s_u=0.23\sigma_p'^{0.8}\sigma_v'^{-0.2} \tag{5.6}$$

where, e is void ratio; ω is water content; G_s is specific weight of soil particles; $\gamma_{t,sat}$ is saturated unit weight of soft soil at final condition; $\gamma_{i,sat}$ is saturated unit weight of soft soil at initial condition; γ_w is unit weight of water; u_0 is the initial pore water pressure; u is the excess pore water pressure; σ'_p is pre-consolidation pressure; σ'_v is vertical effective stress; d is the depth to soil surface at final condition; D is the depth to soil surface at initial condition. Here, the excess pore pressure is unknown and can be calculated using the measured water content, specific gravity and the height of soil.

The calculated excess pore water pressure contours are shown in Figure 5.23. With the use of non-woven geotextile or the smaller horizontal spacing of the drains, the equipotential lines are more horizontal. Then the flow lines, perpendicular to the equipotential lines, tend to be vertical. Moreover, as the distance to HDeG sheet increasing, the equipotential lines tend to be horizontal, then the flow lines tend to be vertical.

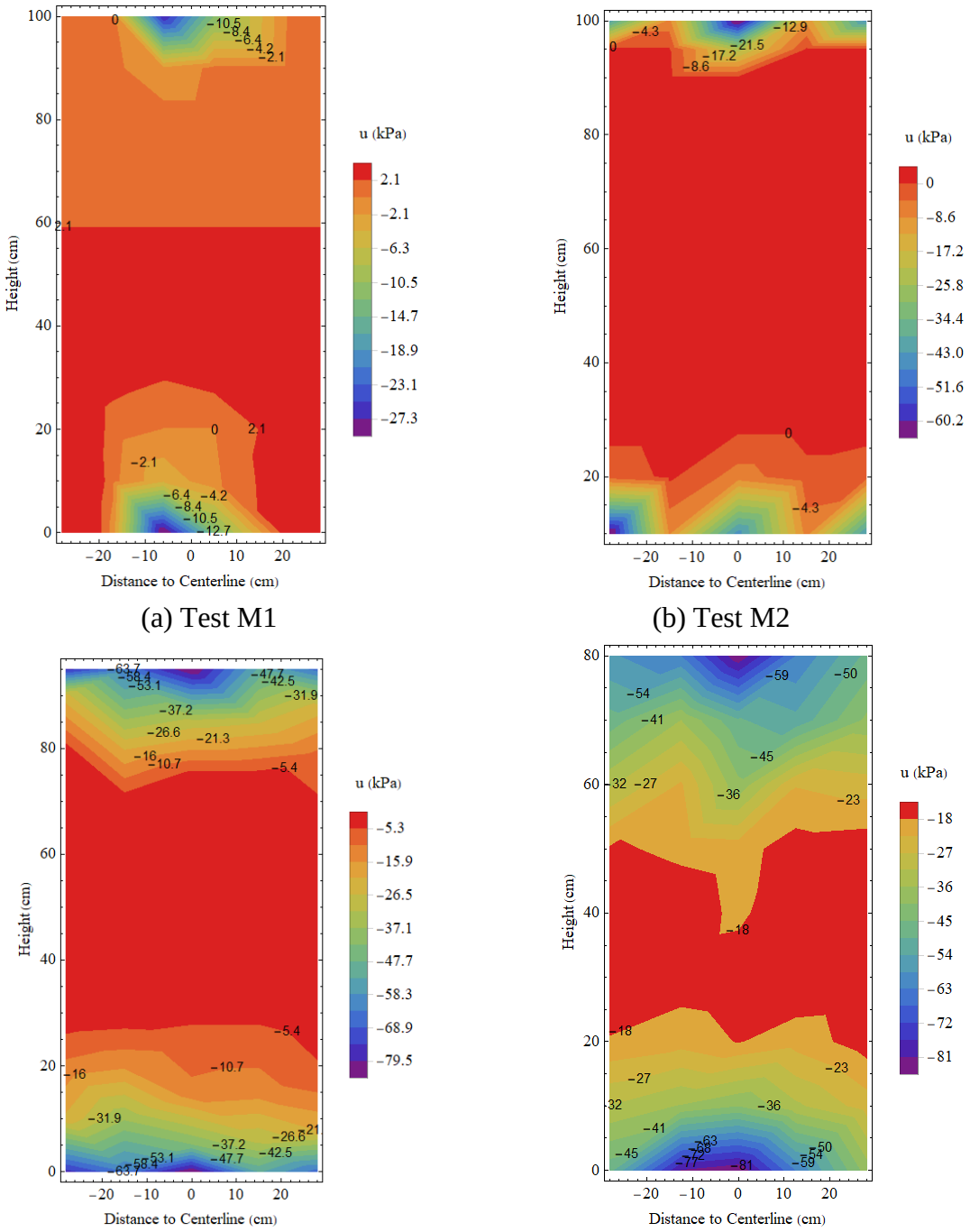

(a) Test M1 (b) Test M2

(c) Test M3 (d) Test M4

Figure 5.23 Calculated equipotential lines: (a) Test M1; (b) Test M2; (c) Test M3 and (d) Test M4 (*u*: Excess pore water pressure)

5.5 Degree of consolidation

The average settlements of four model tests are shown in Figure 5.24. In Test M1, due to the low ratio of the width to the horizontal spacing of drain, 0.0833, the settlement and consolidation rate was much lower than others. With a high ratio of the width to the horizontal spacing of drain, 0.333, such as in Tests M2 and M3, the difference was small. With the use of HDeG with non-woven geotextile, the difference between Tests M3 and M4 was also not significant. With higher ratio of w/s_h or the use of non-woven geotextile, the settlement is larger.

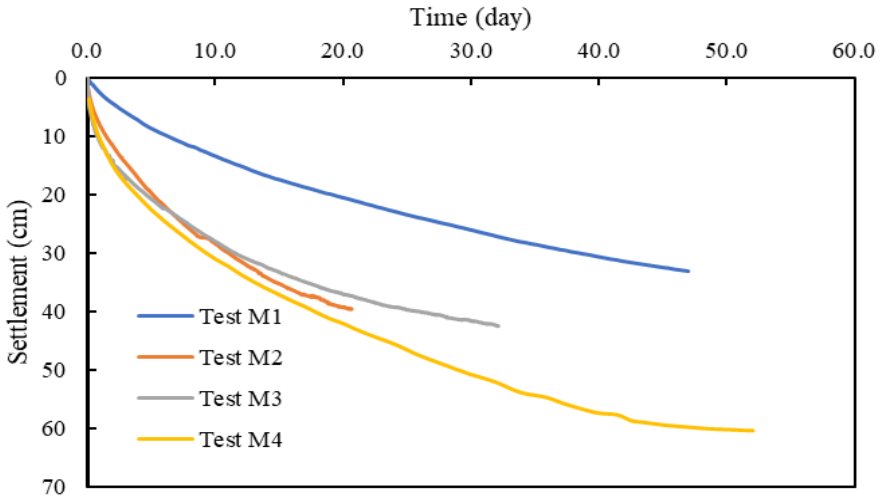

Figure 5.24 Average settlement of four model tests

To calculate the degree of consolidation based on average settlement, the Asoka method (1978) was used to determine the ultimate settlement of four model tests firstly as shown in Figure 5.25. It can be seen from the Figure 5.25 that the ultimate settlement of Test M1 was close to that of Test M2 and the ultimate settlement of Test M3 was close to that of Test M4. To calculate the degree of consolidation based on distributions of excess pore pressure, the linear interpolation between the measured data points of excess pore pressure was used. The degree of consolidation calculated by these two methods are shown in Figure 5.26.

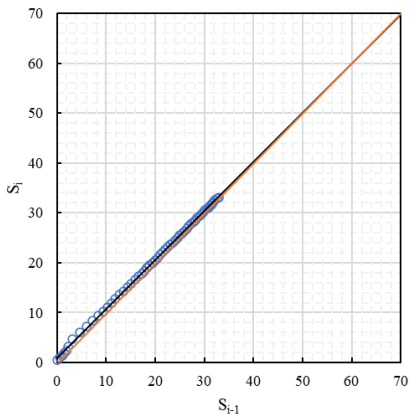

(a) Test M1 (s_{ult} = 60.0 cm)

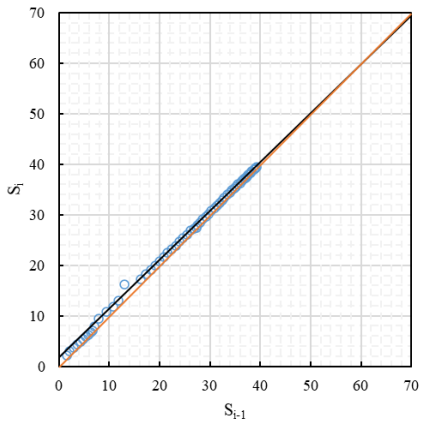

(b) Test M2 (s_{ult} = 60.4 cm)

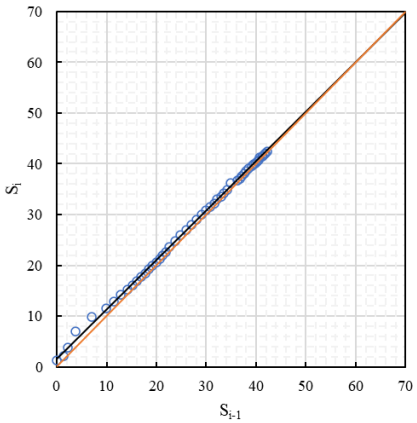

(c) Test M3 (s_{ult} = 64 cm)

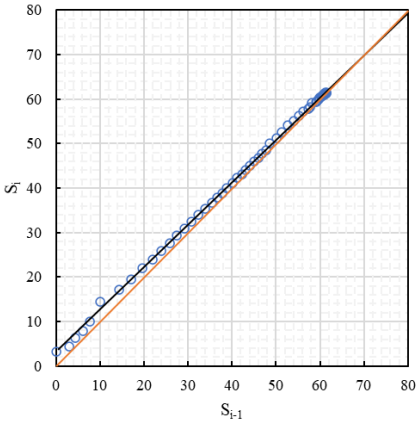

(c) Test M3 (s_{ult} = 71 cm)

Figure 5.25 Ultimate settlement, s_{ult}, of four model tests using Asoka's method: (a) Test M1; (b) Test M2; (c) Test M3 and (d) Test M4

Figure 5.26 shows that the degree of consolidation based on excess pore pressure lagged behind that based on settlement due to the non-linear compressibility. Because of the use of linear interpolation, the degree of consolidation based on excess pore pressure at early stage was higher than the real values. The degree of consolidation of Test M2 was larger than that of Test M1 at the same time, and the degree of consolidation of Test M3 was also larger than that of Test M4 at the same time. The degree of consolidation based on settlement for Tests M2 and M3 were close to each other. Nevertheless, the final degree of consolidation based on the excess pore pressure of Test M3 was larger than that of Test M2. Therefore, the HDeG with non-woven geotextile is more effective for the vacuum consolidation of soft marine clay. The use of HDeG with non-woven

geotextile is more feasible as horizontal drain for land reclamation with multiple layers of soft marine clay fill.

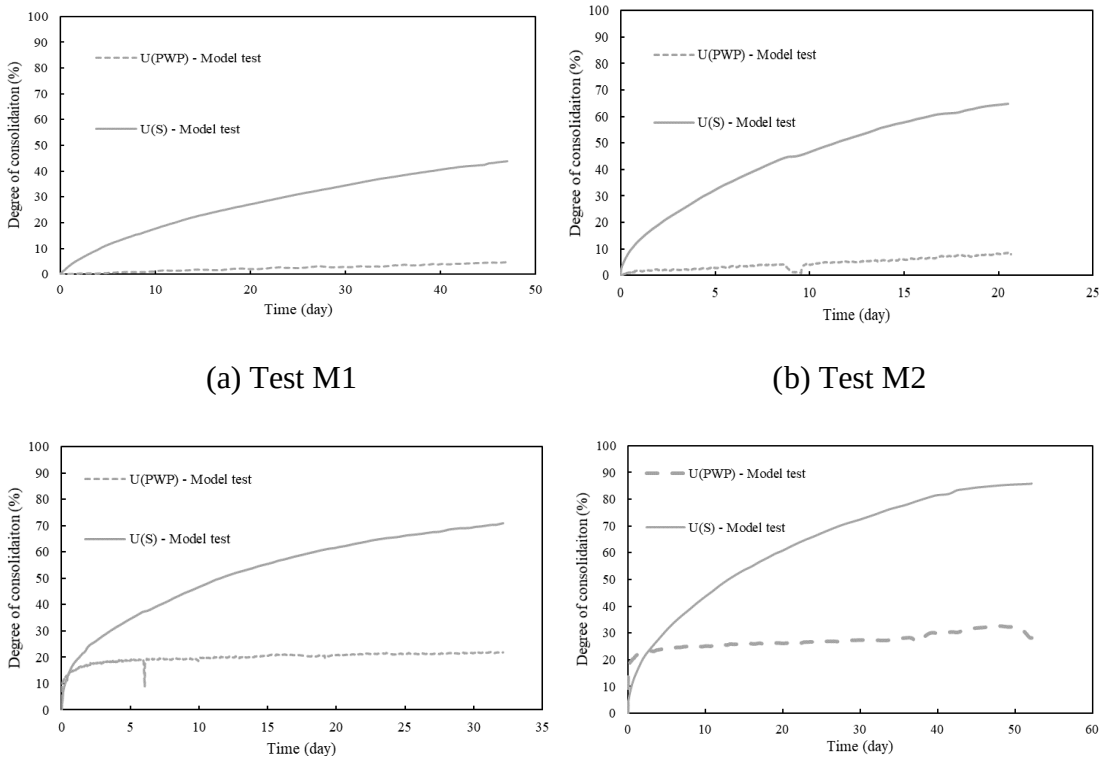

(a) Test M1 (b) Test M2

(c) Test M3 (d) Test M4

Figure 5.26 Degree of consolidation based on settlement and excess pore pressure: (a) Test M1; (b) Test M2; (c) Test M3 and (d) Test M4

5.6 Conclusions

Four model tests were conducted to investigate the effect of different horizontal and vertical spacings of drains and non-woven geotextile on the vacuum consolidation of soft marine clay using HDeG sheet. The following conclusions could be drawn:

(1) The model tests show that the use of HDeG was much more efficient than the use of horizontal drains only for consolidation soft clay. The geotextile in the HDeG played an important role in distributing vacuum pressure and consolidating soil.

(2) The performance of the HDeG was controlled by the horizontal spacing of the drains s_h, the vertical spacing of HDeG s_v, the width of the drain w and the

permittivity of the geotextile k_p. In general, the greater the w/s_h or w/s_v ratio or the higher the k_p, the more efficiency the HDeG.

(3) With the use of HDeG with geotextile of relatively high permittivity, the pore water pressure distribution at the same elevation were more uniform. The flow lines tended to be vertical and the equipotential lines tended to be horizontal. The undrained shear strength and water content distribution contours tended to be horizontal too.

(4) Based on the calculation of degree of consolidation using the monitoring data, the degree of consolidation based on distribution of excess pore pressure lagged behind that based on average settlement due to the non-linear compressibility.

CHAPTER 6 CONSOLIDATION ANALYSIS OF SOFT SOIL THROUGH THE USE OF HDEG SHEET

6.1 Introduction

As discussed in Chapter 4 and 5, with the lower horizontal spacing, the vacuum consolidation using horizontal drain is better. From the construction point of view, the vertical spacing of horizontal drains should not be too small and could be in the range of 1.5 to 3.0 m. Compared to the horizontal spacing or the width of drains, the vertical spacing or the thickness of soft marine clay is relatively large. Therefore, the conventional consolidation theory, such as Terzaghi's method (1956), Hansbo's method (1981), or Hird's method (1992) is not suitable to analyse the vacuum consolidation behaviour using horizontal drains. With the use of HDeG sheet, the transmissivity of geotextile has a great effect on the vacuum consolidation of soft marine clay and the pore water pressure tends to be uniform at same elevation. A small-strain consolidation solution was developed for the design of land reclamation using the proposed HDeG sheet. Moreover, the soft dredged marine clay as fill material in land reclamation is with high water content and high compressibility. The non-linear properties of soil compressibility and permeability should be considered. The large-strain consolidation solution was established to simulate the vacuum consolidation behaviour of soft clay fill using horizontal drains. The finite element method was also developed to analyse and design the land reclamation of soft clay using horizontal drain.

6.2 Small-strain Consolidation solution

By using the vacuum preloading with HDeG sheet, the duration of vacuum consolidation will take for a long time. A consolidation solution using constant coefficient of consolidation makes it more suitable for designing the vacuum preloading of soft marine clay using HDeG sheet in land reclamation.

6.2.1 Horizontal drainage enhanced geotextile

A new analytical solution under plane strain condition was developed for vacuum consolidation of soft clay using HDeG sheet. Due to symmetry, only a quarter unit cell

was used. The analytical model is shown in Figure 6.1. The coordinates are set-up with x in the horizontal direction and z in the vertical direction. The origin of the analytical model is set at the corner, O, of the quarter unit cell. The horizontal dimension for quarter unit cell is half of the horizontal spacing, s_h, of drains. The vertical dimension is the consolidation height, h, which depends on the drainage condition. The vacuum pressure is added in the drain ($0<x<w/2$). w is the width of drain.

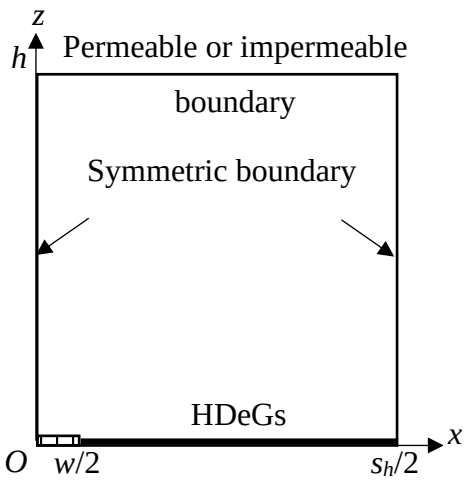

Figure 6.1 Analytical model

6.2.1.1 Assumptions made

Based on the permeability tests of soft clay and transmissivity tests of geotextile in Chapter 4, the in-plane permeability of geotextile used in HDeG was equivalent to that of sand, which was much larger than the permeability of soft clay. Therefore, the horizontal flow in soft clay could be ignored.

(1) The soft soil and geotextile are uniform and fully saturated.

(2) The soil particles and water are incompressible.

(3) The Darcy's law is applicable.

(4) All compressive strains within the soil mass are small and occur in the vertical direction only.

(5) The horizontal flow in soft clay is ignored.

(6) The thickness of HDeG sheet is ignored.

(7) The well resistance of the drain is ignored.

(8) The placement of subsequent layer of soft clay fill is instant.

(9) The coefficient of consolidation is constant.

6.2.1.2 Boundary conditions

Boundary condition for soft clay

The boundary conditions for the excess pore water pressure of a soil element at x and z, *u(x, z, t)*, are listed as follows:

(1) $\frac{\partial u}{\partial z} = 0$, at $z = h$, single drainage

(2) $u = 0$, at $z = h$, double drainage

(3) $u = p(x, t)$, at $z = 0$.

(4) $u = u_0$ (Const), at t = 0

where, *p(x, t)* is the distribution of excess pore water pressure on the HDeG sheets; u_0 is the initial excess pore water pressure which is related to the surcharge and set as a constant value on cross-section. With geomembrane covered on the soil surface, the top boundary is impermeable. Thus the consolidation is under single drainage condition and $h = s_v/2$ as shown in Figure 6.1. Without membrane on the soil surface, the top boundary is permeable. Thus the consolidation for top soil layer is under double drainage condition and *h* is the vertical spacing, s_v, of HDeG sheet.

Boundary conditions for HDeG sheet

As the HDeG sheet consists of drain and geotextile, the vacuum pressure is constant in the drain. Then the boundary conditions for the excess pore water pressure of geotextile, *p(x, t)*, are listed as follows:

(5) $p = -p_{vac}$, at $x = w/2$

(6) $\frac{\partial p}{\partial x} = 0$, at $x = s_h/2$

where, p_{vac} is the absolute vacuum pressure in drain; *w* is the width of drain; s_h is the horizontal spacing of drains.

6.2.1.3 Theoretical derivation

As the boundary conditions for soft soil and geotextile are different, the excess pore water pressure, *u(x, z, t)* and *p(x, t)*, should be analysed individually.

Soft clay

Based on the assumption (6), the governing equation for the excess pore water pressure of soft soil, *u(x, z, t)*, can be expressed by Eq. (6.1).

$$\frac{\partial u_s}{\partial t} = c_v \frac{\partial^2 u_s}{\partial z^2} \tag{6.1}$$

Based on the boundary conditions for soft soil, the solution for soft soil under single drainage condition can be expressed by Eq. (6.2),

$$u(x,z,t) = p(x,t)[1 - v_1(z,t)] + u_0 v_2(z,t) \tag{6.2}$$

and for double drainage condition, the solution is in Eq. (6.3) (Chai and Carter, 2011).

$$u(x,z,t) = p(x,t)[1 - \frac{z}{h} - v_1(z,t)] + u_0 v_2(z,t) \tag{6.3}$$

where, $v_1(z, t)$ and $v_2(z, t)$ are the transient solution for vertical flow. For the solution of $v_1(z, t)$, the governing equation and boundary conditions under single drainage condition can be expressed as Eq. (6.4) to Eq. (6.7)

$$\frac{\partial v_1}{\partial t} = c_v \frac{\partial^2 v_1}{\partial z^2} \tag{6.4}$$

$$v_1(0,t) = 0 \tag{6.5}$$

$$\frac{v_1(h,t)}{\partial z} = 0 \tag{6.6}$$

$$v_1(z,0) = 1 \tag{6.7}$$

Under double drainage condition, the boundary conditions are different as expressed by Eq. (6.8) and Eq. (6.9).

$$v_1(h,t) = 0 \tag{6.8}$$

$$v_1(z,0) = 1 - \frac{z}{h} \tag{6.9}$$

For the solution of $v_2(z, t)$, the governing equation under single drainage condition can be expressed as Eq. (6.10) to Eq. (6.13).

$$\frac{\partial v_2}{\partial t} = c_v \frac{\partial^2 v_2}{\partial z^2} \tag{6.10}$$

$$v_2(0,t) = 0 \tag{6.11}$$

$$\frac{v_2(h,t)}{\partial z} = 0 \tag{6.12}$$

$$v_2(z,0) = 1 \tag{6.13}$$

Under double drainage condition, the top boundary condition is permeable as in Eq. (6.14).

$$v_2(h,t) = 0 \tag{6.14}$$

Therefore, under single drainage condition, the solutions $v_1(z, t)$ and $v_2(z, t)$ are same as shown in Eq. (6.15).

$$v_1(z,t) = v_2(z,t) = \sum_{n=1}^{\infty} \frac{2}{M} sin \frac{Mz}{h} e^{-M^2 T_v} \tag{6.15}$$

where, $M = (2n\text{-}1)\pi/2$, $n \geq 1$; $T_v = C_v t/h^2$.

Under double drainage condition, the solutions $v_1(z, t)$ and $v_2(z, t)$ are shown in Eq. (6.16) and Eq. (6.17).

$$v_1(z,t) = \sum_{n=1}^{\infty} \frac{2}{N} sin \frac{Nz}{h} e^{-N^2 T_v} \tag{6.16}$$

$$v_2(z,t) = \sum_{n=1}^{\infty} \frac{2}{M} sin \frac{2Mz}{h} e^{-4M^2 T_v} \tag{6.17}$$

where, $N = n\pi$, $n \geq 1$; $T_v = C_v t/h^2$.

Geotextile

Based on the assumption (7), the governing equation for the excess pore pressure of geotextile, $p(x, t)$, is in Eq. (6.18) and Eq. (6.19).

$$\theta \frac{\partial^2 p}{\partial x^2} + 2k \frac{\partial u}{\partial z}\Big|_{z=0} = 0, \frac{w}{2} < x \leq \frac{s_h}{2} \tag{6.18}$$

$$p = -p_{vac}, 0 < x \leq \frac{w}{2} \tag{6.19}$$

where, θ is the transmissivity of geotextile sheet; k is permeability of the adjacent soil of HDeG sheet.

By substituting the Eq. (6.2) and Eq. (6.15) into Eq. (6.18), the governing equation for single drainage condition can be expressed by Eq. (6.20).

$$\frac{\partial^2 p}{\partial x^2} - \frac{4k}{\theta h}\sum_{n=1}^{\infty} e^{-M^2 T_v} p = -\frac{4ku_0}{\theta h}\sum_{n=1}^{\infty} e^{-M^2 T_v} \tag{6.20}$$

The solution for Eq. (6.20) is shown in Eq. (6.21).

$$p(x,t) = -\frac{e^{\frac{\lambda w}{2}}(p_{vac} + u_0)(e^{\lambda x} + e^{\lambda s_h} e^{-\lambda x})}{e^{\lambda w} + e^{\lambda s_h}} + u_0 \tag{6.21}$$

where,

$$\lambda = \sqrt{\frac{4k}{\theta h}\sum_{n=1}^{\infty} e^{-M^2 T_v}}$$

And by substituting the Eq. (6.3), (6.16) and (6.17) into Eq. (6.19), the governing equation for double drainage condition can be expressed by Eq. (6.22).

$$\frac{\partial^2 p}{\partial x^2} - \frac{2k}{\theta h}(1 + 2\sum_{n=1}^{\infty} e^{-N^2 T_v})p = -\frac{8ku_0}{\theta h}\sum_{n=1}^{\infty} e^{-4M^2 T_v} \tag{6.22}$$

The solution for Eq. (6.22) is shown in Eq. (6.23).

$$p(x,t) = -\frac{e^{\frac{\mu w}{2}}(p_{vac} + \alpha u_0)(e^{\mu x} + e^{\mu s_h} e^{-\mu x})}{e^{\mu w} + e^{\mu s_h}} + \alpha u_0 \tag{6.23}$$

where,

$$\mu = \sqrt{\frac{2k}{\theta h}(1 + 2\sum_{n=1}^{\infty} e^{-N^2 T_v})}$$

$$\alpha = \frac{4\sum_{n=1}^{\infty} e^{-4M^2 T_v}}{1 + 2\sum_{n=1}^{\infty} e^{-N^2 T_v}}$$

Unit cell

The excess pore water pressure on the quarter unit cell of soft soil and HDeG sheet under single drainage condition can be expressed by Eq. (6.24) and Eq. (6.25).

$$u(x,z,t) = -p_{vac}(1 - \sum_{n=1}^{\infty} \frac{2}{M} sin\frac{Mz}{h} e^{-M^2 T_v}) + u_0 \sum_{n=1}^{\infty} \frac{2}{M} sin\frac{Mz}{h} e^{-M^2 T_v}, 0 < x \leq \frac{w}{2} \quad (6.24)$$

$$u(x,z,t) = \{-p_{vac}\beta(x) + u_0[1-\beta(x)]\}(1 - \sum_{n=1}^{\infty} \frac{2}{M} sin\frac{Mz}{h} e^{-M^2 T_v}) + u_0 \sum_{n=1}^{\infty} \frac{2}{M} sin\frac{Mz}{h} e^{-M^2 T_v}, \frac{w}{2} < x \leq \frac{s_h}{2} \quad (6.25)$$

where, $M = (2n\text{-}1)\pi/2$, $n \geq 1$; $h = s_v/2$; $\beta(x) = \frac{e^{\frac{\lambda w}{2}}(e^{\lambda x} + e^{\lambda s_h} e^{-\lambda x})}{e^{\lambda w} + e^{\lambda s_h}}$; $\lambda = \sqrt{\frac{4k}{\theta h} \sum_{n=1}^{\infty} e^{-M^2 T_v}}$.

The solution under double drainage condition can be expressed by Eq. (6.26) and Eq. (6.27).

$$u(x,z,t) = -p_{vac}\left(1 - \frac{z}{h} - \sum_{n=1}^{\infty} \frac{2}{N} sin\frac{Nz}{h} e^{-N^2 T_v}\right) + u_0 \sum_{n=1}^{\infty} \frac{2}{M} sin\frac{2Mz}{h} e^{-4M^2 T_v}, 0 < x \leq \frac{w}{2} \quad (6.26)$$

$$u(x,z,t) = \{-p_{vac}\beta(x) + \alpha u_0[1 - \beta(x)]\}\left(1 - \frac{z}{h} - \sum_{n=1}^{\infty} \frac{2}{N} sin\frac{Nz}{h} e^{-N^2 T_v}\right) + u_0 \sum_{n=1}^{\infty} \frac{2}{M} sin\frac{2Mz}{h} e^{-4M^2 T_v}, \frac{w}{2} < x \leq \frac{s_h}{2} \quad (6.27)$$

where, $N = n\pi$, $n \geq 1$; $h = s_v$; $\beta(x) = \frac{e^{\frac{\mu w}{2}}(e^{\mu x} + e^{\mu s_h} e^{-\mu x})}{e^{\mu w} + e^{\mu s_h}}$; $\mu = \sqrt{\frac{2k}{\theta h}(1 + 2\sum_{n=1}^{\infty} e^{-N^2 T_v})}$; $\alpha = \frac{4\sum_{n=1}^{\infty} e^{-4M^2 T_v}}{1+2\sum_{n=1}^{\infty} e^{-N^2 T_v}}$. By integrating the Eq. (6.24) and (6.25) over the whole cross-section of quarter unit cell, the degree of consolidation under single drainage condition can be obtained as in Eq. (6.28).

$$U(t) = [\frac{2\left(e^{\lambda s_h} - e^{\lambda w}\right)}{\lambda s_h(e^{\lambda s_h} + e^{\lambda w})} + \frac{w}{s_h}]\left(1 - \sum_{n=1}^{\infty} \frac{2}{M^2} e^{-M^2 T_v}\right) \tag{6.28}$$

By integrating the Eq. (6.26) and (6.27) over the whole cross-section of quarter unit cell, the degree of consolidation under double drainage condition can be obtained as in Eq. (6.29)

$$\begin{aligned} U(t) = \{&\frac{p_{vac} + \alpha u_0}{p_{vac} + 2u_0}\left[\frac{2(e^{\mu s_h} - e^{\mu w})}{\mu s_h(e^{\mu s_h} + e^{\mu w})} + \frac{w}{s_h}\right] \\ &+ \frac{(2-\alpha)u_0}{p_{vac} + 2u_0}\}\left(1 - \sum_{n=1}^{\infty} \frac{2}{M^2} e^{-4M^2 T_v}\right) \end{aligned} \tag{6.29}$$

From Eq. (6.28) and Eq. (6.29), the input parameters are c_v, k_z, θ, w, s_h, s_v, p_{vac}, u_0 and t. When the width of drain, w, is equal to the horizontal spacing, the solutions are the Terzaghi's one-dimensional consolidation solution. Compared with the vacuum pressure in drain, $-P_{vac}$, the initial excess pore water pressure of top layer of soft soil can be ignored. Then the Eq. (6.29) can be simplified as Eq. (6.30).

$$U(t) = [\frac{2(e^{\mu s_h} - e^{\mu w})}{\mu s_h(e^{\mu s_h} + e^{\mu w})} + \frac{w}{s_h}]\left(1 - \sum_{n=1}^{\infty} \frac{2}{M^2} e^{-4M^2 T_v}\right) \tag{6.30}$$

6.2.2 Simplified one-dimensional consolidation solution

A simplified consolidation solution, which is the function of z and t, was developed based on the proposed consolidation solution using constant coefficient of consolidation. By integrating the equations of the excess pore water pressure expressed in Eq. (6.24) and (6.25) along the x axis, the excess pore water pressure of simplified consolidation solution under single drainage condition can be obtained as in Eq. (6.31).

$$\begin{aligned} u_1(z,t) = -\{&(p_{vac} + u_0)\left[\frac{2\left(e^{\lambda s_h} - e^{\lambda w}\right)}{\lambda s_h(e^{\lambda s_h} + e^{\lambda w})} + \frac{w}{s_h}\right] \\ &- u_0\}\left(1 - \sum_{n=1}^{\infty} \frac{2}{M} sin\frac{Mz}{h} e^{-M^2 T_v}\right) \\ &+ u_0 \sum_{n=1}^{\infty} \frac{2}{M} sin\frac{Mz}{h} e^{-M^2 T_v} \end{aligned} \tag{6.31}$$

where, $M = (2n\text{-}1)\pi/2$, $n \geq 1$; $h = s_v/2$; $\beta(x) = \frac{e^{\frac{\lambda w}{2}}(e^{\lambda x} + e^{\lambda s_h} e^{-\lambda x})}{e^{\lambda w} + e^{\lambda s_h}}$; $\lambda = \sqrt{\frac{4k}{\theta h}\sum_{n=1}^{\infty} e^{-M^2 T_v}}$.

By integrating the equations of the excess pore water pressure expressed in Eq. (6.26) and (6.27) along the *x* axis, the excess pore water pressure of simplified consolidation solution under double drainage condition can be obtained as in Eq. (6.32).

$$u_1(z,t) = -\{(p_{vac} + \alpha u_0)\left[\frac{2(e^{\mu s_h} - e^{\mu w})}{\mu s_h(e^{\mu s_h} + e^{\mu w})} + \frac{w}{s_h}\right] - \alpha u_0\left(1 - \frac{z}{h} - \sum_{n=1}^{\infty}\frac{2}{N}sin\frac{Nz}{h}e^{-N^2T_v}\right) + u_0\sum_{n=1}^{\infty}\frac{2}{M}sin\frac{2Mz}{h}e^{-4M^2T_v} \quad (6.32)$$

where, $N = n\pi$, $n \geq 1$; $h = s_v$; $\beta(x) = \frac{e^{\frac{\mu w}{2}}(e^{\mu x} + e^{\mu s_h}e^{-\mu x})}{e^{\mu w} + e^{\mu s_h}}$; $\mu = \sqrt{\frac{2k}{\theta h}(1 + 2\sum_{n=1}^{\infty}e^{-N^2T_v})}$; $\alpha = \frac{4\sum_{n=1}^{\infty}e^{-4M^2T_v}}{1+2\sum_{n=1}^{\infty}e^{-N^2T_v}}$.

In terms of Eq. (6.31) and Eq. (6.32), the excess pore water pressure is a function of *z* and *t*. Therefore, the simplified consolidation solution is under one-dimensional condition. Because of the transmissivity of geotextile, the distribution of excess pore water pressure on HDeG sheet is not uniform essentially as in Eq. (6.25) and Eq. (6.27) and depends on the time, *t*. Based on Eq. (6.31) and Eq. (6.32), an average value as in Eq. (6.33) under single drainage condition and Eq. (6.34) under double drainage condition can be represented the excess pore water pressure on HDeG sheet.

$$p_{eq}(t) = (p_{vac} + u_0)\left[\frac{2\left(e^{\lambda s_h} - e^{\lambda w}\right)}{\lambda s_h(e^{\lambda s_h} + e^{\lambda w})} + \frac{w}{s_h}\right] - u_0 \quad (6.33)$$

$$p_{eq}(t) = (p_{vac} + \alpha u_0)\left[\frac{2(e^{\mu s_h} - e^{\mu w})}{\mu s_h(e^{\mu s_h} + e^{\mu w})} + \frac{w}{s_h}\right] - \alpha u_0 \quad (6.34)$$

where, p_{eq} (t) is the average excess pore water pressure on HDeG sheet, which depends on time *t*.

To simulate the construction of land reclamation with multiple layers of soft clayey soil using finite element method, the detailed modelling of drain geotextile is not convenient. Therefore, the average excess pore water pressure, p_{eq}(t), was proposed to be implemented on vacuum drainage boundary (at the HDeG sheet level) in numerical model under one-dimensional condition for one-dimensional consolidation analysis.

6.2.3 Verification and discussion

To solve the proposed solution, the parameters of c_v, k_z, θ, w, s_h, s_v, p_{vac} and u_0 should be determined firstly. The comparison of the proposed consolidation solution and model tests were conducted. The dimensions and initial conditions of model tests using soft marine clay are shown in Table 6.1. The coefficient of consolidation, c_v, of soft marine clay is 0.4 m^2/yr. the permeability of soft marine clay and transmissivity of geotextile in soft marine clay are expressed as in Eq. (6.35) and (6.36) The settlement and the soil height at different time were calculated using the effective stress and layer-wise summation method. The effective stress was calculated using the distribution of excess pore water pressure based on the Eq. (6.31) and Eq. (6.32) for the use of HDeG sheet.

$$e = 0.931 Log_{10} k + 10.098 \tag{6.35}$$

$$Log_{10}\theta = -5.84\sigma_v'^{0.127} \tag{6.36}$$

Table 6.1 Dimensions and initial conditions of model tests using soft marine clay

Model test	γ_{sat} (kN/m^3)	e_0	Duration (day)	Vacuum (kPa)	Width (m)	Height (m)	HDeG sheet	
							Bottom	Top
1	14.4	2.82	34	-95	1.0	0.74	Drain and double non-woven geotextile sheets	Permeable
2	14.4	2.85	21	-85	1.0	0.74	Drain and single non-woven geotextile sheets	
3	14.2	3.09	32	-85	0.6	1.45	Drain and single non-woven geotextile sheets	
4	14.1	3.28	52	-85	0.6	1.45	Drain and single non-woven geotextile sheets	

*γ_{sat}: saturated unit weigh; e_0: initial void ratio

The settlement and the distributions of excess pore water pressure using the proposed consolidation solution were close to the measured in Model tests 1 to 4 as shown in Figure 6.2 to Figure 6.5. Compared with the excess pore water pressure using the proposed consolidation solution with constant coefficient of consolidation, the measured distributions of excess pore water pressure were not symmetric in vertical direction due to the gravity in Model tests 2 to 4. Overall, the trendline was also similar in terms of the average settlement and the excess pore pressure distributions.

Therefore, the proposed consolidation solution with the consideration of transmissivity is feasible to simulate the vacuum consolidation of soft clay using HDeG sheet. However, the effect of gravity on the consolidation of soft clay can't be considered in the proposed consolidation solution. Under gravity, a more 6 kPa of vertical effective stress was at the bottom in Model tests 3 and 4.

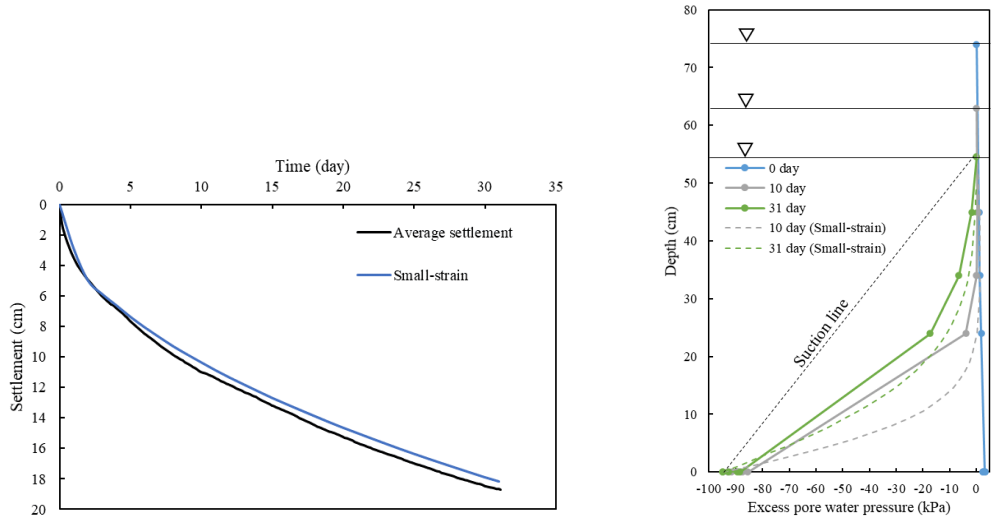

(a) Settlement (b) Excess pore water pressure

Figure 6.2 Settlement and distributions of excess pore water pressure of Model test 1 using proposed consolidation solution

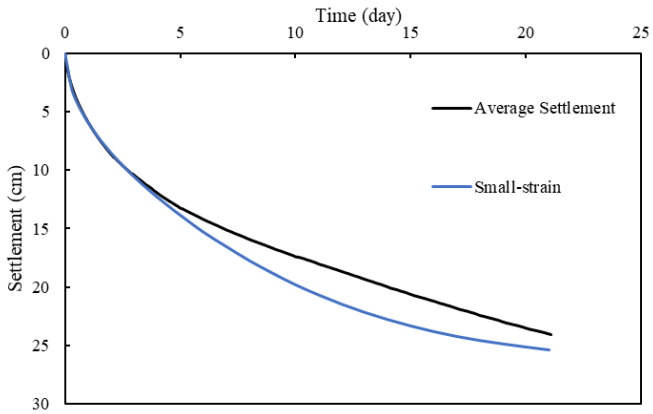

(a) Settlement

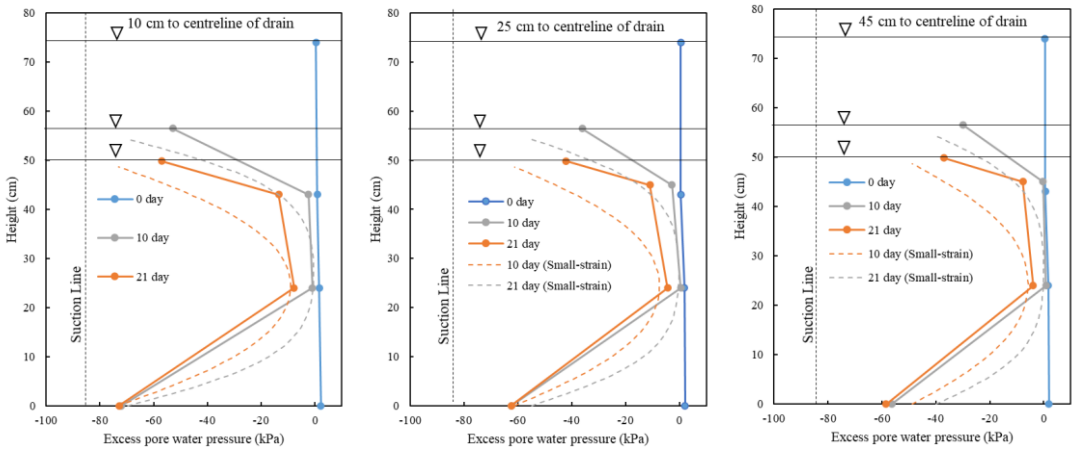

(b) Excess pore water pressure at different distances

Figure 6.3 Settlement and distributions of excess pore water pressure of Model test 2 using proposed consolidation solution

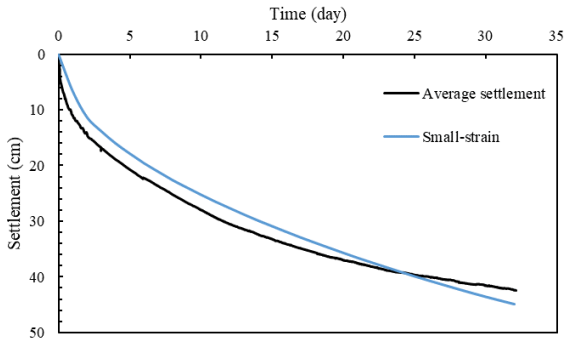

(a) Settlement

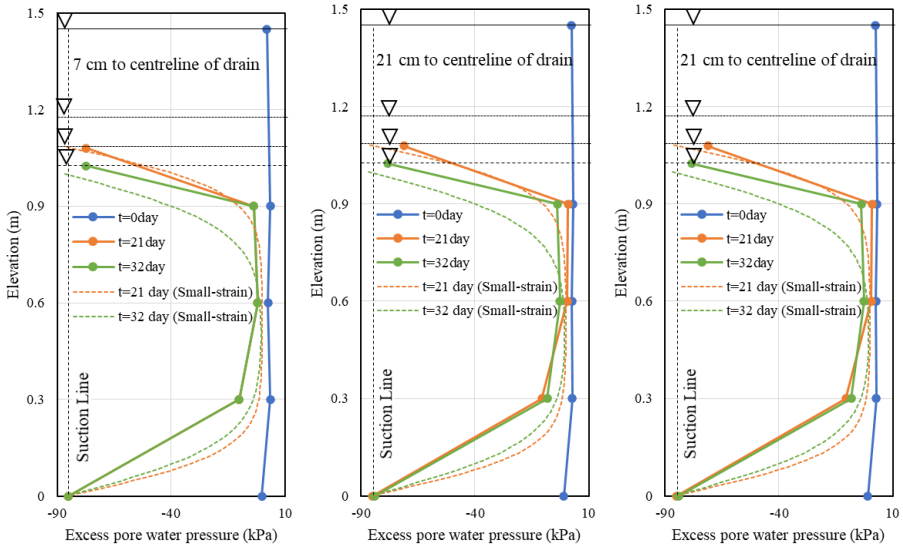

(b) Excess pore water pressure at different distances

Figure 6.4 Settlement and distributions of excess pore water pressure of Model test 3 using proposed consolidation solution

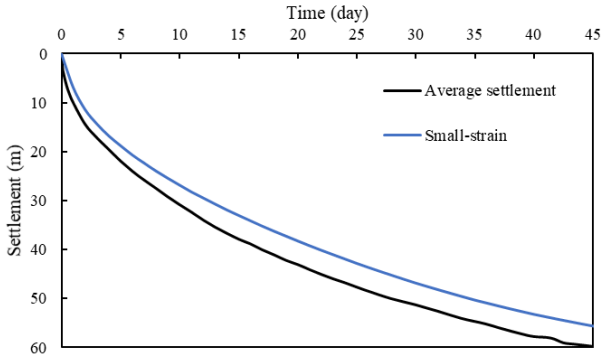

(a) Settlement

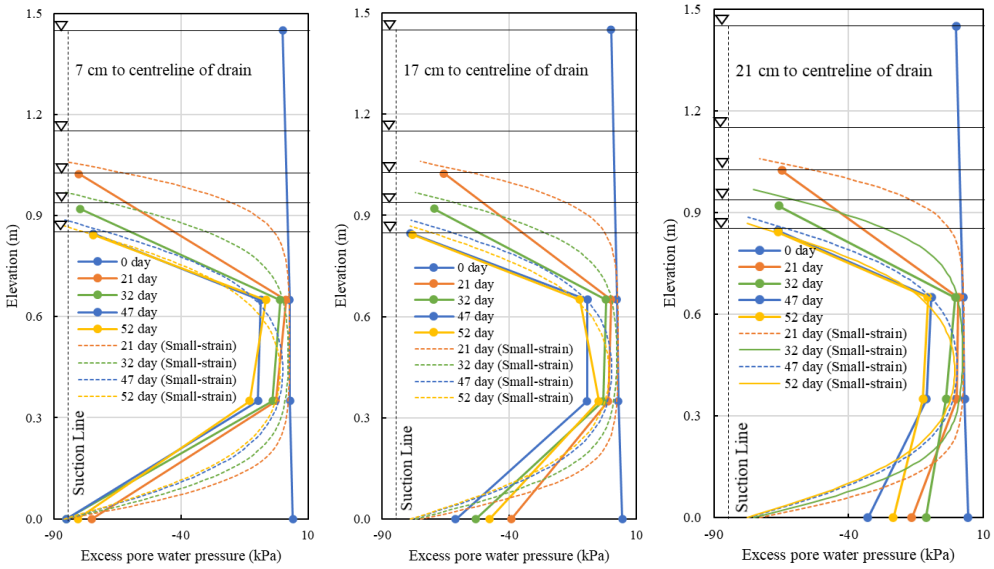

(b) Excess pore water pressure at different distances

Figure 6.5 Settlement and distributions of excess pore water pressure of Model test 4 using proposed consolidation solution

6.2.4 Parametric study

6.2.4.1 Effects of horizontal spacing (s_h)

The effect of the horizontal spacing on the degree of consolidation is represented by the first part of the formula of degree of consolidation as shown in Eq. (6.37) under single drainage condition and Eq. (6.38) under double drainage condition.

$$f(\lambda, s_h) = \frac{2\left(e^{\lambda s_h} - e^{\lambda w}\right)}{\lambda s_h\left(e^{\lambda s_h} + e^{\lambda w}\right)} + \frac{w}{s_h} \tag{6.37}$$

$$f(\mu, s_h) = \frac{2(e^{\mu s_h} - e^{\mu w})}{\mu s_h (e^{\mu s_h} + e^{\mu w})} + \frac{w}{s_h} \tag{6.38}$$

where, w is the width of drain; $\lambda = \sqrt{\frac{4k}{\theta h}\sum_{n=1}^{\infty} e^{-M^2 T_v}}$; $\mu = \sqrt{\frac{2k}{\theta h}(1 + 2\sum_{n=1}^{\infty} e^{-N^2 T_v})}$;

$\alpha = \frac{4\sum_{n=1}^{\infty} e^{-4M^2 T_v}}{1+2\sum_{n=1}^{\infty} e^{-N^2 T_v}}$.

The derivative of Eq. (6.37) to s_h is shown in Eq. (6.39) and that of Eq. (6.38) to s_h is in Eq. (6.40). Both derivatives are negative for $s_h > w$. Hence with the increasing of the horizontal spacing, the value of $f(\lambda, s_h)$ or $f(\mu, s_h)$ decreases and then the degree of consolidation decreases as well.

$$f'(\lambda, s_h) = \frac{e^{\lambda(w+s_h)}\left[(2\lambda + \lambda^2 w)e^{-\lambda(s_h - w)} - (2\lambda + \lambda^2 w)e^{\lambda(s_h - w)} + 4\lambda^2\left(s_h - w - we^{-\lambda(s_h - w)}\right)\right]}{\lambda^2 s_h^2 (e^{\lambda s_h} + e^{\lambda w})^2} \tag{6.39}$$

$$f'(\mu, s_h) = \frac{e^{\mu(w+s_h)}\left[(2\lambda + \lambda^2 w)e^{-\mu(s_h - w)} - (2\lambda + \lambda^2 w)e^{\mu(s_h - w)} + 4\mu^2\left(s_h - w - we^{-\mu(s_h - w)}\right)\right]}{\mu^2 s_h^2 (e^{\mu s_h} + e^{\mu w})^2} \tag{6.40}$$

6.2.4.2 Effects of vertical spacing (s_v)

Given the soil property of soft clay, with the increase in vertical spacing, s_v, the drainage path increases, then the T_v decreases. Due to the reduction of T_v, the degree of consolidation as in Eq. (6.42) under a single drainage condition or in Eq. (6.43) under a double drainage condition decreases.

$$\xi(h) = 1 - \sum_{n=1}^{\infty} \frac{2}{M^2} e^{-M^2 T_v} \tag{6.42}$$

$$\xi(h) = 1 - \sum_{n=1}^{\infty} \frac{2}{M^2} e^{-4M^2 T_v} \tag{6.43}$$

The effect of vertical spacing on the value of $f(\lambda, s_h)$ or $f(\mu, s_h)$, which depends on the vertical spacing, can be expressed as Eq. (6.44) or Eq. (6.45) which is part of the formula of λ or μ.

$$g_1(h) = \frac{1}{h}\sum_{n=1}^{\infty} e^{-M^2 T_v} \tag{6.44}$$

$$g_2(h) = \frac{1}{h}(1 + 2\sum_{n=1}^{\infty} e^{-N^2 T_v}) \tag{6.45}$$

For vertical spacing ranging from 1.5 m to 3.0 m, the difference in the value of $g_1(h)$ or $g_2(h)$ under different vertical spacings is small as shown in Figure 6.6. Therefore, for different vertical spacings, the difference of λ or μ is small. Therefore, the difference in the value of $f(\lambda, s_h)$ or $f(\mu, s_h)$ under different vertical spacings is small and can be ignorable. This means the effect of vertical spacing on the transmission of the excess pore water pressure on HDeG sheet is insignificant.

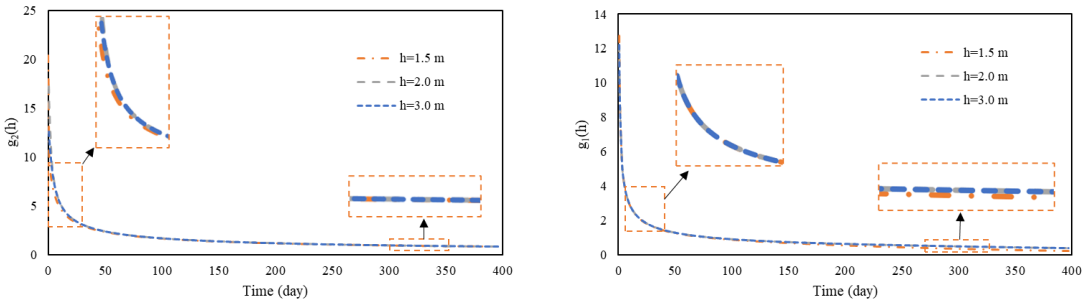

(a) Double drainage condition (b) Single drainage condition

Figure 6.6 Value of $g_1(h)$ and $g_2(h)$: (a) Double drainage condition and (b) Single drainage condition

6.2.4.3 Effects of transmissivity (θ)

As the λ and μ are the function of the transmissivity of geotextile, the derivative of Eq. (6.37) to λ is given in Eq. (6.46) and that of Eq. (6.38) to μ in Eq. (6.47). Both derivatives are negative when λ >0 or μ >0.

$$f'(\lambda, s_h) = \frac{2e^{\lambda(w+s_h)}\left[e^{-\lambda(s_h-w)} - e^{\lambda(s_h-w)} + 2\lambda(s_h - w)\right]}{\lambda^2 s_h^2 (e^{\lambda s_h} + e^{\lambda w})^2} \tag{6.46}$$

$$f'(\mu, s_h) = \frac{2e^{\mu(w+s_h)}\left[e^{-\mu(s_h-w)} - e^{\mu(s_h-w)} + 2\mu(s_h - w)\right]}{\mu^2 s_h^2 (e^{\mu s_h} + e^{\mu w})^2} \tag{6.47}$$

As the transmissivity of HDeG sheet increases for a specific soft soil, the value of λ or μ decreases. Hence the value of $f(\lambda, s_h)$ or $f(\mu, s_h)$ increases. It implies that the degree of consolidation increases.

6.2.5 Stage loading method for land reclamation

By using the new vacuum consolidation method with HDeG sheet, the soft dredged marine clay is filled in the containment pond and followed by the placement of HDeG sheet, layer by layer. For the former dredged marine clay layer, the current top-soil layer can be served as a surcharge. Then the placement of soft marine clay layer is simplified as a stage loading. For top-layer soil without geomembrane, the consolidation behaviour is under double drainage condition, but for sub-layer soil, it is under single drainage condition only. Based on proposed small-strain consolidation theory, the degree of consolidation for the vacuum consolidation with multiple layers of soft dredged marine clay using HDeG sheet can be simplified as follows. The initial excess pore water pressure of top-layer soil is ignored.

(1) Suppose at time t_1, the first step load, p_1, is applied. The degree of consolidation for top-soil layer at t_1 is calculated by Eq. (6.30) and denoted as U_0. Then the degree of consolidation after the first step load applied at t_1 is:

$$U_1 = \frac{U_0 p_{vac}}{2(p_{vac} + p_1)}$$

(2) With U_1 known, an imaginary time t_{10} can be obtained from Eq. (6.28). Under p_1, the degree of consolidation is calculated using time $t_{10}+\Delta t$.

(3) For the sub-soil layers, suppose at time t_i, the total applied load is p_i, and the degree of consolidation with respect to p_i is U_i. A load increment Δp_j, is applied immediately at time t_i. Then the degree of consolidation U_i with respect to the load $p_j = p_i + \Delta p_j$ at t_i is:

$$U_j = \frac{U_i(p_{vac} + p_i)}{p_{vac} + p_j}$$

(4) Given the U_i. known, an imaginary time t_{j0} can be obtained from Eq. (6.30). Under p_j, the degree of consolidation is calculated using time $t_{j0} + \Delta t$.

6.3 Large-strain consolidation solution

When soft clay is used as fill materials for land reclamation, the soft clay is high in both water content and compressibility. The non-linear properties of soil compressibility and permeability should be considered (Gibson, 1967 and 1981). A large-strain consolidation solution under a plane strain condition was developed for the vacuum consolidation using prefabricated drain and HDeG sheet.

The unit cell of soft clay and horizontal drains for the large-strain consolidation solution is shown in Figure 6.7. s_h is the horizontal spacing of drains; s_v is the vertical spacing of horizontal drains; θ is the transmissivity of geotextile in soft clay; γ_s is the saturated unit weight of soft clay; γ_w is the unit weight of water; e_0 is the initial void ratio, k is the permeability of soft clay. For top-soil layer with open condition, the symmetric boundary at drain level was assumed.

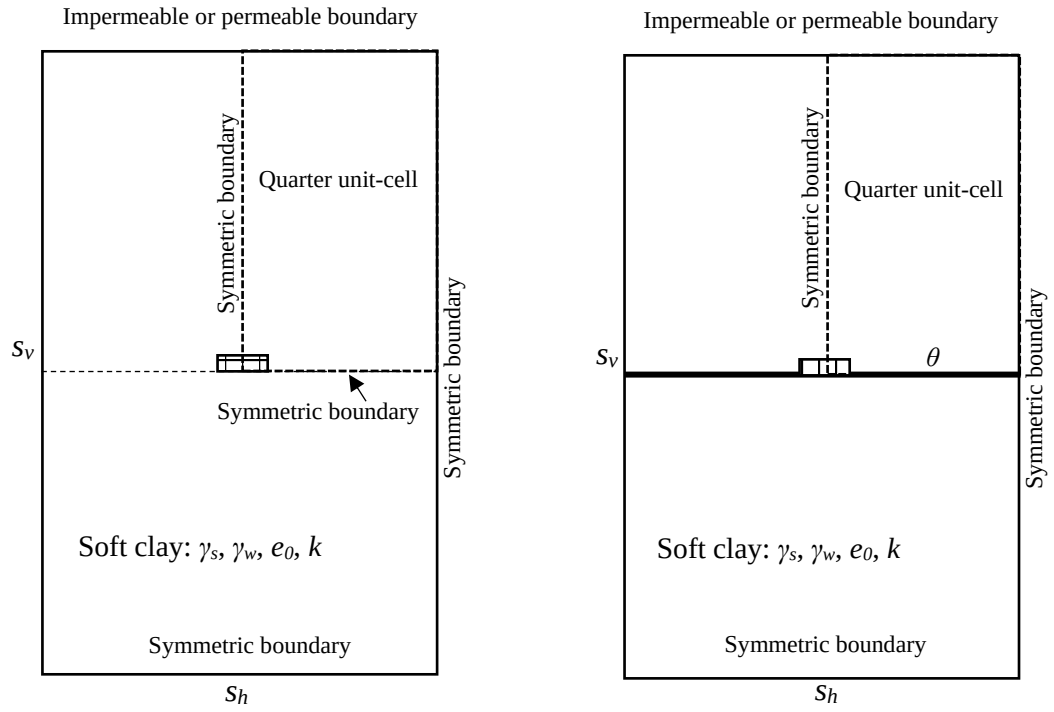

(a) Prefabricated drain (b) HDeG sheet

Figure 6.7 Rectangular unit cell: (a) Prefabricated drain and (b) HDeG sheet

6.3.1 Assumptions

(1) Darcy's law is valid.

(2) The soil is uniform.

(3) The well resistance is ignored.

(4) All compressive strains within the soil mass occur in vertical direction.

(5) The thickness of drain and non-woven geotextile is ignored.

(6) The density of water and soil particle are constant.

(7) The placement of subsequent layer of soft clay is instantly and simplified as a stage loading on underlying layers.

6.3.2 Theoretical derivations

Because of the symmetric geometry of the horizontal unit cell, see in Figure 6.7, only the quarter of horizontal unit cell was considered as in Figure 6.8. h is the consolidation height, which depends on the drainage condition. The Lagrange coordinate (*a*) and Euler coordinate $\xi = \xi(a)$ were applied. The coordinates were set-up with *x* in the horizontal direction and *a* in the vertical direction. The origin of the analytical model was set at the corner, *O*, of the quarter unit cell. The relationship of two coordinates is shown in Eq. (6.48). *u(x, a, t)* is the excess pore water pressure in soft clay under Lagrange coordinate.

$$\frac{\partial \xi}{\partial a} = \frac{1+e}{1+e_0} \tag{6.48}$$

where, *e* is the void ratio at time t; e_0 is the initial void ratio.

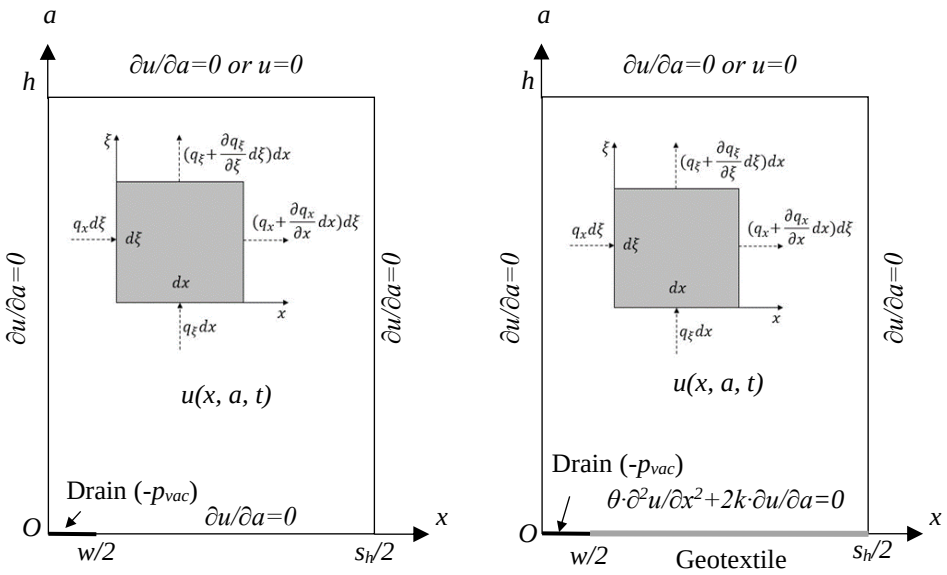

(a) Prefabricated drain (b) HDeG sheet

Figure 6.8 Analytical model for large-strain consolidation solution (p_{vac}: absolute vacuum pressure)

6.3.2.1 Boundary conditions

The boundary conditions for analytical model are shown in Eq. (6.49) to (6.51).

$$\frac{\partial u}{\partial x} = 0, x = 0 \; or \frac{s_h}{2} \tag{6.49}$$

$$u = -p_{vac}, 0 \leq x \leq \frac{w}{2} \tag{6.50}$$

$$u_0 = \Delta p, \; t = 0 \tag{6.51}$$

where, Δp is surcharge on soft clay; p_{vac} is the absolute vacuum pressure. The initial excess pore pressure, u_0, depends on the surcharge. For the use of prefabricated horizontal drain, the boundary condition at $a = 0$ is shown in Eq. (6.52).

$$\frac{\partial u}{\partial a} = 0, a \; = \; 0 \tag{6.52}$$

For the use of, the boundary condition on geotextile is shown in Eq. (6.53).

$$\theta \frac{\partial^2 u}{\partial x^2} + 2k \frac{\partial u}{\partial a} = 0, a \; = \; 0 \tag{6.53}$$

where, θ is the transmissivity of geotextile in soft soil.

Under single drainage condition, the boundary condition at $a = h$ is shown in Eq. (6.54).

$$\frac{\partial u}{\partial a} = 0, a \; = \; h \tag{6.54}$$

Under double drainage condition, the excess pore pressure at $a = h$ is set as 0 kPa as shown in Eq. (6.55).

$$u = 0, a = \; h \tag{6.55}$$

6.3.2.2 Governing Equation

Based on assumption (7), the total stress is constant for every stage loading, which can be expressed by Eq. (6.56).

$$\frac{\partial \sigma'}{\partial t} + \frac{\partial u}{\partial t} = 0 \tag{6.56}$$

where, σ' (kPa) is the effective stress; u (kPa) is the excess pore water pressure.

For the vacuum consolidation, the water flow is in both vertical and horizontal directions as in Eq. (6.57). The non-linear relationships of e-σ' and e-k were used to predict the

consolidation behaviour of soft clay. Since the soil strain only occurs in vertical direction, the governing equations of soft clay are expressed in Eq. (6.58).

$$\frac{\partial \varepsilon_v}{\partial t} = \frac{\partial q_\xi}{\partial \xi} + \frac{\partial q_x}{\partial x} \tag{6.57}$$

$$\frac{\partial u}{\partial t} = -\frac{(1+e_0)^2}{\gamma_w}\frac{d\sigma'}{de}\frac{\partial}{\partial a}\left(\frac{k}{1+e}\frac{\partial u}{\partial a}\right) - \frac{1+e}{\gamma_w}\frac{d\sigma'}{de}\frac{\partial}{\partial x}\left(k\frac{\partial u}{\partial x}\right) \tag{6.58}$$

where, ε_v is volume strain; γ_w is unit weight of water; q_ξ and q_x are the flow rate in vertical and horizontal directions in Euler coordinate; k is the permeability of soft clay. In this problem, the vertical and horizontal permeability are same for soft clay.

6.3.3 Calculation procedure

As there is no close-form solution for the large-strain consolidation solution, the finite differential method (FDM) was used to solve the analytical solution.

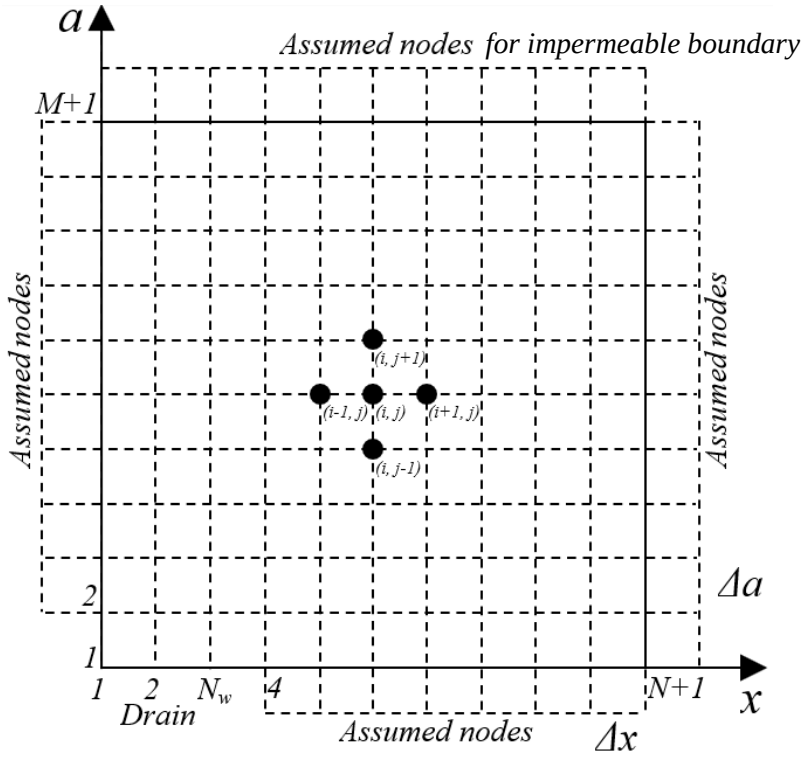

Figure 6.9 Finite difference grid at time $t = t_l$

The rate of excess pore water pressure to time, $\partial u/\partial t$, was approximated using the first forward difference equation and the second partial derivatives of excess pore water pressure in vertical and horizontal directions, $\partial^2 u/\partial a^2$ and $\partial^2 u/\partial x^2$, were approximated

using the second central difference equation. The finite differential formulas at $t = t_l$ are shown in Eq. (6.59) (Mitchell and Griffiths, 1980).

$$u_{i,j}^{l+1} = u_{i,j}^{l} + \Delta t \left[-\frac{(1+e_0)^2}{\gamma_w} \frac{d\sigma'^{l}_{i,j}}{de_{i,j}^{l}} \frac{k_{i,j}^{l}}{\left(1+e_{i,j}^{l}\right)} \frac{u_{i,j+1}^{l} - 2u_{i,j}^{l} + \Delta u_{i,j-1}^{l}}{\Delta a^2} - \frac{k_{i,j}^{l}\left(1+e_{i,j}^{l}\right)}{\gamma_w} \frac{d\sigma'^{l}_{i,j}}{de_{i,j}^{l}} \frac{u_{i+1,j}^{l} - 2u_{i,j}^{l} + u_{i-1,j}^{l}}{\Delta x^2} \right] \tag{6.59}$$

At the impermeable boundary, an assumed row or column of nodes was set beyond the boundary. The finite differential formulas for Eq. (6.49), (6.52) and (6.54) are shown in Eq. (6.60) and Eq. (6.61).

$$u_{i-1,j}^{l} = u_{i+1,j}^{l}, x = x_1 \; or \; x_{N+1} \tag{6.60}$$

$$u_{i,j-1}^{l} = u_{i,j+1}^{l}, a = a_1 \; or \; a_{M+1} \tag{6.61}$$

To solve the boundary condition on geotextile with the consideration of transmissivity, θ, the Gauss-Seidel method was applied as shown in Eq. (6.62). Then the n+1 approximation for excess pore water pressure, $u_{i,1}^{n+1}$, is the true solution.

$$\theta \frac{u_{i+1,1}^{n} - 2u_{i,1}^{n+1} + u_{i-1,1}^{n+1}}{\Delta x^2} + 2k_{i,j}^{t} \frac{u_{i,2}^{l+1} - u_{i,1}^{n+1}}{\Delta a} = 0, a = a_1 \tag{6.62}$$

For the permeable boundary in drain and at soil surface, the assume nodes are not required and the finite differential formulas are shown in Eq. (6.63) and Eq. (6.64).

$$u_{i,M+1}^{l} = 0, a = a_{M+1} \tag{6.63}$$

$$u_{i,1}^{l} = -p_{vac}, i = 1 \; to \; N_w + 1 \tag{6.64}$$

The excess pore water pressure at initial condition, which depends on the surcharge is shown in Eq. (6.65).

$$u_{i,j}^{l} = u_0 \tag{6.65}$$

The grid spacings in vertical and horizontal directions are Δa and Δx, and Δt is the time interval. The convergence condition is shown in Eq. (6.66),

$$Max\left(\frac{c_v \Delta t}{\Delta a^2}, \frac{c_h \Delta t}{\Delta x^2}\right) \leq 0.25 \tag{6.66}$$

where, c_v and c_h are the average coefficients of consolidation in vertical direction and horizontal directions. As the use of soft clay, two coefficients of consolidation are same

in this study. By using the finite differential method, the settlement and the distributions of excess pore water pressure on the cross-section of unit-cell can be calculated.

6.3.4 Verification and discussion

The comparison of the large-strain consolidation solution and model tests are conducted. The dimensions and initial conditions of model tests using soft marine clay are shown in Table 6.2. To solve the large-strain consolidation solution, the spacings Δa and Δx which were set as 0.01 m and the time interval Δt was set as 0.2 hr. The drain was 100 mm in width and the thickness was ignored. The vacuum pressure, $-p_{vac}$ = -85 kPa, was added at drain nodes.

Table 6.2 Dimensions and initial conditions of model tests using soft marine clay

Model test	γ_{sat} (kN/m^3)	e_0	Duration (day)	Vacuum (kPa)	Width (m)	Height (m)	HDeG sheet	
							Bottom	Top
1	14.4	2.82	34	-95	1.0	0.74	Drain and double non-woven geotextile sheets	Permeable
2	14.4	2.85	21	-85	1.0	0.74	Drain and single non-woven geotextile sheets	
3	14.2	3.09	32	-85	0.6	1.45	Drain and single non-woven geotextile sheets	
4	14.1	3.28	52	-85	0.6	1.45	Drain and single non-woven geotextile sheets	
5	14.2	3.09	103	-85	1.0	0.80	Prefabricated horizontal drain	Permeable
6	14.1	3.23	47	-85	0.6	1.35	Prefabricated horizontal drain	
7	14.0	3.42	21	-85	0.6	1.43	Prefabricated horizontal drain	

*γ_{sat}: saturated unit weigh; e_0: initial void ratio

To predict the consolidation behaviour of soft marine clay, the stress-strain relationship of soft marine clay was described using the compression curves from the laboratory consolidation tests, Oedometer and Consolidometer tests. As the soft marine clay is under normal consolidation condition during vacuum consolidation analysis, the equations of normal consolidation lines, proposed in Chapter 4, can be expressed in Eq. (6.67). The non-linear permeability of soft marine clay is in Eq. (6.35).

$$e = -\frac{(e_0 - 1.94)}{Log_{10}6} Log_{10}\sigma_v' + e_0, \sigma_v' < 6kPa \qquad (6.67)$$

$$e = -0.7Log_{10}\frac{\sigma_v'}{6} + 1.94, \sigma_v' < 100kPa$$

$$e = -0.4Log_{10}\frac{\sigma_v'}{100} + 1.05, \sigma_v' < 1000kPa$$

where, e_0 is the initial void ratio; σ'_v is the vertical effective stress.

The distributions of excess pore water pressure and the settlement of Model tests 1 to 4 from testing, small-strain and large-strain consolidation solutions are shown in Figure 6.10 to Figure 6.13. For Model tests 1 to 4, The results from small-strain and large-strain consolidation solutions were close. The settlement and excess pore water pressure distributions using large-strain consolidation solution were close to the measured. The excess pore water pressure on HDeG sheet using large-strain consolidation solution were also close to the measured.

The settlement and excess pore water pressure of Model test 5 using large-strain consolidation solution were larger a bit than the measured. Compared with the observed uniform soil surface, the large differential deformation on soil surface was obtained using large-strain consolidation solution. That is due to the assumption that the soil strain is only in vertical direction. Therefore, the large-strain consolidation solution is better to simulate the consolidation behaviour using HDeG sheet because the vertical soil strain is the main.

The results of Model test 6 and 7 using large-strain consolidation solution are shown in Figure 6.15 and Figure 6.16. The settlement and excess pore water pressure distributions of Model tests 6 to 7 using large-strain consolidation solution were close to the measured. With thick, soft soil in Model tests 6 and 7, the effect of the assumption that only vertical strain on the results using large-strain consolidation solution is not significant.

Therefore, the proposed large-strain consolidation solution is feasible to simulate the vacuum behaviour of soft clay using horizontal drains. But the large-strain consolidation solution is more suitable for the vacuum consolidation with thick, soft soil using prefabricated drains or with HDeG sheet because the vertical soil strain is the main.

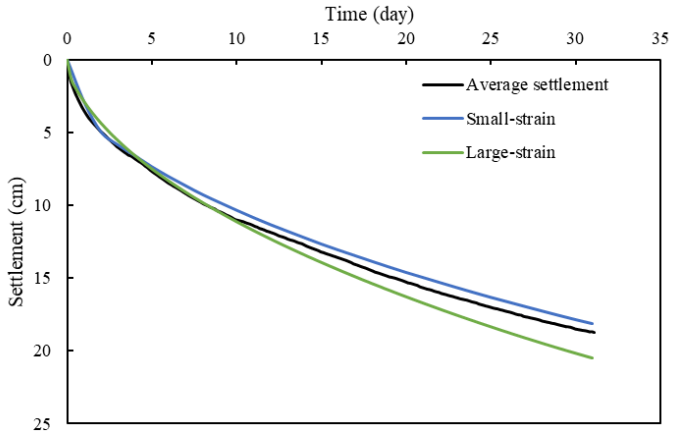

(a) Settlement

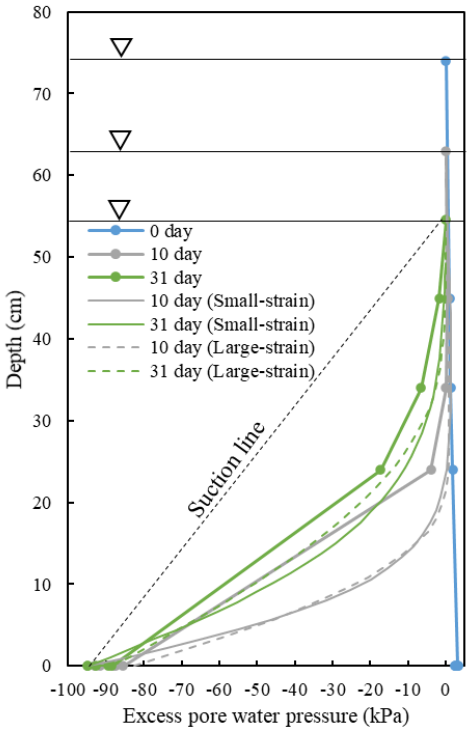

(b) Distribution of excess pore water pressure

Figure 6.10 Distributions of excess pore water pressure and settlement of Model test 1 using large-strain consolidation solution

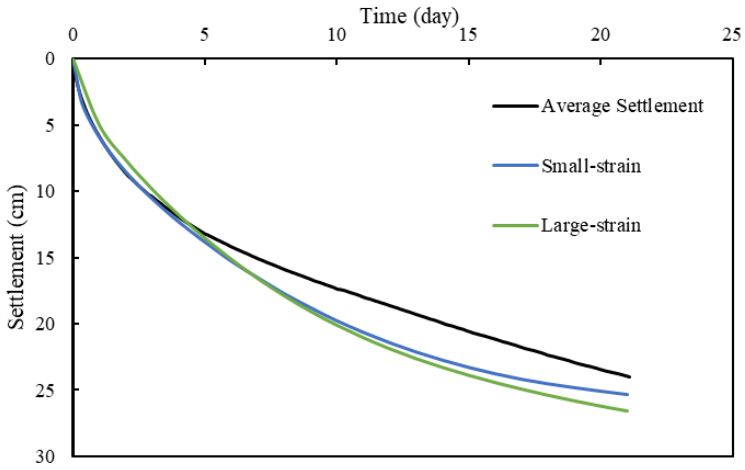

(a) Settlement

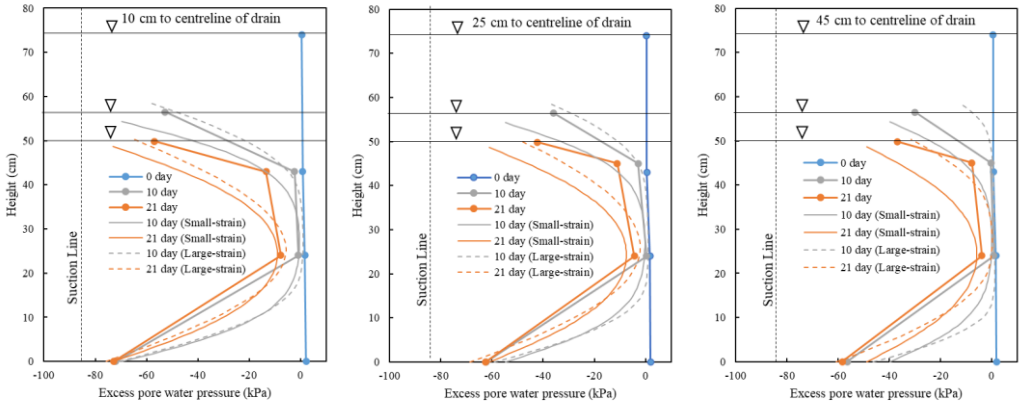

(b) Excess pore water pressure at different distances

Figure 6.11 Distributions of excess pore water pressure and settlement for Model test 2 using large-strain consolidation solution

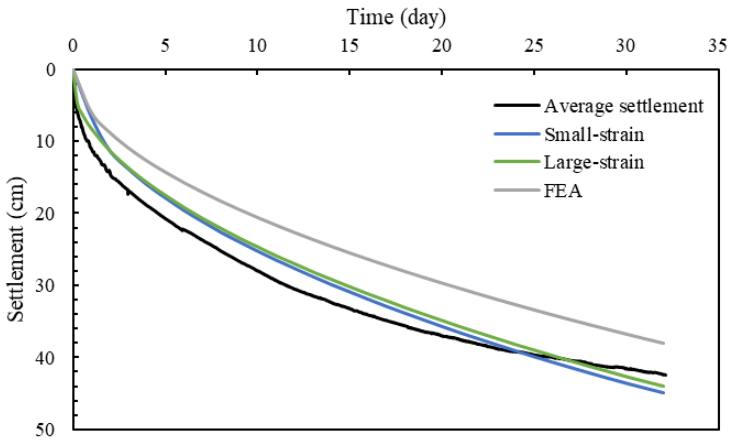

(a) Settlement

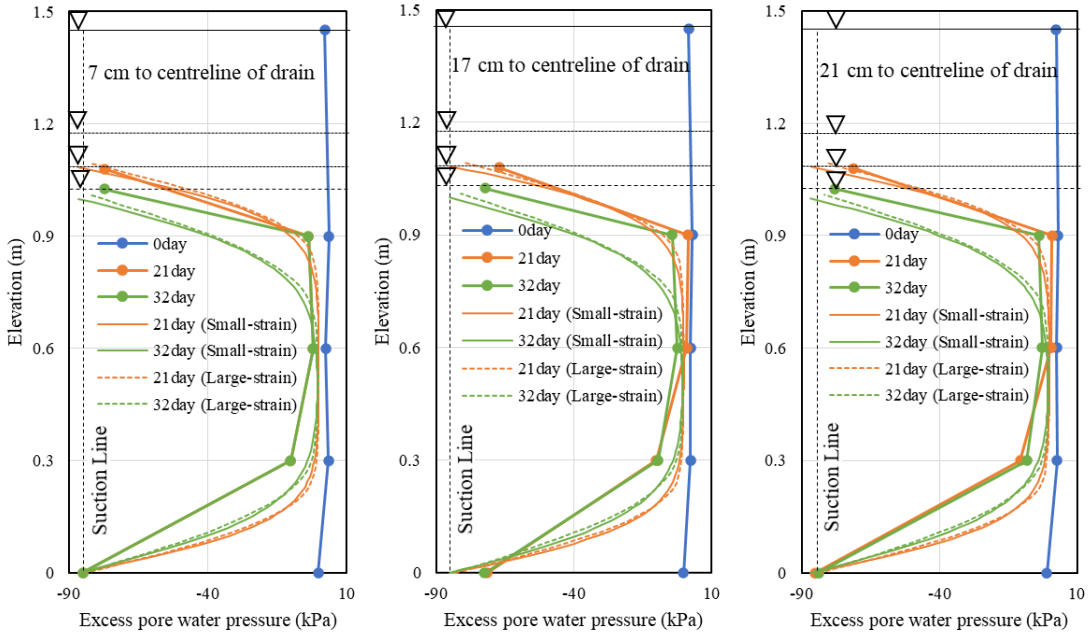

(b) Excess pore water pressure at different distances

Figure 6.12 Distributions of excess pore water pressure and settlement for Model test 3 using large-strain consolidation solution

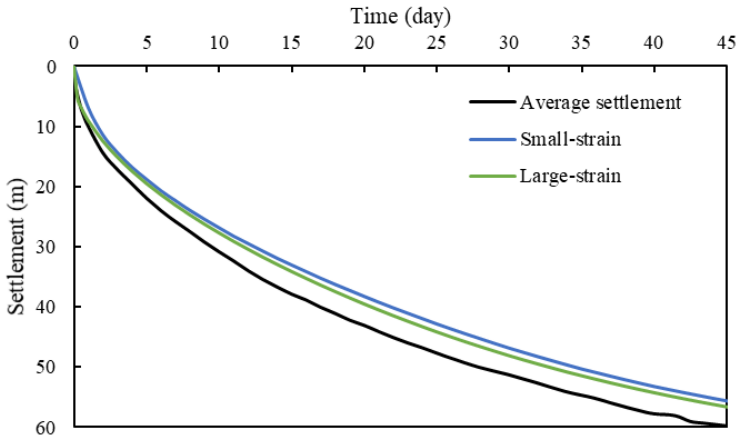

(a) Settlement

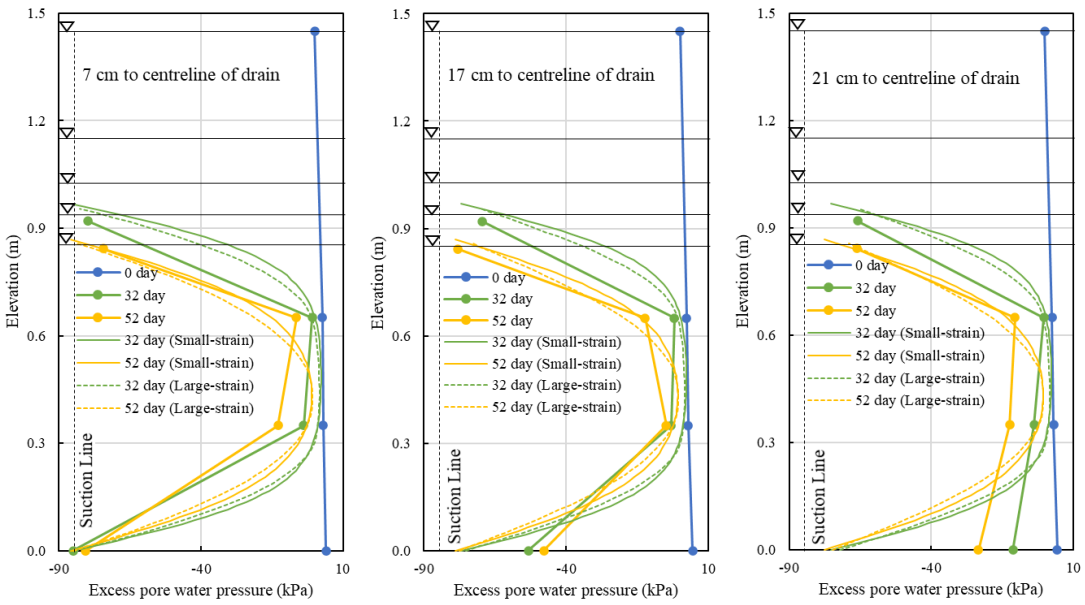

(b) Excess pore water pressure at different distances

Figure 6.13 Distributions of excess pore water pressure and settlement for Model test 4 using large-strain consolidation solution

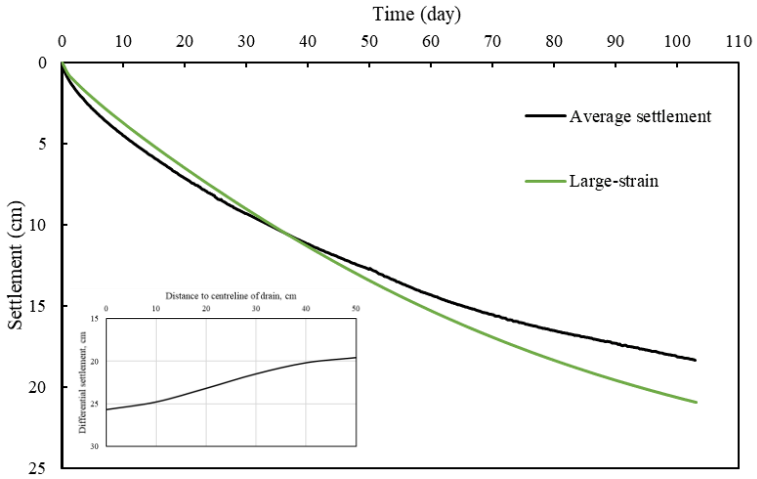

(a) Settlement

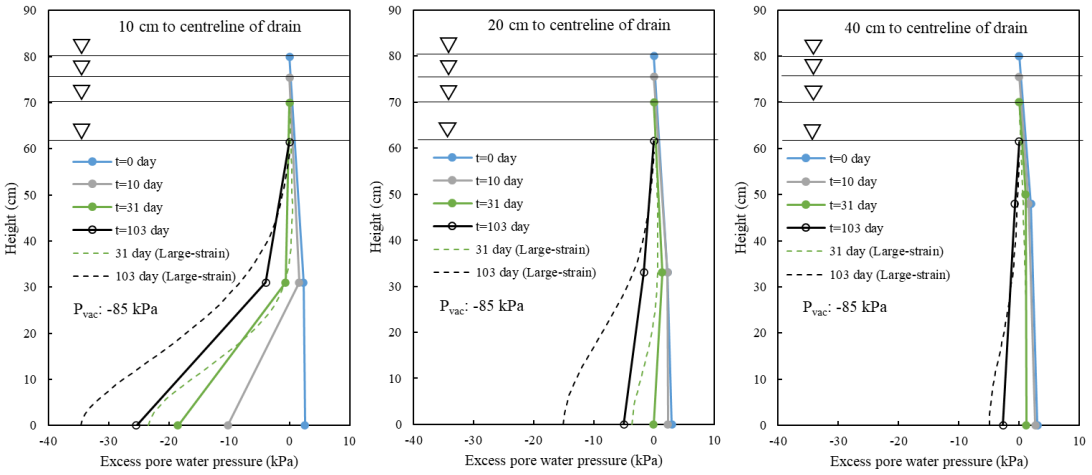

(b) Excess pore water pressure at different distances

Figure 6.14 Distributions of excess pore water pressure and settlement of Model test 5 using large-strain consolidation solution (P_{vac}: Vacuum pressure)

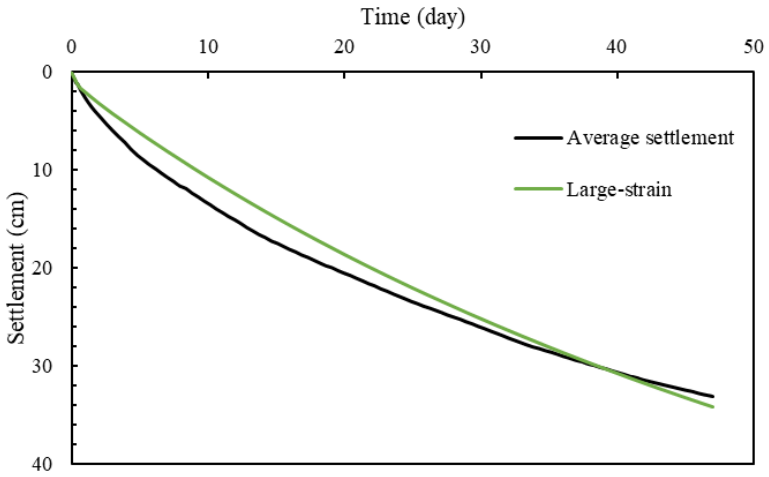

(a) Settlement

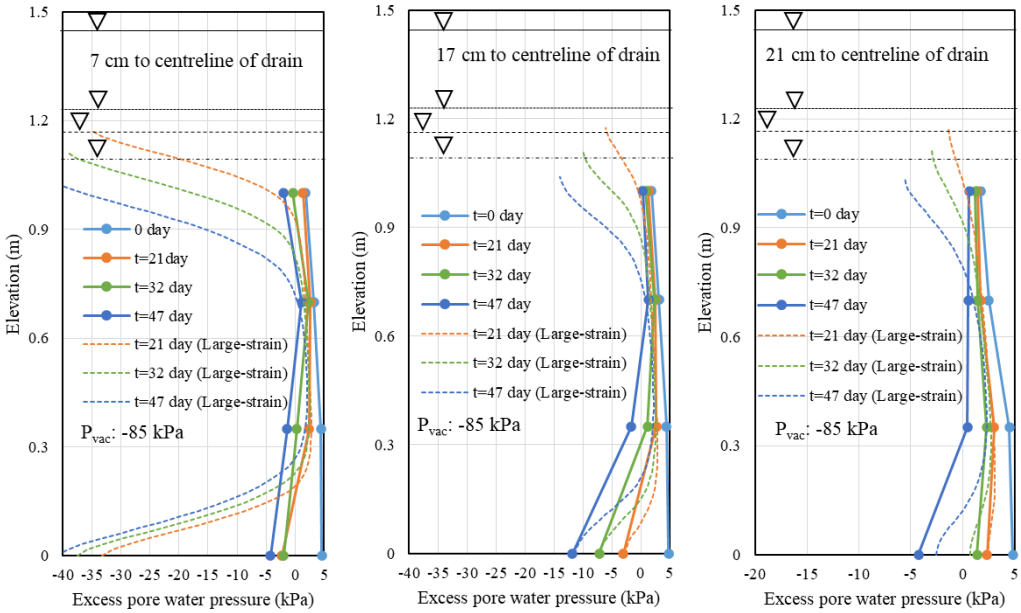

(b) Excess pore water pressure at different distances

Figure 6.15 Distributions of excess pore water pressure and settlement of Model test 6 using large-strain consolidation solution (P_{vac}: Vacuum pressure)

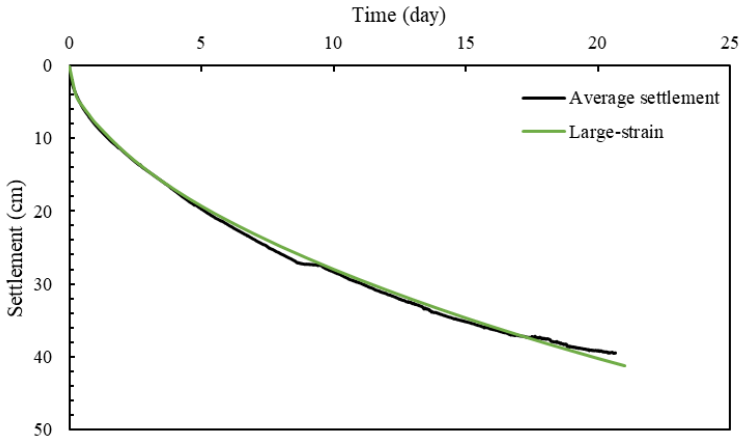

(a) Settlement

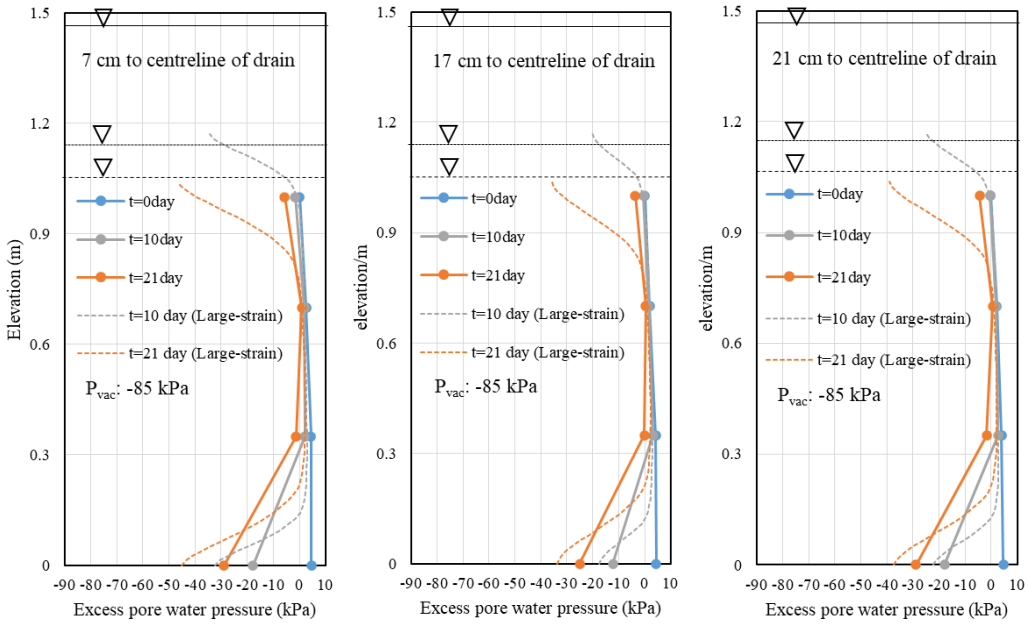

(b) Excess pore water pressure at different distances

Figure 6.16 Distributions of excess pore water pressure and settlement of Model test 7 using large-strain consolidation solution (P_{vac}: Vacuum pressure)

6.4 Numerical analysis

6.4.1 Numerical model in two-dimensional condition

Finite element analyses (FEA) were used to simulate the model tests under a plane strain condition by using the commercial software 2D ABAQUS/Standard. The numerical models are shown in Figure 6.17. The soil strain was in vertical and horizontal directions which is consistent with consolidation behaviour of soil in model tests. The transient coupled pore pressure/effective stress analysis was used to integrate the continuity equation and heat transfer equation in consolidation theory, which is related to the time increments. The 4-node bilinear displacement and pore pressure (CPE4P) element was applied to the soil material and the mesh grid was 0.01m. The dimensions and initial conditions of seven model tests using soft marine clay are shown in Table 6.3. The HDeG with non-woven geotextile was used in Model tests 1 to 4 and the prefabricated drain was used in Model tests 5 to 7.

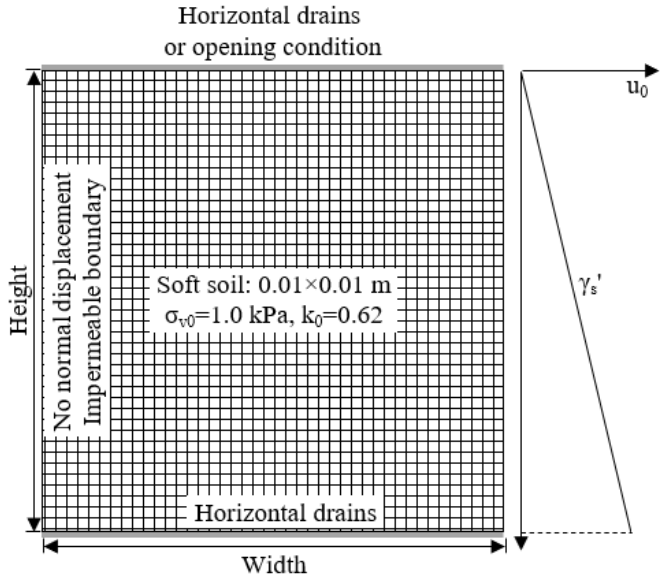

Figure 6.17 Mesh grid for numerical models (σ_{v0}: initial vertical effective stress; k_0: coefficient of lateral earth pressure at rest; u_0: initial excess pore pressure)

Table 6.3 Dimensions and Initial conditions of model tests using soft marine clay

Model test	γ_{sat} (kN/m^3)	e_0	Duration (day)	Vacuum (kPa)	Width (m)	Height (m)	HDeG sheet	
							Bottom	Top
1	14.4	2.82	34	-95	1.0	0.74	Drain (2mm), Geotextile element, 10cm	Permeable
2	14.4	2.85	21	-85	1.0	0.74	Drain (2mm), Geotextile element, 10cm	
3	14.2	3.09	32	-85	0.6	1.45	Drain (2mm), Geotextile element, 10cm, 5cm	
4	14.1	3.28	52	-85	0.6	1.45	Drain (2mm), Geotextile element, 10cm	
5	14.2	3.09	103	-85	1.0	0.80	Drain (2mm), 10cm	Permeable
6	14.1	3.23	47	-85	0.6	1.35	Drain (2mm), 5cm	
7	14.0	3.42	21	-85	0.6	1.43	Drain (2mm), 5cm, 10cm	

*γ_{sat}: Saturated unit weigh; e_0: initial void ratio

As the soft marine clay is under normal consolidation condition during vacuum consolidation analysis, the stress-strain relationship of soft marine clay was also

described using normal consolidation lines as in Eq. (6.67) and inputted into the numerical models. The compression index at slurry stage (below 6 kPa) was affected by the initial void ratio. Thus, the deformation of self-weight consolidation of soft marine clay was considered using the normal consolidation lines and initial excess pore pressure as in Figure 6.17. The excess pore water pressure was calculated using the buoyant unit weight of soft marine clay, γ'_s. In consolidation theory, the dissipation of excess pore water pressure depended on the permeability of porous material. The relationship of void ratio and permeability from the consolidation and permeability tests of soft marine clay as in Eq. (6.35) was inputted into the numerical models.

The modified cam-clay model was used for soft marine clay. The piecewise linearly clay hardening curve as shown in Figure 6.18 was used to model the increase of yield stress in hydrostatic compression in soft marine clay under consolidation. This curve is calculated using Eq. (6.68) and (6.69). The parameters for modified cam-clay model are shown in Table 6.4. By inputting the piecewise linearly clay hardening curve, the compression index was not required. The recompression index, κ, was 0.03 based on the Oedometer and Consolidometer tests. The coefficient, M, the slope of critical state line was 0.882, which was calculated using the friction angle, φ = 22.6°. A small initial effective stress should be set for the soft marine clay in numerical model. Here the initial effective stress was set as 1 kPa under k_0 condition. Thus the initial yield stress, P_{c0}, in hydrostatic compression of soft marine clay was 1 kPa.

$$(\frac{p_c - p}{\frac{p_c}{2}})^2 + (\frac{q}{M\frac{p_c}{2}})^2 = 1 \tag{6.68}$$

$$\varepsilon_{vol} = \frac{e_1 - e}{1 + e_1} \tag{6.69}$$

where,

$$p = \frac{2k_0 + 1}{3}\sigma'_v$$

$$q = (1 - k_0)\sigma'_v$$

$$k_0 = 1 - sin\varphi'$$

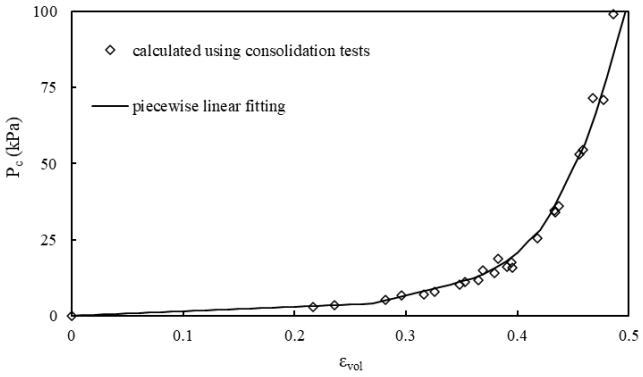

Figure 6.18 The piecewise hardening relationship for Modified Cam-clay model for soft marine clay

Table 6.4 Soil parameter in modified cam-clay model of soft marine clay

κ	φ' (°)	M	P_{c0} (kPa)
0.03	22.6	0.882	1.0

The drain was modelled as rectangular shape with 3 mm in thickness. The negative excess pore pressure was set at the perimeter of the drain, -95 kPa for Model test 1 and -85 kPa for Model test 2 to 7. The non-woven geotextile was modelled using geotextile element. The subroutine for geotextile element was similar to the PVD element developed by Peng and Liu (2005). However, the change of non-linear transmissivity with the effective stress on geotextile can be considered in geotextile element. The compressibility (see Figure 6.19) and in-plane permeability, the transmissivity over the thickness of geotextile, in soft marine clay were inputted as parameters for the geotextile element.

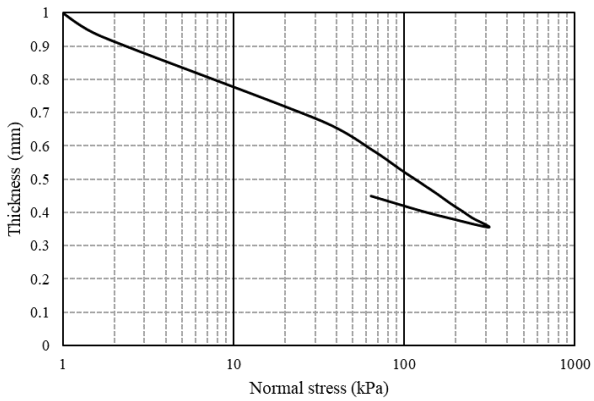

Figure 6.19 Thickness of non-woven geotextile under different normal stress

The zero-pore water pressure was set on the boundary where drainage was permitted such as the top surface for Model tests 1 and 5. The normal displacement was fixed at the lateral and bottom boundaries.

6.4.2 Numerical model in one-dimensional condition

As the detail modelling of drain in rectangular shape and geotextile using geotextile element was time-consuming for multiple layers of soft clay for land reclamation. A numerical simulation using average excess pore pressure on HDeG sheet was proposed to model the vacuum consolidation using HDeG sheet. The numerical model was similar as in Section 6.4.1. The difference was that the average pore water pressure, $p_{eq}(t)$, as in Eq. (6.33) or Eq. (6.34), representing the excess pore water pressure on HDeG sheet, was set at vacuum drainage boundary as in Figure 6.20. The comparison of 1D numerical model and the Model tests 1 to 4 were conducted to verify this method. The unit weight, initial void ratio, the initial height, compressibility, and permeability of soft marine clay in Model tests 1 to 4 are same as in Section 6.4.1. The average pore water pressure of Model tests 1 to 4 are shown in Figure 6.21.

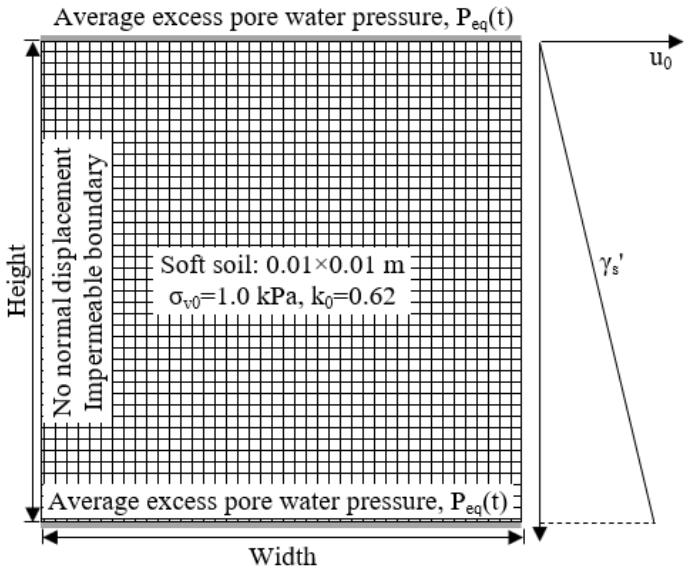

Figure 6.20 Numerical model with average excess pore pressure on HDeG sheet for Model test 1 to 4

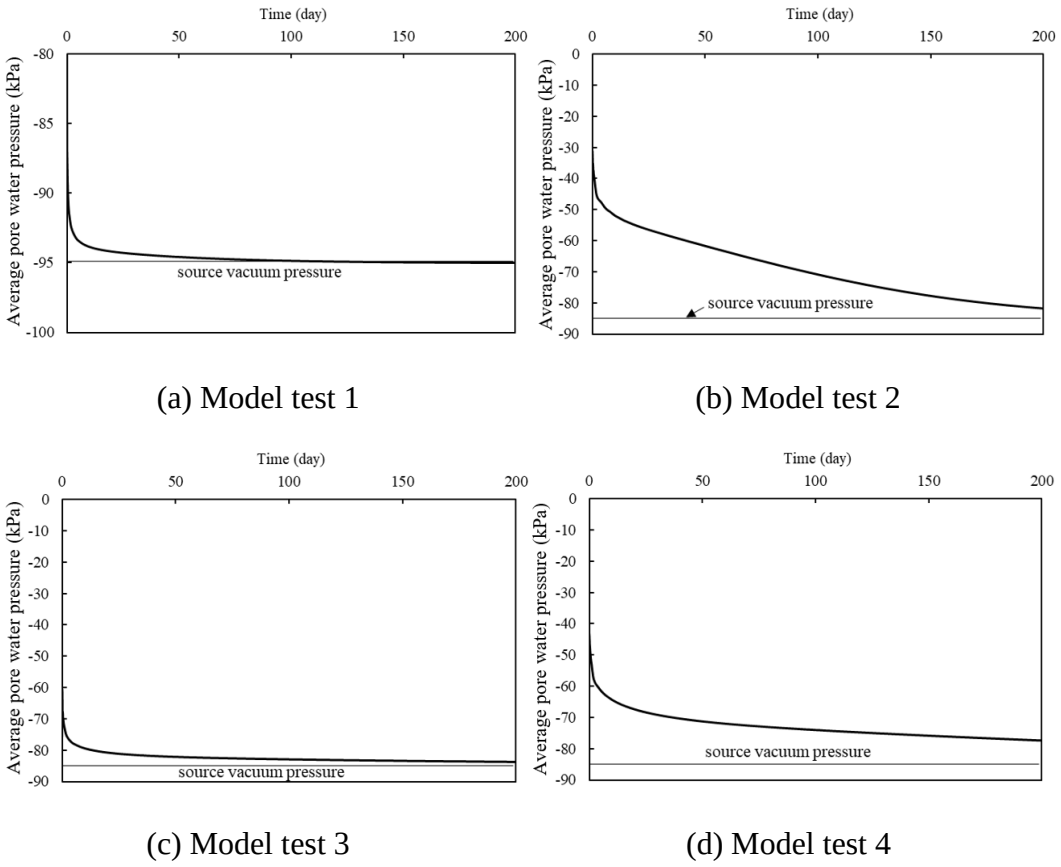

Figure 6.21 Average pore water pressure for 1D numerical models representing the pore water pressure distribution on HDeG sheet: (a) Model test 1; (b) Model test 2; (c) Model test 3 and (d) Model test 4

6.4.3 Results and discussion

6.4.3.1 Excess pore water pressures and settlements

The contours of excess pore water pressure and settlement of Model tests 1 are shown in Figure 6.22. The excess pore water pressure and settlement were uniform at same elevation. The distributions of excess pore water pressure and the average settlement of Model test 1 from the model tests, small-strain and large-strain consolidation solutions and FEA are shown in Figure 6.23. The contours of excess pore water pressure and settlement of Model test 5 are shown in Figure 6.24. The distributions of excess pore water pressure and average settlement of Model test 5 from the model tests, large-strain consolidation solution and FEA are shown in Figure 6.25.

The average settlements using FEA were close to the measured and the calculated using Theoretical solutions. That is because the opening condition in Model tests 1 and 5

resulted in the uniform soil surface observed during testing. Hence, the average settlement on the four measurement points was close to the average surface settlement of soil and the simulated settlement using FEA. The excess pore pressure distributions of Model test 1 using FEA were lower than the measured and the calculated. However, the trendlines were similar. The excess pore pressure distributions of Model test 5 using FEA were close to the measured.

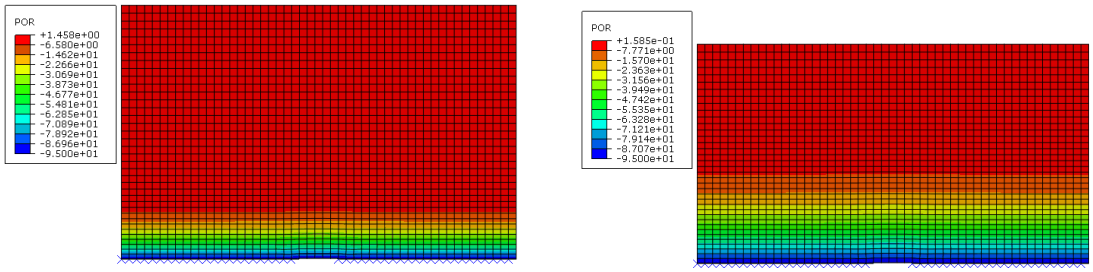

(a) Excess pore water pressure on 10th day (b) Excess pore water pressure on 31st day

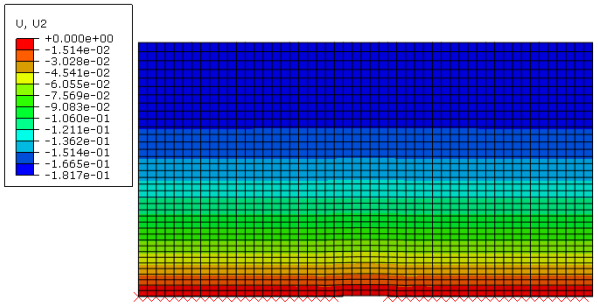

(c) Settlement on 31st day

Figure 6.22 Contours of excess pore water pressure and settlement of Model test 1 (POR: Pore water pressure; U2: Settlement)

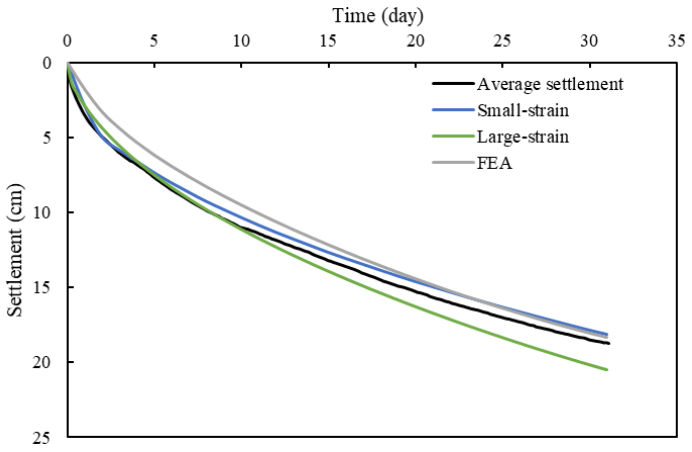

(a) Settlement

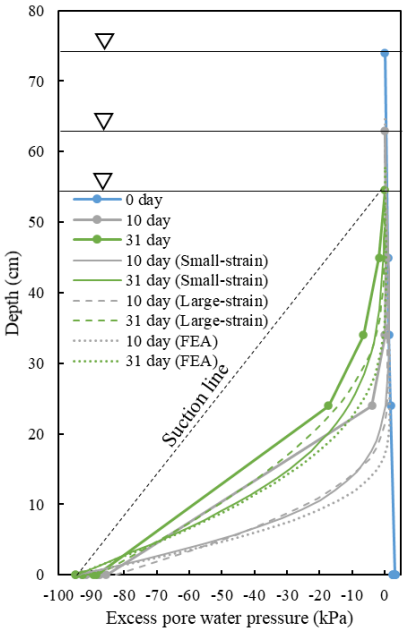

(b) Excess pore water pressure Distribution

Figure 6.23 Distributions of excess pore water pressure and settlement at selected sections using FEA for Model test 1

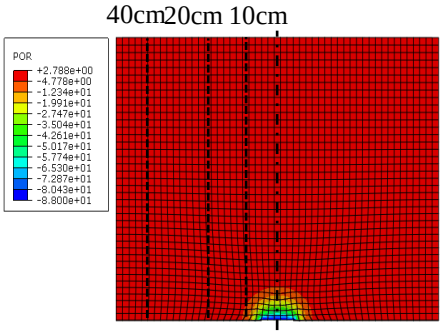

(a) Excess pore water pressure on 10th day

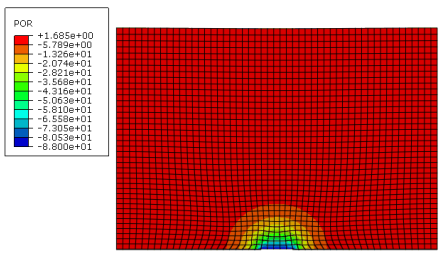

(b) Excess pore water pressure on 31st day

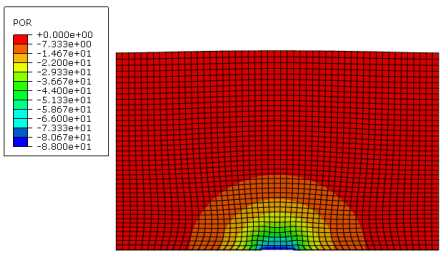

(c) Excess pore water pressure on 103th day

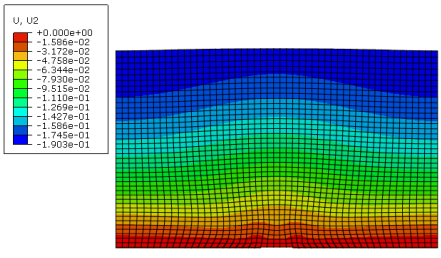

(d) Settlement on 103th day

Figure 6.24 Contours of excess pore water pressure and settlement of Model test 5 (POR: Pore water pressure; U2: Settlement)

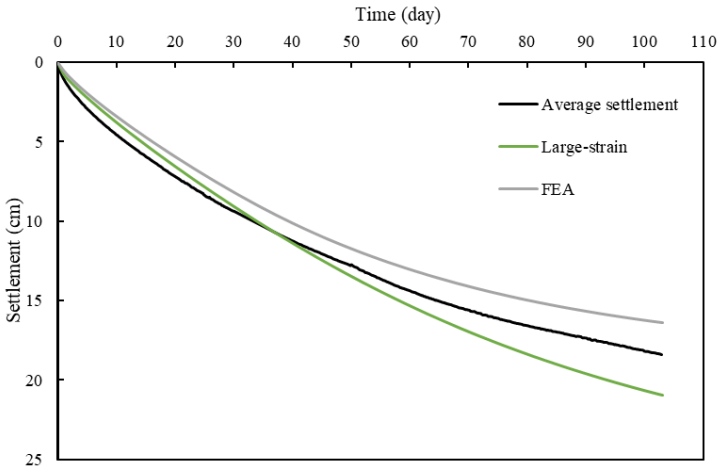

(a) Settlement

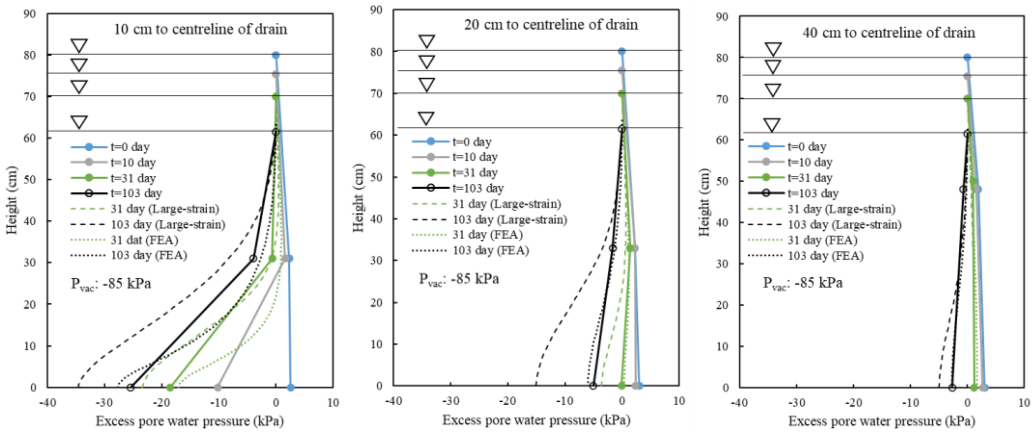

(b) Excess pore water pressure distributions at different distances

Figure 6.25 Distributions of excess pore water pressure and settlement at selected sections using FEA for Model test 5 (P_{vac}: Vacuum pressure)

The contours of excess pore water pressure and settlement of Model tests 2, 3 and 4 with the used of HDeG sheet are shown in Figure 6.26 to Figure 6.28. and the contours of excess pore water pressure and settlement of Model tests 6 and 7 with the used of drain only are shown in Figure 6.29 and Figure 6.30. Compare with the simulation results of Model test 6 and 7, the excess pore water pressure and the settlement in Model tests 2, 3 and 4 were more uniform.

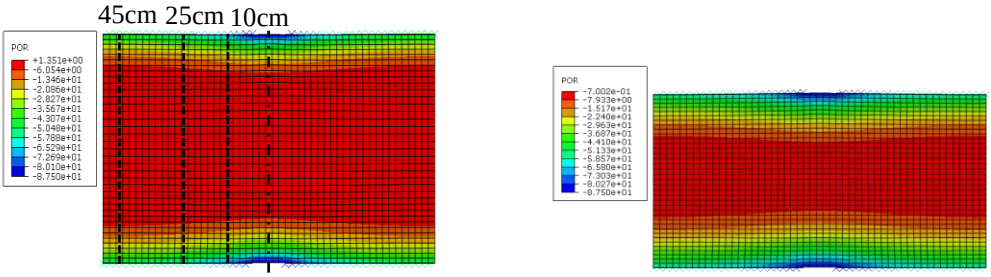

(a) Excess pore water pressure on 10th day (b) Excess pore water pressure on 21st day

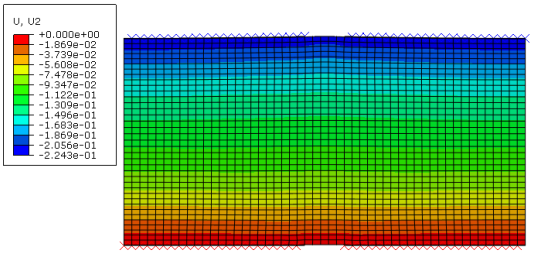

(c) Settlement on 21st day

Figure 6.26 Contours of excess pore water pressure and settlement of Model test 2

(POR: Pore water pressure; U2: Settlement)

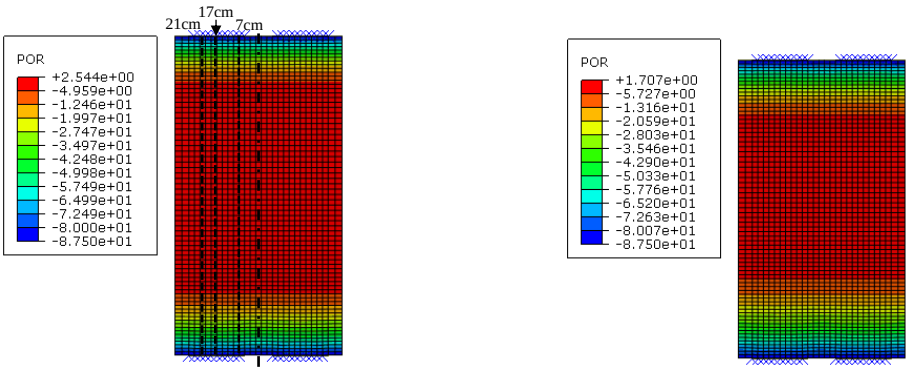

(a) Excess pore water pressure on 21st day (b) Excess pore water pressure on 32nd day

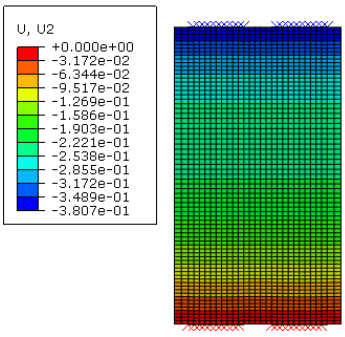

(c) Settlement on 32nd day

Figure 6.27 Contours of excess pore water pressure and settlement of Model test 3

(POR: Pore water pressure; U2: Settlement)

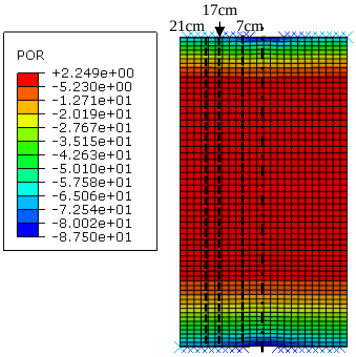

(a) Excess pore water pressure on 21st day

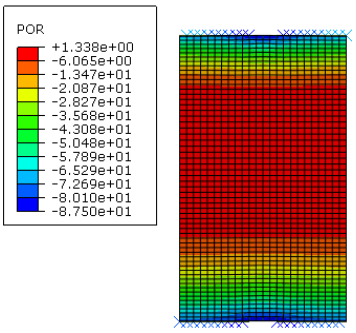

(b) Excess pore water pressure on 32nd day

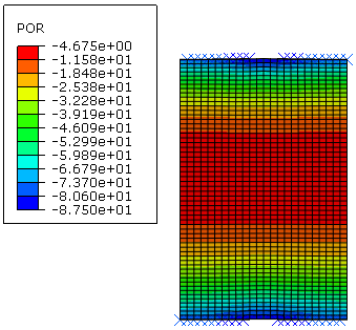

(c) Excess pore water pressure on 47th day

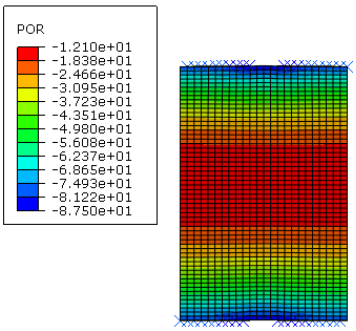

(d) Excess pore water pressure on 52nd day

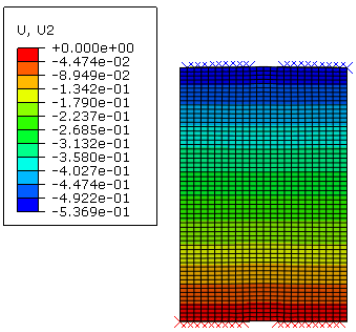

(c) Settlement on 52nd day

Figure 6.28 Contours of excess pore water pressure and settlement of Model test 4 (POR: Pore water pressure; U2: Settlement)

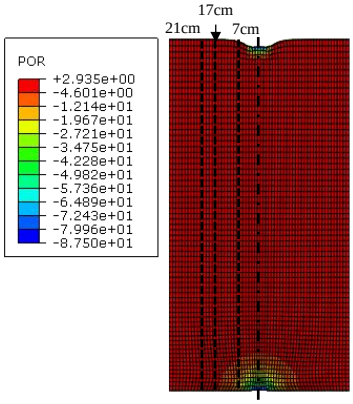

(a) Excess pore water pressure on 21st day

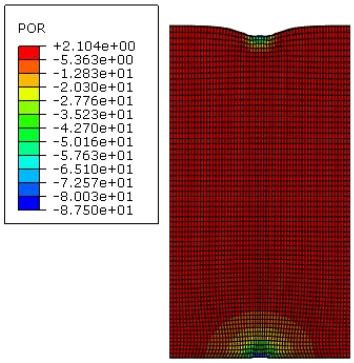

(b) Excess pore water pressure on 32nd day

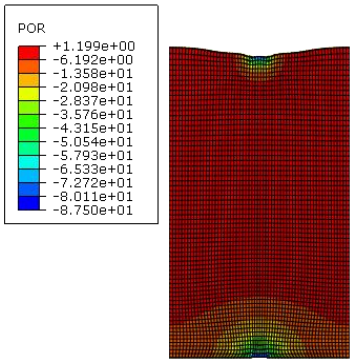

(c) Excess pore water pressure on 47th day

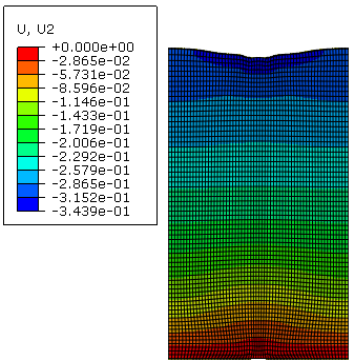

(d) Settlement on 47th day

Figure 6.29 Contours of excess pore water pressure and settlement of Model test 6 (POR: Pore water pressure; U2: Settlement)

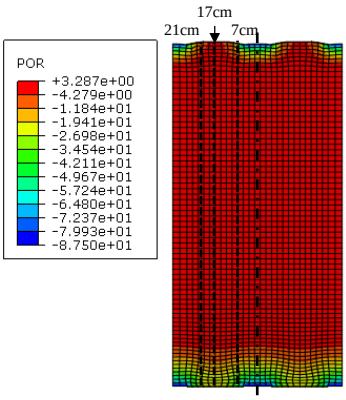

(a) Excess pore water pressure on 10th day

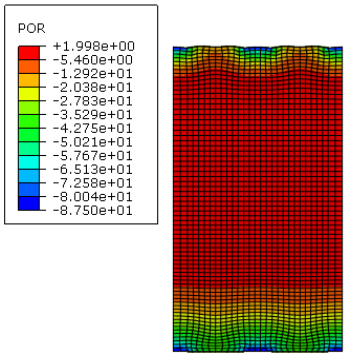

(b) Excess pore water pressure on 21st day

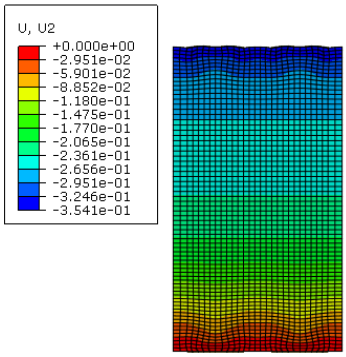

(c) Settlement on 21st day

Figure 6.30 Contours of excess pore water pressure and settlement of Model test 7 (POR: Pore water pressure; U2: Settlement)

Based on the selected specific cross-sections, the calculation and simulation results for Model tests 2, 3 and 4 with the use of HDeG sheet and Model tests 6 and 7 with the use of drain only under sealed soil surface are shown in Figure 6.31 to Figure 6.35. The average settlements predicted using FEA were lower than the measured and the calculated using theoretical solutions. The distributions of excess pore water pressures using FEA were consistent with those measured. However, relatively lower pore water pressure distributions were obtained from FEA. This is consistent with the lower settlement prediction. The numerical prediction could simulate the effect of geotextile as the different pore water pressure distributions in Model test 3 and 4 were captured by the FEA.

The comparison of the model tests and FEA with average pore water pressure, P_{eq}, on HDeG sheet were conducted for Model tests 1 to 4. The average settlement and the distributions of excess pore water pressure using FEA with average pore water pressure were close to the measured. The settlement was a bit lower than the measured, but the trendline was similar. That is partly because the measurement points on soil surface were not enough. In Mode test 1, with the good transmissivity, the excess pore pressure on HDeG sheet was uniform. Therefore, the results of 1D and 2D numerical simulation were same. In Model test 2, the distributions of excess pore pressure using FEA were close to the measured at the middle distance (25 cm to centreline of drain). In Model tests 3 and 4, the distributions of excess pore pressure using FEA were also close to the measured at the middle distance (17 cm to centreline of drain). Hence, the excess pore water pressure using FEA with average pore water pressure on HDeG sheet is the

average values on cross-section. In a word, the one-dimensional numerical model with average pore water pressure on HDeG sheet is feasible and valid to simulate the vacuum consolidation of soft clay using HDeG sheet.

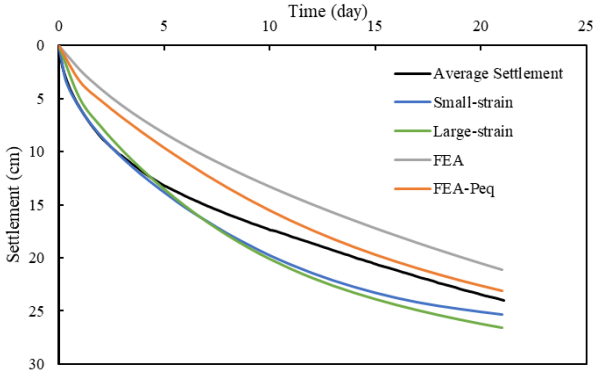

(a) Settlement

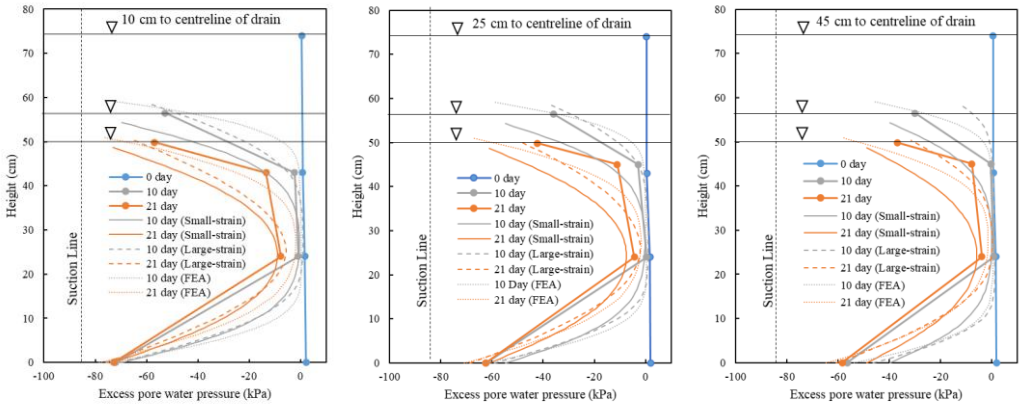

(b) Excess pore water pressure distributions at different distances

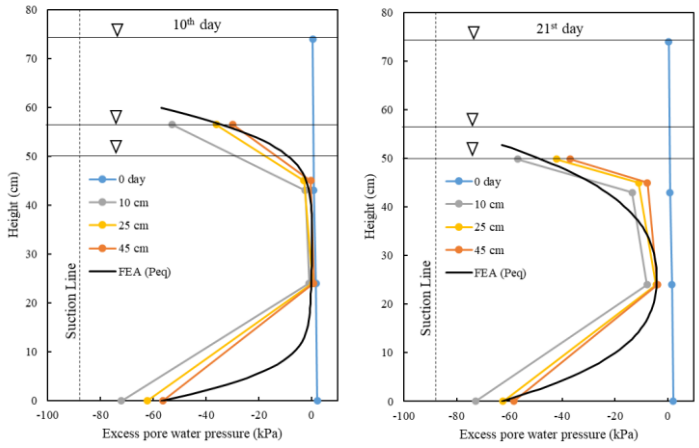

(c) Excess pore water pressure distributions at different days using FEA with average excess pore pressure

Figure 6.31 Distributions of excess pore water pressure and average settlement using FEA for Model test 2 (P_{eq}: average excess pore pressure on HDeG sheet)

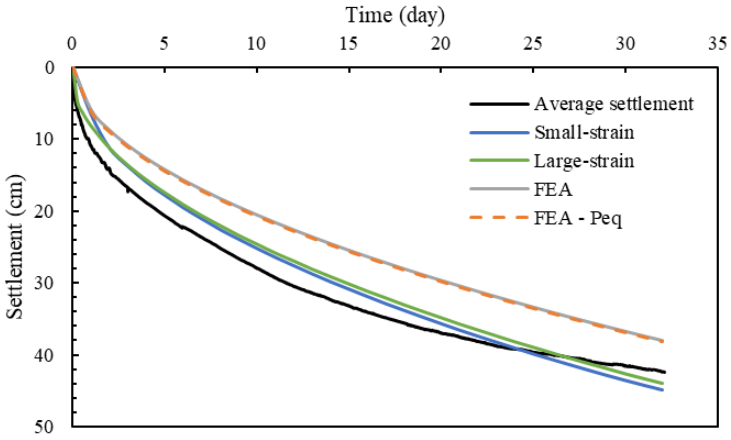

(a) Settlement

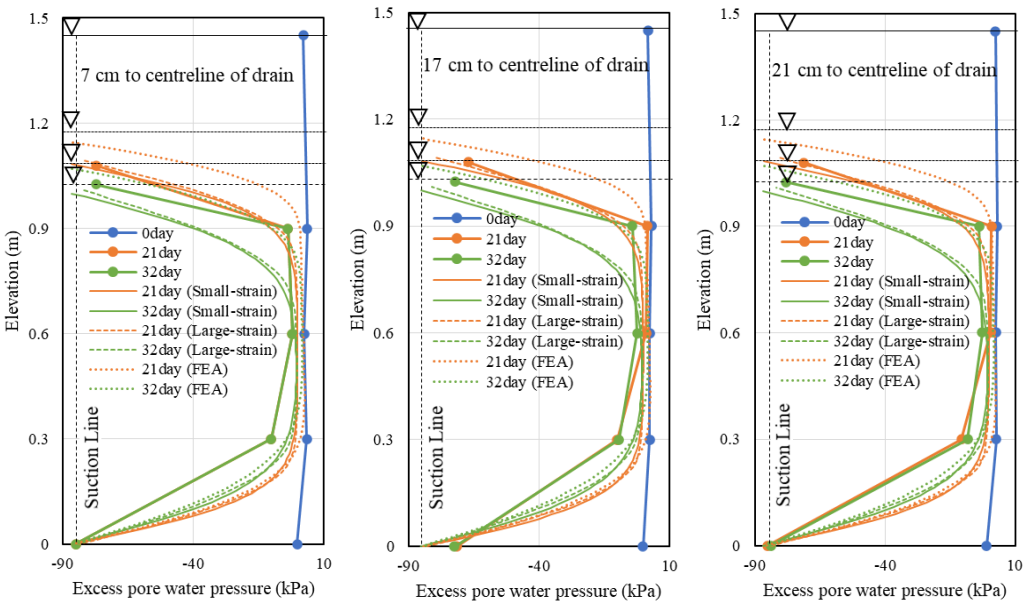

(b) Excess pore water pressure distributions at different distances

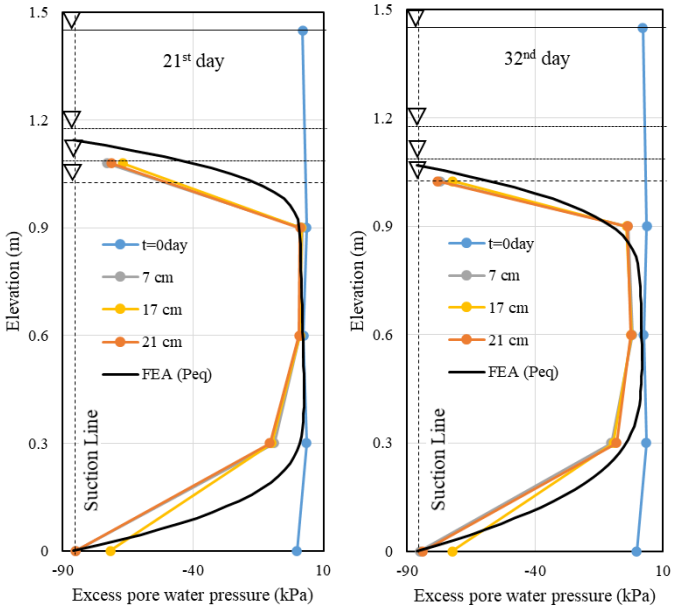

(c) Excess pore water pressure distributions at different days using FEA with average excess pore pressure

Figure 6.32 Distributions of excess pore water pressure and average settlement using FEA for Model test 3 (P_{eq}: average excess pore pressure on HDeG sheet)

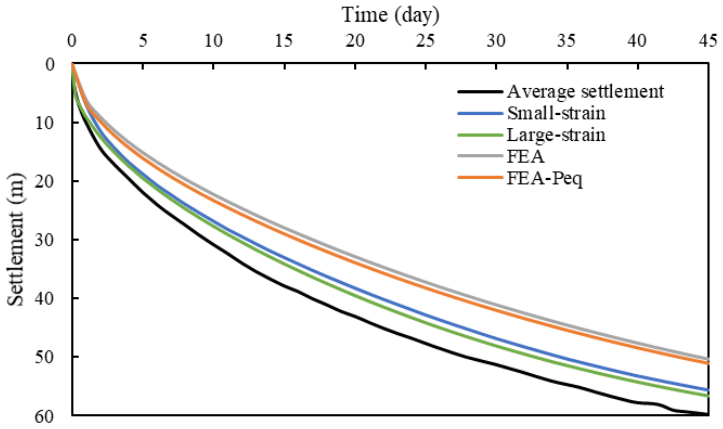

(a) Settlement

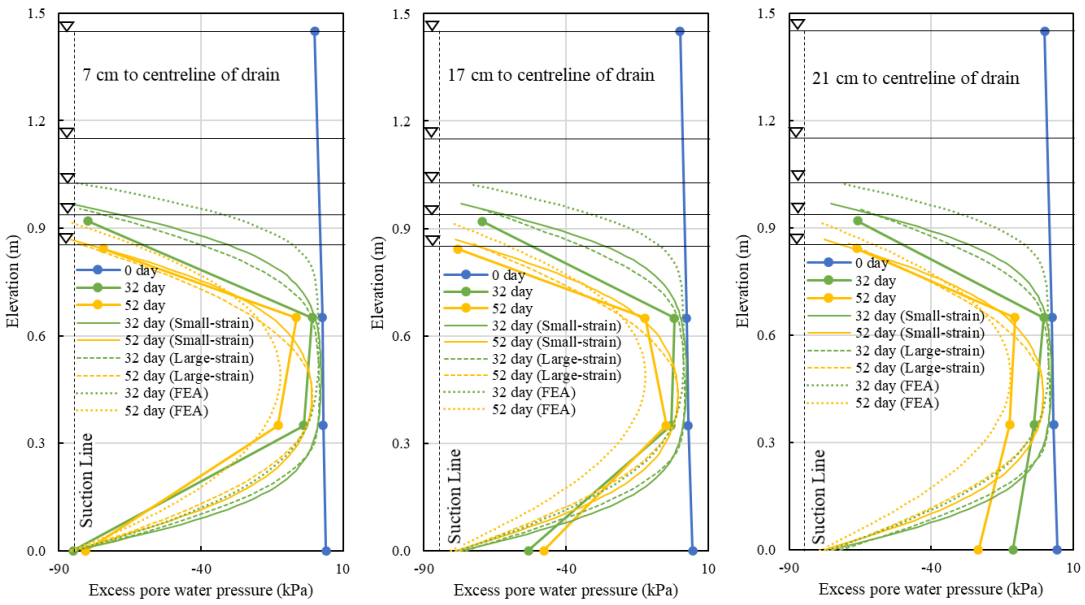

(b) Excess pore water pressure distributions at different distances

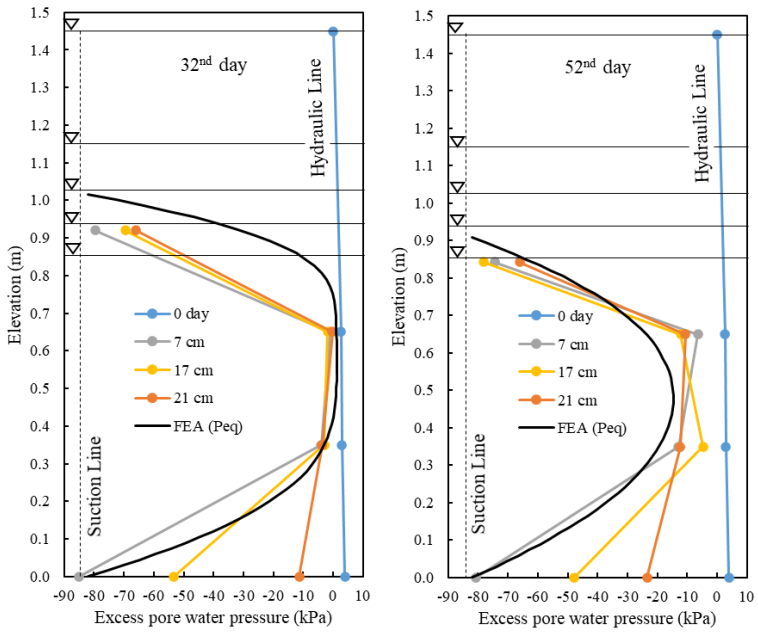

(c) Excess pore water pressure distributions at different days using FEA with average excess pore pressure

Figure 6.33 Distributions of excess pore water pressure and average settlement using FEA for Model test 4 (P_{eq}: average excess pore pressure on HDeG sheet)

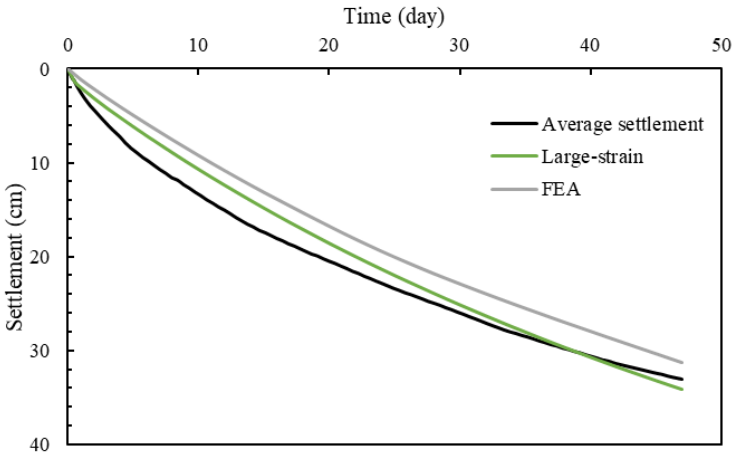

(a) Settlement

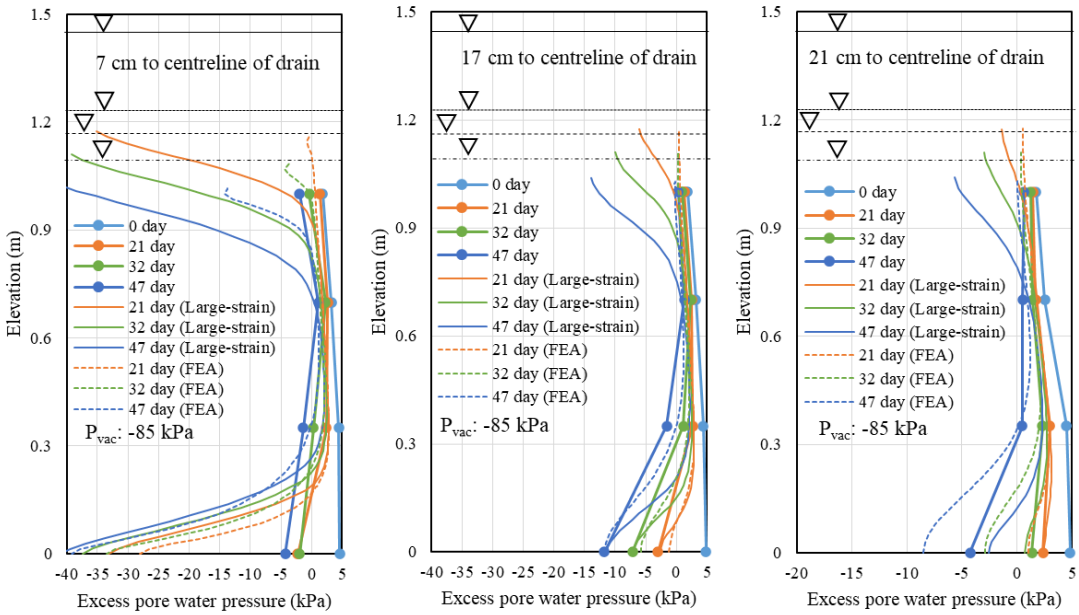

(b) Excess pore water pressure distributions at different distances

Figure 6.34 Distributions of excess pore water pressure and average settlement using FEA for Model test 6 (P_{vac}: Vacuum pressure)

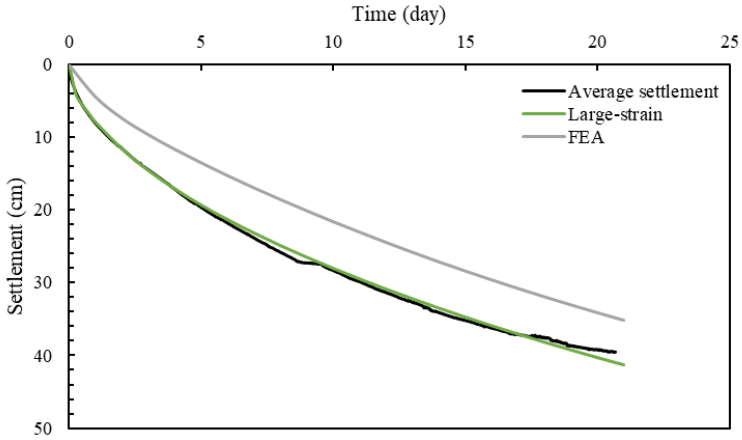

(a) Settlement

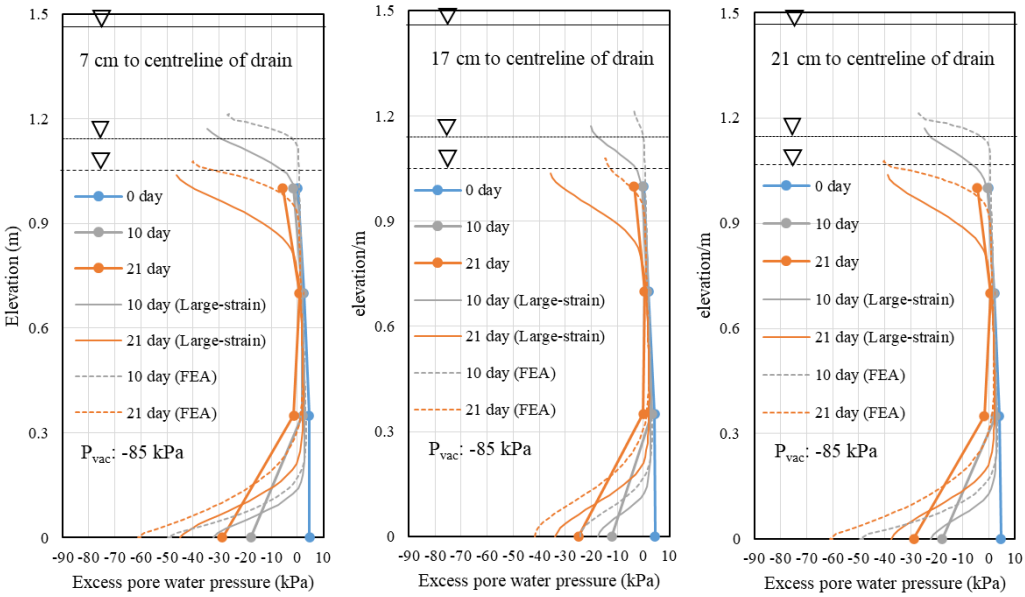

(b) Excess pore water pressure at different distances

Figure 6.35 Distributions of excess pore water pressure and average settlement using FEA for Model test 7 (P_{vac}: Vacuum pressure)

6.4.3.2 Seepage analysis

The flow fields of Model tests 3 and 4 with the use of HDeG sheet and Model tests 6 and 7 with the use of drain only using FEA at the end of vacuum consolidation are shown in Figure 6.38 to Figure 6.37. The equipotential lines of Model test 3 were thus almost horizontal. For Model test 4, beyond 15 cm around the drain, the equipotential lines were almost horizontal. Therefore, except the areas in 15 cm around the HDeG, the flow lines tend to be vertical as shown in Figure 6.36b and Figure 6.37b. For Model tests 6 and 7,

the flow lines beyond 30 cm around the drains were close to be vertical. Therefore, with the use of non-woven geotextile, the equipotential lines tend to be more uniform, then flow lines tend to be vertical. That is consistent with the results of Model tests.

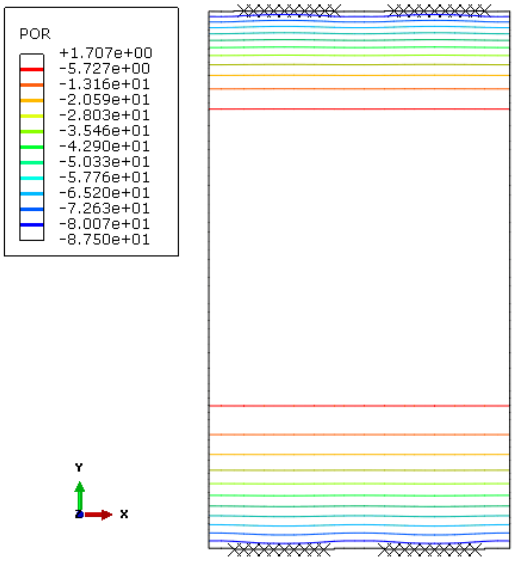

(a) Equipotential lines

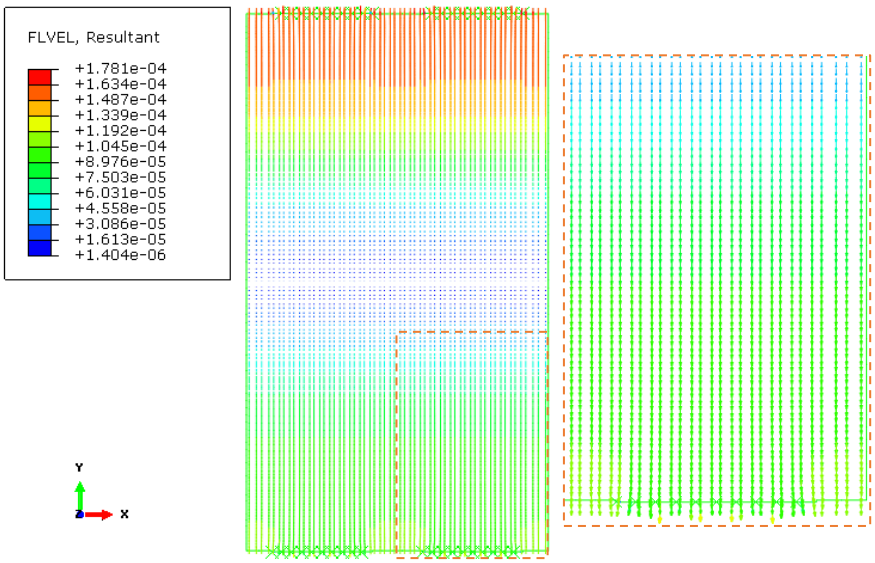

(b) Flow lines

Figure 6.36 Equipotential and flow lines of Model test 3 at 32nd day using FEA (POR: Excess pore pressure; FLVEL: Flow velocity)

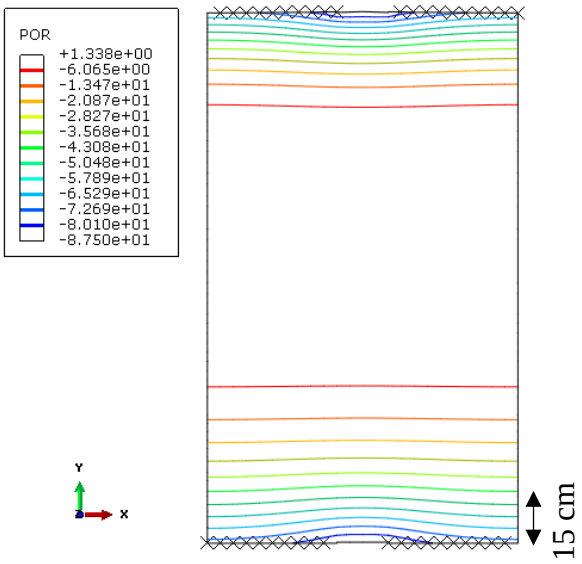

(a) Equipotential lines

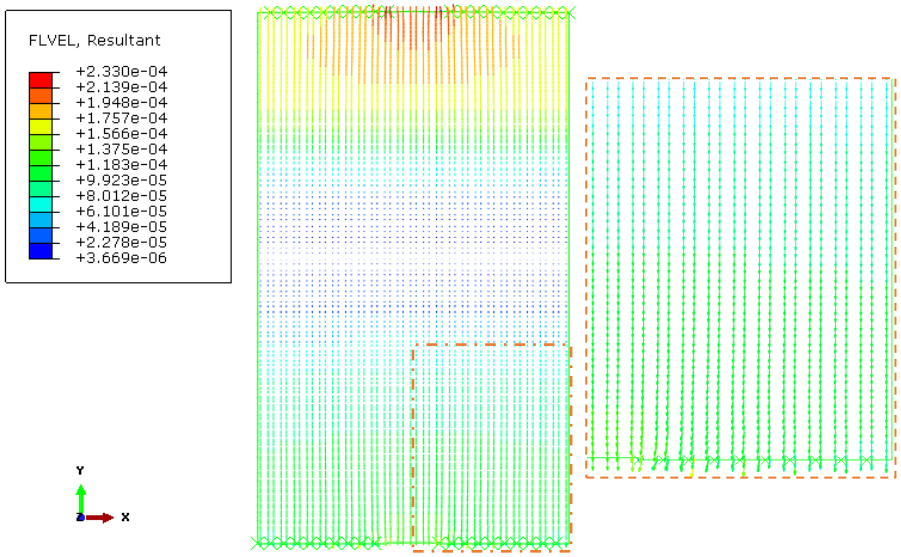

(b) Flow lines

Figure 6.37 Equipotential and flow lines of Model test 4 at 52nd day using FEA (POR: Excess pore pressure; FLVEL: Flow velocity)

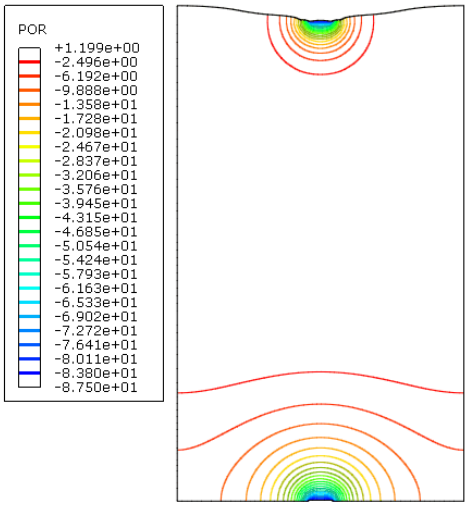

(a) Equipotential lines

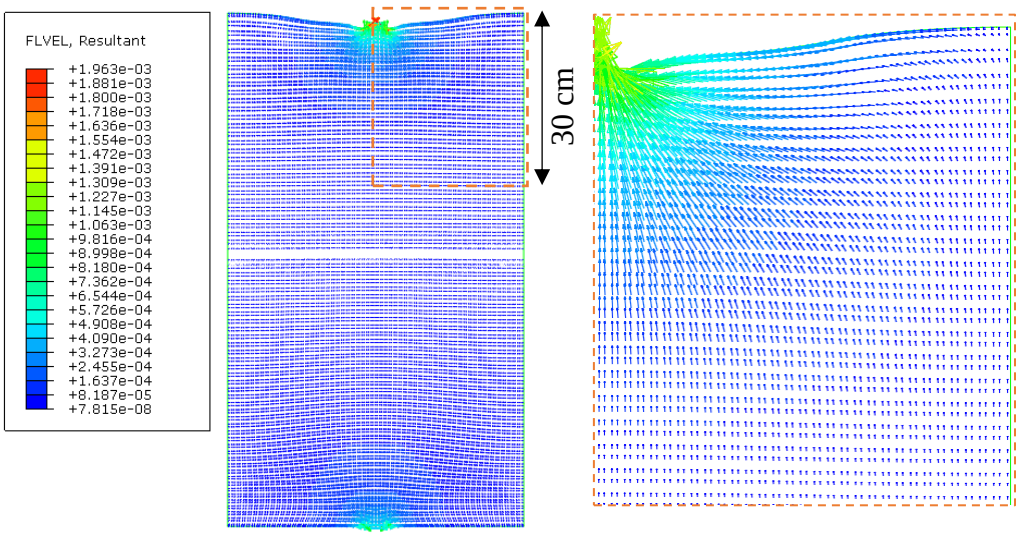

(b) Flow lines

Figure 6.38 Equipotential and flow lines of Model test 6 at 47th day using FEA (POR: Excess pore pressure; FLVEL: Flow velocity)

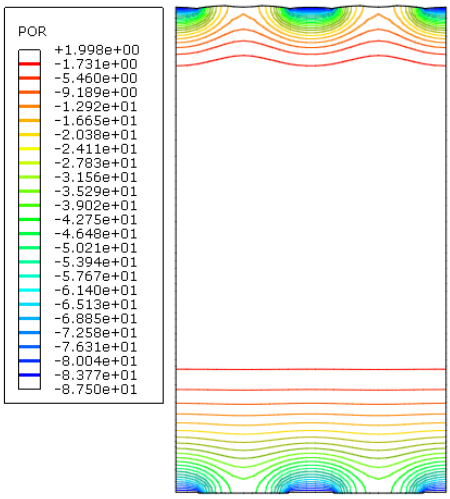

(c) Equipotential lines

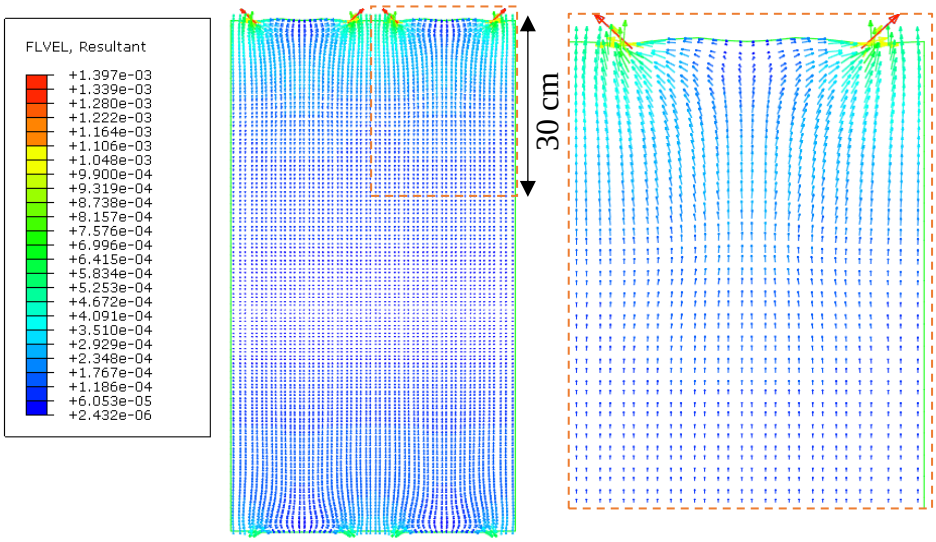

(b) Flow lines

Figure 6.39 Equipotential and flow lines of Model test 7 at 21st day using FEA (POR: Excess pore pressure; FLVEL: Flow velocity)

6.5 Comparison and discussion

6.5.1 Excess pore water pressure on HDeG sheet

With enough pore pressure transducers at horizontal drain level for Model tests 1, 2 and 5, the distributions of pore water pressure on HDeG sheet are shown in Figure 6.40. Because the analytical models are symmetric, the distributions of excess pore water pressure on half of HDeG sheet using theoretical solutions and FEA were presented. Due to the use of constant initial excess pore water pressure for small-strain consolidation solution, the distributions of excess pore water pressure on top and bottom HDeG sheet in unit cell are same. From Figure 6.40, with the use of HDeG sheet, the excess pore water pressure on HDeG sheet reduced gradually from that in drain which should be same with the excess pore pressure on drainage boundary under free drainage condition.

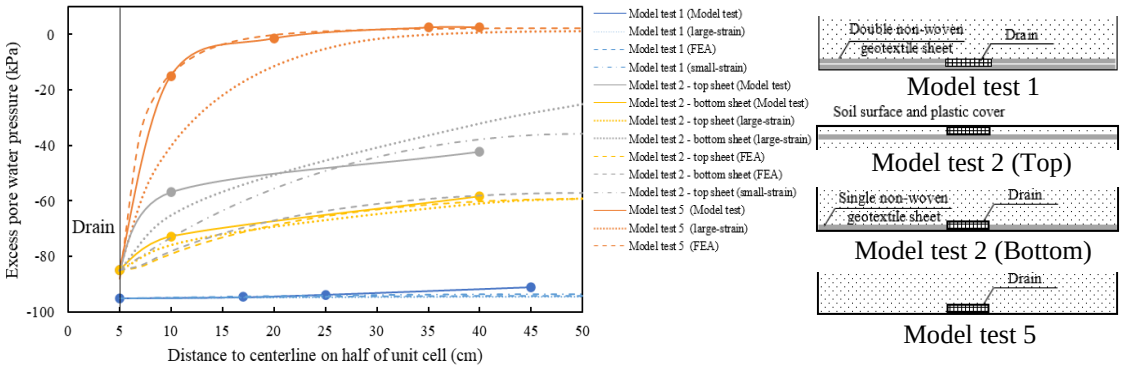

Figure 6.40 Distribution of excess pore pressure on HDeG sheet in Model tests 1, 2 and 5

In Model test 1, because of the high transmissivity of double non-woven geotextile, the distributions of excess pore water pressure using all methods were similar and close to the source vacuum pressure (-96 kPa). The excess pore water pressure distributions of Model tests 2 using large-strain consolidation solution were closer to the measured. But those using FEA were close to the measured on bottom HDeG sheet and those using small-strain consolidation solution were close to the measured on top HDeG sheet. Compared with that using large-strain consolidation solution, the distributions of excess pore water pressure using FEA at horizontal drain level of Model test 5 were closer to the measured. Therefore, the geotextile element with the consideration of transmissivity in FEA and the theoretical consolidation solutions are effective to simulate the excess

pore water pressure distribution on HDeG sheet. However, the numerical simulation of vacuum consolidation using prefabricated horizontal drain using FEA agrees well with the model test.

6.5.2 Degree of consolidation

The degree of consolidation using theorical consolidation solutions and FEA are compared with the calculated degree of consolidation using measured settlement and pore water pressure as shown in Figure 6.41. The degree of consolidation based on the excess pore water pressure was calculated using the measured data based on linear extrapolation and weighted average method. Thus, the degree of consolidation based on excess pore water pressure using measured data at early stage was much higher than the predicted. The degree of consolidation based on the average settlement was larger than that based on the excess pore water pressure. That is because the non-linear compressibility and the under estimation using few pore water pressure data.

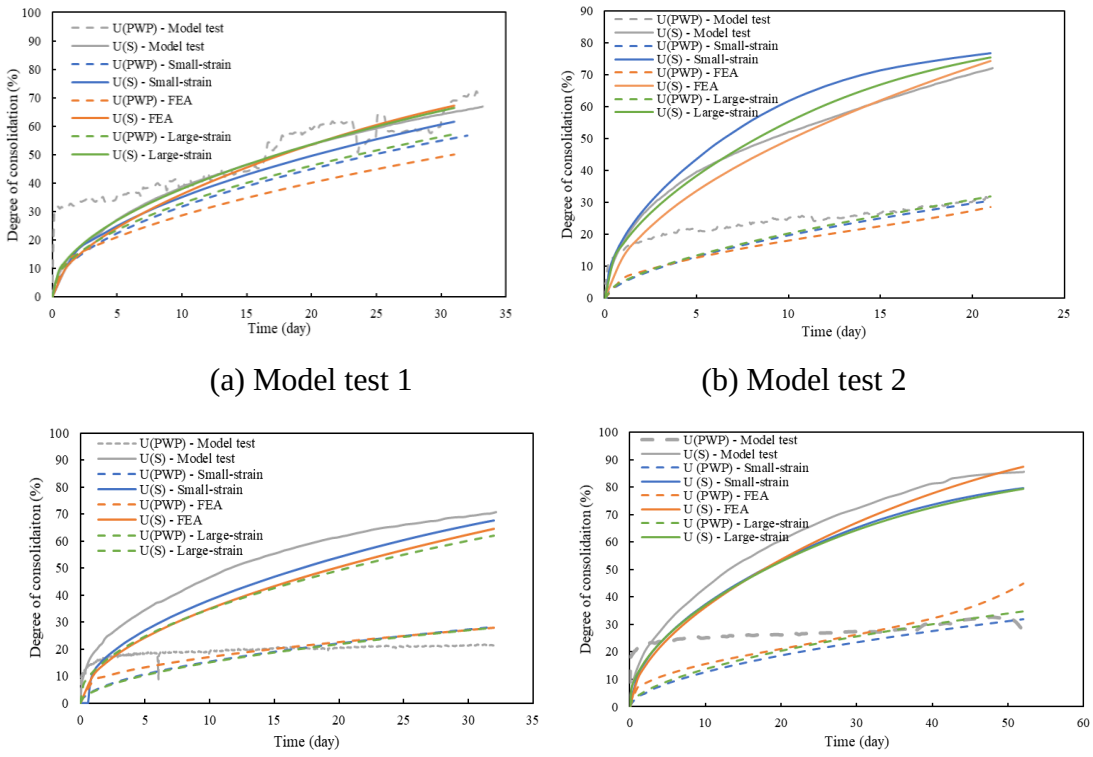

(a) Model test 1 (b) Model test 2

(c) Model test 3 (d) Model test 4

Figure 6.41 Degree of consolidation based on measured data, theoretical solutions and FEA for the use of non-woven geotextile: (a) Model test 1; (b) Model test 2; (c) Model test 3; (d) Model test 4 (S: Settlement; PWP: Excess pore pressure)

For Model tests 1 to 4 with the use of HDeG sheet, the degree of consolidation, as in Figure 6.41, using theoretical solutions and FEA was much close to the calculated degree of consolidation. Hence, the theoretical solutions and FEA are suitable to analyze the vacuum consolidation behaviour of soft soil using HDeG sheet.

6.6 Degree of consolidation transferring

Based on the theoretical and numerical analyses, the degree of consolidation based on settlement is larger than that based on excess pore water pressure distribution. Therefore, the difference between the degree of consolidation based on settlement and that based on excess pore water pressure distribution should be investigated.

6.6.1 Theoretical derivations

Based on Terzaghi's theory, the degree of consolidation based on the distribution of excess pore water pressure can be expressed by Eq. (6.68) under single drainage condition. The degree of consolidation based on the settlement is shown in Eq. (6.69)

$$U_u = \frac{\bar{\sigma}_t HW}{\sigma_\infty HW} \tag{6.68}$$

$$U_s = \frac{S_t}{S_\infty} \tag{6.69}$$

where, $\bar{\sigma}_t$ is the weighted average effective stress on whole cross-section of unit cell at time *t*; σ_∞ is final uniform effective stress on whole cross-section of unit cell; *H* and *W* are the height and width of the cross-section of a rectangular unit cell for vacuum consolidation using horizontal drains.

Under the final condition, the final settlement can be calculated using Eq. (6.70).

$$S_\infty = \frac{c_c H}{(1+e_0)} \log_{10} \sigma_\infty \tag{6.70}$$

Moreover, two methods can be used to calculate the settlement at time *t* using compression curves of soft soil as expressed by Eq. (6.71) or Eq. (6.72). Here, the constant compression index, C_c, and recompression index, C_r, are assumed. As the soft marine clay is used as fill materials, the initial effective stress is set as 1 kPa and the soil is always under normal consolidation during the vacuum consolidation. In Eq. (6.71), the settlement at time *t* is calculated based on the weighted average effective stress on whole cross-section of unit cell. In Eq. (6.72), the settlement at time *t* is calculated using

layer-wise summation method. Here, the whole cross-section is divided into *n* uniform layers in *H* direction (vertical direction). For each layer, the thickness is set as Δz and the weighted average effective stress for layer *i* is $\bar{\sigma}_i$ as in Figure 6.42.

$$\bar{S}_t = \frac{c_c H}{(1+e_0)} \log_{10} \bar{\sigma}_t \tag{6.71}$$

$$S_t = \frac{c_c H}{(1+e_0)} \log_{10} (\prod_{i=1}^{n} \bar{\sigma}_i)^{\frac{1}{n}} \tag{6.72}$$

where,

$$n\bar{\sigma}_t = \sum_{1}^{n} \bar{\sigma}_i \tag{6.73}$$

$$(\prod_{i=1}^{n} \bar{\sigma}_i)^{\frac{1}{n}} \leq \bar{\sigma}_t \tag{6.74}$$

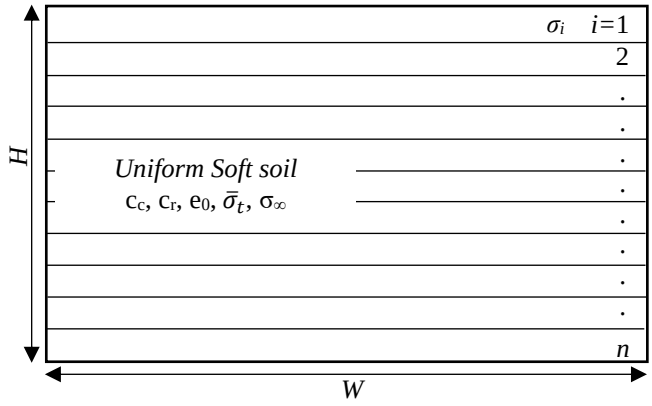

Figure 6.42 Subdivided soil layers

Based on inequality of arithmetic and geometric means, only when the effective stress is uniform on the whole cross-section of unit cell, the terms at both sides as in Eq. (6.74) will be equal. So, the settlement calculated by Eq. (6.72) is less than that calculated by Eq. (6.71) at time *t*. For non-uniform distribution of pore water pressure at time *t*, the settlement calculated by Eq. (6.72) should be closer to the measured settlement. This phenomenon confirmed the effectiveness of layer-wise summation method for the calculation of settlement of soil foundation under loading.

Under final condition with uniform distribution of excess pore water pressure, the final effective stress, σ_∞, is uniform on the whole cross-section of unit cell. Thus, the final

settlement calculated by Eq. (6.71) and Eq. (6.72) are the same. Moreover, the ratio of two calculated settlements as in Eq. (6.71) and Eq. (6.72) is following:

$$k = \frac{\log_{10}(\prod_{i=1}^{n} \bar{\sigma}_i)^{\frac{1}{n}}}{\log_{10} \bar{\sigma}_t} \tag{6.75}$$

$$k = \frac{1}{n}\sum_{1}^{n} f(\bar{\sigma}_i) \tag{6.76}$$

$$f(\bar{\sigma}_i) = \log_{\bar{\sigma}_t} \bar{\sigma}_i \tag{6.77}$$

From Eq. (6.76), the ratio *k* is the mean value of the algebraic summation of $f(\bar{\sigma}_i)$. At initial stage, the effective stress on cross-section is from 1 kPa to vacuum pressure. The ratio *k* at initial stage is smallest. And as the increasing of effective stress, the ratio *k* turns to be 1 at the final stage. Hence, the Eq. (6.69) can be expressed as Eq. (6.78).

$$U_S = k\frac{Log10[\bar{\sigma}_t]}{Log10[\sigma_\infty]} \tag{6.78}$$

Therefore, the conversion equation for the degree of consolidation based on settlement and excess pore water pressure can be obtained as Eq. (6.79).

$$U_U = \sigma_\infty^{\frac{U_S}{k}-1} \tag{6.79}$$

Based on Eq. (6.79), the degree of consolidation using excess pore water pressure should lag behind the degree of consolidation using settlement during the vacuum consolidation of soft soil using horizontal drains. But they are the same at the final stage of consolidation. The ratio *k* changes with the elapse of time and depends on the distribution of excess pore water pressure. To estimate the degree of consolidation based on the excess pore water pressure, the ratio *k* is assumed to be 1, then the Eq. (6.79) can be simplified as Eq. (6.80).

$$U_U = \sigma_\infty^{U_S-1} \tag{6.80}$$

Under double drainage condition, the final effective stress distribution is linear from top surface with zero pore water pressure to the vacuum drainage boundary. The degree of consolidation based on excess pore water pressure should be expressed as Eq. (6.81).

$$U_u = \frac{\bar{\sigma}_t HW}{\bar{\sigma}_\infty HW} \tag{6.81}$$

And two methods to calculate the final settlement are expressed as Eq. (6.82) and Eq. (6.83).

$$S_\infty = \frac{c_c H}{(1+e_0)} \log_{10}(\prod_{i=1}^{n} \bar{\sigma}_{\infty i})^{\frac{1}{n}} \tag{6.82}$$

$$\bar{S}_\infty = \frac{c_c H}{(1+e_0)} \log_{10} \bar{\sigma}_\infty \tag{6.83}$$

where, $\bar{\sigma}_\infty$ is the weighted average final effective stress.

$$\bar{\sigma}_\infty = \frac{1}{n} \sum_{1}^{n} \bar{\sigma}_{\infty i} \tag{6.84}$$

$$(\prod_{i=1}^{n} \bar{\sigma}_{\infty i})^{\frac{1}{n}} < \bar{\sigma}_\infty \tag{6.85}$$

The ratio *s* of two calculated final settlement can be expressed as Eq. (6.86).

$$s = \frac{1}{n} \sum_{1}^{n} \log_{\bar{\sigma}_\infty} \bar{\sigma}_{\infty i} \tag{6.86}$$

The conversion equation can be expressed as Eq. (6.88)

$$U_S = \frac{k}{s} \frac{Log10[\bar{\sigma}_t]}{Log10[\bar{\sigma}_\infty]} \tag{6.87}$$

$$U_U = \sigma_\infty^{\frac{sU_S}{k}-1} \tag{6.88}$$

Here, the ratio *k* and *s* are less than 1, even at the final stage. Therefore, the ratio of *s/k* depends on the excess pore pressure distribution and can be larger than 1.

6.6.2 Comparisons of model tests and theoretical or numerical analyses

Based on the conversion equation, the calculated degree of consolidation based on pore water pressure of Model test 2 are shown in Figure 6.43 as an example. By using conversion equation as in Eq. (6.80), the calculated degree of consolidation based on excess pore water pressure was calculated using the degree of consolidation based on measured settlement. The calculated degree of consolidation using conversion equation was close to the theoretical solutions and FEA. The calculated degree of

consolidation using conversion equation was lower than that using measured pore water pressure at early stage. This phenomenon is mainly due to the use of the linear extrapolation for the calculation of degree of consolidation using measured pore water pressure data points.

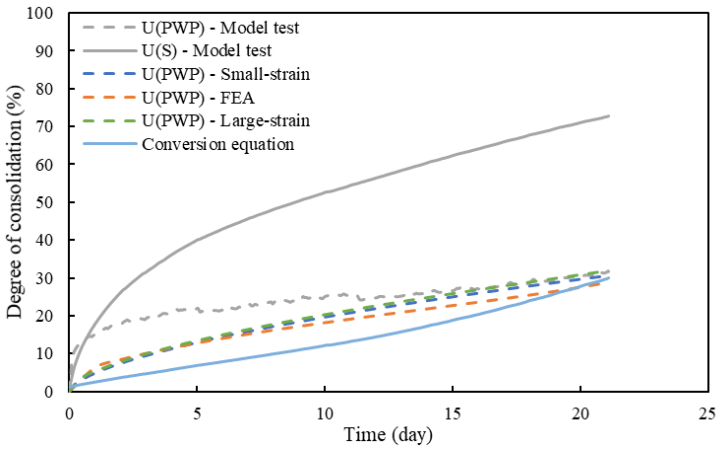

Figure 6.43 Degree of consolidation for Model test 2 (S: Settlement; PWP: Excess pore pressure)

6.7 Conclusions

In this chapter, the theoretical solutions and finite element analyses were proposed and verified by the model tests using HDeG sheet.

(1) The proposed theoretical solutions and adopted finite element analyses were feasible to simulate the vacuum consolidation behaviour of soft clay. The proposed theoretical solutions were suitable for consolidation of soft clay using HDeG sheet and vacuum preloading.

(2) As the horizontal spacing of horizontal drains or the vertical spacing of HDeG sheet increases, the degree of consolidation decreased. With the increase in transmissivity of geotextile, the degree of consolidation increased.

(3) Finite element analyses with the use of the average pore water pressure for HDeG sheet were feasible to simulate the consolidation of soft soil using HDeG sheet and vacuum preloading.

(4) The degree of consolidation interpreted from settlement was larger than that interpreted from pore pressure due to the non-linear compressibility. An equation to convert the degree of consolidation based on settlement to that

based on pore water pressure or verse versa was proposed. The effectiveness of the conversion equation was verified using the measured data, theoretical solutions and FEA.

CHAPTER 7 HORIZONTAL DRAINAGE ENHANCED GEOTEXTILE SHEET WITH ELECTRO-OSMOSIS OR LIME LINER

7.1 Introduction

The performance of the horizontal drainage enhanced geotextile sheet (HDeG sheet) can be further enhanced using other means. In this chapter, the use of electroosmosis or lime liner together with HDeG sheet is explored. For the use of HDeG sheet, the pore water pressure gradient loss around HDeG sheet is relatively large. This is because the soil around HDeG sheet gets consolidated first and its permeability reduces much more than the other soil and the clogging of geotextile sheet which acts as a filter to the horizontal drains (Chu et al., 2004; Chai and Miura, 2002). As mentioned in Chapters 4 and 5, the HDeG sheet is more feasible for land reclamation. In this Chapter, the use of electro-osmosis and lime treatment to accelerate the consolidation rate or to optimize the HDeG sheet was investigated. Based on the laboratory tests, HDeG sheet enhanced by electrical HDeG sheet or lime liner were proposed.

To design the electrical HDeG sheet, the selection of the electrode materials is an important step. For the use of lime, a liner approach was explored with the intention to improve the permeability of soft soil around the HDeG sheet. The configuration of the lime liner enhanced HDeG sheet and the effectiveness was investigated.

7.2 Selection of electrode materials

One of the key components in electro-osmosis is electrode materials. A study for the selection of the most suitable material to be used as electrode for this project as well for future practical applications was carried out first. Due to the anode passivation on copper electrode, steel or carbon electrode would be more feasible for electro-osmosis consolidation. To avoid the gravity induced water flow, the electro-osmosis consolidation tests were conducted with horizontal flow. Two types of electrodes were tried: porous steel plate electrodes and woven carbon felt electrodes.

7.2.1 Experimental set-up

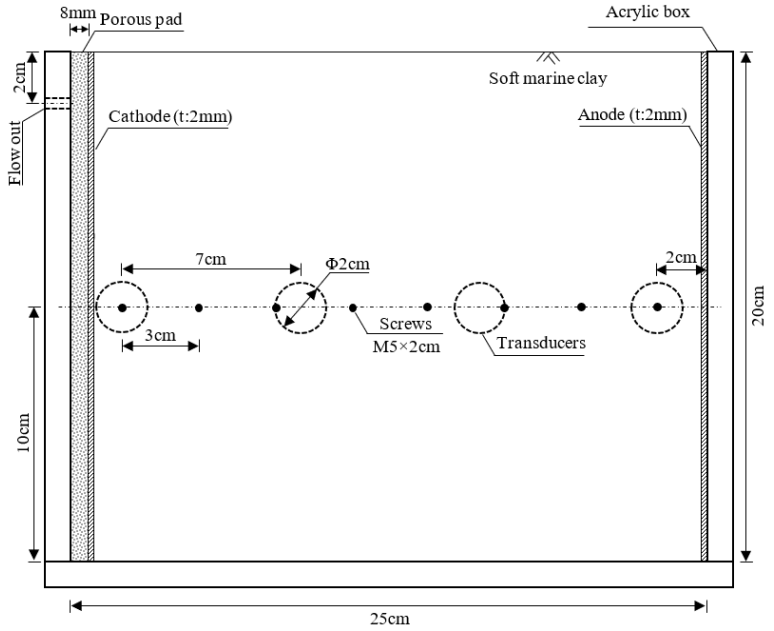

(a) Elevation view

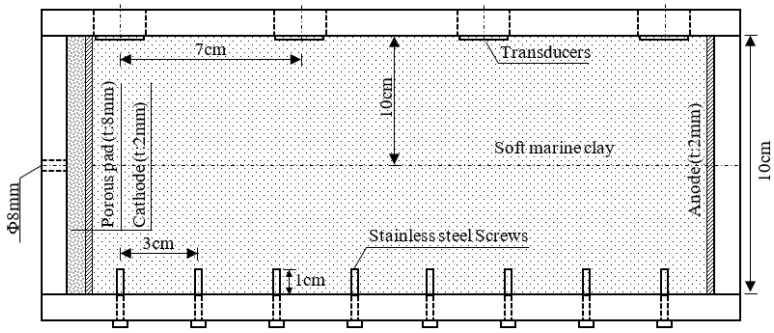

(b) Top view

Figure 7.1 Electro-osmosis testing device: (a) Elevation view and (b) Top view

A PVC box with 0.25 m in length, 0.1 m in width and 0.2 m in height was used for the electro-osmosis tests as shown in Figure 7.1. Four small-sized pore pressure transducers were used to measure the pore water pressure responses (Figure 7.1). The transducers were fixed at the middle of the box with 0.07 m spacing in between to measure the pore pressure at 4 different positions. KYOWA BPR-A-S 200 kPa brand pore pressure transducers were used. It had a 0.02 m outside diameter as shown in Figure 7.2. Eight stainless steel screws (M5×2cm) with 0.03 m spacing in between were fixed at the middle of box on the opposite side of the transducers (see Fig. 7.1b) to measure the voltage distribution. The screws were penetrated into the soft clay about 0.01 m. A DC power supply (Instek SPD-3606) with 6A of maximum current and 120V of maximum

voltage as shown in Figure 7.3 was used to provide the voltage and current. Two types of electrodes were used. The first was steel plate of 1.0 mm thick with round holes as shown in Figure 7.4. It had 1.43E-7 Ω·m in electrical resistivity. The other one was woven carbon felt with 1.0 mm in thickness and 5E-4 to 8E-4 Ω·m in electrical resistivity.

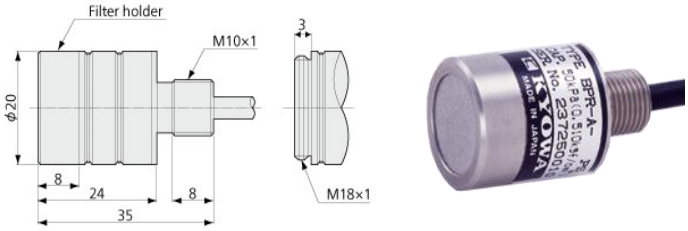

Figure 7.2 Use of Small-size pore pressure transducers in the model tests

Figure 7.3 DC power supply (Instek SPD-3606)

(a) Steel plate with round holes (thickness: 1mm)

(b) Woven carbon felt (thickness: 1mm)

Figure 7.4 Two types of electrodes: (a) steel plate with round holes and (b) woven carbon felt

7.2.2 Testing Procedure

The salinity and water content of soft soil were 16.77‰ and 120%, respectively. The sample was mixed by sea water and wet marine clay and put in a vacuum chamber with a vacuum of - 80 kPa for 8 hours to remove air bubbles. The soft marine clay was placed into the top of box. The steel electrodes were used for Test 1 as shown in Figure 7.5a. The carbon felt electrodes were used for Test 2 as shown in Figure 7.5b. A layer of non-woven geotextile with 1 mm in thickness was used to wrap the electrodes (1 mm in thickness) to filtrate the soil particles. At cathode, a porous pad with 8 mm thick was placed behind the electrode to hold water. Near cathode, a hole with 8 mm in diameter and 0.02 m below the top of box (Figure 7.1a) was used to collect the discharged water during the electro-osmosis. A constant current, about 3.3 A, was applied. The test period was about 4.8 hrs.

(a) Using steel plate as electrode (Test 1)

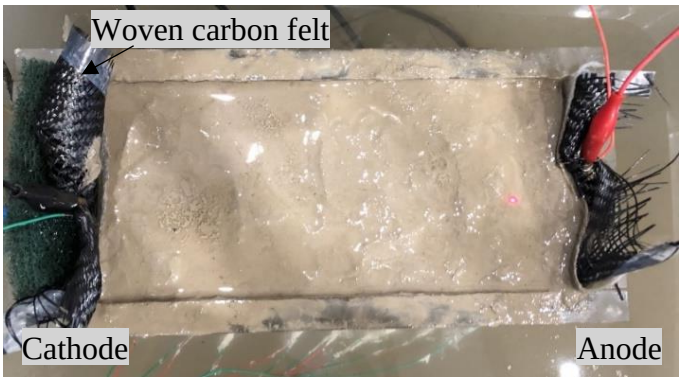

(b) Using carbon felt as electrode (Test 2)

Figure 7.5 Test setup for Test 1 and 2 under pure electro-osmosis with horizontal flow: (a) Using steel plate as electrode (Test 1) and (b) Using carbon felt as electrode (Test 2)

Because of the oxidation reactions at anode, as in Eq. (7.1) and Eq. (7.2), and high current on electrodes, the box and soil were over heated. Water was used to cool down the test box. As the electrical resistivity of the carbon felt was much larger than that of steel material, the carbon felt was broke into pieces at the interface of air and water after 2 hours due to the massive heat at the anode. Another piece of carbon felt was replaced during this test.

$$Fe \rightarrow Fe^{3+} + 3e^{-} \quad (7.1)$$

$$2Cl^{-} \rightarrow Cl_2 + 2e^{-} \quad (7.2)$$

7.2.3 Test results

The disassembled electrodes are shown in Figure 7.6 and Figure 7.7 after testing. In Test 1, the steel plate at anode was corroded and iron ions were released into soft soil. In Test 2, chlorine was released at anode and light-yellow water bubble was observed. The volume of the discharged water collected in Test 1 was around 300 mL which was slightly more than around 270 mL of water collected in Test 2. The measured pH values of the discharged water from the two tests were 13.6 and 13.4, respectively, which were similar.

Figure 7.6 Test 1 using pure electro-osmosis and steel plate as electrode

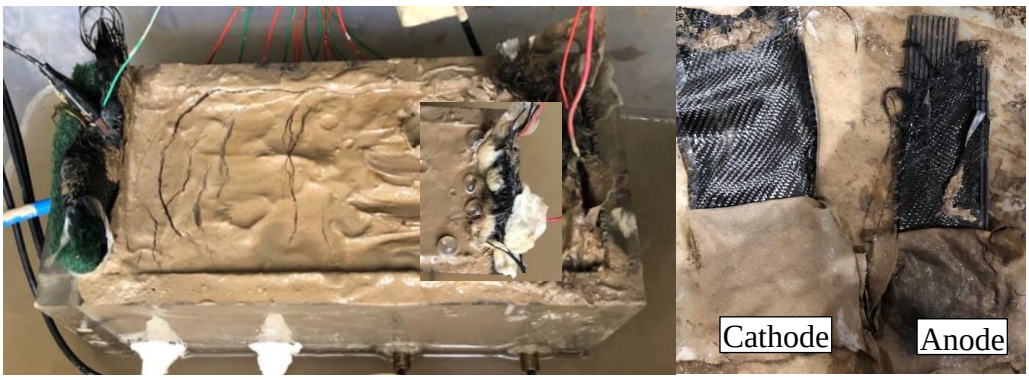

Figure 7.7 Test 2 using pure electro-osmosis and carbon felt as electrode

- Water content

In each test, five soil samples were collected at 0.1 m above the bottom of the soil at an even interval from cathode to anode. The final water contents of the two tests are similar as shown in Figure 7.8. The average water contents were 95.1% for Test 1 and 95.2% for Test 2, respectively. The water reduction was larger than the discharged water because of water electrolysis and evaporation during sampling.

Under DC current, the pore water flowed from anode to cathode. The reduction of water content was about 40% at anode and 20% at cathode. The reduction of water content near cathode was due to water migrating to cathode and water electrolysis. As a result of the uneven reduction of water content at cathode and anode, the soil surface was also uneven based on observation. The maximum differential settlement was 3 to 4 cm. The cracks at the soil surface were formed near cathode as shown in Figure 7.6 and Figure 7.7.

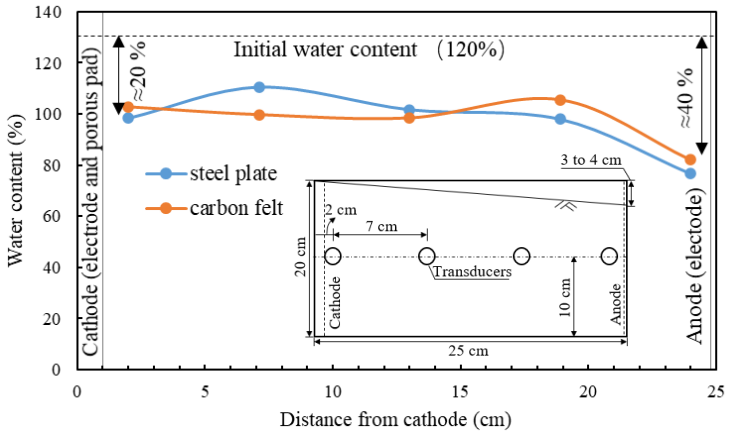

Figure 7.8 Water content of two tests

- Voltage distribution

The voltage distributions in the soil in the two model tests are shown in Figure 7.9 and Figure 7.10. The voltage gradient, v_x, was calculated from the middle straight-line section as shown in Figures 7.9 and 7.10. Compared with the voltage gradient using carbon felt, the voltage gradient using steel plate was reduced largely from beginning. This was due to the increase in iron ions in pore water which increased the electrical conductivity of soft soil. However, the gradients of two tests gradually became close to each other and kept steady, 0.55 V/cm for Test 1 and 0.59 V/cm for Test 2. Therefore,

the efficiency using steel or carbon felt electrodes was comparable based on the testing results.

The potential loss, the reduction of voltage at the interface of electrode and soft soil, was increasing for two tests. The potential loss for using carbon felt was much higher than that using steel plate which can be ignorable. This is because the chlorine or hydrogen was released on electrodes and the polarization voltage on anode of carbon felt. The polarization voltage is the change in the electric potential of an electrode produced during electrolysis.

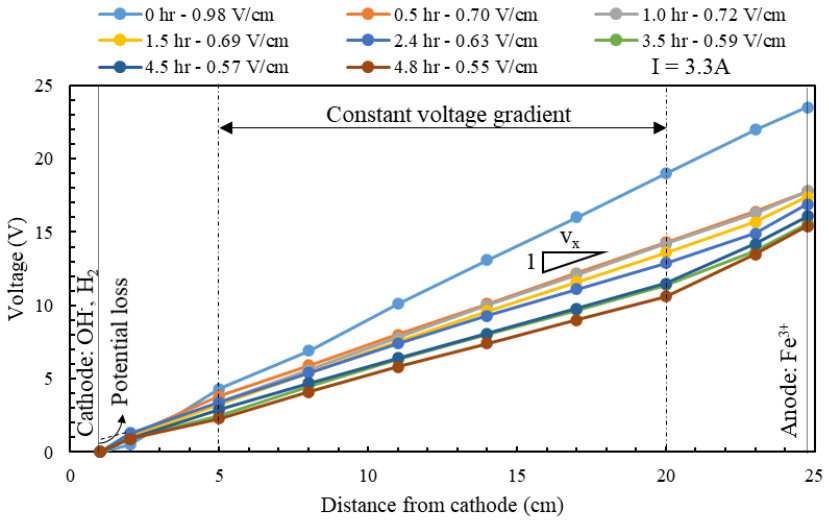

Figure 7.9 Voltage distribution in Test 1 using steel plate electrodes (v_x: voltage gradient)

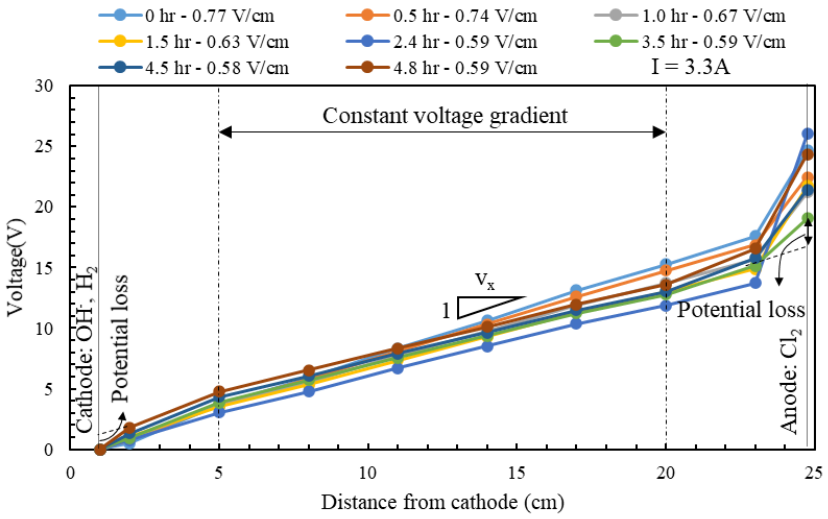

Figure 7.10 Voltage distribution in Test 2 using carbon felt electrodes (v_x: voltage gradient)

- Pore water pressure

The pore water pressures monitored in the two model tests are shown in Figure 7.11. The pore water pressure near the anode was the lowest and increased from the anode to the cathode. The pore water pressure near the anode in Test 2 was lower than that in Test 1 by about 3 kPa, which was because when steel plate was used, the voltage gradient near the anode was larger than that using carbon felt as shown in Figure 7.11.

As the voltage gradients at the cathode were similar and nearly constant irrespective of whether steel plate or carbon felt was used, the reductions of pore water pressure (T-1) near the cathode were close in both tests: 6.3 kPa for Test 1 and 5.1 kPa for Test 2. The change of pore water pressure at T-2 and T-3 were synchronous in two tests due to the constant voltage gradient. As the constant voltage gradient was similar in both tests, the reductions of pore water pressure at T-2 and T-3 in two tests were close, about 6.75 kPa for test 1 and 8.83 kPa for test 2. Based on the results, the difference in the pore water pressure responses between the two tests was not significant.

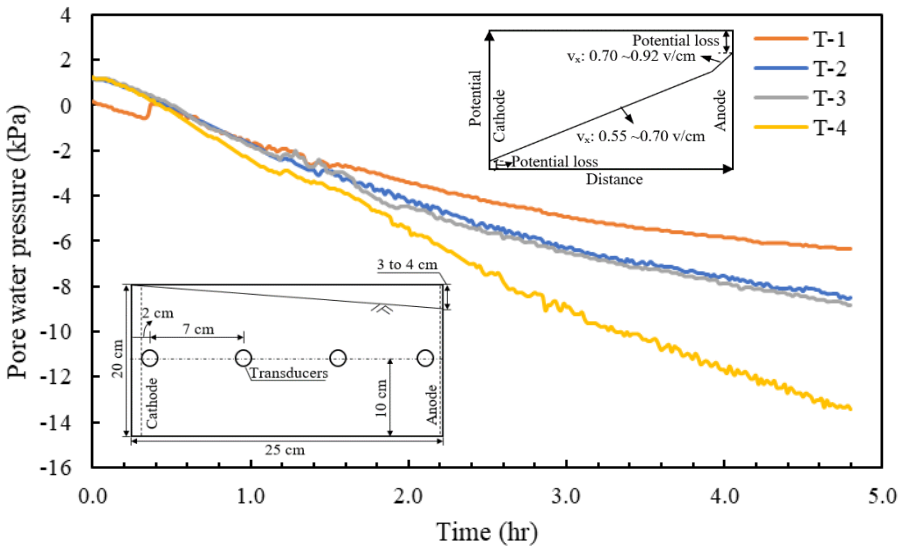

(a) Test 1 using steel plate electrodes

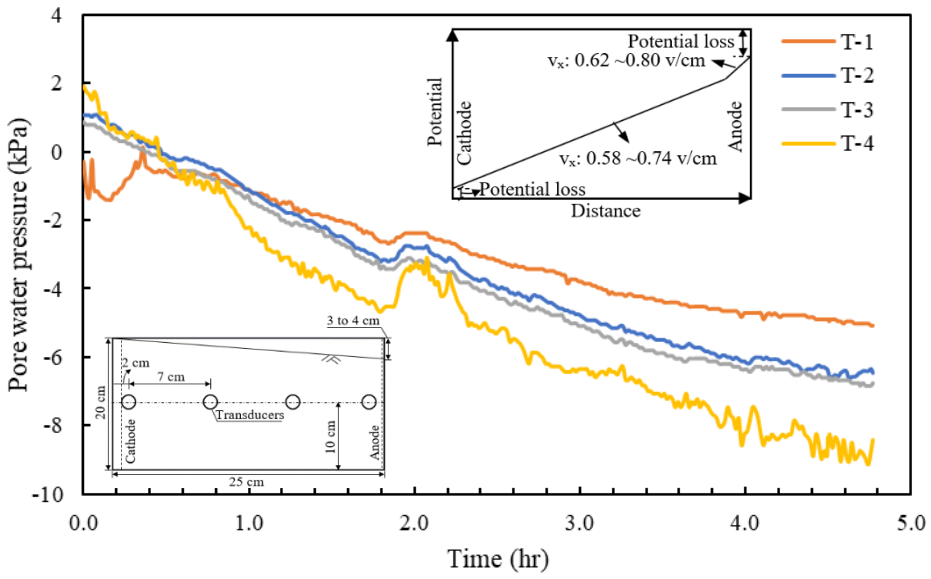

(b) Test 2 using carbon felt electrodes

Figure 7.11 Measured pore water pressure: (a) Test 1 using steel plate electrodes and (b) Test 2 using carbon felt electrodes

Based on the data and discussion presented above, the efficiency of electro-osmosis using steel was slightly better than that using carbon felt given a specific dimension of electrically conductive material. Due to the flexibility and lightweight of carbon felt, the carbon felt electrodes could be placed on the whole reclamation pond. Hence, the use of carbon felt electrodes could be much better than that using metal electrodes. Therefore, the carbon felt was considered more feasible for electro-osmosis consolidation of clay for land reclamation project.

7.3 Effectiveness of carbon felt and horizontal drains

As the woven carbon felt was more feasible for electro-osmosis consolidation, the combination of carbon felt and horizontal drain was proposed for the treatment of soft soil in land reclamation. The chlorine and hydrogen could be removed through horizontal drains. Some vacuum consolidation model tests were conducted to investigate the effectiveness of carbon felt used together with the horizontal drain. However, a connection between carbon felt and conductive wires at the interface of water and air should be developed to avoid the high polarization voltage and corrosion of carbon felt.

7.3.1 Testing setup

The test box of 0.2 m in length, 0.1 m in width and 0.3 m in height was used. The detail of the box is shown in Figure 7.12. Three small-sized pore pressure transducers, KYOWA BPR-A-S 200kPa brand, were used to measure the pore pressure at 3 different elevations along the height. One laser sensor was used to measure the settlement of the center point at the top of the soil surface. A vacuum pump was used to provide the vacuum pressure through the horizontal drain. The vacuum container with lime solution was used to remove the chlorine and store the discharged water. Same as the tests described in Section 7.2.1, the DC power supply was applied for electro-osmosis and eight stainless steel screws were used to measure the voltage distribution along the height of the soil sample.

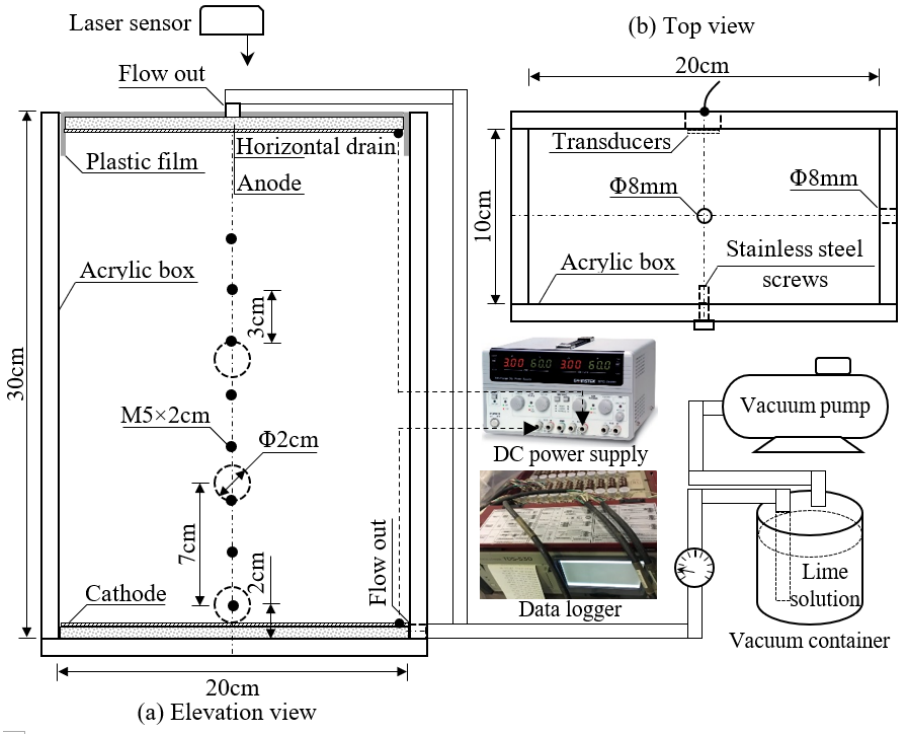

Figure 7.12 Model tests using carbon felt and horizontal drain: (a) Elevation view and (b) Top view

7.3.2 Testing procedure

The initial water content of soft marine clay was about 125% and the salt content was about 32.5‰. The initial height of soft marine clay sample was 0.28 m. A porous pad (8 mm thick) wrapped with non-woven geotextile (1 mm thick) was used as a horizontal drain. The carbon felt (1 mm thick) with steel or conductive plastic connector was placed

next to the horizontal drain. A plastic film was used to cover the top of the horizontal drain. A syringe needle was put into the drain and connected with a vacuum gauge to measure the vacuum pressure in the drain. The vacuum pressure applied was -65 kPa.

The dimension of carbon felt electrodes were 0.195 m in length and 0.095 m in width. Two types of connectors were used to connect the conductive wires with the woven carbon felt as shown in Figure 7.13. A thick steel bracket as shown in Figure 7.13a was used to connect with the carbon felt to provide sufficient allowance for corrosion. Conductive plastic as shown in Figure 7.13b was also used. The electrical resistivity of the conductive plastic was about 1 Ω·m and the melting point was about 200°C. It was hoped the conductive plastic connector would survive the high temperature generated during electro-osmosis. Based on previous studies (Leong et al., 2006), the applicable current density was from 21 A/m^2 to 100 A/m^2, which is 0.39 A to 1.85 A referred to the specific dimension of electrodes used in the model tests.

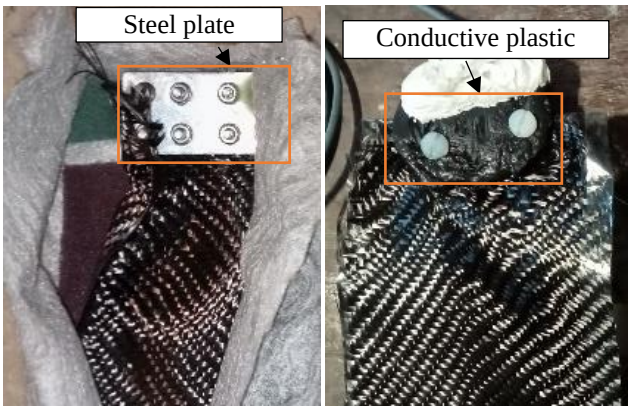

Figure 7.13 Connection with carbon felt (a) Steel connector and (b) Conductive plastic connector

A summary of the consolidation model tests conducted is shown in Table 7.1. To avoid the top drain and electrode touching the upper transducer, the tests were terminated when the settlement reached 0.095 m. After testing, the final height of the soil sample was 0.185 m, which was close to the top transducers. The water content was measured at different locations along the height as shown in Figure 7.14.

In Models T3, T4 and T7, a current of 3A was used for steel connector and 1A was used for conductive plastic connector was used. However, these currents were too high. A large amount of heat was released and unable to dissipated under vacuum pressure, so

that the electrodes and horizontal drain was broken into pieces and the box was also melt down. Then the tests had to be stopped prematurely.

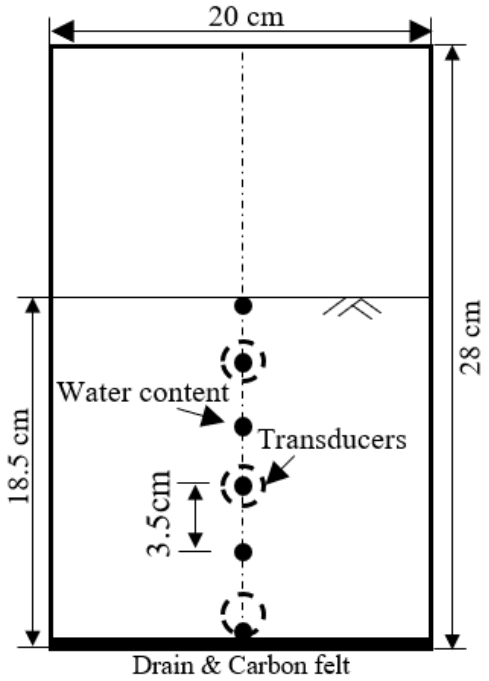

Figure 7.14 Locations where water contents of the soil were measured

Table 7.1 Summary of tests using carbon felt for electro-osmosis tests

Model	Condition	Vacuum pressure (kPa)	Connector	Current, *I* (A)	Initial water content (%)	Duration, *Td* (hr)
T1	VC	-65	---	---	125.1	60.0
T2	EO	---	Steel	1.0	125.9	46.0
T3	EO	---	Conductive plastic	1.0	125.9	43.4
T4	EO+VC	-65	Steel	3.0	125.6	13.6
T5	EO+VC	-65	Steel	1.0	124.3	54.0
T6	EO+VC	-65	Steel	0.5	125.9	46.0
T7	EO+VC	-65	Conductive plastic	1.0	124.9	27.6
T8	EO+VC	-65	Conductive plastic	0.5	124.9	48.0

*Initial height of soil sample: 28 cm
*Termination condition: 9.5 cm of settlement
*EO: Electro-osmosis; VC: Vacuum consolidation

7.3.3 Testing results

- Settlement and pore water pressure

The settlement versus time curves measured for all the Models are curved in Figure 7.15a and Figure 7.16a. During Models T2 and T3 in which only electro-osmosis was used, the carbon felt was uplifted by gas bubbles due to the release of hydrogen at the cathode. Hence, the surface settlement for these model tests was fluctuant. The surface settlement appears to increase with the increase in current.

The pore-water pressure variations versus time curves measured for all the Models are shown in Figure 7.15b and Figure 7.16b. By using electro-osmosis only, the reductions of excess pore water pressure were much lower, especially for the transducer T-3 in Model T2. The change of excess pore water pressure for T-1 and T-2 in Model T2 was synchronous, which is consistent with Test 1 and Test 2 using electro-osmosis only under horizontal flow. The excess pore water pressure for transducers T-1, T-2 and T-3 in Model T3 was affected by the large amount of heat released from the conductive plastic connector. The final reductions of excess pore water pressures in Models T2 and T3 mainly ranged from 5 to 8 kPa.

The reductions of excess pore water pressure in T-1, T-2 and T-3 using vacuum pressure and electro-osmosis were larger than the simple summation of those using vacuum consolidation or electro-osmosis only at same time. For example, the excess pore water pressure at 45^{th} day for T-1, T-2, and T-3 were -3.5, -3.2 and -40.5 kPa in Model T1, -4.4, -4.3 and -7.1 kPa in Model T2, -20.9, -19.4 and -50.0 kPa in Model T5. The summations of the excess pore water pressure of same transducer in Model T1 and T2 was lower than the excess pore water pressure at corresponding transducer in Model T5. Therefore, the excess pore water pressure in the soil was affected by the coupling of vacuum consolidation and electro-osmosis. Compared with vacuum consolidation only, the soft soil was subjected to additional loading induced by the coupling of vacuum consolidation and electro-osmosis. Hence, the settlement was larger than that using vacuum pressure or electro-osmosis only at same time.

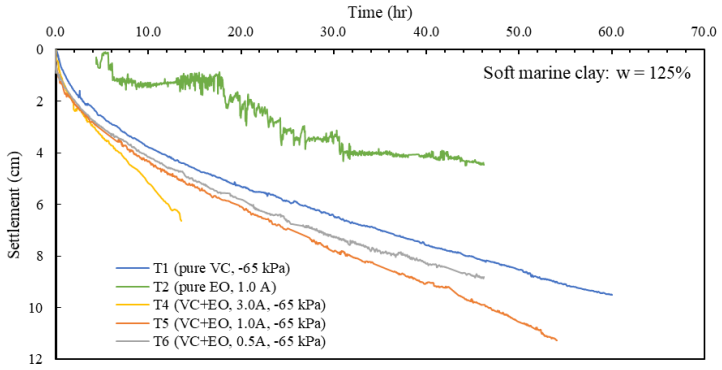

(a) Settlement

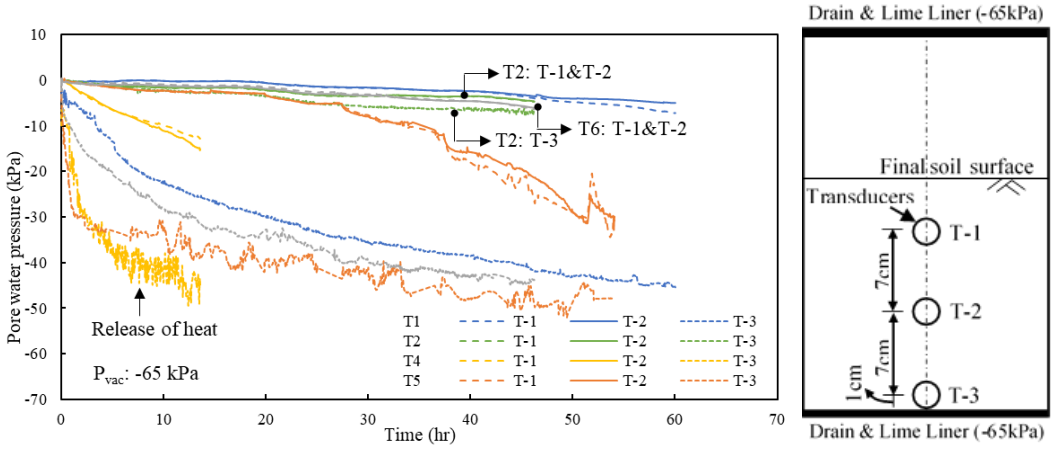

(b) Pore water pressure

Figure 7.15 Test results from model tests using steel connector: (a) Settlement and (b) Pore-water pressure (VC: Vacuum consolidation; EO: Electro-osmosis)

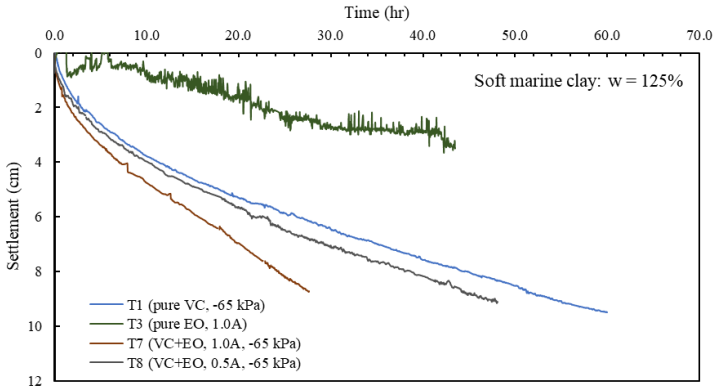

(a) Settlement

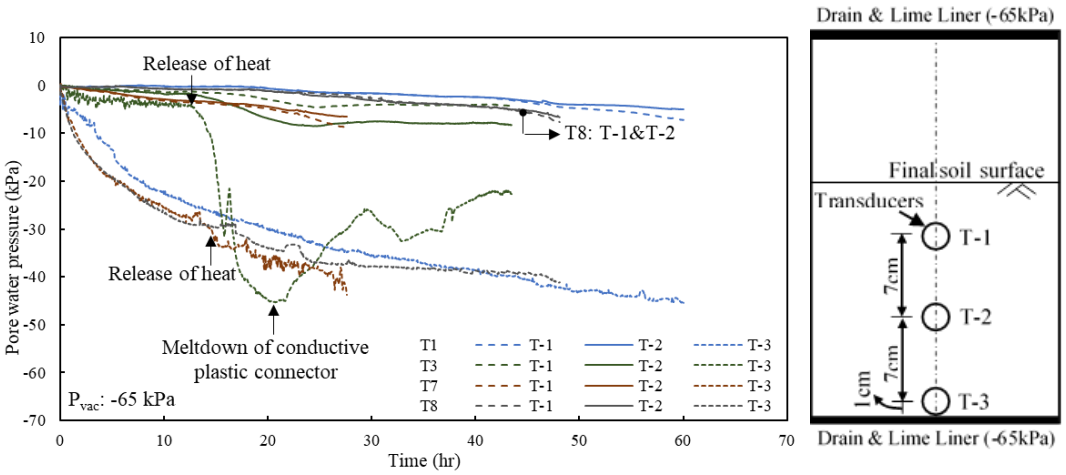

(b) Pore water pressure

Figure 7.16 Test results from model tests using conductive plastic connector: (a) Settlement and (b) Pore-water pressure (VC: Vacuum consolidation; EO: Electro-osmosis)

- Degree of consolidation

The ultimate settlements, S_∞, were obtained using the Asoka's method (1978). With the use of electro-osmosis, the ultimate settlement was larger than that using vacuum pressure only due to a larger reduction of excess pore water pressure induced by the coupling of vacuum consolidation and electro-osmosis. The degree of consolidation (DoC) based on settlement is shown in Figure 7.17. The final degree of consolidation was around 60%.

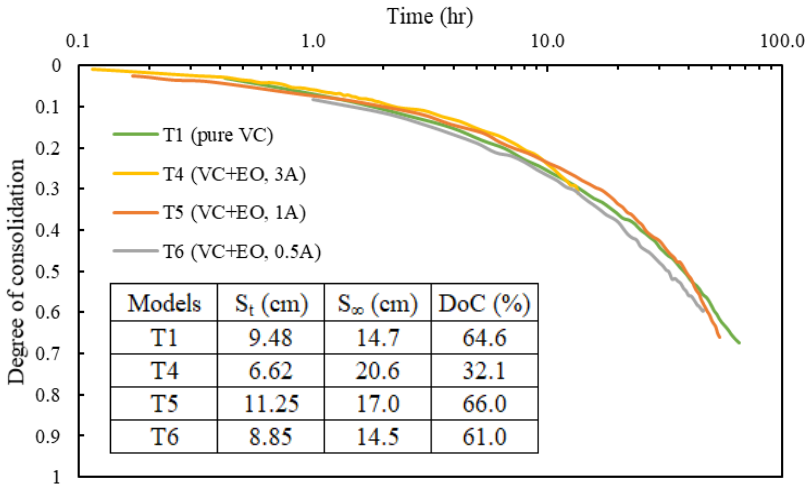

Models	S_t (cm)	S_∞ (cm)	DoC (%)
T1	9.48	14.7	64.6
T4	6.62	20.6	32.1
T5	11.25	17.0	66.0
T6	8.85	14.5	61.0

(a) Steel connector

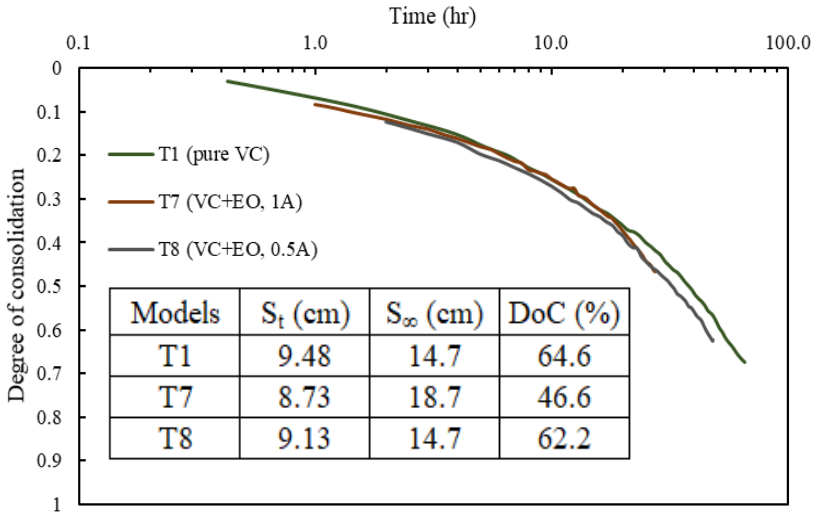

Models	S_t (cm)	S_∞ (cm)	DoC (%)
T1	9.48	14.7	64.6
T7	8.73	18.7	46.6
T8	9.13	14.7	62.2

(b) Conductive plastic connector

Figure 7.17 Degree of consolidation for electro-osmosis tests: (a) Steel connector and (b) Conductive plastic connector (S_t: Settlement; S_∞: Ultimate settlement; DoC: Degree of consolidation)

- Water content

The measured water contents along the height for different Models are shown in Figure 7.18. For Models T2 and T3 using electro-osmosis only, the water content was reduced from the initial water content, 125%, to 75% at the anode. For Models using 1A current, the reduction of water content was more, from 75% to 40% in Model T5 and from 79% to 42% in Model T7. For Models T6 and T8 using 0.5A current, the reduction of water content was close to that using vacuum consolidation only. However, for Models T6 and T8 using 0.5A current, the durations (*Td*), 46 hrs for Model T6 and 48 hrs for Model T8, were shorter than that in Model T1 using vacuum consolidation only.

The comparison of the measured and estimated settlement is shown in Table 7.2. The estimated settlement was calculated using the reduction of average water content of saturated soil in Models. The average specific gravity of soil after testing was measured, 2.695. The measured and estimated settlement in Model T1 was close. For the Models using electro-osmosis, the differences of the measured and estimated settlement were larger than that of Model T1, especially in Model T4. That is because the evaporation of soil during sampling due to the release of heat in electro-osmosis model tests.

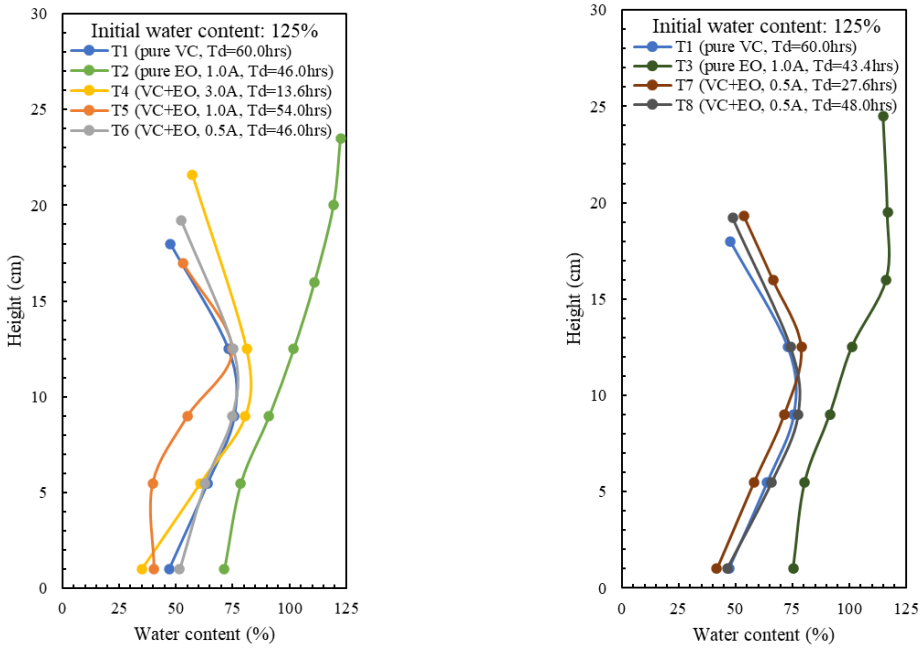

(a) Models using steel connector (b) Models using conductive plastic connector

Figure 7.18 Water content measured in model tests: (a) Models using steel connector and (b) Models using conductive plastic connector (VC: Vacuum consolidation; EO: Electro-osmosis; Td: Test duration)

Table 7.2 Comparison of measured and estimated settlement: (a) Models using steel connector and (b) Models using conductive plastic connector

(a) Models using steel connector

Model	T1	T2	T4	T5	T6
ω_0 (%)	125.1	125.9	125.6	124.3	125.9
$\omega_{t\text{-}avg}$ (%)	66.4	96.7	70.0	55.7	68.1
$s_{t\text{-}cal}$ (cm)	9.7	4.6	7.6	11.5	9.2
s_t (cm)	9.5	4.5	6.6	11.3	8.9

(b) Models using conductive plastic connector

Model	T1	T3	T7	T8
ω_0 (%)	125.1	125.9	124.9	124.9
$\omega_{t\text{-}avg}$ (%)	66.4	101.0	67.8	67.7
$s_{t\text{-}cal}$ (cm)	9.7	3.7	9.1	9.4
s_t (cm)	9.5	3.5	8.7	9.1

- Compressibility of soil in electro-osmosis tests

The calculated effective stress and void ratio of soil in electro-osmosis model tests are shown in Figure 7.19. The effective stress was calculated by using the measured pore water pressure. The void ratio was calculated by using the measured water content and specific gravity. The data points of effective stress and void ratio of soil in electro-osmosis model tests were deviated from that of original marine clay, which means the change of the mineral of soil particles.

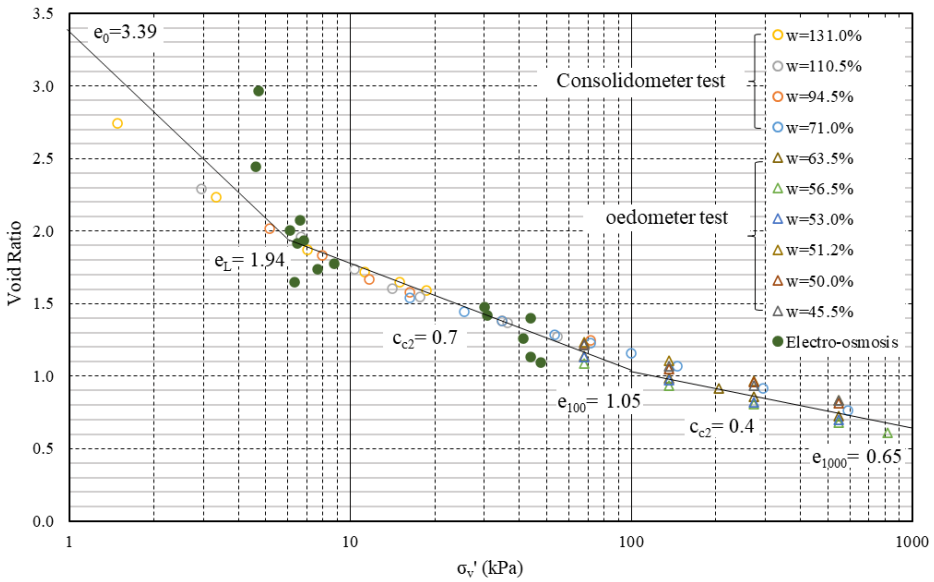

Figure 7.19 Measured data of effective stress versus void ratio in Models using electro-osmosis and vacuum consolidation

- Voltage distribution

The voltage distributions along the soil height in model tests using electro-osmosis are shown in Figure 7.20. As time elapsed, the potential loss at anode was increasing. Larger increase in potential loss occurred for Model T4 with 3A current and Models T3 and T7 with 1A current. In terms of the connection method, the steel connector was thermally stable in Model tests with lower than or equal to 1A current, whereas the conductive plastic connector was thermally stable in Model tests with lower or equal to 0.5A current. The voltage gradients were stable with time due to the same salt content and constant current.

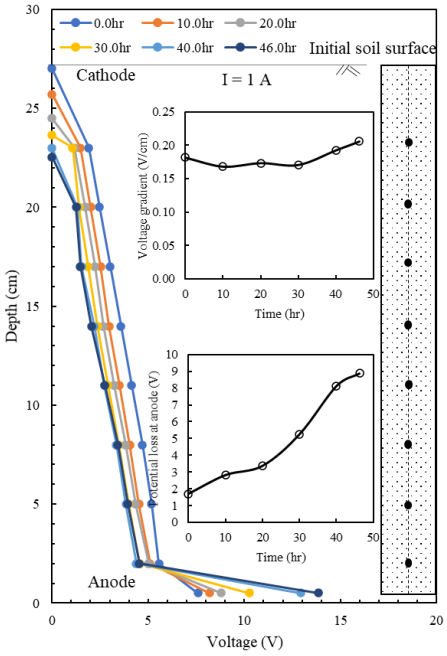

(a) Model T2

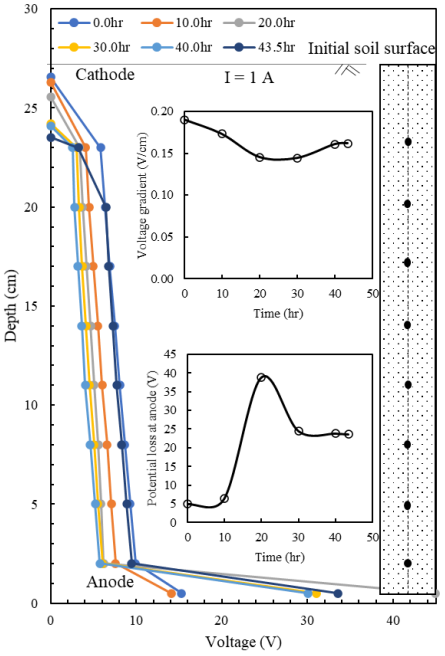

(b) Model T3

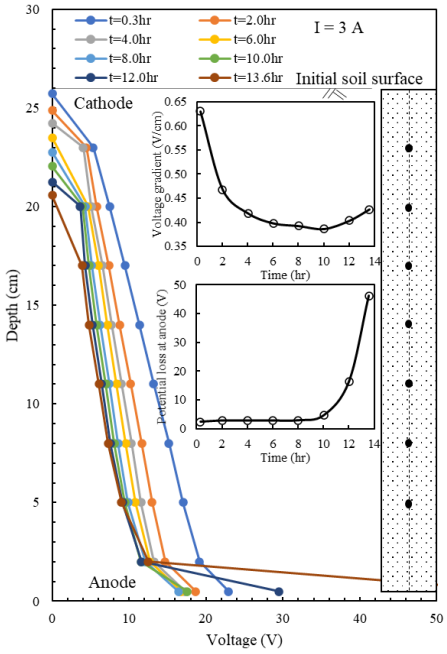

(c) Model T4

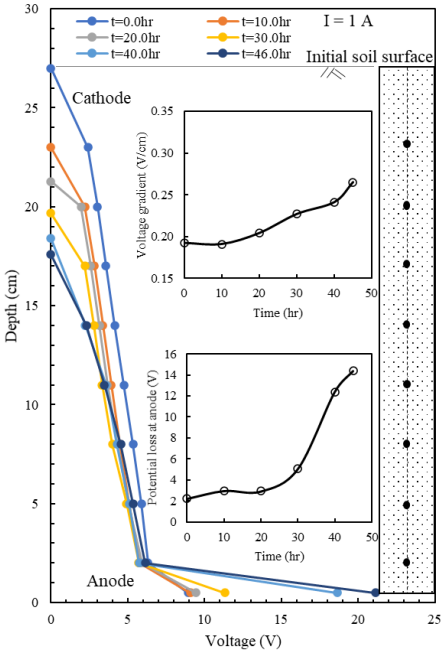

(d) Model T5

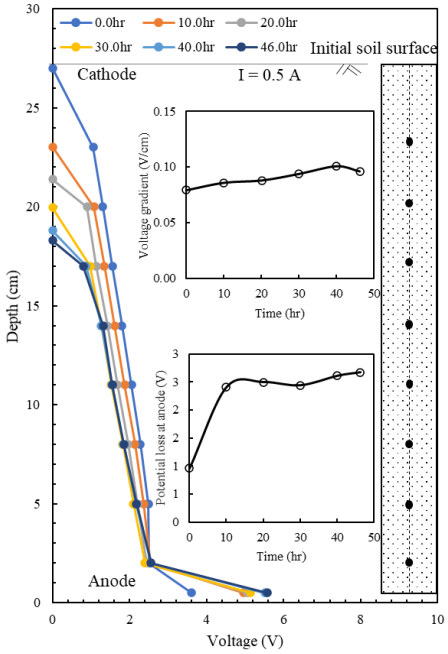

(e) Model T6

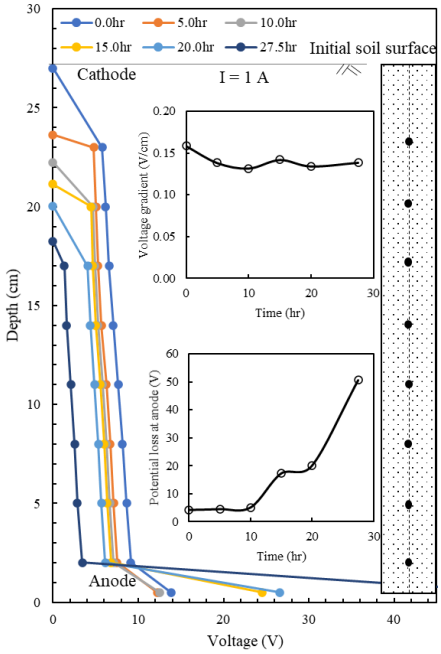

(f) Model T7

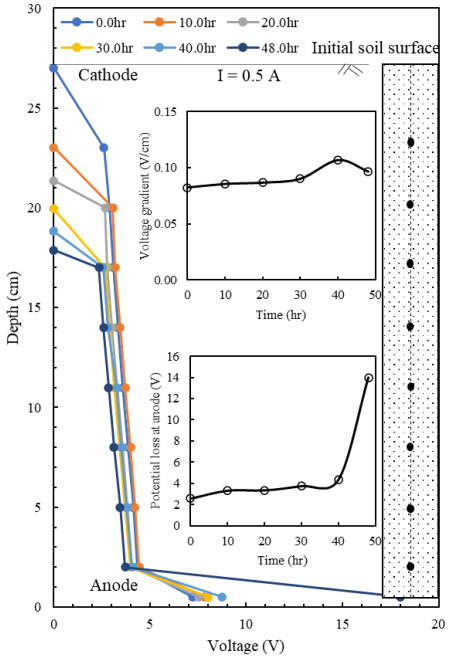

(g) Model T8

Figure 7.20 Voltage distribution in all Model tests: (a) Model T2; (b) Model T3; (c) Model T4; (d) Model T5; (e) Model T6; (f) Model T7; (g) Model T8 (I: Current)

Based on the testing data, the larger settlement and reduction of excess pore water pressure were induced when a combined vacuum preloading and electro-osmosis was

applied. In terms of settlement, the use of 1A current is better to consolidate the soft soil. However, the thermal stability of the connection still needs to be improved.

7.4 Configuration of electrical HDeG or e-HDEG

The combination of horizontal drain and woven carbon felt was effective to consolidate the soft clay. To combine the woven carbon felt and HDeG sheet, the ideal design for the electrical HDeG sheet is shown in Figure 7.21. The drain and woven carbon felt are combined with two non-woven geotextile sheets. The horizontal spacing of prefabricated drains is 0.6 m. The thickness of non-woven geotextile and carbon felt is 1 mm. The total width of the electrical HDeG sheet is 3 m.

By using non-woven geotextile, the transmissivity of non-woven geotextile is enough to use as drainage path and remove the chlorine or hydrogen produced on carbon felt. By using the carbon felt, the proposed electrical HDeG sheet is flexible and lightweight. Therefore, the proposed electrical HDeG sheet can be rolled up and transported to the reclaimed location.

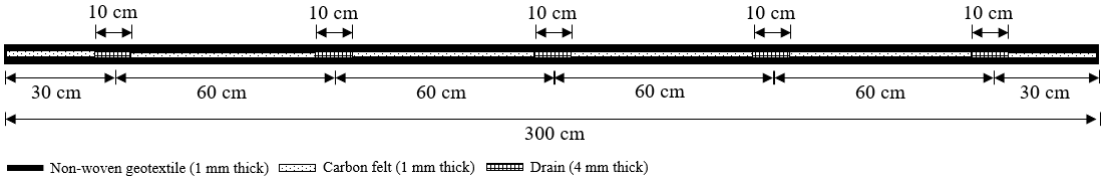

Figure 7.21 Ideal Design of electrical HDeG sheet

7.5 Model tests using lime liner

Previous studies (Broms, 1999) have shown that when soil is treated using lime, the permeability of the soil may increase. To enhance the efficiency of HDeG sheet, in particular, the property of the soil at the interface of HDeG with the soil, lime was used as a liner for HDeG. Four small-sized model tests were conducted to evaluate the efficiency of lime liner.

7.5.1 Testing set-up

The testing setup was similar to that presented in Section 7.3.1. The test box used was 0.2 m in length, 0.1 m in width and 0.3 m in height. The positions of the lime liners used for the model tests are shown in Figure 7.22.

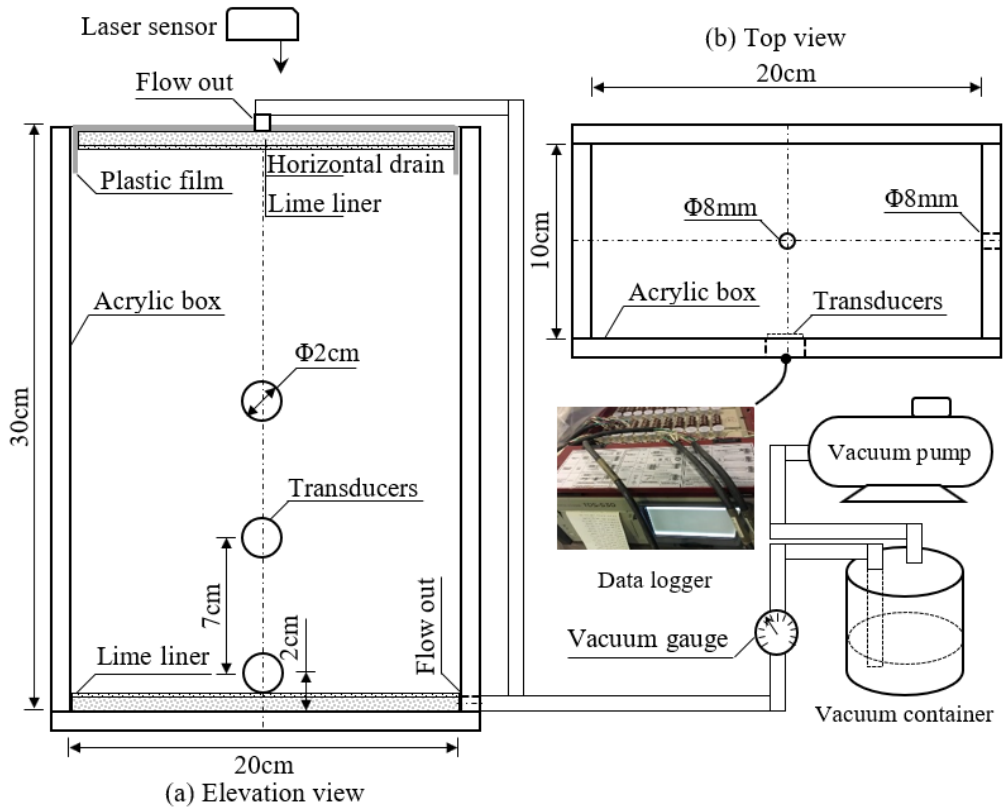

Figure 7.22 Model tests using lime liner and horizontal drain: (a) Elevation view and (b) Top view

To investigate the soil properties of lime treated soil, few oedometer tests using lime and clay slurry mixture were conducted and the results are shown in Figure 7.23. Lime and clay slurry was mixed using hydrate lime, 2% dry weight of clay. The mixture was consolidated under a pressure of 80 kPa. To assess the performance of the lime liner, oedometer tests on clay sample with hydrate lime applied only on the surface together with a layer of non-woven geotextile were also carried out. As a compare, an oedometer test on marine clay without any treatment was also carried out.

The e – log σ_v' curves obtained from the oedometer tests are shown in Figure 7.24a. The use of lime liner did not change much the compressibility of the clay. The void ratio versus permeability in a semi-log plot are shown in Figure 7.24b. The data from oedometer tests as well as permeability tests of the original marine clay and the lime treated soil are plotted. It can be seen that the permeability of soil treated by hydrate lime or with the use of a lime liner was 2 to 3 times of that of original marine clay. However, when the effective stress was higher than 100 kPa (or when the void ratio is less than 1.0) for the soil treated using lime liner, the difference in the permeability

became small. Therefore, the relatively high permeability of lime treated soil is mainly due to the soil structure induced by cation exchange. To verify this point, the specific gravity was also measured for soil after oedometer tests. As shown in Table 7.3. The specific gravities of lime treated soil were higher than that of the original marine clay. The more thorough the treatment, the bigger the changes. This is an indication that the composition of the marine clay had changed after lime treatment.

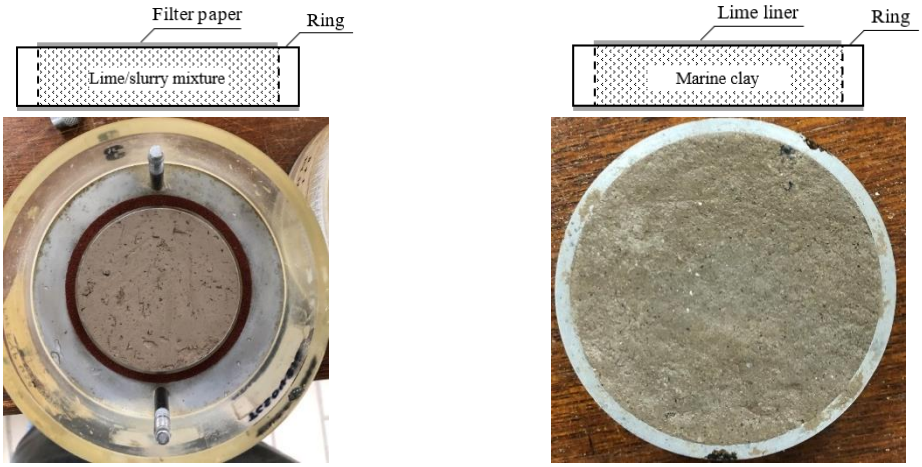

(a) Lime/clay mixture (b) Marine clay with lime liner

Figure 7.23 Oedometer tests: (a) lime/clay mixture and (b) marine clay with lime liner

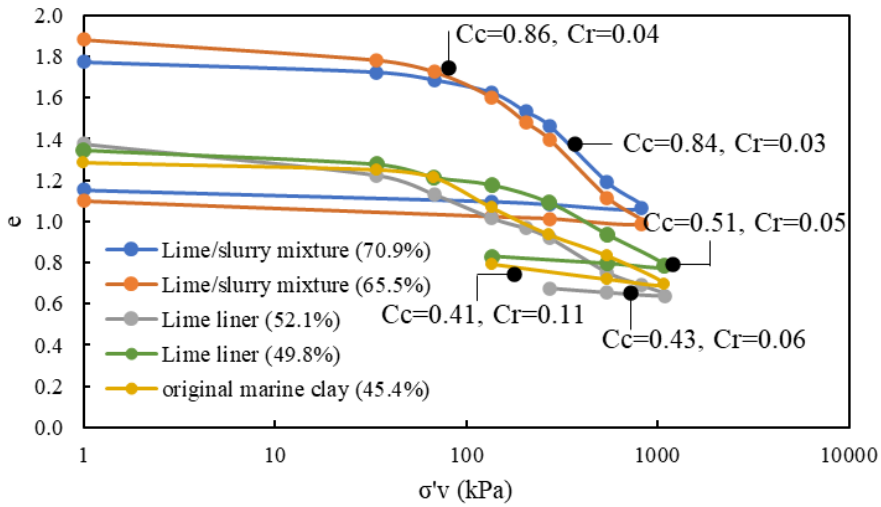

(a) Compressibility

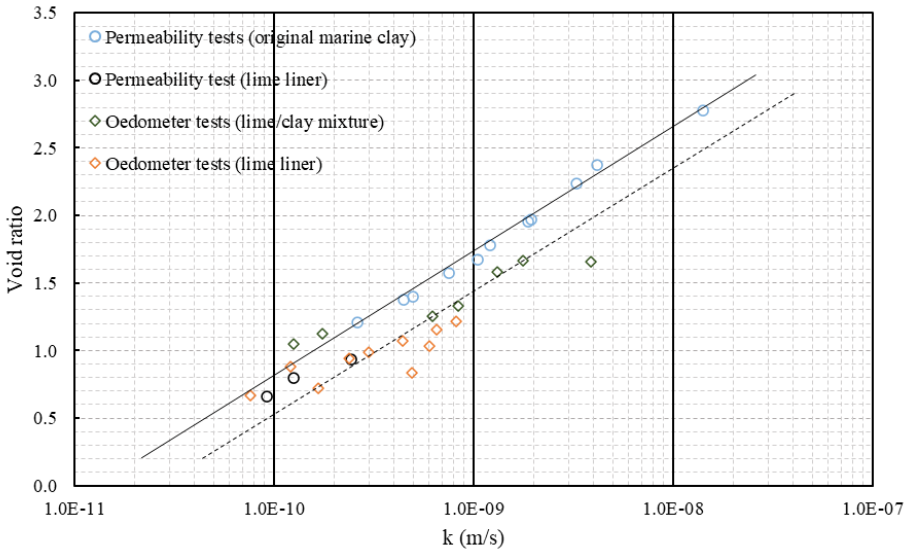

(b) Permeability

Figure 7.24 Compressibility and permeability of original marine clay and lime treated soil: (a) Compressibility and (b) Permeability

Table 7.3 Specific gravity of lime treated soil and original marine clay

	Original marine clay	Marine clay with lime liner	Lime/slurry mixture
Specific gravity (G_s)	2.691	2.715	2.735

7.5.2 Testing procedure

The horizontal drain and lime liner was separated by using a non-woven geotextile sheet. The porous pad was used as horizontal drain. A layer of quick lime was put in between the non-woven geotextile sheets as lime liner as in Figure 7.25 and immersed in water first before testing. The initial water content of soft marine clay was around 125% for model tests. The initial height of soft marine clay was about 28 cm. A plastic film was covered on the top horizontal drain and lime liner. A syringe needle was used in the same way as described in Section 7. 3.1 to measure the vacuum pressure in horizontal drain. The applied vacuum pressure was -90 kPa. A summary of all the model tests is given in Table 7.4. Setting time, Ts, used in the table refers to the duration after the test

setup and before the start of testing. After testing, the water content was measured at different locations along the height as in Figure 7.14. The specific gravity was measured using the dry samples of soil.

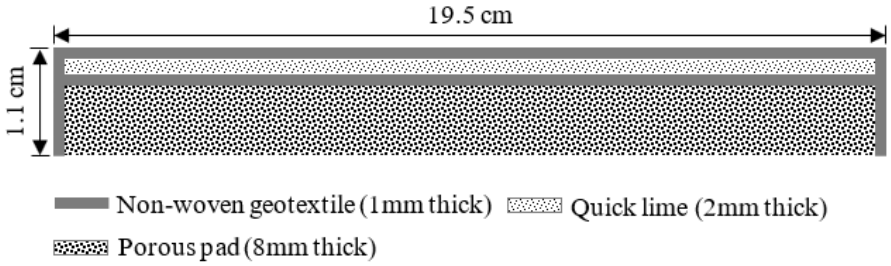

Figure 7.25 Horizontal drain and lime liner

Table 7.4 Summary of Model tests using lime liner

Model	Condition	Vacuum pressure (kPa)	Setting time, *Ts* (hr)	Water content (%)	Duration, *Td* (hr)
L1	VC	-90	---	125.1	68.5
L2	VC+LL	-90	0	124.9	50.0
L3	VC+LL	-90	17.0	123.2	71.5
L4	VC+LL	-90	65.7	125.9	48.5
L5	VC+LL	-90	116.0	125.9	47.4

*Initial height of soil sample: 28 cm
*Termination condition: 9.5 cm of settlement
*LL: Lime liner; VC: Vacuum consolidation

7.5.3 Testing results

- Settlements and pore water pressures

The surface settlements versus time curves for all the 4 tests are shown in Figure 7.26a. When the lime liner was used, the settlements were larger a bit than that using vacuum pressure only. The pore water pressures versus time curves for the four Model tests are shown in Figure 7.26b. The reductions of excess pore pressure in Models L2 to L5 were larger than that in Model L1 using vacuum pressure only. With the use of lime liner or the longer setting time, the reduction of excess pore pressure was faster.

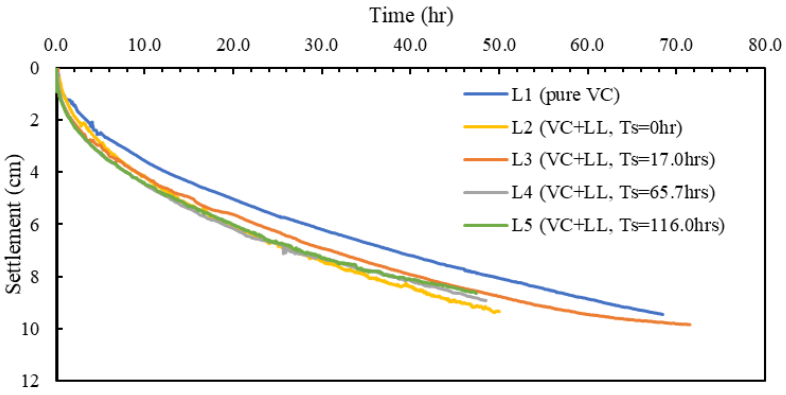

(a) Settlement

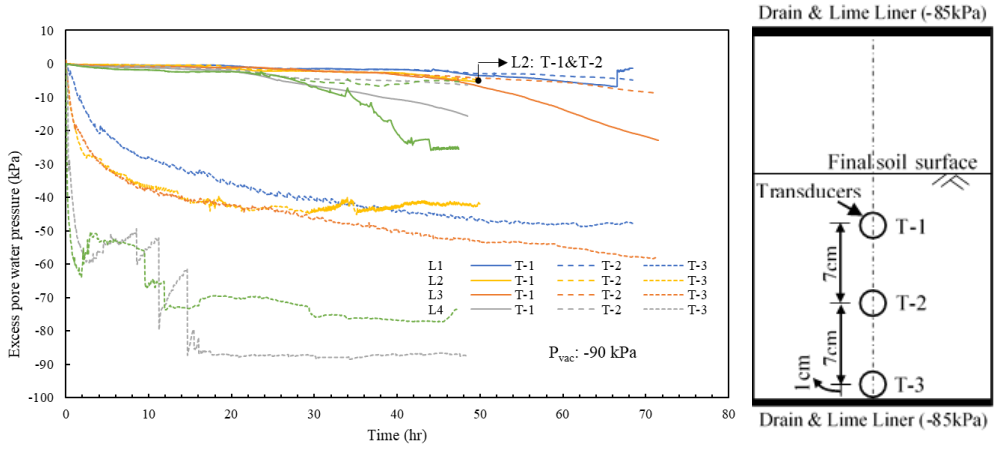

(b) Pore water pressure

Figure 7.26 Measured settlement and pore water pressure: (a) Settlement and (b) Pore water pressure (VC: Vacuum consolidation; LL: Lime liner; *Ts*: Setting time)

- Water content and specific gravity

The measured water contents at similar settlement and specific gravity are shown in Figure 7.27. With the use of lime liner, the reduction of water content was slightly more than that using vacuum consolidation only. The specific gravity along height of treated soil was in between those of original marine clay and lime and clay mixture as in Figure 7.27b. Therefore, the cation exchange of soil particles in soft soil along height was achieved. Because the cation exchange depends on the calcium ion diffusion, the specific gravity near the lime liner tended to be larger than that in the middle of soft soil. The average specific gravity of lime liner treated soil was 2.71.

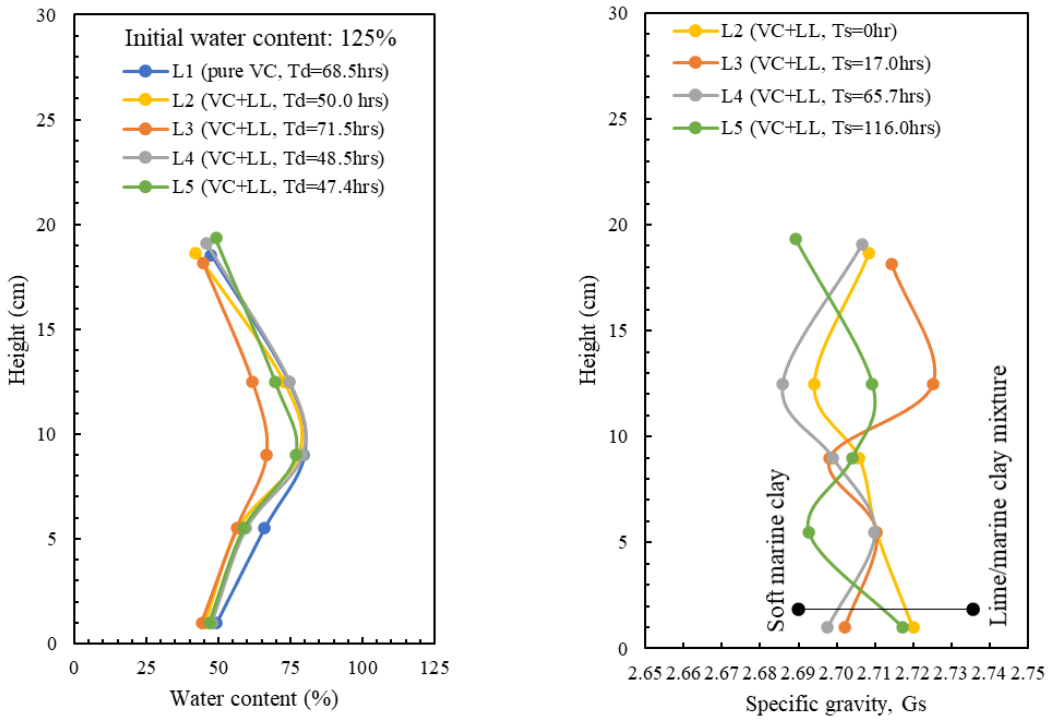

(a) Water content (b) Specific gravity

Figure 7.27 Water content and specific gravity of soil along height after testing: (a) water content and (b) specific gravity (VC: Vacuum consolidation; LL: Lime liner; *Td*: Test duration; Ts: Setting time)

The comparison of the measured and estimated settlement in the model tests using lime liner and vacuum consolidation is shown in Table 7.5. The estimated settlement was calculated using the reduction of average water content and specific gravity. The measured and estimated settlement were consistent.

Table 7.5 Comparison of the measured and estimated settlement

Model	L1	L2	L3	L4	L5
ω_0 (%)	125.1	124.9	123.2	125.9	125.9
$\omega_{t\text{-}avg}$ (%)	68.3	63.9	58.7	66.2	64.7
$s_{t\text{-}cal}$ (cm)	9.6	9.8	10.4	9.4	9.3
s_t (cm)	9.45	9.35	9.85	8.92	8.65

- Compressibility of soil in model tests using lime liner

Same as presented in Section 7.3.3, the calculated effective stress and void ratio of soil in model tests using lime liner are shown in Figure 7.28. The data points of effective stress and void ratio of soil in electro-osmosis model tests were also slightly deviated from that of original marine clay.

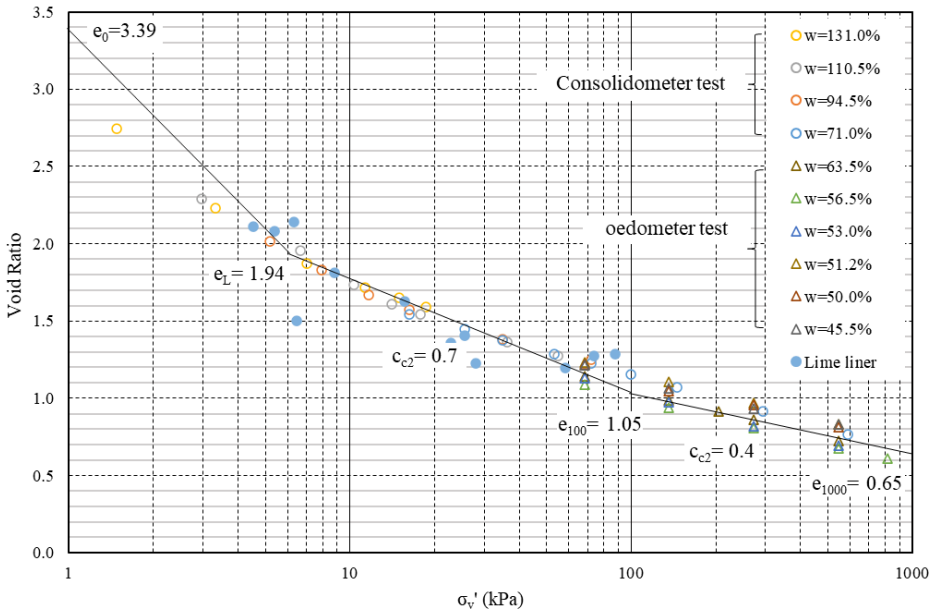

Figure 7.28 Measured data of effective stress versus void ratio in Models using lime liner and vacuum consolidation

- Degree of consolidation

The ultimate settlement was obtained using the Asoka's method (1978) as in Table 7.6.

Table 7.6 Ultimate settlement

Model	S_t (cm)	S_∞ (cm)	DoC (%)
L1	9.45	13.15	71.88
L2	9.35	12.50	74.80
L3	9.85	11.20	87.95
L4	8.92	11.61	76.84
L5	8.65	11.25	76.89

The excess pore water pressure distributions along the height are shown in Figure 7.29. With the use of lime liner or the longer setting time, the reductions of excess pore water

pressure near horizontal drain were larger than those using vacuum pressure only, such as the excess pore water pressure of transducers T-1 and T-3 in Models L3, L4 and L5. That is because the cation exchange induced by lime liner, so that the coefficient of consolidation or the permeability of soft soil was improved, especially for the soil next lime liner.

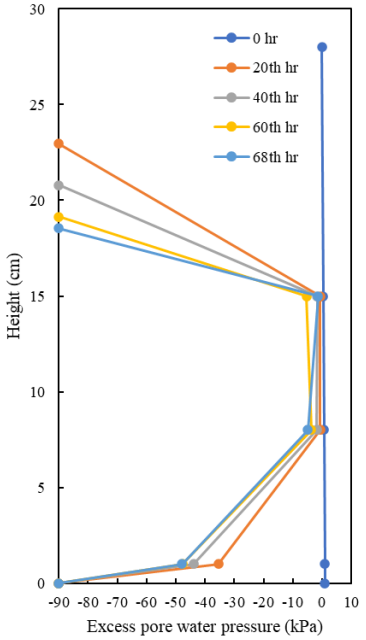

(a) Model L1

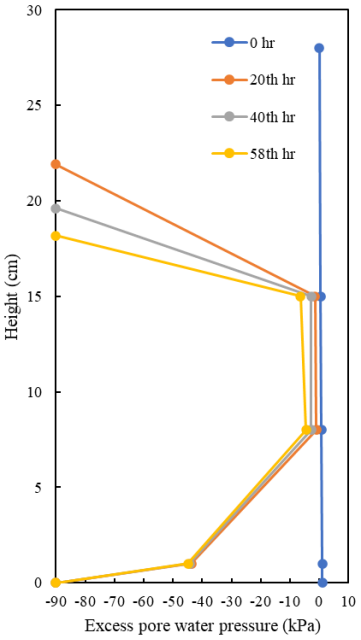

(b) Model L2

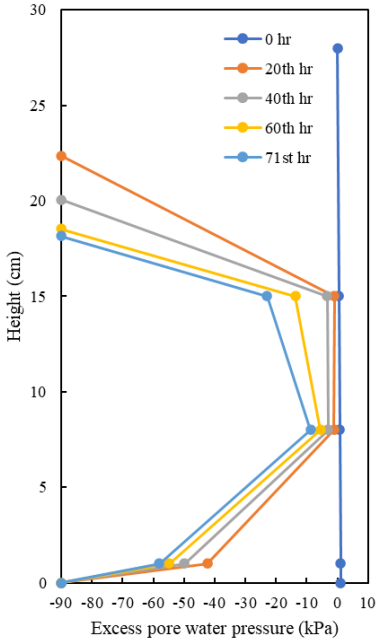

(c) Model L3

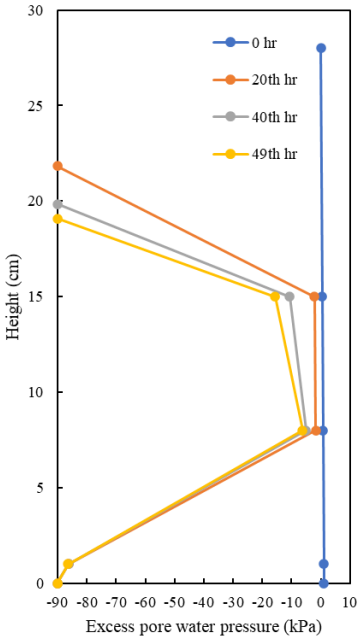

(d) Model L4

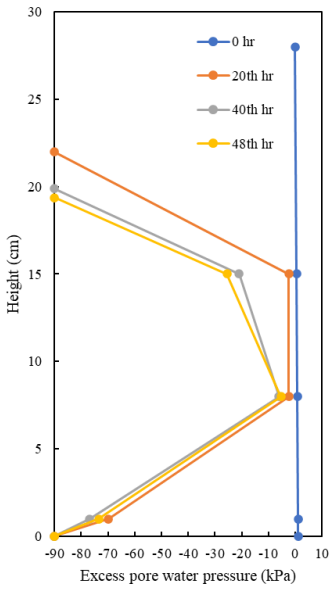

(e) Model L5

Figure 7.29 Excess pore water pressure distribution along height of all model tests: (a) Model L1; (b) Model L2; (c) Model L3; (d) Model L4; (e) Model L5

The degree of consolidation based on settlement and excess pore water pressure for all model tests are shown in Figure 7.30. With the use of lime liner, the degree of consolidation based on settlement for Models L2 to L5 were close and larger than that of Model L1. Compared with Models L2 and L3, the degree of consolidation based on excess pore water pressure for Models L4 and L5 were much larger than that of Model L1. Therefore, the lime liner is effective to treat the soft soil. In terms of the degree of consolidation based on excess pore water pressure, the setting time had an effect on the consolidation of soft soil due to calcium ion diffusion.

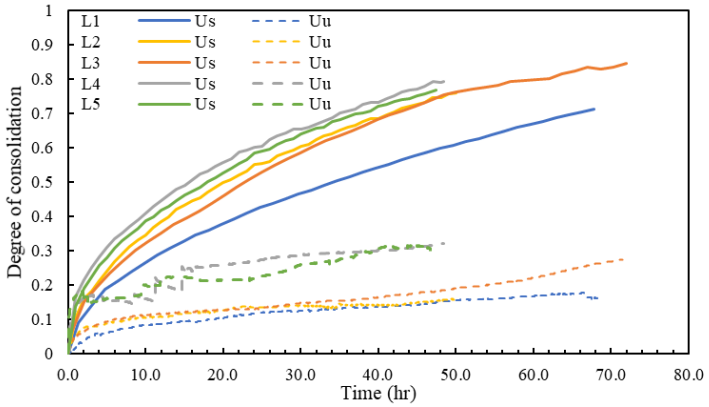

Figure 7.30 Degree of consolidation of model tests (Us: Degree of consolidation based on settlement; Uu: Degree of consolidation based on excess pore water pressure)

7.6 Configuration of lime liner enhanced HDeG sheet

As the use of lime liner and horizontal drain is feasible for the consolidation of soft clay, the new design of lime liner enhanced HDeG sheet is proposed in Figure 7.31. The horizontal spacing of prefabricated drains is 0.6 m and the total width is 3 m. To form the lime liner enhanced HDeG sheet conveniently, the quick lime is placed in between two non-woven geotextile sheets as lime liner. During the installation of lime liner enhanced HDeG sheet, the quick lime will react with seawater into hydrate lime. Same with the electrical HDeG sheet, the lime liner enhanced HDeG sheet have good transmissivity and flexibility, which make it is convenient for transportation and installation.

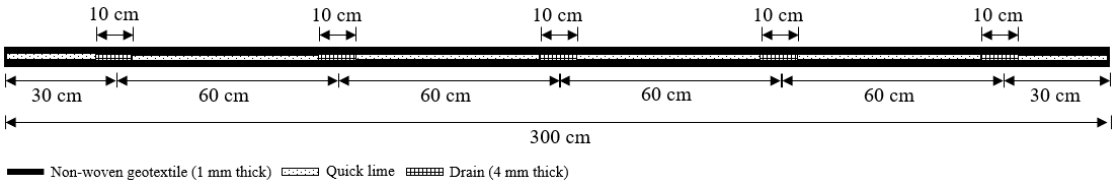

Figure 7.31 Ideal design of lime liner enhanced HDeG sheet

7.7 Conclusions

The following conclusions can be drawn from the model tests:

(1) A method to combine electro-osmosis with HDeG or the use of e-HDeG for consolidation of soft clay was proposed. Both carbon felt and steel plate could be used as electrode for electro-osmosis. However, carbon felt was a better choice due to its flexibility and lightweight. The model tests showed that electro-osmosis using carbon felt was effective in accelerating the vacuum consolidation of soft marine clay. Nevertheless, the connector for the wires and the carbon felt still need to be improved.

(2) Larger settlement and greater reduction in excess pore water pressure were induced by the coupling of vacuum consolidation and electro-osmosis.

(3) The use of lime liner to enhance the performance of HDeG or lime liner enhanced HDeG was proposed. The permeability of the lime treated soil was improved for about 2 – 3 times because of the soil structure induced by cation exchange of soil particle. The efficiency of the use of lime liner was verified using small

consolidation tests under surcharge or vacuum pressure. The setting time had an effect on the consolidation of soft soil due to calcium ion diffusion. With longer setting time, the reduction of excess pore pressure was larger.

CHAPTER 8 CONTAINMENT STRUCTURE USING VERTICAL WALL AND SUCTION CAISSONS

8.1 Introduction

One important component in a land reclamation project is the containment structure. For land scarce Singapore, land reclamation has been carried out along most of the coastal areas in the past. Future land reclamation will have to be carried out in relative deep water (Chu *et al.*, 2009a; Chu and Guo, 2016). Furthermore, as the global mean sea level (MSL) is projected to rise by 0.6 - 1.3 m till 2100 (Horton, 2020), a taller seawall or a higher ground elevation is also required. In this case, the conventional sand bund method is no longer applicable for containment structures as it requires too much fill materials to build. The use of vertical concrete seawalls becomes a good alternative. When seawalls or other coastal defence systems are constructed on soft marine deposits, suction caissons can be employed as foundations (Chu et al., 2012; Guan et al., 2018). In this chapter, a conceptual design and related construction procedure using vertical seawall and suction caisson foundations as containment structure for land reclamation in Singapore was proposed. The stability and deformation analyses conducted using analytical and numerical methods.

8.2 Conceptual design for containment structure using vertical seawall and suction caissons

Suction caisson is one of the suitable foundation types for seawall constructed on thick marine clay deposit in relatively deep seawater. The conceptual design for seawall with suction caisson foundations used as containment structure for land reclamation is shown in Figure 8.1(a). The design configuration of the suction caisson foundation and the seawall on top of the foundation is given in Figure 8.1(b). It can be seen from Figure 8.1(b) that the suction caisson foundation consists of 4 identical concrete suction caissons connected together by a top slab and vertical webs. Part of the reasons for using 4 suction caissons is to facilitate installation. The use of 4 suction caissons as a group enables the vertical settlement of the caissons to be uniform to avoid titling by

controlling the suction applied to each cylinder. The seawall comprises a series of single cylinders and vertical webs sitting on top of the suction caisson foundation as shown in Figure 8.1(b).

In terms of construction sequence, the 4 suction caissons and the upper cylinders as the seawall are installed section by section. The suction caissons and the upper cylinders can be cast and assembled together as a whole at a casting yard. The assembly is towed to the required position and penetrated into the required depth under the hydrostatic pressure outside and the suction inside the chambers of caissons which are sealed at the bottom by the seabed clay. The upper concrete cylinders can also be installed separately on top of the suction caisson foundation after the foundation are installed. The joints between seawall and suction caisson foundation are grouted using cement grout after the installation of two adjacent segments.

After the seawall has been installed, the soft dredged marine clay and horizontal drainage enhanced non-woven geotextile sheets (HDeG sheet) will be placed within the containment structure for land reclamation. During the placement of soft marine clay, the lateral earth pressure will increase which results in the reduction of the stability of seawall.

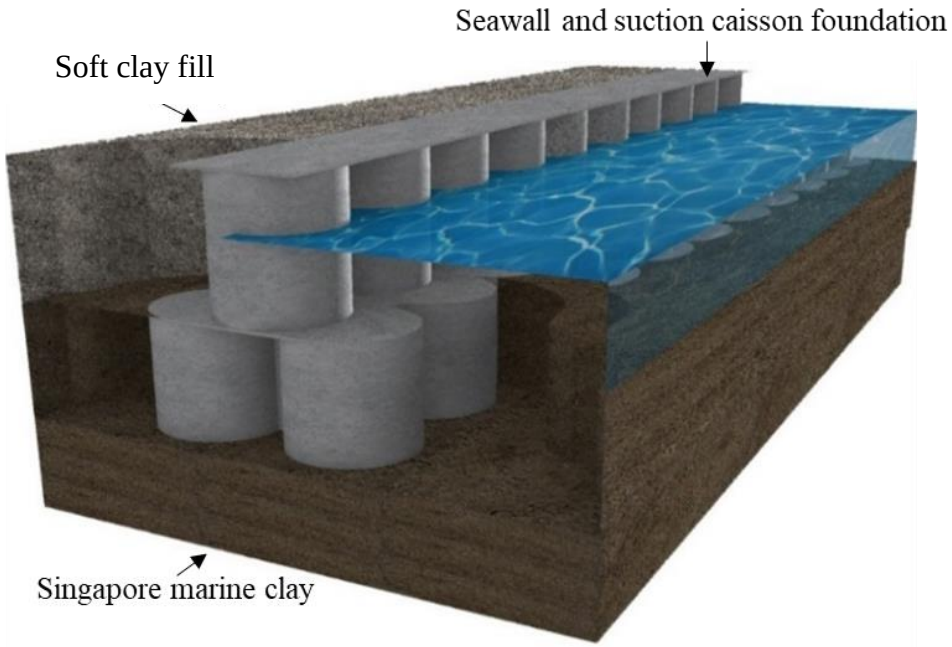

(a) Use of vertical seawall and suction caissons for containment structure

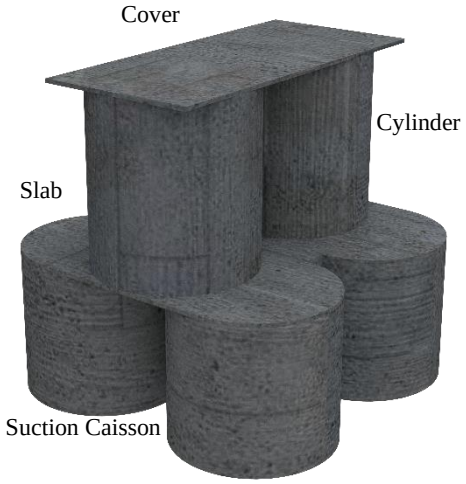

(b) One unit of the seawall structure

Figure 8.1 Proposed containment structure for land reclamation

8.3 Stability analyses of containment structure under backfill

8.3.1 Site conditions

An idealised site condition in Singapore is shown in Figure 8.2. The seabed soil consists of 15 m upper marine clay, 5 m intermediate stiff clay and 20 m lower marine clay as in Figure 8.2. The cemented sand is below the lower marine clay. The soil parameters of Singapore marine clay are given in Table 8.1 (Arulrajah and Bo, 2008; Chu et al., 2009b; Bo et al., 2013). The undrained shear strength of upper marine clay and lower marine clay was considered increasing with the increase of depth or OCR. The average undrained shear strength, 79 kPa, was used for the intermediate marine clay. The ratio of horizontal permeability to vertical permeability for Singapore marine clay was set about 1.5. The effective friction angle was set about 23° for upper and lower marine clay, and 28.5° for intermediate marine clay. The soil properties of Singapore marine clay are shown in Table 8.1.

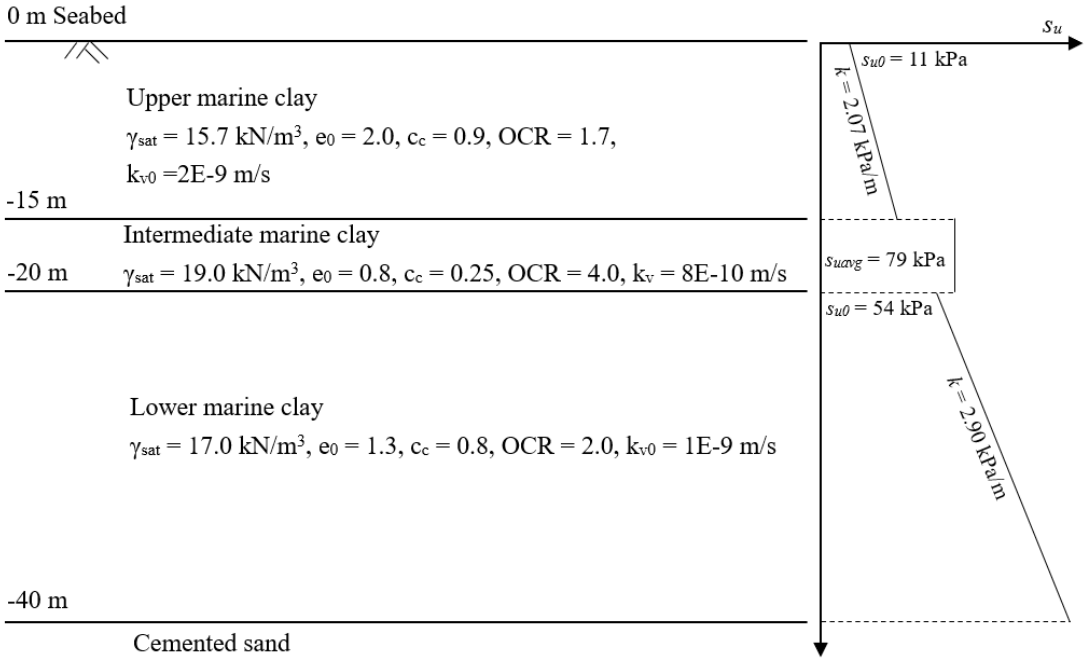

Figure 8.2 Soil profile of Singapore marine clay

Table 8.1 Soil properties of Singapore marine clay

Properties		Upper marine clay	Intermediate marine clay	Lower marine clay
Unit weight	γ_{sat} (kN/m^3)	15.7	19.0	17.0
Undrained modulus	E_{u0} (MPa)	3.85	27.65	19.25
Empirical correlation	c_u/σ'_{v0}	0.37	---	0.42
Undrained shear strength	c_{u0} (kPa)	11	79	55
Gradient of undrained shear strength	k_{cu} (kPa/m)	2.07	---	2.90
Initial void ratio	e_0	2.0	0.8	1.3
Friction angle	φ' (°)	23	28.5	23
Compression index	c_c	0.9	0.25	0.80
Recompression index	c_r	0.1	0.05	0.16
Coefficient of consolidation (horizontal)	c_h (m^2/yr)	3.0	7.5	4.0
Coefficient of consolidation (vertical)	c_v (m^2/yr)	0.6	3.0	1.1
Permeability (horizontal)	k_h (m/day)	3.0E-9	1.2E-9	1.5E-9
Permeability (vertical)	k_v (m/S)	2.0E-9	8.0E-10	1.0E-9
Coefficient of permeability	c_k	0.3e_0	---	0.3e_0
Over-consolidation ratio	OCR	1.7	4.0	2.0

The unit weight of sea water, γ_w, is 10.05 kN/m^3. The mean sea level is located at +1.64 mCD. The properties of soft clay fill used for land reclamation are similar with the soft marine clay as in Table 8.2. The saturated unit weight of soft clay fill was set as 14.2 kN/m^3. The initial water content and void ratio were 111.5 % and 3.0, respectively. The compressibility and permeability of soft clay were expressed as in Eq. (8.1) and Eq. (8.2). The recompression index is 0.1.

$$e = -1.36Log_{10}\sigma_v' + e_0, \sigma_v' < 6kPa$$

$$e = -0.7Log_{10}\frac{\sigma_v'}{6} + 1.94, \sigma_v' < 100kPa \quad (8.1)$$

$$e = -0.4Log_{10}\frac{\sigma_v'}{100} + 1.05, \sigma_v' < 1000kPa$$

$$e = 0.931Log_{10}k + 10.098 \quad (8.2)$$

where, e_0 is the initial void ratio; σ'_v is the vertical effective stress; k is the permeability of soft clay fill.

Table 8.2 Soil parameters of soft clay fill

Unit weight, γ_{sat} (kN/m^3)	Water content, ω (%)	Initial void ratio, e_0	Initial permeability, k_0 (m/s)	Coefficient of consolidation, c_v (m^2/yr)	Recompression index, c_r
14.2	111.5	3.0	3.2E-8	0.4	0.1

8.3.2 Design of suction caissons and seawall

The seawall is designed as an offshore containment structure for land reclamation. The geometry of one unit of seawall with suction caisson foundation is shown in Figure 8.3. The diameter of the suction caisson will be the same as that of the cylinder. The outer diameter, *D*, of caissons or cylinders is 20 m and the corresponding width, *W*, of suction caisson foundation is 43 m. The width of concrete web between the suction caissons or the cylinders is 3 m. Three water depths below the mean sea level are assumed for the stability analyses, about 8.5 m, 12.5 m and 16.5 m. The top surface of the seawall is 6 m above the mean sea level. Three different heights, *H*, of seawall corresponding to three different sea water depths, d_w, are considered as 14.5 m, 18.5 m and 22.5 m, respectively. The penetration depth, *d*, of suction caisson foundation is set to be 15 m based on soil profile. In practice, the suction caisson foundation will penetrate the

marine clay for up to 0.5 m under its self-weight. The upper cylinder has a concrete cover and was filled with fluid inside, like sea water in this case. The width of the cover is the same as the outer diameter of the cylinder. The thickness, *t*, in every part is assumed as 0.5 m here and the structure is made of concrete with a unit weight of 25 kN/m^3.

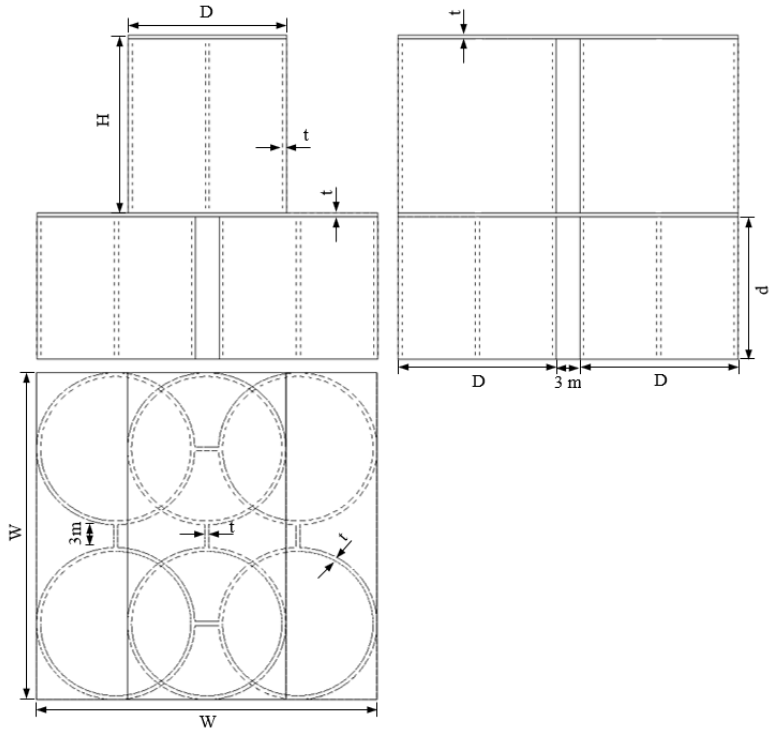

Figure 8.3 Three views diagram for the new containment bund (*t*: thickness, 0.5 m)

Table 8.3 Geometry of seawall and seawater depths

Height of seawall, *H* (m)	Seawater depth, d_w (m)	Diameter, *D* (m)	Width of foundation, *W* (m)	Depth of foundation, *d* (m)	Thickness, *t* (m)
14.5	8.5	20	43	15	0.5
18.5	12.5				
22.5	16.5				

8.3.3 Soil improvement works

To improve the stability of seawall, sand compaction piles (SCPs) would be used to improve the upper marine clay next to the suction caissons on the seaside to enhance the

stability of the seawall. The SCPs should be installed after the installation of the suction caissons, but before the placement of soft clay fill. With the use of SCPs, the lateral displacement of the seawall will be reduced and the stability of the seawall will be improved as shown by other case studies (Chu et al., 2000; Han et al., 2007; Chai et al., 2012; Jiang et al., 2013; Kamash et al., 2014).

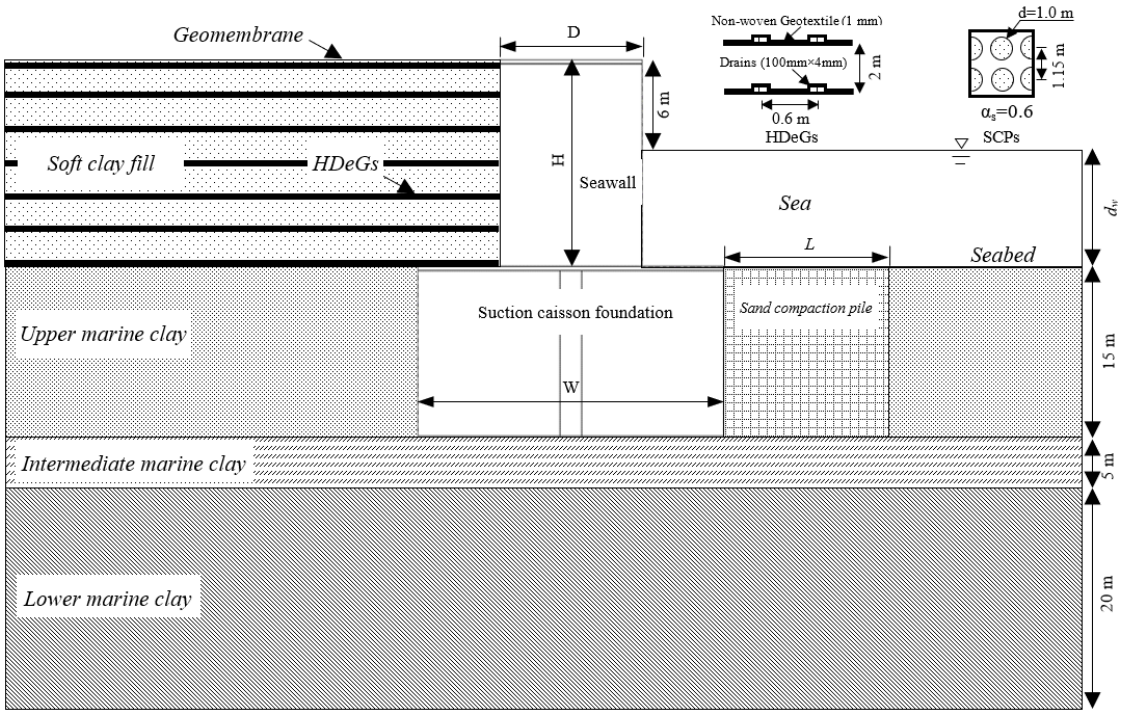

Figure 8.4 Analytical model for the stability analyses (*L*: width of SCPs treated marine clay)

The penetrated depth of SCPs should be the same as the penetration depth of the suction caissons. The effect of different widths, *L*, of SCPs treated marine clay or different rows of SCPs on the stability of seawall was considered. The sand compaction piles with 1.0 m in diameter were distributed in a rectangular shape with the spacing of 1.15 m from centre to centre as shown in Figure 8.4, which resulted in a replacement ratio of 0.6. The replacement ratio is calculated as A_s/A, A_s is the area of cross-section of SCPs and A is the area of unit-cell of SCPs treated marine clay. The parameters of SCPs are shown in Table 8.4. The saturated unit weight of the sand compaction piles is 20 kN/m^3 and its internal friction angle is 35°.

Table 8.4 Soil parameters for sand compaction piles

Unit weight, γ_{sat} (kN/m^3)	Modulus, E (MPa)	Friction angle, φ' (˚)	Initial void ratio, e_0	Coefficient of lateral earth pressure at rest, k_0	Permeability, k (m/day)
20.0	50	35	0.6	0.43	0.864

The HDeG consists of a single non-woven geotextile sheet and drains with 0.6 m horizontal spacing as shown in Figure 8.5. The first layer of HDeG is laid on the seabed first using an offshore barge. The soft clay fill is placed to cover completely the HDeG before vacuum pressure is applied. The above process is repeated by the placement of another layer of HDeG and another layer of soft clay fill until the soft clay fill reaches the designated height. The vertical spacing of the HDeG sheet is set as 2 m. A layer of geomembrane is used to cover the top of the HDeG sheet to seal the entire land reclamation area for vacuum consolidation. The advantage of this design is to enable the soft clay fill to be improved layer by layer using vacuum pressure in the early stage of consolidation and the fills placed subsequently on top becomes the additional surcharge. In this way, the construction time for land reclamation can be much reduced. The HDeG sheet not only provide vacuum pressure, but also work as a drain for water dissipation and discharge during consolidation.

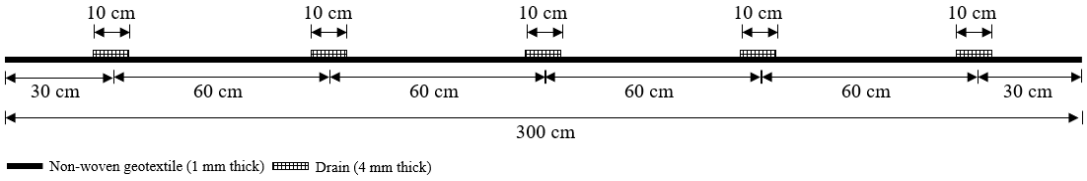

Figure 8.5 Horizontal drainage enhanced geotextile

With the use of HDeG sheet, the vacuum preloading is considered to be -60 kPa and applied after 15 days of infilling. For illustration purpose, the period of the placement of soft clay fill and HDeG sheet for one layer is assumed to be one month. The top surface of the soft clay fill will be covered by geomembrane. One meter of sand layer with a unit weight of 20.0 kN/m^3 will be placed on the geomembrane too. Further vacuum preloading will be applied to consolidate the top layer of soft clay fill and the rest of the clay fill for another 2 to 6 months. The design ground level of the improved soil will be controlled to be the same as the top level of the seawall. The total layers of

soft marine clay are 11 layers for 14.5 m of seawall height, 15 layers for 18.5 m of seawall height, and 18 layers for 22.5 m of seawall height. The total original thickness of soft marine clay is estimated to be 22 m for H = 14.5 m, 30 m for H = 18.5 m, and 36 m for H = 22.5 m.

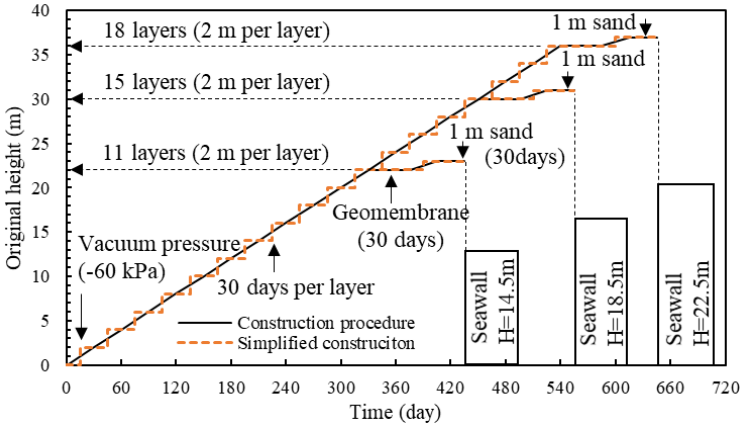

Figure 8.6 Construction procedure

The vertical coefficient of consolidation of soft clay fill and the upper marine clay are assumed to be 0.4 m^2/yr and 0.6 m^2/yr, respectively. Based on the small-strain consolidation solution and design procedure as proposed in Chapter 6. By using the proposed formula for the degree of consolidation of small-strain consolidation solution, the degree of consolidation based on pore water pressure, U_u, for each layer of soft clay fill was calculated. The degrees of consolidation for first layer under three different heights of seawall, H, are shown in Figure 8.7. By using the proposed conversion equation, the degree of consolidation based on settlement, U_s, was calculated. The settlement, s_{ti}, for each layer can be calculated using the degree of consolidation based on settlement and the ultimate settlement, $s_{\infty i}$, obtained using Terzaghi's method. The summaries of the calculation for each layer under different heights of seawall are shown in Table 8.5 to Table 8.7. Based on the degree of consolidation based on pore water pressure, the effective stress, σ_t, and improved undrained shear strength, c_u, can be calculated for each layer of soft clay fill. The excess pore water pressure distributions in soft clay fill and upper marine clay can also be calculated using the excess pore pressure formula of the proposed small-strain consolidation solution as shown in Figure 8.8. The degree of consolidation based on the pore water pressure and settlement and the undrained shear strength of upper marine clay can also be calculated using the proposed small-strain consolidation solution.

Based on the calculation as in Table 8.5 to Table 8.7, the average values of degree of consolidation (DoC), undrained shear strength, c_u, and the settlement, s_t, of soft clay fill and upper marine clay can be obtained. The degree of consolidation based on pore water pressure, DoC_u, and settlement, DoC_s, at the end of vacuum consolidation is 42.0% and 82.0% for H = 14.5 m, 44.0% and 83.0% for H = 18.5 m, 45.2% and 84.0% for H = 22.5 m. The degrees of consolidation, DoC_u and DoC_s of upper marine clay is 4.1% and 31.3% for H = 14.5 m, 4.2% and 34.1% for H = 18.5 m, and 4.3% and 35.8% for H = 22.5 m. The average undrained shear strength of soft clay fill and upper marine clay were obtained. The final ground elevations of soft clay fill and sand layer above seabed are 14.06 m for H = 14.5 m, 18.46 m for H = 18.5 m, and 21.69 m for H = 22.5 m.

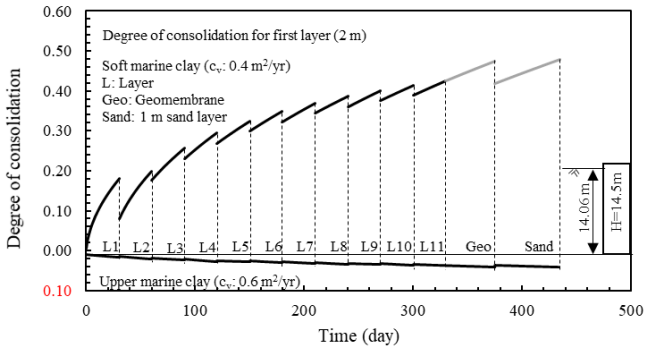

(a) H = 14.5 m

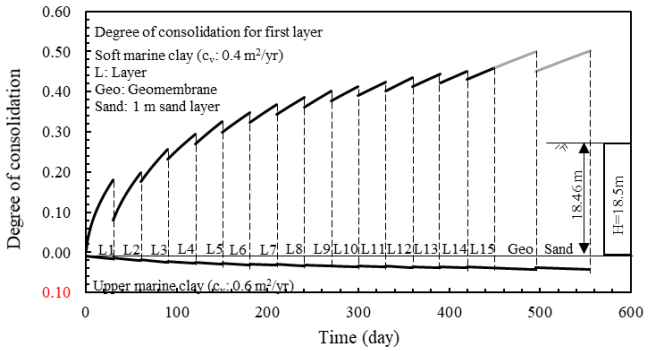

(b) H = 18.5 m

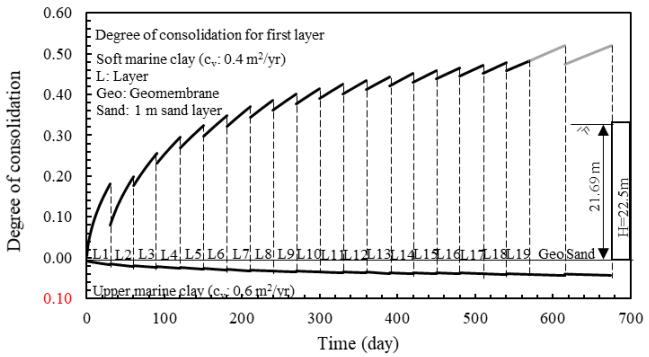

(c) H = 22.5 m

Figure 8.7 Degree of consolidation based on pore pressure for first layer

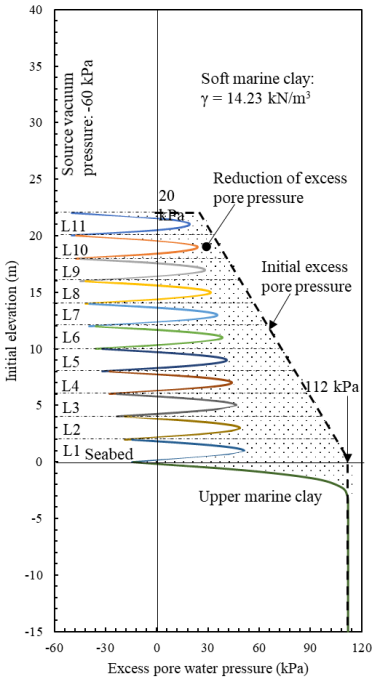

(a) H = 14.5 m

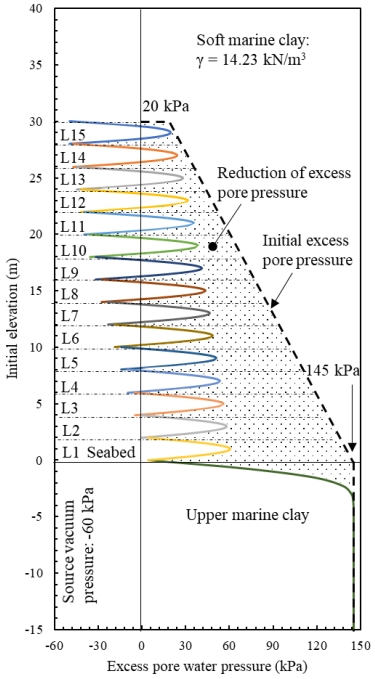

(b) H = 18.5 m

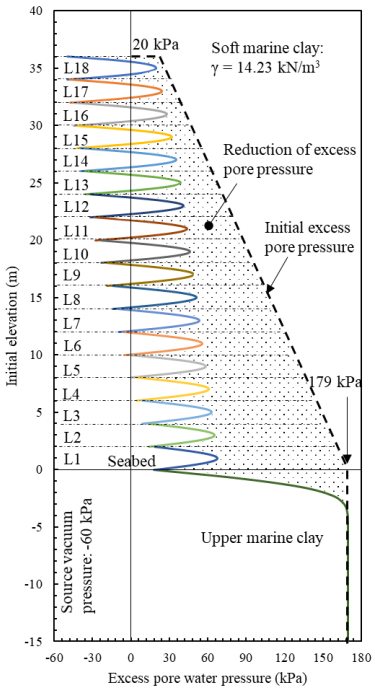

(c) H = 22.5 m

Figure 8.8 Excess pore water pressure distributions of soft marine clay and upper marine clay after construction

Table 8.5 Calculation of the vacuum consolidation of soft clay fill of H = 14.5 m

Layers / Time (day)		1	2	3	4	5	6	7	8	9	10	11
DoC_u	30	0.18										
	60	0.20	0.18									
	90	0.26	0.20	0.18								
	120	0.30	0.26	0.20	0.18							
	150	0.33	0.30	0.26	0.20	0.18						
	180	0.35	0.33	0.30	0.26	0.20	0.18					
	210	0.37	0.35	0.33	0.30	0.26	0.20	0.18				
	240	0.39	0.37	0.35	0.33	0.30	0.26	0.20	0.18			
	270	0.40	0.39	0.37	0.35	0.33	0.30	0.26	0.20	0.18		
	300	0.41	0.40	0.39	0.37	0.35	0.33	0.30	0.26	0.20	0.18	
	330	0.42	0.41	0.40	0.39	0.37	0.35	0.33	0.30	0.26	0.20	0.18
	375	0.47	0.47	0.46	0.45	0.43	0.42	0.40	0.37	0.35	0.31	0.25
	435	0.48	0.47	0.46	0.45	0.45	0.43	0.42	0.40	0.38	0.36	0.33
σ_∞ (kPa)		168	159	151	143	134	126	118	109	101	93	84
$s_{\infty i}$ (m)		1.02	1.02	1.01	1.01	1.00	1.00	0.99	0.98	0.98	0.95	0.93
DoC_s		0.86	0.85	0.85	0.84	0.83	0.83	0.82	0.80	0.79	0.77	0.75
s_{ti} (m)		0.87	0.86	0.86	0.85	0.83	0.82	0.81	0.79	0.77	0.73	0.70
h_{ti} (m)		1.13	1.14	1.14	1.15	1.17	1.18	1.19	1.21	1.23	1.27	1.30
σ_t (kPa)		81	75	69	64	60	54	50	44	38	33	28
u_0 (kPa)		108	99	91	83	74	66	58	49	41	33	24
OCR		1.00	1.00	1.00	1.00	1.00	1.00	1.00	1.00	1.00	1.01	1.16
c_u (kPa)		19.4	17.9	16.7	15.4	14.5	13.0	11.9	10.5	9.2	8.1	7.5
h_t (m)		13.15										

DoC_u: degree of consolidation based on pore water pressure; DoC_s: degree of consolidation based on settlement; σ_∞: Surcharge; σ_t: final effective stress for each layer; $s_{\infty i}$: ultimate settlement for each layer; s_{ti}: final settlement for each layer; h_{ti}: final thickness for each layer; u_0: initial pore water pressure; OCR: over-consolidation ratio for each layer; c_u: undrained shear strength for each layer; h_t: final thickness of soft clay fill.

Table 8.6 Calculation of the vacuum consolidation of soft clay fill of H = 18.5 m

Time (day) \ Layers		1	2	3	4	5	6	7	8	9	10	11	12	13	14	15
DoC_u	30	0.18														
	60	0.20	0.18													
	90	0.26	0.20	0.18												
	120	0.30	0.26	0.20	0.18											
	150	0.33	0.30	0.26	0.20	0.18										
	180	0.35	0.33	0.30	0.26	0.20	0.18									
	210	0.37	0.35	0.33	0.30	0.26	0.20	0.18								
	240	0.39	0.37	0.35	0.33	0.30	0.26	0.20	0.18							
	270	0.40	0.39	0.37	0.35	0.33	0.30	0.26	0.20	0.18						
	300	0.41	0.40	0.39	0.37	0.35	0.33	0.30	0.26	0.20	0.18					
	330	0.42	0.41	0.40	0.39	0.37	0.35	0.33	0.30	0.26	0.20	0.18				
	360	0.43	0.42	0.41	0.40	0.39	0.37	0.35	0.33	0.30	0.26	0.20	0.18			
	390	0.44	0.43	0.42	0.41	0.40	0.39	0.37	0.35	0.33	0.30	0.26	0.20	0.18		
	420	0.45	0.44	0.43	0.42	0.41	0.40	0.39	0.37	0.35	0.33	0.30	0.26	0.20	0.18	
	450	0.46	0.45	0.44	0.43	0.42	0.41	0.40	0.39	0.37	0.35	0.33	0.30	0.26	0.20	0.18
	495	0.50	0.49	0.49	0.48	0.47	0.47	0.46	0.45	0.43	0.42	0.40	0.37	0.35	0.31	0.25
	555	0.51	0.50	0.49	0.49	0.48	0.47	0.46	0.45	0.44	0.43	0.42	0.40	0.38	0.36	0.33
σ_{zc} (kPa)		201	193	184	176	168	159	151	143	134	126	118	109	101	93	84
s_{zi} (m)		1.04	1.03	1.03	1.02	1.02	1.02	1.01	1.01	1.00	1.00	0.99	0.98	0.98	0.95	0.93
DoC_s		0.87	0.87	0.86	0.86	0.86	0.85	0.85	0.84	0.83	0.83	0.82	0.80	0.79	0.77	0.75
s_{ti} (m)		0.90	0.89	0.89	0.88	0.87	0.86	0.86	0.85	0.83	0.82	0.81	0.79	0.77	0.73	0.70
h_{ti} (m)		1.10	1.11	1.11	1.12	1.13	1.14	1.14	1.15	1.17	1.18	1.19	1.21	1.23	1.27	1.30
σ_t (kPa)		103	97	90	86	81	75	69	64	59	54	50	44	38	33	28
u_0 (kPa)		141	133	124	116	108	99	91	83	74	66	58	49	41	33	24
OCR		1.00	1.00	1.00	1.00	1.00	1.00	1.00	1.00	1.00	1.00	1.00	1.00	1.00	1.01	1.16
c_u (kPa)		24.6	23.2	21.6	20.7	19.4	17.9	16.7	15.4	14.2	13.0	11.9	10.5	9.2	8.1	7.5
h_t (m)		17.55														

DoC_u: degree of consolidation based on pore water pressure; DoC_s: degree of consolidation based on settlement; σ_{zc}: Surcharge; σ_t: final effective stress for each layer; s_{zi}: ultimate settlement for each layer; s_{ti}: final settlement for each layer; h_{ti}: final thickness for each layer; u_0: initial pore water pressure; OCR: over-consolidation ratio for each layer; c_u: undrained shear strength for each layer; h_t: final thickness of soft clay fill.

Table 8.7 Calculation of the vacuum consolidation of soft marine clay of H = 22.5 m

Time (day) \ Layers		1	2	3	4	5	6	7	8	9	10	11	12	13	14	15	16	17	18
DoC_u	30	0.18																	
	60	0.20	0.18																
	90	0.26	0.20	0.18															
	120	0.30	0.26	0.20	0.18														
	150	0.33	0.30	0.26	0.20	0.18													
	180	0.35	0.33	0.30	0.26	0.20	0.18												
	210	0.37	0.35	0.33	0.30	0.26	0.20	0.18											
	240	0.39	0.37	0.35	0.33	0.30	0.26	0.20	0.18										
	270	0.40	0.39	0.37	0.35	0.33	0.30	0.26	0.20	0.18									
	300	0.41	0.40	0.39	0.37	0.35	0.33	0.30	0.26	0.20	0.18								
	330	0.42	0.41	0.40	0.39	0.37	0.35	0.33	0.30	0.26	0.20	0.18							
	360	0.43	0.42	0.41	0.40	0.39	0.37	0.35	0.33	0.30	0.26	0.20	0.18						
	390	0.44	0.43	0.42	0.41	0.40	0.39	0.37	0.35	0.33	0.30	0.26	0.20	0.18					
	420	0.45	0.44	0.43	0.42	0.41	0.40	0.39	0.37	0.35	0.33	0.30	0.26	0.20	0.18				
	450	0.46	0.45	0.44	0.43	0.42	0.41	0.40	0.39	0.37	0.35	0.33	0.30	0.26	0.20	0.18			
	480	0.47	0.46	0.45	0.44	0.43	0.42	0.41	0.40	0.39	0.37	0.35	0.33	0.30	0.26	0.20	0.18		
	510	0.47	0.47	0.46	0.45	0.44	0.43	0.42	0.41	0.40	0.39	0.37	0.35	0.33	0.30	0.26	0.20	0.18	
	540	0.48	0.47	0.47	0.46	0.45	0.44	0.43	0.42	0.41	0.40	0.39	0.37	0.35	0.33	0.30	0.26	0.20	0.18
	585	0.48	0.48	0.47	0.47	0.46	0.45	0.44	0.43	0.42	0.41	0.40	0.39	0.37	0.35	0.33	0.30	0.26	0.20
	645	0.52	0.51	0.51	0.51	0.50	0.49	0.49	0.48	0.47	0.47	0.46	0.45	0.43	0.42	0.40	0.37	0.35	0.31
σ_o (kPa)		225	217	208	201	193	184	176	168	159	151	143	134	126	118	109	101	93	84
s_{oi} (m)		1.05	1.04	1.04	1.04	1.03	1.03	1.02	1.02	1.01	1.01	1.01	1.00	0.99	0.99	0.98	0.96	0.94	0.93
DoC_s		0.88	0.88	0.87	0.87	0.87	0.86	0.86	0.86	0.85	0.85	0.84	0.83	0.83	0.82	0.80	0.79	0.77	0.75
s_{ti} (m)		0.92	0.91	0.91	0.90	0.89	0.89	0.88	0.87	0.86	0.85	0.84	0.83	0.82	0.81	0.79	0.76	0.73	0.69
h_{ti} (m)		1.08	1.09	1.09	1.10	1.11	1.11	1.12	1.13	1.14	1.15	1.16	1.17	1.18	1.19	1.21	1.24	1.27	1.31
σ_i (kPa)		117	112	106	102	97	91	86	81	75	70	65	60	54	49	43	38	32	26
u_0 (kPa)		165	157	148	141	133	124	116	108	99	91	83	74	66	58	49	41	33	24
OCR		1.0	1.0	1.0	1.0	1.0	1.0	1.0	1.0	1.0	1.0	1.0	1.0	1.0	1.0	1.0	1.0	1.0	1.1
c_u (kPa)		28.0	26.8	25.5	24.4	23.2	21.9	20.6	19.4	18.1	16.9	15.7	14.3	13.1	11.8	10.4	9.1	7.7	6.5
h_t (m)		20.81																	

DoC_u: degree of consolidation based on pore water pressure; DoC_s: degree of consolidation based on settlement; σ_{oi}: Surcharge; σ_i: final effective stress for each layer; s_{oi}: ultimate settlement for each layer; s_{ti}: final settlement for each layer; h_{ti}: final thickness for each layer; u_0: initial pore water pressure; OCR: over-consolidation ratio for each layer; c_u: undrained shear strength for each layer; h_t: final thickness of soft clay fill.

Table 8.8 Degree of Consolidation of soft clay fill and upper marine clay after consolidation

Parameters \ Dimension		Height of seawall (m)		
		14.5	18.5	22.5
Soft marine clay	DoC_u (%)	42.0	44.0	45.5
	$DoCs$ (%)	82.0	83.0	84.0
	h_0 (m)	22	30	38
	S_t (m)	8.87	12.43	16.12
	$c_{u\text{-}avg}$ (kPa)	12.68	15.05	17.40
	e_t	1.388	1.342	1.304
Upper marine clay	DoC_u (%)	4.06	4.20	4.28
	$DoCs$ (%)	31.3	34.1	35.8
	S_t (cm)	11.01	13.56	15.11
	c_{u0} (kPa)	12.05	12.26	12.41
	k (kPa/m)	1.85	1.80	1.77
	e_t	2.0	1.99	1.99

DoC_u: degree of consolidation based on pore water pressure; DoC_s: degree of consolidation based on settlement; h_0: initial thickness of soft clay fill; s_t: final settlement; $c_{u\text{-}avg}$: average undrained shear strength of soft clay fill; e_t: final average void ratio; c_{u0}: undrain shear strength of improved upper marine clay at seabed; k_{cu}: gradient of undrained shear strength of improved upper marine clay.

8.3.4 Hydrological conditions and wave loads

According to the offshore hydrological data in Singapore, the wave parameters including the probable maximum wave height in 25 years are shown in Table 8.9 (Chew and Wei, 1980). The critical condition where the wave force is under trough is considered for the wave force. The vertical circular surface of the caisson cylinders is simplified as the vertical straight surface, which is a more conservative design according to Torum et al. (2012). In this paper, the wave force is calculated based on the British standard BS 6349-1 (2000). For long vertical structure, the reflective conditions can be applied and the wave can be considered as standing wave. The wave force under trough was calculated based on the Sainflou theory (Sainflou, 1928).

Table 8.9 Wave parameters

wave height H_{inc} (m)	wave period T (s)	wavelength L (m)	γ_w (kN/m^3)
1.7	5.0	35.4	10.05

8.3.5 Stability analyses

For preliminary design, it is highly desirable to have an analytical method to check the stability of seawalls with respect to the selection of suction caisson foundations such as sizes and depth of penetration. For this purpose, a Microsoft Excel based analytical

design method was developed. The worst design condition is taken as when all the soft marine clay or sand fill had been placed and the vacuum preloading has stopped. Therefore, the short-term stability of the seawalls and suction caisson foundations at this condition is estimated in the analytical analyses.

The seawall on suction caisson foundation is simplified as retaining wall on strip foundation. The simplified design model was in terms of unit length with 37 m in width of strip foundation and 14 m in width of retaining wall based on same area. The treated clay fill and marine clay are assumed to be under an undrained condition and the sand compaction piles under a drained condition. A parametric study with different widths, *L*, or rows of SCPs is carried out to obtain the optimum width or row for the SCPs. The sand compaction piles are simplified as sand compaction walls with 0.7 m wide based on same area method (Cooper and Rose, 1999; Abusharar and Han, 2011; Zhang 2014). The free body diagram for the stability analyses of simplified seawall and suction caisson foundation is shown in Figure 8.9.

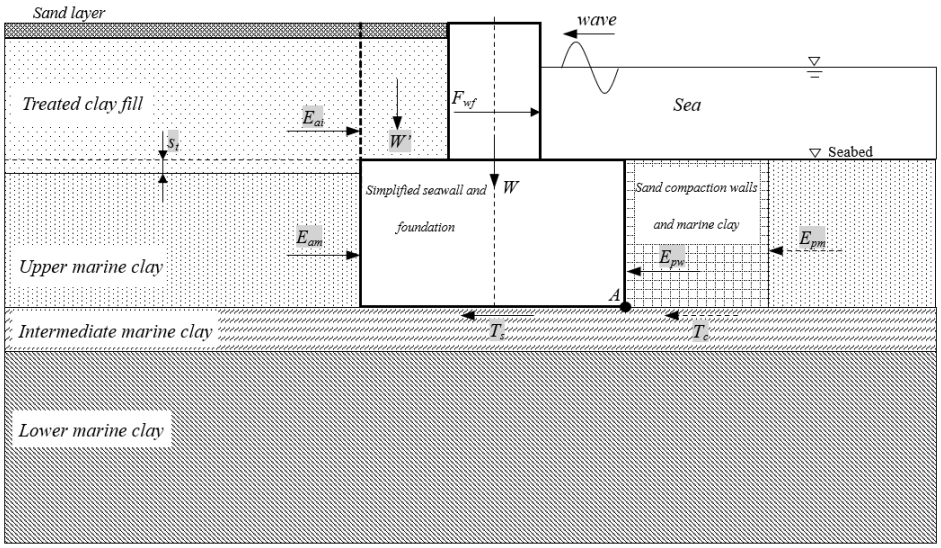

Figure 8.9 Free body diagram for the simplified seawall on suction caisson foundation

8.3.5.1 Wave force

Based on the Sainflou theory, the distribution of wave pressure on the simplified seawall is shown in Figure 8.9. From the mean sea level to the trough of wave, the wave pressure increases from 0 kPa to P_1. From the trough to the seabed, the wave pressure reduces from P_1 to P_2. The formulas of P_1 and P_2 are shown in Eq. (8.1) and Eq. (8.2).

$$P_1=\gamma_w(H_{inc}-H_{0c}) \tag{8.1}$$

$$P_2=\frac{\gamma_w H_{inc}}{cosh\frac{2\pi d_w}{L}} \tag{8.2}$$

where, H_{inc} is the incident wave height; γ_w is the unit weight of seawater; d is the sea water depth; L is the wavelength; H_{0c} is calculated by Eq. (8.3).

$$H_{0c}=\frac{\pi H_{inc}^2}{L}coth\frac{2\pi d_w}{L} \tag{8.3}$$

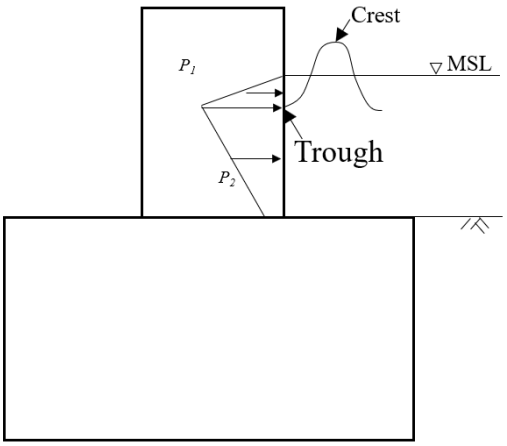

Figure 8.10 Distribution of wave pressure on seawall

8.3.5.2 Lateral stability

For lateral stability, two failure modes should be considered for different widths, L, of SCPs treated marine clay as in Figure 8.11. In the first failure mode, the passive zone in upper marine clay and the horizontal shear strength at the bottom of SCPs treated marine clay are mobilized for the case of relatively few rows of SCPs. In the second failure mode, the passive zone in the SCPs treated marine clay is mobilized for the case of the relatively large numbers of rows of SCPs (Nakamura et al., 2006).

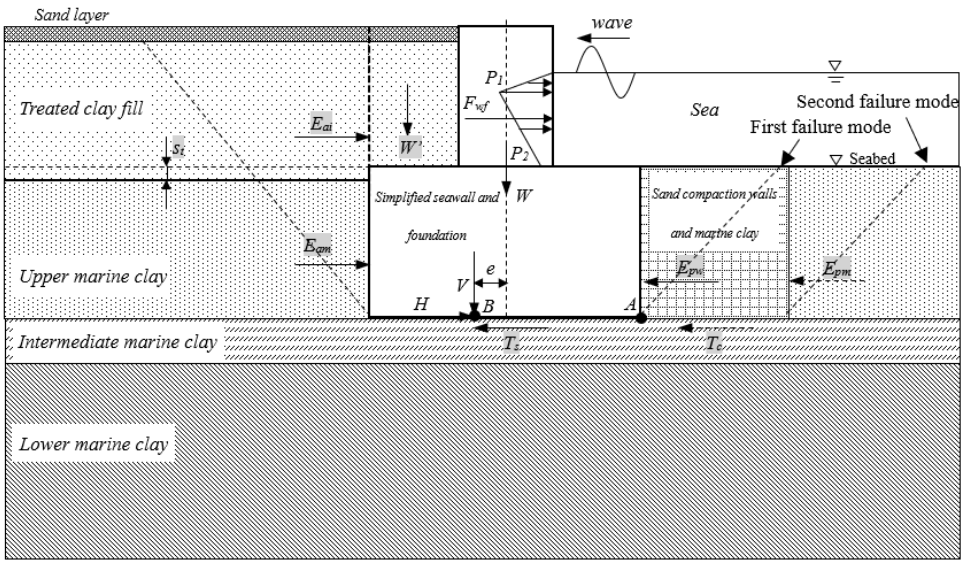

Figure 8.11 Two failure modes for lateral stability

The simplified seawall and foundation are subjected to the wave force under trough, F_{wf}, the active thrust of upper marine clay, E_{am}, and the active thrust of treated clay fill and sand layer, E_{ai}, as shown in Figure 8.9. Additionally, in first failure mode, the simplified structure is subjected to the passive resistance of upper marine clay, E_{pm}, and the sliding resistance, T_s and T_c, at the bottom of simplified foundation and SCPs treated marine clay. In second failure mode, the simplified structure is subjected to the passive resistance of SCPs treated marine clay, E_{pw}, which is calculated using Eq. (8.4) and the sliding resistance at the bottom of simplified foundation, T_s. The factor of safety, FoS_l, for lateral stability is calculated by Eq. (8.5) for the first failure mode and Eq. (8.6) for the second failure mode.

$$E_{pw}=(1-\alpha_s)E_{pm}+\alpha_s E_{ps} \tag{8.4}$$

$$FoS_l = (E_{pm}+T_s+T_c)/(E_{ai}+ E_{am} +F_{wf}) \tag{8.5}$$

$$FoS_l = (E_{pw}+T_s)/(E_{ai}+ E_{am} +F_{wf}) \tag{8.6}$$

The active thrust, E_{am}, of the upper marine clay and the passive resistance of the upper marine clay, E_{pm}, under undrained condition and the passive resistance of the sand compaction piles, E_{ps}, under drained condition were calculated using Rankine's theory (Kitazume, 2005). The active thrust, E_{ai}, imposed by the treated clay fill under undrained condition and sand layer under drained condition was also calculated using Rankine's

theory. The sliding resistances, T_s and T_c, are calculated using the undrained shear strength of the upper marine clay at the bottom of the simplified foundation or SCPs treated upper marine clay.

8.3.5.3 Combined overturning and bearing capacity

In terms of the combined overturning and bearing capacity, the rotation centre is set at the outside bottom corner of the simplified foundation, point A, as shown in Figure 8.9.

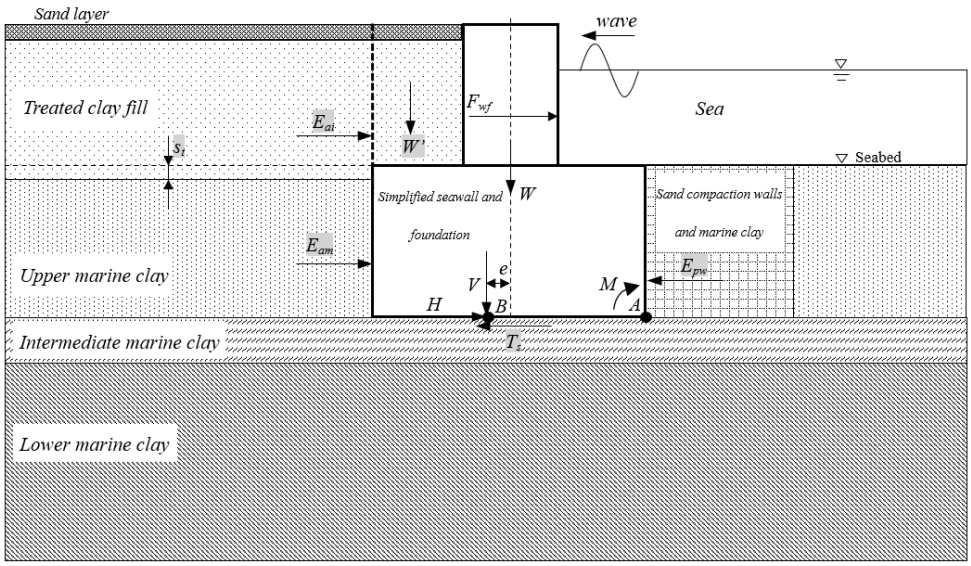

Figure 8.12 Free body diagram for combined overturning and bearing capacity

The factor of safety, FoS_v, is calculated using Eq. (8.7).

$$FoS_v = q_u/q_v \tag{8.7}$$

where, q_u is the bearing capacity of the simplified foundation; q_v is the foundation pressure.

The simplified seawall and foundation are subjected to the active thrusts of upper marine clay, sand layer and treated clay fill, the passive resistance of the SCPs treated upper marine clay, the self-weight of the seawall and the suction caisson foundation, the wave force under trough on seawall and the eccentrically additional vertical load. The additional vertical load is the weight of treated clay fill on the slab, W', as shown in Figure 8.9. With the eccentrical vertical load, the foundation pressure can be calculated using Eq. (8.8).

$$q_v = V/(B-2e) \tag{8.8}$$

where, V is the total vertical load acting at point B, which consists of the self-weight of seawall, suction caisson foundation and additional vertical load as shown in Eq. (8.9); B is the simplified width of simplified foundation; e is the eccentric of total vertical load and can be calculated by Eq. (8.10) and Eq. (8.11).

$$V = W' + W \tag{8.9}$$

$$e = M/V \tag{8.10}$$

$$M = M_{ai} + M_{am} + M_{wf} - M_{pw} - M_{w'} - M_w \tag{8.11}$$

where, W' is the weight of treated marine clay on slab; W is the self-weight of seawall and suction caisson foundation; M is the net moment on the structure; M_{ai} is the moment from active thrust of treated clay fill and sand layer; M_{am} is the moment from active thrust of upper marine clay. M_{wf} is the moment from wave force; M_{pw} is the moment from passive resistance of SCPs treated upper marine clay; $M_{w'}$ is the moment from the weight of treated clay fill and sand layer on slab; M_w is the moment from self-weight of seawall and suction caisson foundation.

As the suction caisson foundation belongs to shallow foundation in this case, the bearing capacity can be calculated based on the Hansen's ultimate bearing capacity theory under undrained condition as shown in Eq. (8.12).

$$q_u = s_u N_c (1 + d'_c - i'_c) + \gamma' d \tag{8.12}$$

where, N_c is bearing capacity factor and equal to 5.14; d'_c is depth factor; i'_c is inclination factor; γ' is buoyant unit weight of upper marine clay; d is penetration depth of suction caisson foundation. The undrained shear strength, s_u, is the weighted average value referred to the maximum calculation depth below the foundation, z_{max}, which is equal to 0.6B under undrained condition.

8.3.5.4 Overall stability

The circular failure mode is assumed to analyse the overall stability. It is assumed that the failure surface cuts through the inside bottom corner of simplified foundation, point C, and SCPs treated upper marine clay or the outside bottom corner of SCPs treated upper marine clay as shown in Figure 8.13.

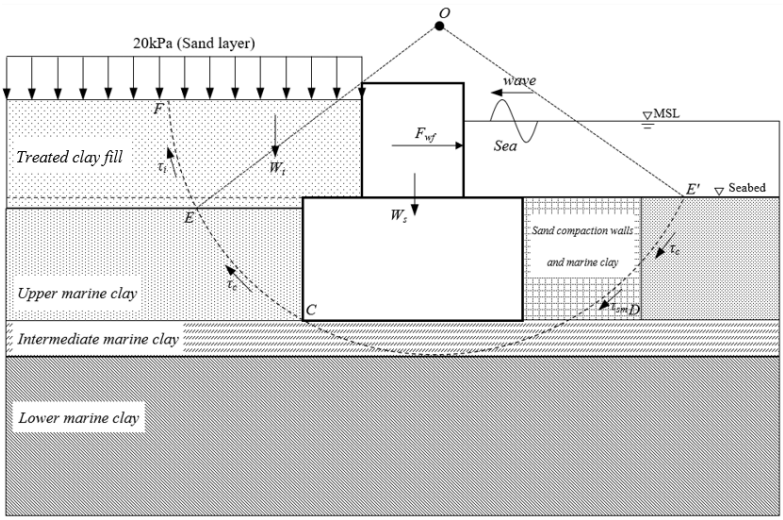

Figure 8.13 Failure mode for overall stability

The undrained shear strength of marine clay, τ_c, and treated clay fill, τ_i, are used as the shear strength on the circular failure surface. The shear strength of sand compaction walls and adjacent upper marine clay, τ_{sm}, are calculated individually with the consideration of replacement ratio (Kitazume, 2005). Because of the strength recovery, the undrained shear strength of upper marine clay in SCP treated soil zone is 1.2 times of the original undrained shear strength. The factor of safety, FoS_o, for overall stability is calculated using Eq. (8.13) referred to rotation centre O.

$$FoS_o = (M_{\tau c}+M_{\tau i}+M_{scp})/(M_w+M_{ws}+M_{wf}) \quad (8.13)$$

where $M_{\tau c}$ is the moment of the undrained shear strength of marine clay on the circular failure surface. $M_{\tau i}$ is the moment of the undrained shear strength of treated clay fill; M_{scp} is the moment of the shear strength of SCPs treated upper marine clay. M_{ws} is the moment of the weight of treated clay fill inside failure surface and the simplified uniform pressure referred to sand layer; M_w is the moment of the self-weight of seawall and suction caisson foundation; M_{wf} is the moment of the wave force under trough on the simplified seawall. In this problem, the linear programming method is used to get the centre O of the circular failure surface related to the minimum factor of safety of overall stability.

8.3.6 Verification using finite element analyses

The FEA simulation was conducted using Plaxis 2D to investigate the effects of sand compaction piles on the stability of the seawall and verify the reliability of the overall

stability in the analytical method. For illustration, the finite element model for 14.5 m seawall height is shown in Figure 8.14. The dimensions of the seawall and suction caisson foundation were listed in Table 8.3. The width of seawall and suction caisson foundation were simplified to be 14 m and 37 m. The simplified suction caisson foundation and seawall were modelled as rigid body. The equivalent unit weight of the simplified seawall and foundation with the consideration of the soil plugs and infilling sea water was used. The Mohr-Coulomb model under an undrained condition was used for the marine clay and treated clay fill, and that under a drained condition was used for sand compaction piles. Four different rows of sand compaction piles, 22, 26, 30, and 34, were assumed in the study. The sand compaction piles were modelled as sand compaction walls (SCWs) with 0.7 m in width based on same area. The soil parameters of sand were shown in Table 8.4. The improved undrained shear strength and the thickness of treated clay fill and upper marine clay were inputted. The seabed soil parameters were shown in Table 8.1. The soil parameters of improved treated clay fill and upper marine clay were shown in Table 8.4 and Table 8.8. The default strength reduction coefficient, 0.7, for the interface of soil and the seawall or suction caisson foundation was used. The fixed normal displacement was applied in the boundary. The factors of safety were obtained using the strength reduction method under undrained conditions.

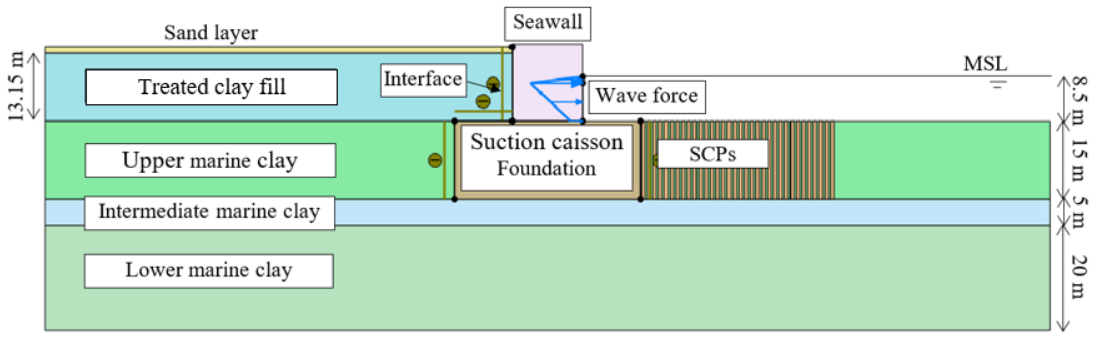

Figure 8.14 Finite element model of stability analyses for 14.5 m of seawall height

8.3.7 Comparison between analytical and numerical methods

The factors of safety obtained from the analytical method are shown in Figure 8.15 and Table 8.10. Those using finite element analyses are shown in Figure 8.16. In terms of lateral stability, with the increase in the rows of SCPs, the lateral stability is transferred from the first failure mode to the second failure mode. Therefore, the critical number of the rows of SCPs is 26 or 30 m in width of SCPs improved marine clay.

Compared with the analytical method, the factors of safety of overall stability using FEA are slightly smaller. As the rows of SCPs increases, the factors of safety increase too. In terms of overall stability, the critical row of SCPs is 18 rows of SCPs for analytical method and 26 rows of SCPs for FEA, which are consistent with those obtained from lateral stability using analytical method.

The failure surfaces obtained from the overall stability for 14.5 m of seawall height using analytical and numerical methods are shown in Figure 8.17 and Figure 8.18, respectively. The locations of failure surfaces using analytical method are similar to those using numerical method. When the number of rows of SCPs is more than 18, the factor of safety for overall stability using analytical method becomes constant. This is because that all the failure surfaces with minimum factor of stability cut through the SCPs treated marine clay as shown in Figure 8.17(c). When the number of rows is below 18, the failure surfaces using analytical method cut through the outside corner of SCPs treated upper marine clay. When the rows of SCPs are 18, the factors of safety for the failure surface cutting through the SCPs treated soil and that cutting through the outside corner of SCPs treated soil are the same about 1.69. When the rows of SCPs are 26, two failure surfaces are observed in the overall stability using numerical method. One cut through the SCPs treated soil and the other one passed the outside corner of SCPs treated soil. When the rows of SCPs were above 26, the failure surface was close to that of lateral stability. Therefore, 26 rows of SCPs which is about 30 m in width of SCPs treated marine clay is effective for the improvement of stability of seawall.

The above results have demonstrated the effectiveness of the stability analysis methods for seawall using. However, in terms of 22.5 m of seawall height, the stability analyses using analytical and numerical methods are not enough, more soil improvement works need to be studied to stabilize the seawall and suction caisson foundation. Based on the stability analyses, the seawall and suction caisson foundation with 20 m diameter of caissons or cylinders and 30 m wide of SCPs treated marine clay is more stable and proposed to be used for the design of containment bund for land reclamation.

Table 8.10 Factor of Stability using analytical emthod for overturning stability and bearing capacity

H (m) / Factor of safety	14.5	18.5	22.5
Overturning stability	4.11	2.79	2.38
Bearing capacity	3.57	2.61	2.12

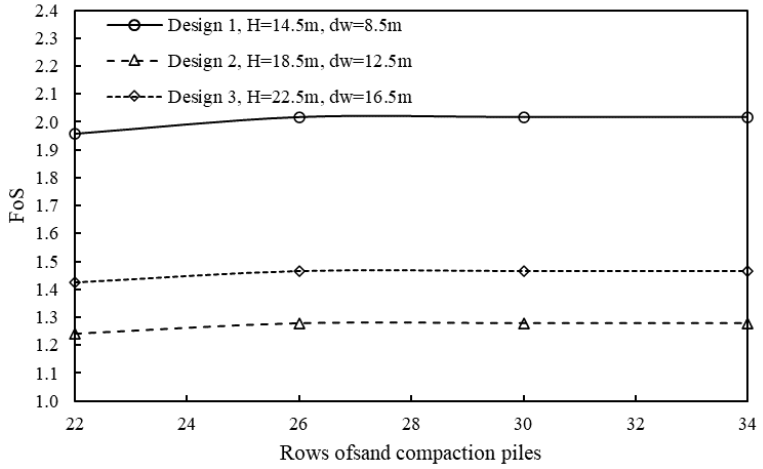

Figure 8.15 Factor of safety (FoS) for lateral stability analyses using analytical method considering different rows of SCPs

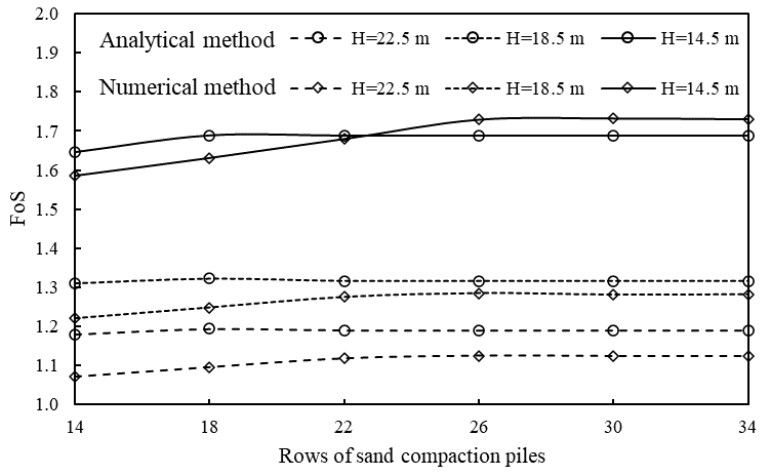

Figure 8.16 Factor of safety (FoS) for overall stability analyses for three designs using analytical and numerical methods considering different rows of SCPs

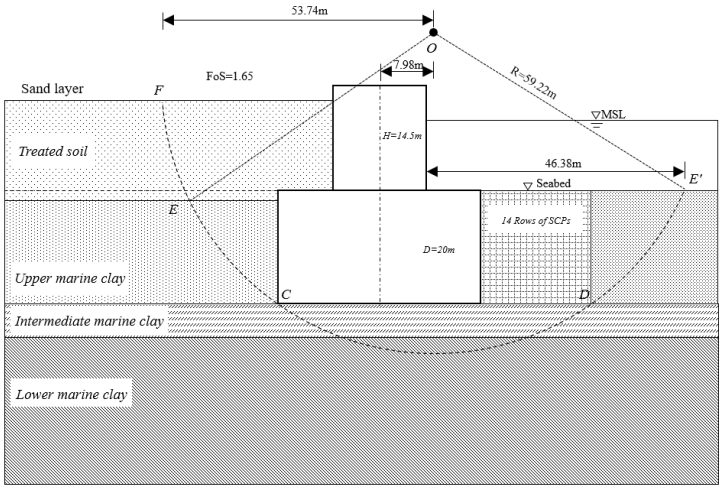

(a) 14 Rows of SCPs

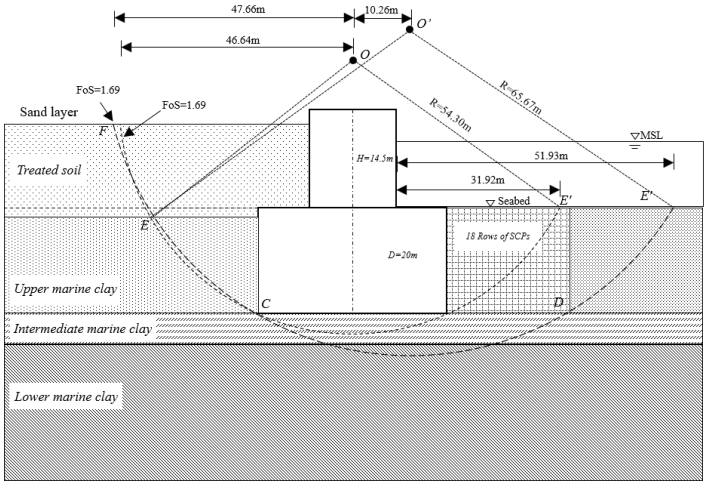

(b) 18 Rows of SCPs

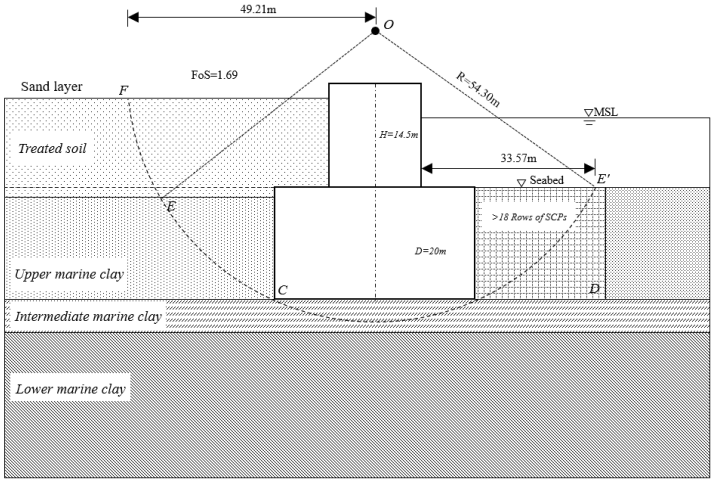

(b) more than 18 Rows of SCPs

Figure 8.17 Failure surfaces of overall stability using analytical method

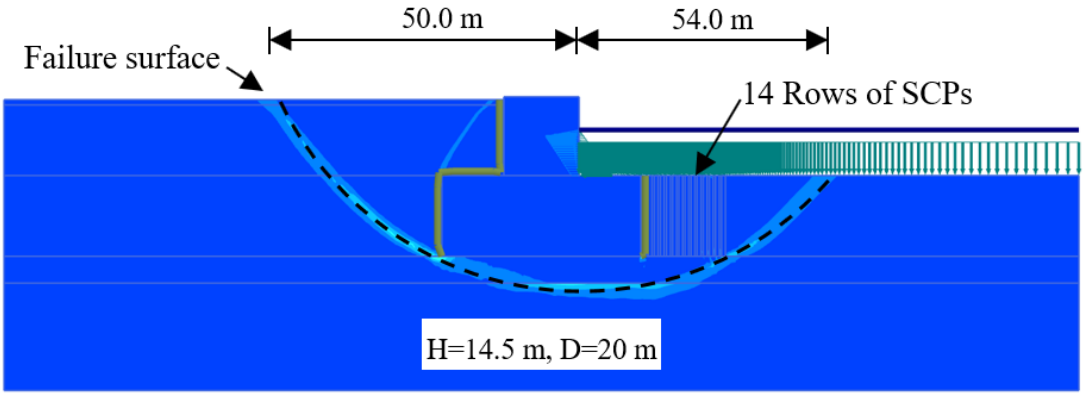

(a) 14 rows of SCPs

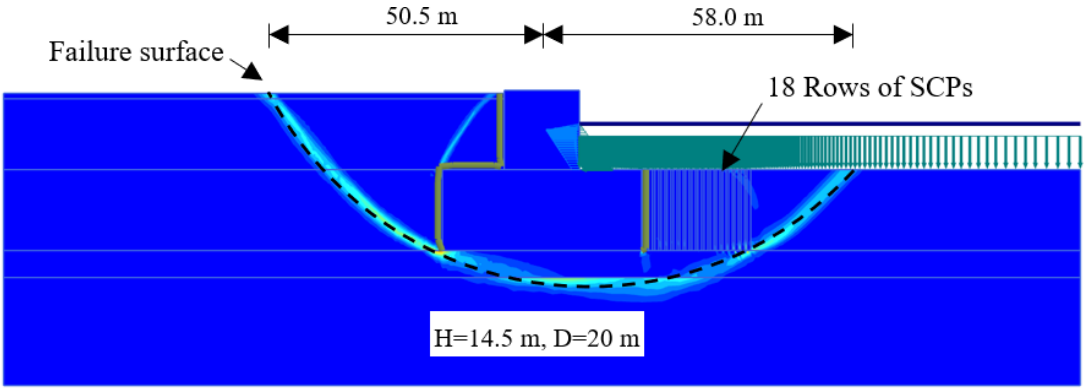

(b) 18 rows of SCPs

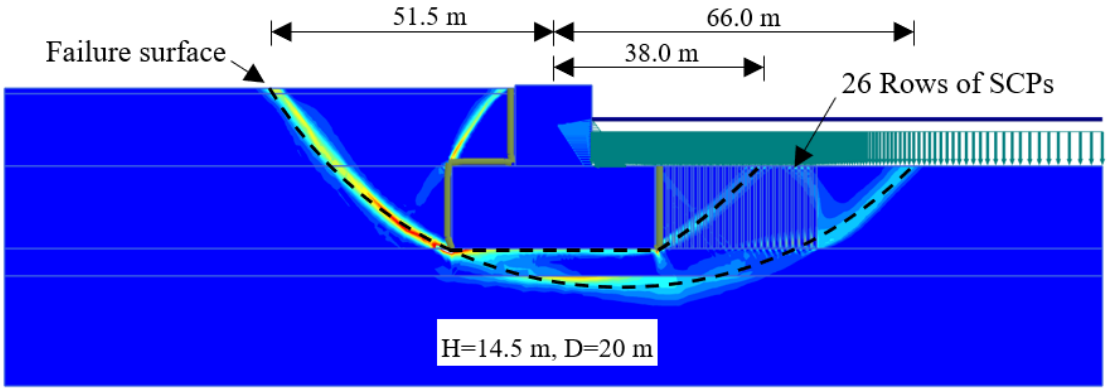

(c) 26 rows of SCPs

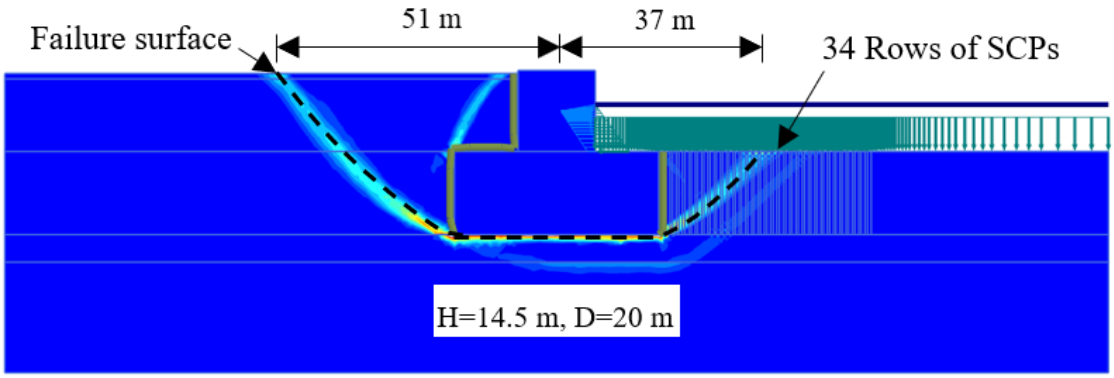

(d) 34 rows of SCPs

Figure 8.18 Overall stability of seawall using finite element method

8.3.8 Effects of diameter of caissons on the stability

Since the design with H = 14.5 m was much stable, the different geometries were investigated. Three diameters of caissons, D, and the corresponding width, W, of suction caisson foundation were proposed as in Table 8.11.

Table 8.11 Geometry of seawall

D (m)	15.0	17.5	20.0
W (m)	33.0	38.0	43.0

By using the proposed three geometries, the analytical method and the finite element method were also conducted. the factors of safety for the proposed geometries are shown in Table 8.12, Figure 8.19 and Figure 8.20. with the decrease of diameter of caissons, the factors of safety decreased. However, in terms of the three proposed geometries, the factors of safety were enough. Thus, all the three structures with different diameters of caissons were stable enough to be used as containment bund for land reclamation.

Table 8.12 Factor of Stability using analytical method for overturning stability and bearing capacity for 14.5 m of seawall height

D (m) / Factor of safety	15.0	17.5	20.0
Overturning stability	2.65	3.33	4.11
Bearing capacity	2.94	3.27	3.57

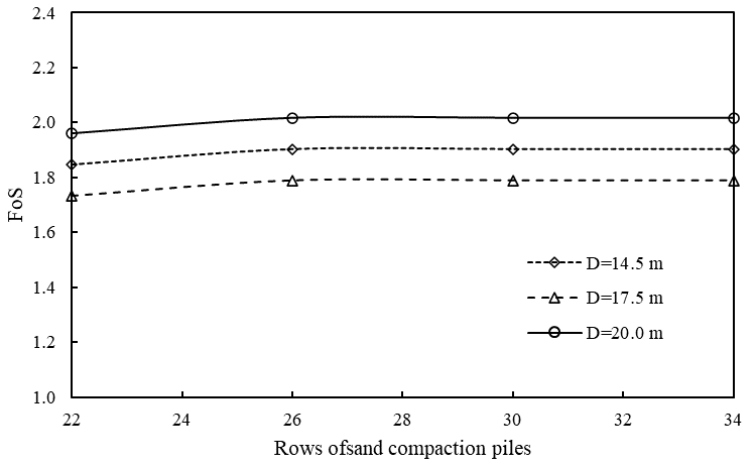

Figure 8.19 Factor of safety (FoS) for lateral stability analyses for 14.5 m of seawall height using analytical method considering different rows of SCPs

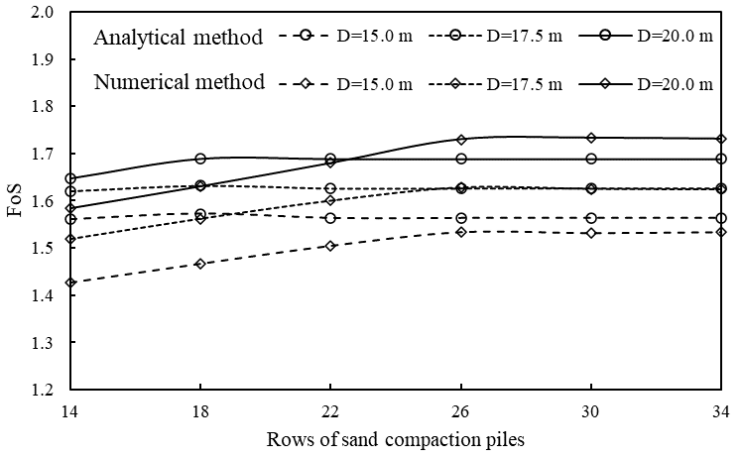

Figure 8.20 Factor of safety (FoS) for overall stability analyses for 14.5 m of seawall height using analytical and numerical methods considering different rows of SCPs

8.4 Deformation of seawall during land reclamation

8.4.1 Numerical model

The numerical model for land reclamation of soft clay fill with seawall as containment bund is shown in Figure 8.21. The numerical model was based on the preliminary design of seawall. As the cemented sand is below the lower marine clay, only the Singapore marine clay was modelled. The soil properties of Singapore marine clay were same with those in section 8.3.1. The soil properties of soft clay fill were same as the previous study. Every layer of soft clay fill was 2 m in thickness, 3.0 of initial void ratio and 14.2

kN/m^3 of unit weight. Therefore, the initial effective stress was set as 1 kPa. The modified Cam-clay model was applied for Singapore marine clay and soft clay fill. For soft clay fill, the piece-wise hardening method was also used as discussed in Chapter 6. The soil parameters of soft clay fill and marine clay input into numerical models are shown in Table 8.13. The proposed seawall and suction caisson foundation with 20 m in diameter of caissons or cylinders were modelled as simplified seawall with 14 m in width and strip foundation with 37 m in width using rigid body. Their parameters were shown in Table 8.3. The Mohr-Coulomb model was applied for sand compaction piles. The soil properties of sand were listed in Table 8.4.

Table 8.13 Soil parameters for finite element analyses

Soil layer	Unit weight γ (kN/m^3)	λ	κ	M	P_{c0} (kPa)	k_0 (m/s)	c_k	e_0
Soft clay fill	14.2	---	0.030	0.882	1.0	2.2E-8	0.93	3.0
Upper marine clay	15.7	0.391	0.043	0.898	72.4	2.0E-9	0.60	2.0
Intermediate marine clay	19.0	0.109	0.022	1.135	408.0	8.0E-10	---	0.8
Lower marine clay	17.0	0.348	0.070	0.898	404.1	1.0E-9	0.39	1.3

The interaction between the soft clay fill and the upper marine clay was modelled using the tie method with same deformation and pore water pressure at connected nodes. The tie method was also used to model the interaction between the suction caisson foundation and the Singapore marine clay. As the deformation of soft marine clay during vacuum consolidation using HDeG sheet was large, the interaction between the soft clay fill and the seawall was modelled using contact property with frictionless interface. The two contact pairs were kept contact under vacuum pressure. Based on preliminary study, 26 rows of SCPs were feasible to stabilize the seawall and suction caisson foundation. Therefore, 26 rows of sand compaction walls were modelled and the tie method was used to model the interaction between SCPs and upper marine clay. The normal deformation at the lateral boundary is fixed and the deformation at the bottom is also fixed. The CPE4P elements with a degree of pore pressure were used for soil. The CPE4 elements were used for seawall and suction caisson foundation as shown in Figure 8.22.

The HDeG sheet consisted of drains with 0.6 m horizontal spacing and a Tencate TS10 non-woven geotextile sheet as shown in Figure 8.4. The equivalent pore water pressure on HDeG sheet as shown in Figure 8.23 was set at vacuum drainage boundary at the beginning of every layer and the source vacuum pressure was set as -60 kPa. During the infilling of soft marine clay, the top surface was set as zero-pore pressure boundary.

The linear infilling stage for every layer was set about 15 days, which was modelled by the linear increasing of body force. The construction period for every layer of soft marine clay and HDeG sheet was 30 days. After the full infilling of soft clay fill, a layer of geomembrane was covered on the ground surface for 30 days and 20 kPa of uniform pressure as 1 m sand surcharge was placed on geomembrane for 60 days. After the land reclamation, the vacuum pressure was turned off and three more months of consolidation of soil was calculated. The summary of stage construction is shown in Table 8.14.

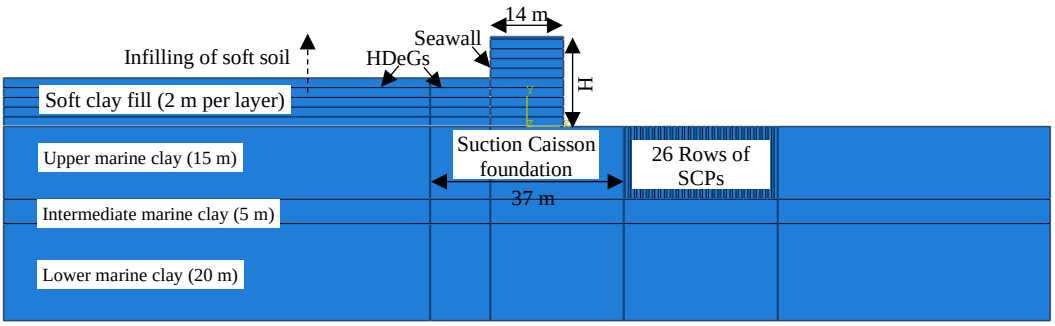

Figure 8.21 Numerical model

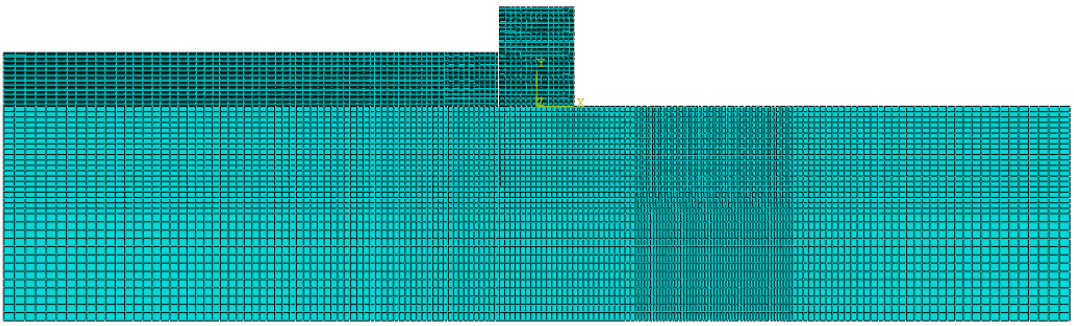

Figure 8.22 Mesh

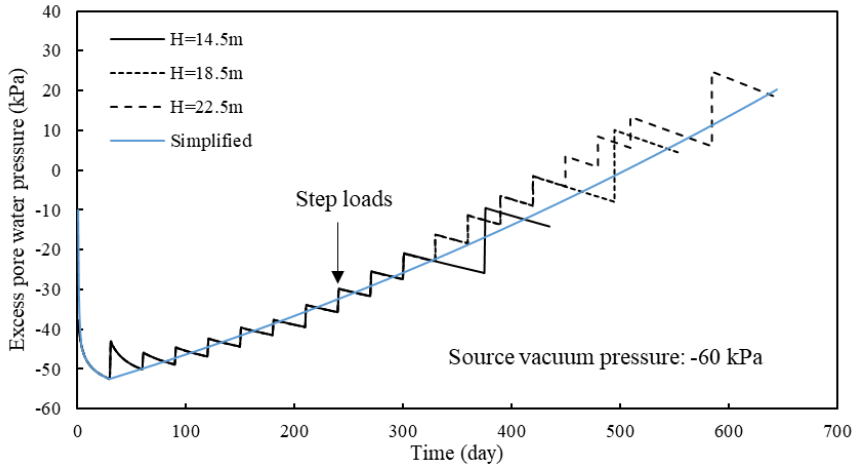

Figure 8.23 Average excess pore water pressure on HDeG sheet under stage loading

Table 8.14 Construction stage of land reclamation of soft soil using seawall and HDeG sheet

Stage	Duration (day)	Source vacuum pressure (kPa)
Soft marine clay layers and HDeG sheet	30	-60
Geomembrane	30	-60
Sand surcharge (20 kPa)	60	-60
After vacuum consolidation	90	0

8.4.2 Deformation of seawall and soft marine clay

The vectors of deformation of simplified seawall and suction caisson foundation are shown in Figure 8.24 to Figure 8.26. The seawall and suction caisson foundation moved outward to seaside during the land reclamation. The horizontal displacement of the whole model is shown in Figure 8.27 to Figure 8.29. The sand compaction piles are effective to reduce the horizontal deformation of upper marine clay induced by seawall and suction caisson foundation.

The sliding and settlement at the top outside corner of seawall are shown in Figure 8.30. The maximum deflections which is the ratio of the outward sliding to the height of seawall, are about 1.13%, 1.19% and 1.98% respectively for different heights of seawall.

The settlement of soft marine clay is shown in Figure 8.31. The total settlement of soft clay fill for different heights of seawall were about 8.44 m, 11.89 m and 14.49m, respectively. Then the corresponding ground surfaces of soft marine clay and sand layer were 14.6 m, 19.1 m and 22.5 m above the seabed respectively, which are close to the results of the proposed theoretical analyses, 14.06 m for H = 14.5 m, 18.46 m for H = 18.5 m, and 21.69 m for H = 22.5 m. The settlements of upper marine clay were about 19.3 cm, 22.3 cm and 24.2 cm for different heights, which are much larger than those using the theoretical analyses. This is due to the high permeability or high coefficient of consolidation of upper marine clay at reloading stage with an OCR of 1.7.

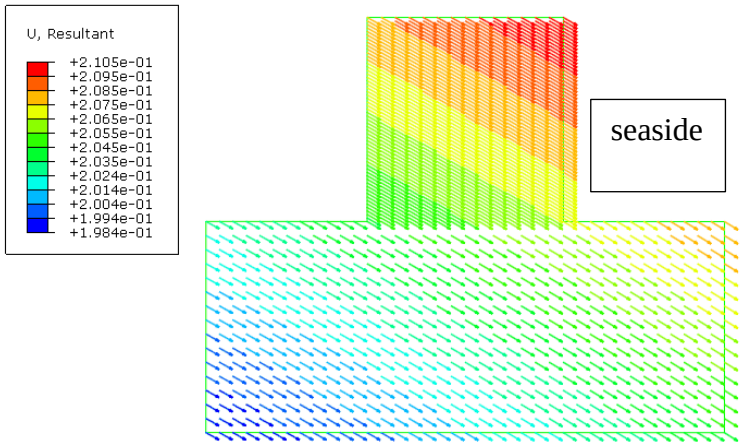

(a) Deformation at the end of vacuum consolidation

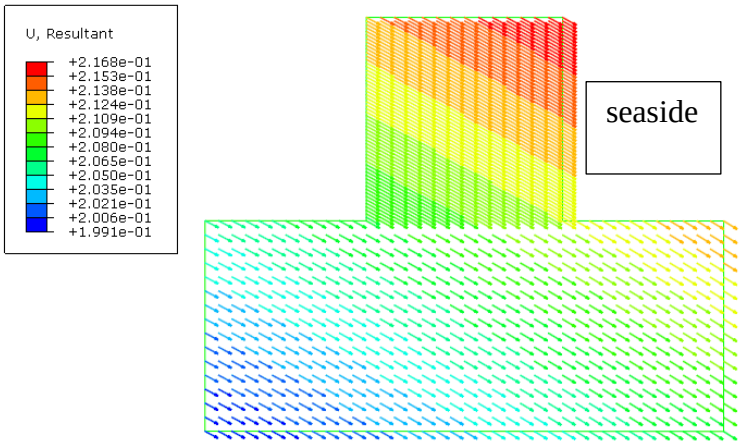

(b) Deformation after vacuum pressure turnoff

Figure 8.24 Deformation of seawall with 14.5 in height

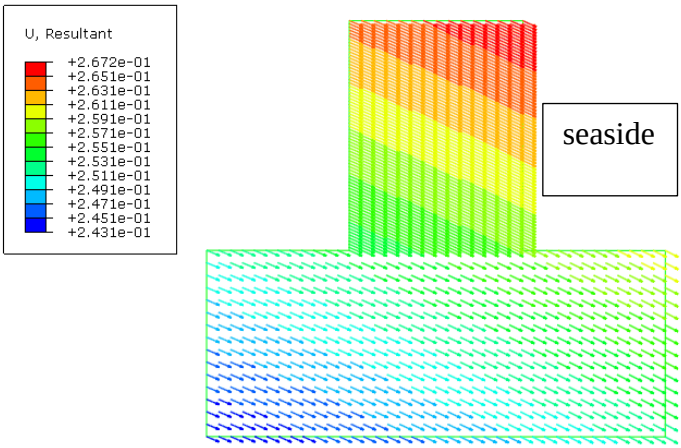

(a) Deformation at the end of vacuum consolidation

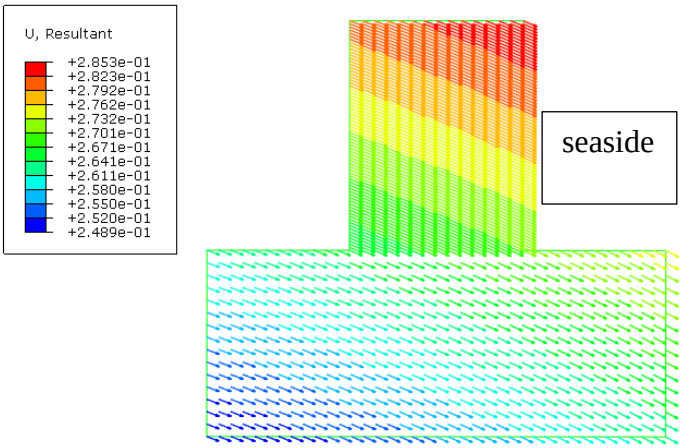

(b) Deformation after vacuum pressure turnoff

Figure 8.25 Deformation of seawall with 18.5 in height

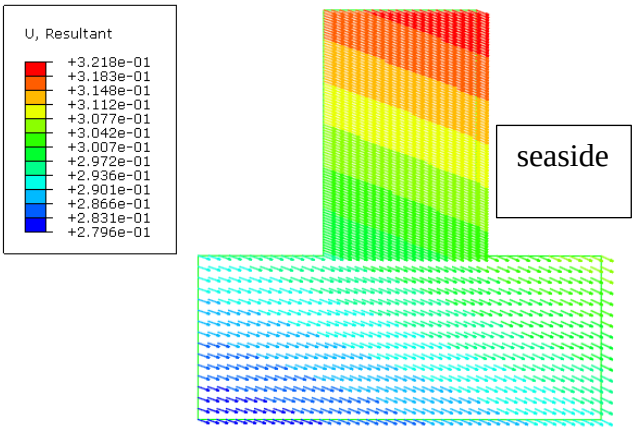

(a) Deformation at the end of vacuum consolidation

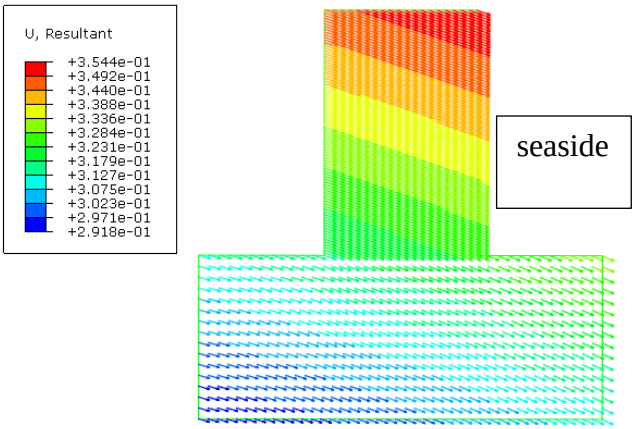

(b) Deformation after vacuum pressure turnoff

Figure 8.26 Deformation of seawall with 22.5 in height

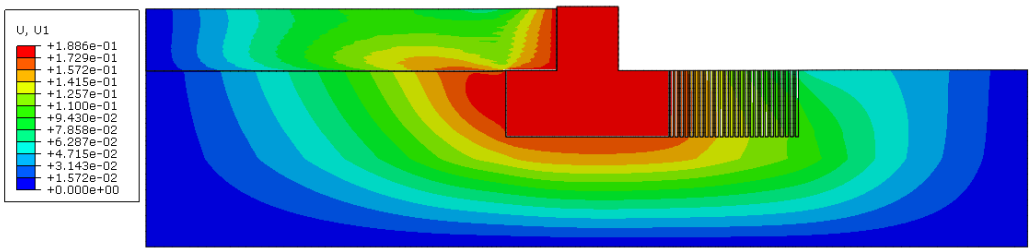

(a) horizontal displacement at the end of vacuum consolidation

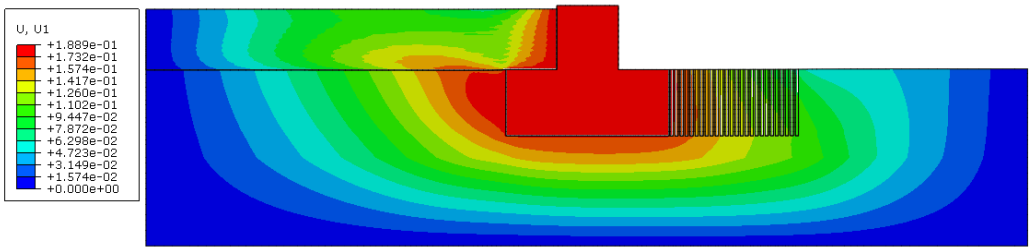

(b) horizontal displacement after vacuum pressure turnoff

Figure 8.27 Deformation in numerical model with 14.5 m in seawall height

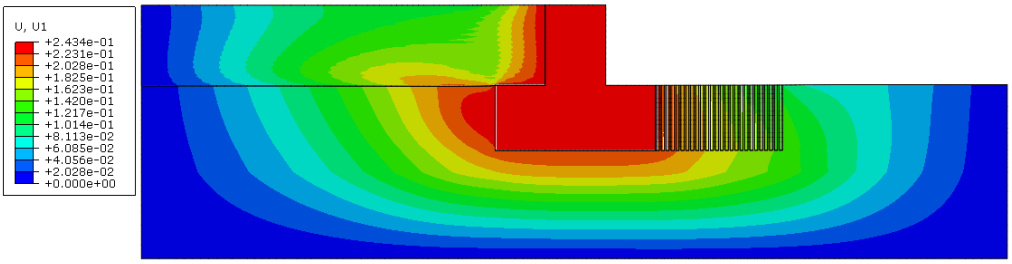

(a) horizontal displacement at the end of vacuum consolidation

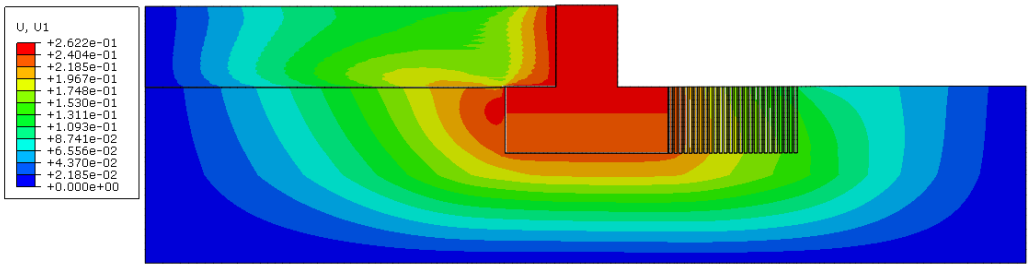

(b) horizontal displacement after vacuum pressure turnoff

Figure 8.28 Deformation in numerical model with 18.5 m in seawall height

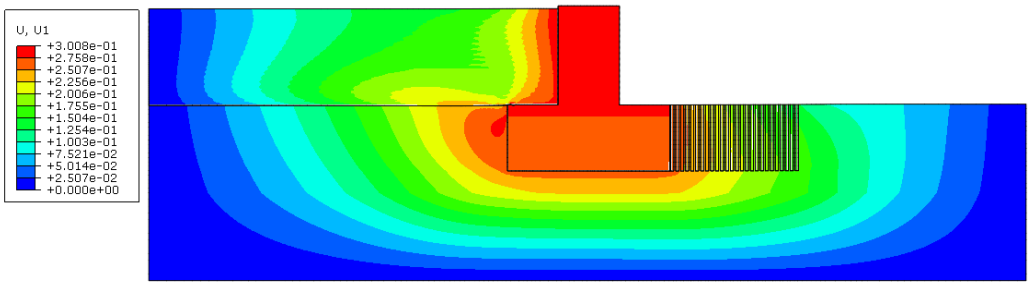

(a) horizontal displacement at the end of vacuum consolidation

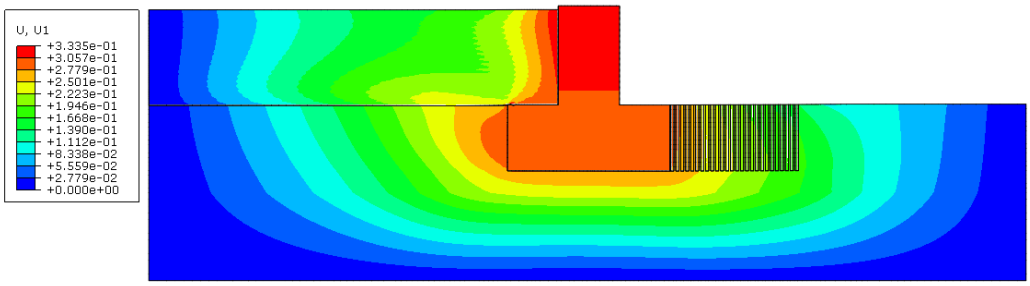

(b) horizontal displacement after vacuum pressure turnoff

Figure 8.29 Deformation in numerical model with 22.5 m in seawall height

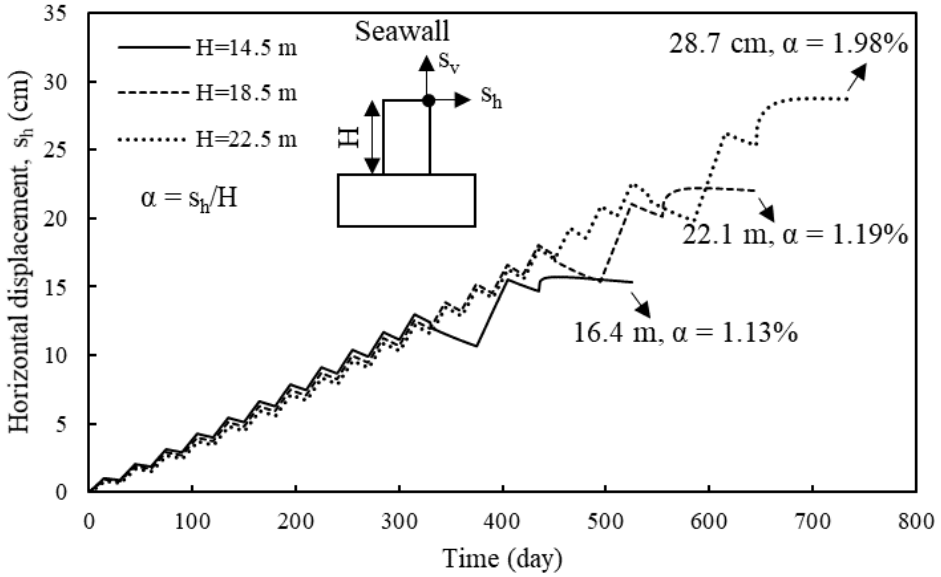

(a) Horizontal displacement

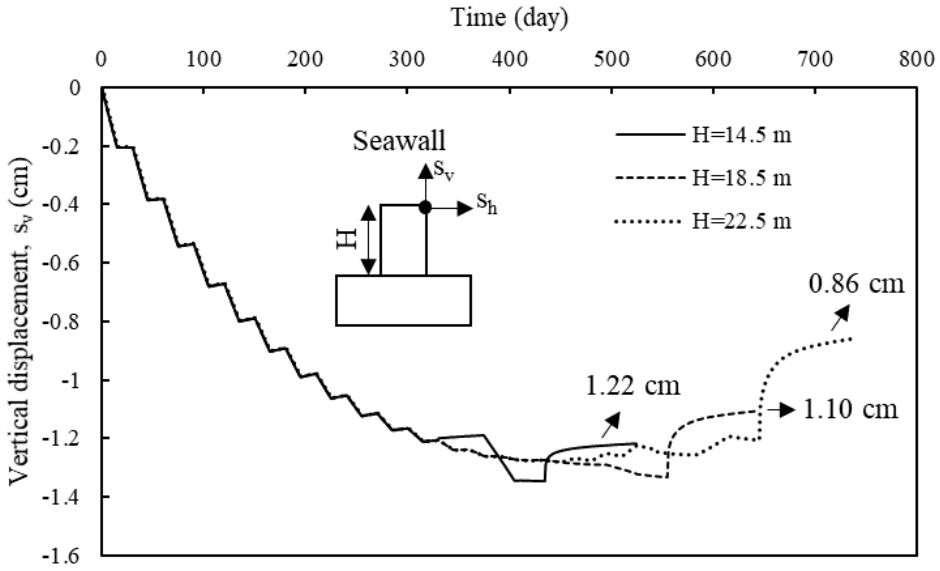

(b) Vertical displacement

Figure 8.30 Displacement at top corner of seawall

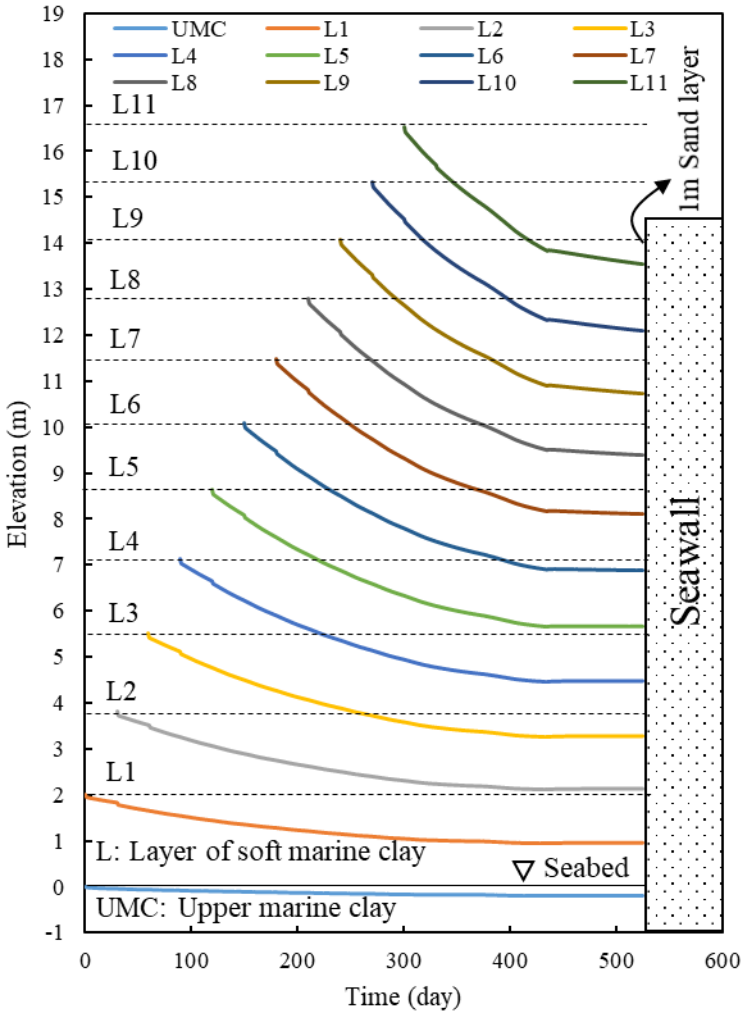

(a) Seawall with 14.5 m in height

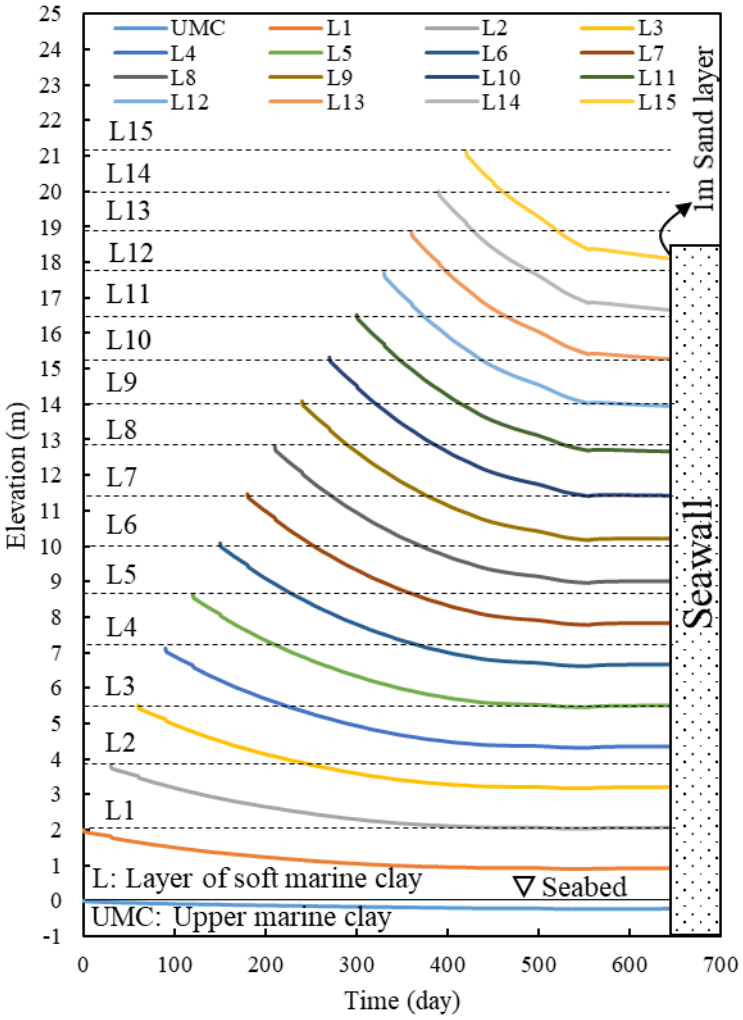

(b) Seawall with 18.5 m in height

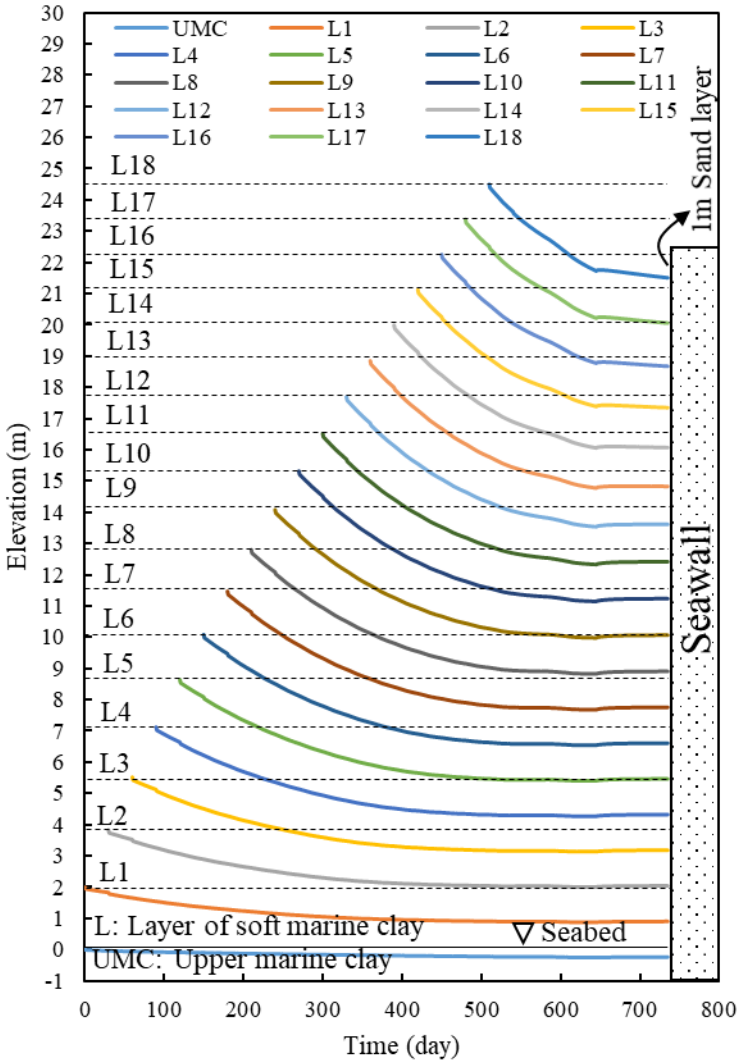

(c) Seawall with 22.5 m in height

Figure 8.31 Deformation of upper marine clay and soft marine clay

8.4.3 Pore water pressure distributions

The contours of excess pore water pressure in soft clay fill and Singapore marine clay are shown in Figure 8.32. The pore water pressure distributions in the upper marine clay and the soft clay fill are shown in Figure 8.33. Due to the relatively high permeability or coefficient of consolidation at the reloading stage, the excess pore pressures in upper marine clay were larger than those obtained from the theoretical analyses as in Figure 8.8.

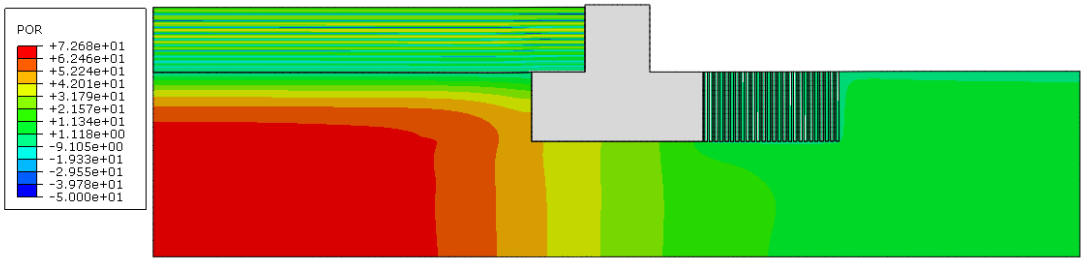

(a) Excess pore pressure for 14.5 in height of seawall

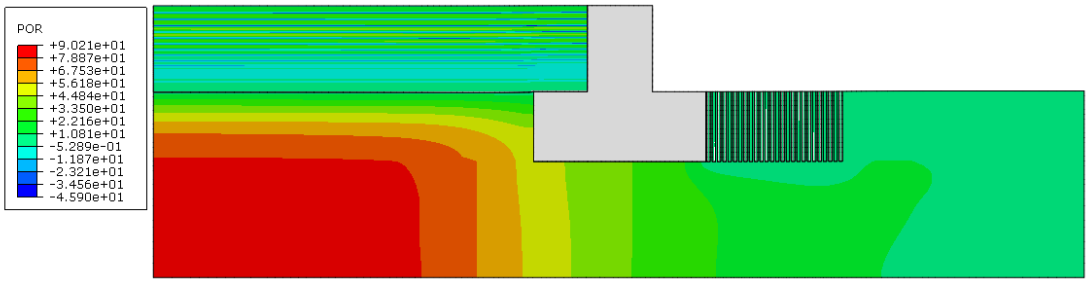

(b) Excess pore pressure for 18.5 in height of seawall

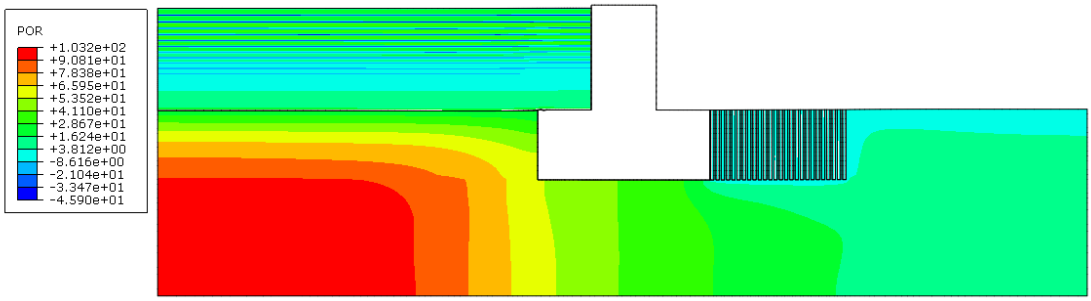

(c) Excess pore pressure for 22.5 in height of seawall

Figure 8.32 Excess pore pressure in numerical model

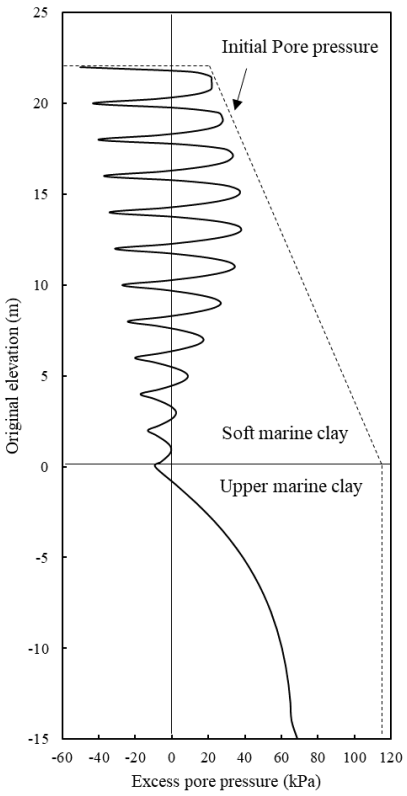

(a) Seawall with 14.5 m in height

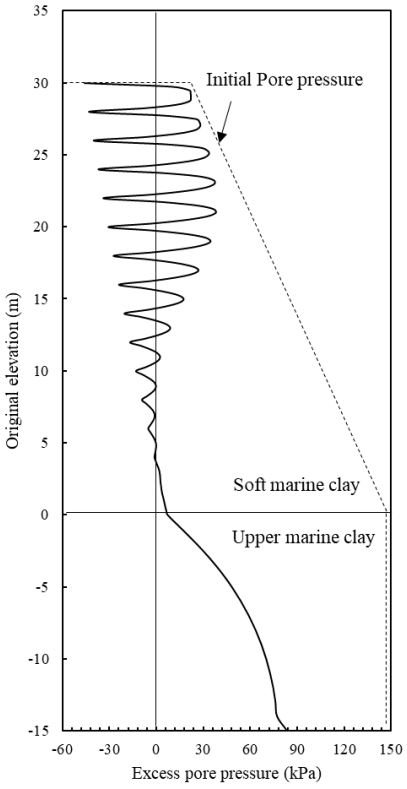

(b) Seawall with 18.5 m in height

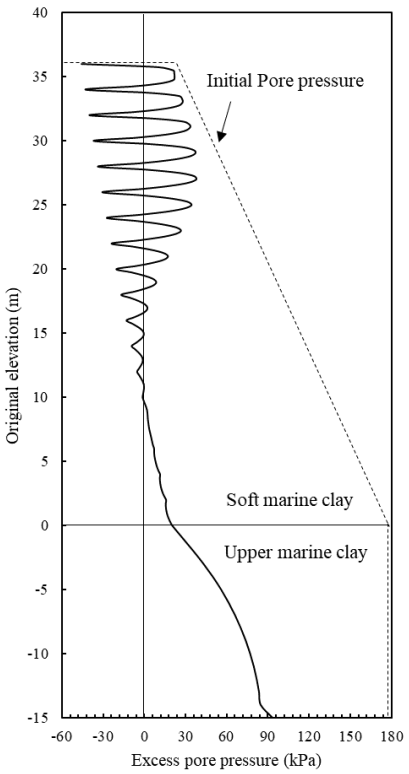

(c) Seawall with 22.5 m in height

Figure 8.33 Excess pore pressure distributions in soft marine clay and upper marine clay after construction

8.4.4 Lateral earth pressure distribution on seawall

After land reclamation, the lateral earth pressure distribution of soft clay fill on seawall is shown in Figure 8.34. The ratio of lateral earth pressure to the vertical effective stress was close to the coefficient of active earth pressure. The lateral earth pressure at the top surface of soft marine clay was larger than that of the theoretical calculation and close to 20 kPa which is because the uniform pressure, 20 kPa, was imposed directly on soil surface as sand surcharge.

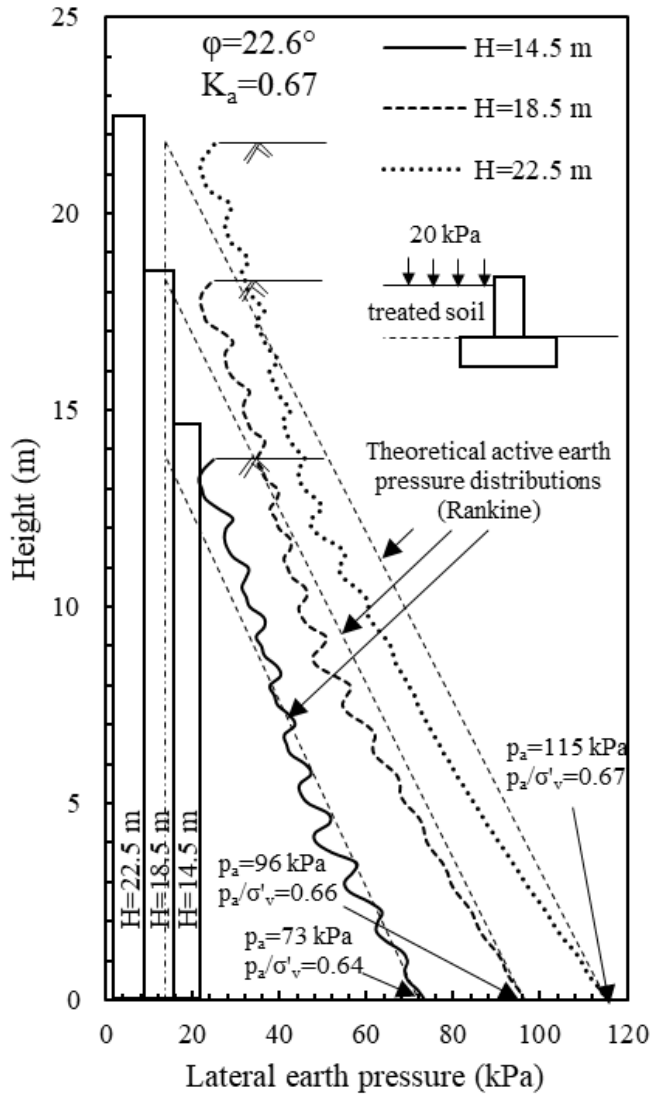

Figure 8.34 Lateral earth pressure on seawall after land reclamation

8.5 Stability of containment structure for land reclamation with improvement of seabed clay

In the analyses presented earlier, the need to treat the seabed clay was not taken into consideration. However, when the seabed soil is very soft, the seabed soil also needs to be treated to reduce the settlement of the reclaimed land. In this case, the seawall stability analysis procedure adopted could be different. An alternative method for land reclamation with treatment of the upper marine clay was proposed in this section.

One of the cost-effective methods to treat the seabed marine clay was to use PVDs as the land reclamation fill could be considered as surcharge. the schematical arrangement for soil improvement and seawall design is shown in Figure 8.35.

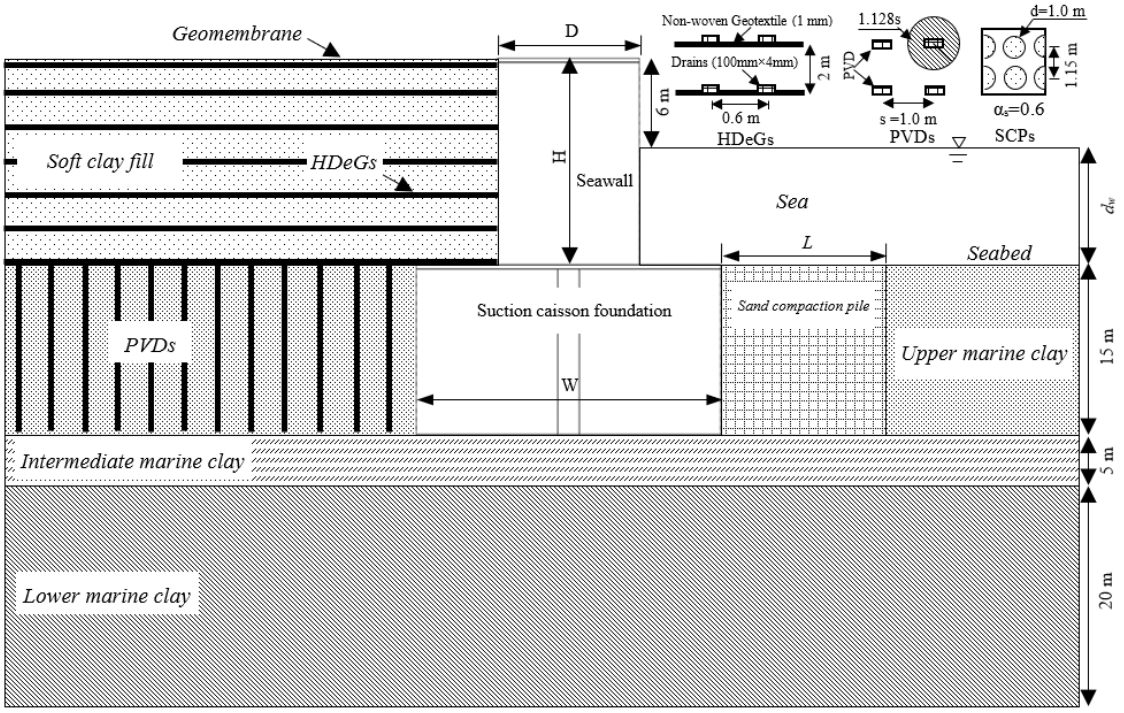

Figure 8.35 Proposed alternative method to improve the stability of containment structure using HDeG sheet and PVDs

PVDs were assumed to be installed in a rectangular pattern with 1 m spacing as shown in Figure 8.35. the PVDs could be installed into the upper marine clay using an offshore barge. After the installation of PVDs, the fist layer of HDeG was laid on the seabed. As the PVDs was in contact with HDeG, the upper marine clay would be consolidated under the same vacuum pressure too in addition to the weight of soft clay fill placed subsequently.

For soft clay fill, the coefficient of consolidation was 0.4 m^2/yr. The degree of consolidation was calculated using the proposed solution. For upper marine clay, the vertical and horizontal coefficient of consolidation were taken as 0.6 m^2/yr and 2.0 m^2/yr, respectively. The degree of consolidation was calculated using the Hansbo's solution (Hansbo, 1979) and Carrillo's equation (Carrillo, 1942). The parameters for Hansbo's solution are shown in Table 8.15. The radius of the smear zone was taken as 4 times of

the radius of the drain and the horizontal permeability of upper marine cay was considered to be 2 times that of the smeared soil.

Table 8.15 Parameter for Hansbo's solution

c_v (m^2/yr)	c_h (m^2/yr)	k_h/k_s	d_w	d_e	d_s	s	n	F(n)
0.6	2.0	2	0.067	1.128	0.268	4	16.84	3.46

*k_h/k_s: Ratio of horizontal permeability in upper marine clay and smear zone; d_w; Diameter of drain; d_e: Diameter of unit cell of PVDs treated soil; d_s: Diameter of smear zone; n: d_e/d_s; F(n): $F(n)=\mathrm{Ln}(n/s)-0.75+k_h/k_s\mathrm{Ln}(s)$

The total thickness of soft clay fill was 24 m for H = 14.5 m, 32 m for H = 18.5 m and 40 m for H = 22.5 m. The construction duration of land reclamation using HDeG sheets and PVDs was 465 days, 585 days and 705 days, respectively. The soil parameters of the improved soft clay fill and upper marine clay was shown in Table 8.16. The degree of consolidation, settlement, and the improved undrained shear strength under different seawall heights were computed. The degrees of consolidation for soft clay fill and upper marine clay after construction were 42.5 % and 90.5 % for H = 14.5 m, 44.4 % and 94.8 % for H = 18.5 m and 45.9 % and 97.2 % for H = 22.5 m The final elevation of ground surface after construction was 13.6 m, 17.2 m and 21.3 m, respectively.

Table 8.16 Updated soil parameters of soft clay fill and upper marine clay after consolidation

(a) Improved soft clay fill

Height of seawall (m)	Thickness (m)	Consolidation Duration (day)	*DoC* (%)	s_t (m)	e_t	γ_c (kN/m^3)	c_u (kPa)
14.5	24	465	42.5	9.73	1.38	17.0	13.3
18.5	32	585	44.4	13.32	1.33	17.2	15.6
22.5	40	705	45.9	17.02	1.30	17.3	17.8

(b) Improved upper marine clay

Height of seawall (m)	*DoC* (%)	*OCR*	s_t (m)	γ_m (kN/m^3)	c_{u0} (kPa)	k_{cu} (kPa/m)
14.5	90.5	1.38	1.70	17.7	38.2	2.38
18.5	94.8	1.25	2.44	18.8	56.3	2.50
22.5	97.2	1.23	2.72	19.2	65.1	2.59

DoC: degree of consolidation based on pore water pressure; s_t: final settlement of upper marine clay; e_t: final void ratio; γ_c: final unit weight of clay fill; γ_m: final unit weight of upper marine clay; c_u: undrained shear strength of treated clay fill; C_{u0}: undrained shear strength at seabed; k_{cu}: gradient of undrained shear strength of upper marine clay.

From Table 8.16, the undrained shear strength of upper marine clay inside the containment structure was improved. The average undrained shear strength of treated clay fill was 13.3 kPa, 15.6 kPa and 17.8 kPa. The undrained shear strength of improved upper marine clay at seabed was 38.2 kPa, 56.3 kPa and 60.1 kPa, respectively. Based on Eq. (8.5) and (8.6) for lateral stability, as the increase of undrained shear strength of upper marine clay inside the containment structure, the active thrust, E_{am}, of improved upper marine clay reduced. Otherwise, based on Eq. (8.13) for overall stability, as the increase of undrained shear strength of upper marine clay inside the containment structure, the resistance, $M_{\tau c}$, of marine clay was also increased. Thus, the factors of safety were improved and the containment structure will be more stable.

Supposed that the same improvement width of SCPs, 26 rows of SCPs, were used for the stability analyses. The Factors of safety for the land reclamation using HDeG sheets and PVDs are shown in Table 8.17. Compared with the stability analyses in Section 8.3, the factors of safety for the land reclamation using HDeG sheets and PVDs were increased largely.

Table 8.17 Factor of safety for land reclamation using HDeG sheets and PVDs

Height of seawall (m)	FoS_l	FoS_v	FoS_o
14.5	2.71	3.86	1.98
18.5	2.33	3.63	1.78
22.5	1.80	2.92	1.53

8.6 Conclusions

(1) A new type of seawall was proposed as a containment structure for land reclamation in relatively deep seawater. A simple analytical method for stability

analyses of the proposed seawall was suggested and its application was illustrated using design examples together with the proposed design procedure.

(2) Sand compaction piles were proposed to be used to treat the seabed clay in front of the suction caissons to enhance the stability of the seawall. The effect of the range of improvement using sand compaction piles was investigated using finite element analysis. The stability of the seawall in terms of overall stability under the critical condition using the proposed analytical method was also verified using the results of the finite element analysis. The results were similar and thus the proposed stability analyses method was supported by the finite element analysis. Based on the finite element analysis, the maximum deflection at top of seawall was less than 1/100 of the height of seawall.

(3) The consolidation process of the soft clay fill used for land reclamation using the HDeG and vacuum preloading method was analysed. The settlement of each layer with time as well as the pore water pressure variations in the clay fill could be calculated. These values were used to update the soil parameters for the seawall stability analysis. The vertical and horizontal displacement of the seawall as well as the deformation of the soils at different stages of consolidation of the soft clay fill were calculated using finite element analysis. The pore water pressure distributions in the soil were also calculated.

(4) A method to use PVDs to improve the seabed soil together with the improvement of the soft clay fill was also proposed. It could be seen from the analytical analysis that the improvement of seabed soil would enhance the stability of the seawall. More detailed numerical analysis could be carried out as a further study.

CHAPTER 9 CONCLUSIONS AND RECOMMENDATIONS

9.1 Conclusions

Preloading using either fill surcharge or vacuum pressure and PVDs is common method for the treatment of soft clayey soil. When the soft soil is too soft, a working platform needs to be formed. In this study, a modified Broms' method was proposed for the formation of a working platform. As there are difficulties in the use of PVDs with preloading for land reclamation projects such as time consuming and large uncertainties in design, a preloading method using horizontal drainage enhanced geotextile (HDeG) and vacuum pressure was proposed for the treatment of soft clay fill for land reclamation. The performance of HDeG sheet for vacuum preloading was investigated using model tests. The finite element analyses and theoretical consolidation solutions were also adopted to simulate the vacuum consolidation behaviour of soft soil in the model tests. A method to construct vertical seawall as containment structure for land reclamation using concrete cylinders and suction caissons was also proposed.

The use of HDeG sheet offers the following advantages: (1) The HDeG sheets is easy to transport and install; (2) The HDeG sheet can be kept in position due to the geotextile sheet and confinement of soft cohesive soil; (3) A working platform is not required; (4) Vacuum pressure can be applied through the horizontal drains to accelerate the consolidation of soft clayey soil as early as the first few meters of soft clayey soil was placed; (5) The placement of soft soil can be considered as the surcharge for the previous soft clay fill; (6) The containment bund does not have to be built as high as the maximum height of the slurry; (7) More reliable prediction of the settlement and the amount of fills to be placed can be made; and (8) The duration of land reclamation will be reduced substantially and the overall construction cost can be reduced. The following conclusions can be summarised from the studies presented in this thesis:

Stabilization of working platform using modified Broms' method

(1) A modified Broms' method was proposed to use geotextile tubes to form sand berms on top of the geotextile sheet placed on soft ground. A field trial on the use of the modified Broms' method was also carried out. The results obtained from the field trial

confirmed that the proposed method was easier to implement and could reduce uncertainties involved in both design and construction as the dimension and stability of the sand berms could be better maintained.

(2) An analytical solution for the modified Broms' method was proposed to calculate the tensile stresses and tensile strains in the geotextile and the deformed profile of the geotextile sheet. The design procedure based on the proposed methods for modified Broms' method was developed.

(3) The proposed analytical solution was also validated using finite element analyses. The analytical predictions agreed well with FE analyses and reasonably well with the field monitoring data.

Model tests for vacuum consolidation of soft clayey soil using HDeG sheet

(4) The consolidation of soft soil using HDeG and vacuum was more effective than the use of a horizontal drain and vacuum alone. The vacuum pressure could be distributed almost uniformly across the entire HDeG with double non-woven geotextile sheets. With HDeG using a single non-woven geotextile sheet, the pore water pressure distribution along the geotextile was not uniform, but within -60 to -80 kPa and the value was reducing with time. The geotextile in the HDeG played an important role in distributing vacuum pressure and consolidating soil.

(5) High degree of consolidation in terms of settlement was obtained when HDeG was used with vacuum for the consolidation of soft marine clay in the model tests. One layer of HDeG with double non-woven geotextile sheets performed better than that using two layers of HDeG with single layer of non-woven geotextile. Whether one layer or two layers of non-woven geotextile is more effective in terms of both performance and cost needs further study.

(6) The transmissivity of geotextile had a significant effect on the transmission of vacuum pressure in the soil. The transmissivity of non-woven geotextile was affected by the type of soil it embedded and the normal stress. For this reason, a method to measure the transmissivity of geotextile in soil was proposed and used in this study.

(7) The performance of the HDeG was controlled by the horizontal spacing of the drains s_h, the vertical spacing of HDeG s_v, the width of the drain w and the permittivity of the

geotextile k_p. In general the greater the w/s_h or w/s_v ratio or the higher the k_p, the more efficiency the HDeG.

(8) With the use of HDeG with geotextile of relatively high permittivity, the pore water pressure distribution at the same elevation were more uniform. The flow lines tended to be vertical and the equipotential lines tended to be horizontal. The undrained shear strength and water content distribution contours tended to be horizontal too.

Consolidation analyses of soft clayey soil using HDeG sheet

(9) The proposed theoretical solutions and adopted finite element analyses were feasible to simulate the vacuum consolidation behaviour of soft clay. The proposed theoretical solutions were suitable for consolidation of soft clay using HDeG sheet and vacuum preloading.

(10) As the horizontal spacing of horizontal drains or the vertical spacing of HDeG sheet increased, the degree of consolidation decreased. With the increase in transmissivity of geotextile, the degree of consolidation increased.

(11) Finite element analyses with the use of the average pore water pressure for HDeG sheet were feasible to simulate the consolidation of soft soil using HDeG sheet and vacuum preloading.

(12) Based on the calculation of degree of consolidation using the monitoring data, the degree of consolidation based on distribution of excess pore pressure lagged behind that based on average settlement due to the non-linear compressibility. An equation to convert the degree of consolidation based on settlement to that based on pore water pressure or verse versa was proposed. The effectiveness of the conversion equation was verified using the measured data, theoretical solutions and FEA.

HDeG sheet with electro-osmosis or lime liner

(13) A method to combine electro-osmosis with HDeG or the use of e-HDeG for consolidation of soft clay was proposed. Both carbon felt and steel plate could be used as electrode for electro-osmosis. However, carbon felt was a better choice due to its flexibility and lightweight. The model tests showed that electro-osmosis using carbon felt was effective in accelerating the vacuum consolidation of soft marine clay. Nevertheless, the connector for the wires and the carbon felt still need to be improved.

(14) Larger settlement and greater reduction in excess pore water pressure were induced by the coupling of vacuum consolidation and electro-osmosis.

(15) The use of lime liner to enhance the performance of HDeG or lime liner enhanced HDeG was proposed. The permeability of the lime treated soil was improved for about 2 – 3 times because of the soil structure induced by cation exchange of soil particle. The efficiency of the use of lime liner was verified using small consolidation tests under surcharge or vacuum pressure. The setting time had an effect on the consolidation of soft soil due to calcium ion diffusion. With longer setting time, the reduction of excess pore pressure was larger.

Design of containment structure for land reclamation

(16) A new type of seawall was proposed as a containment structure for land reclamation in relatively deep seawater. A simple analytical method for stability analyses of the proposed seawall was suggested and its application was illustrated using design examples together with the proposed design procedure.

(17) Sand compaction piles were proposed to be used to treat the seabed clay in front of the suction caissons to enhance the stability of the seawall. The effect of the range of improvement using sand compaction piles was investigated using finite element analysis. The stability of the seawall in terms of overall stability under the critical condition using the proposed analytical method was also verified using the results of the finite element analysis. Based on the finite element analysis, the maximum deflection at top of seawall was less than 1/100 of the height of seawall.

(18) The consolidation process of the soft clay fill used for land reclamation using the HDeG and vacuum preloading method was analysed. The settlement of each layer with time as well as the pore water pressure variations in the clay fill could be calculated. These values were used to update the soil parameters for the seawall stability analysis. The vertical and horizontal displacement of the seawall as well as the deformation of the soils at different stages of consolidation of the soft clay fill were calculated using finite element analysis. The pore water pressure distributions in the soil were also calculated.

(19) A method to use PVDs to improve the seabed soil together with the improvement of the soft clay fill was also proposed. It could be seen from the analytical analysis that the improvement of seabed soil would enhance the stability of the seawall. More detailed numerical analysis could be carried out as a further study.

9.2 Recommendations

Due to time constraints, some aspects of the present study could not be completed or investigated further. Some recommendations and suggestions for further studies are proposed.

(1) An analytical solution needs to be developed to predict the transmissivity of non-woven geotextile in soft clayey soil. However, the reduction of transmissivity of non-woven geotextile in soft clayey soil depends on the clay content and normal effective stress. Hence, the transmissivity tests using different types of soft clay should be conducted. An analytical model for the transmissivity of non-woven geotextile in soft clay with different clay content should be studied.

(2) As the transmissivity affects the vacuum consolidation of soft clayey soil, the parametric studies of the transmissivity on the performance of HDeG sheet should be conducted for the selection of geotextile.

(3) The carbon felt is feasible to be combined with horizontal drains for the treatment of soft clayey soil. However, the more thermal stable connector of metal wires and carbon felt need to be developed.

(4) The large-scale model tests using electrical HDeG sheet should be conducted to evaluate the performance of electrical HDeG sheet and determine the commencing time for the use of electro-osmosis.

(5) By using the lime liner and horizontal drains, the cation exchange of soil particles depends on the calcium diffusion. Hence, the theoretical analyses for the calcium diffusion in porous material should be studied.

(6) To improve the stability of containment bund using caisson, The use of PVDs for the treatment of upper marine clay is an alternative selection. Further studies on the alternative method should be conducted.

REFERENCES

Abusharar, S.W., Han, J., 2011. Two-dimensional deep-seated slope stability analysis of embankments over stone column-improved soft clay. *Eng. Geol*. 120 (1–4): 103–110.

ALF TØRUM, ANNETTE JAHR and ØIVIND ARNTSEN, 2012. Wave force on a composite breakwater with circular cylinder caissons. Coastal Engineering Journal, 54(4).

Almeida, M.S.S., Ferreira, C.A.M., 1993. Field in situ and laboratory consolidation parameters of a very soft clay. In Predictive Soil Mechanics, Proceedings of the Worth Memorial Symposium. Thomas Telford, London, UK, pp. 73–93.

Asadi, A., Huat, B. B., Nahazanan, H., Keykhah, H. A., 2013. Theory of electroosmosis in soil. International Journal of Electrochemical Science, 8 (1): 1016–1025

Alvarez, I.E., Rubio, R., Ricalde, H., 2007. Beach restoration with geotextile tubes as submerged breakwaters in Yucatan, Mexico. Geotextiles and Geomembranes, 25 (4): 233-241.

Archer, G. G., Wang, P., 1990. The Dielectric Constant of Water and Debye-Hückel Limiting Law Slopes. Journal of Physical and Chemical Reference Data. 19 (2): 371–411.

Abiera, H.O., Miura, N., Bergado, D.T., Nomura, T. 1999. Effect of using electro-conductive PVD in the consolidation of reconstituted Ariake clay. Geotechnical Engineering Journal, 30(2): 67–82.

Arulrajah, A., Nikraz, H., Bo, M.W., 2005. In-situ testing of Singapore marine clay at Changi. Geotechnical and Geological Engineering, 23: 111–130.

Arulrajah, A., Bo, M.W., 2008. Characteristics of Singapore Marine Clay at Changi. Geotechnical and Geological Engineering, 26: 431-441.

Barron, R.A., 1948. Consolidation of fine-grained soils by drain wells. Transactions, ASCE, 113: 718-754.

Basu, D., Prezzi, M., 2007. Effect of the smear and transition zones around prefabricated vertical drains installed in a triangular pattern on the rate of soil consolidation. International Journal of Geomechanics, ASCE 7(1): 34–43.

Been, K., Sills, G.C., 1981. Self-weight consolidation of soft soils: an experimental and theoretical study Geotechnique, (31)4: 519-535.

Bergado, D.T., Alfaro, M.C., Balasubramaniam, A.S., 1993. Improvement of soft Bangkok clay using vertical drains, Geotextiles and Geomembranes, 12(5): 615–663.

Bergado, D.T., Anderson, L.R., Miura, N., Balasubramaniam, A.S., 1996. Soft Ground Improvement in Lowland and Other Environments, ASCE Press, ASCE, NY.

Bergado, D.T., Balasubramaniam, A.S., Fannin, R.J., Holtz, R.D., 2002. Prefabricated vertical drains (PVDs) in soft Bangkok clay: a case study of the New Bangkok International Airport project, Canadian Geotechnical Journal, 39: 304–315.

Bjerrum, L., Moum, J., Eide, O. 1967. Application of electroosmosis to a foundation problem in a Norwegian quick clay. Géotechnique, 17(3): 214–235.

British Standarts Institution, 1994. Maritime structures —Part 1: Code of practice for general criteria. BS 6349-1:2000. British Standarts Institution, London, UK.

British Standarts Institution, 1994. Code of Practice for Earth Retaining Structures. BS 8002. British Standarts Institution, London, UK.

Bo, M.W., Chu, J., Low, B.K.,Choa, V., 2003b. Soil Improvement: Prefabricated Vertical Drain Technique: Thomson Learning.

Bo, M.W. & Choa, V. 2004. Reclamation and Ground Improvement. Thomson.

Bo, M.W., Chu, J., Choa, V., 2005. The Changi East reclamation project in Singapore. Chapter. 9, Ground Improvement Case Histories, B. Indraratna & J. Chu (Eds.), Elsevier: 247-276.

Bo, M. W., Arulrajah, A., Nikraz, H., 2007. Preloading and prefabricated vertical drains design for foreshore land reclamation projects: a case study. Proceedings of the Institution of Civil Engineers - Ground Improvement. 11(2): p. 67-76.

Bo, M.W., 2008. Compressibility of ultra-soft soil. WORLD SCIENTIFIC.

Bourges-Gastand, S., Stoltz, G., Dolez, P., Blond, E., Touze-Follz, N., 2015. Laboratory device to characterise electrokinetic geosynthetic composites for fluid fine tailings dewatering. Can. Geotech. J. 52 (4): 505-514.

Broms, B. B., 1987. Stabilization of very soft clay using geofabric. Geotextiles and Geomembranes, 5(1): 17-28.

Cantre, S., 2002. Geotextile tubes-analytical design aspects. Geotextiles and Geomembranes, 20(5), 305-319.

Carrillo, N., 1942. Simple two- and tree-dimensional cases in the theory of consolidation of soils. J. Math. Phys. 21, 1-5.

Casagrande, L. 1948. Electro-osmosis. Proceedings, 2nd International Conference on Soil Mechanics and Foundation Engineering, Rotterdam, 1: 218-223.

Casagrande, A., 1952. Electro-osmotic stabilization of soils. J. Boston Soc. Civ. Eng. ASCE 39, 51-83.

Casagrande L, 1983. Stabilisation of soils by means of electro-osmosis state-of-the-art. Journal of the Boston Society of Civil Engineers ASCE 69(2): 255–302.

Chai, J. C., Miura N., 1999. Investigation of factors affecting vertical drain behavior. Journal of Geotechnical Engineering, ASCE 125(3): 216–226.

Chai, J.-C., Miura, N., 2002. Long-term transmissivity of geotextile confined in clay. In: Delmas, Ph., Gourc, J.P. (Eds.), Proc. 7th Inter. Conf. on Geosynthetics, Nice, France, vol. 1. Balkema Publishers, pp. 155-158.

Chai, J. C., Miura, N., Bergado, D. T. 2008. Preloading clayey deposit by vacuum pressure with cap-drain: Analyses versus performance. Geotexiles and Geomembranes, 26: 220-230.

Chai, J. C., Horpibulsuk, S., Shen, S.L. Carter, J., 2014. Consolidation analysis of clayey deposits under vacuum pressure with horizontal drains. Geotextiles and Geomembranes. 42.

Chai, J. C., Bergado, D. T., Shen, S. L., 2013. Modelling prefabricated vertical drain improved ground in plane strain analysis. Proceedings of the Institution of Civil Engineers – Ground Improvement 166(2): 65–77.

Chai, J. C., Nguyen, D.Q., 2013. Geocomposite induced consolidation of clayey soils under stepwise loads. Geotextiles and Geomembranes. 37. 99–108.

Chen, H., Bao, X.C., 1983. Analysis of soil consolidation stress under the action of negative pressure. Proceedings 8th European Conference on Soil Mechanics and Foundation Engineering, Helsinki, 2: 591-596.

Cheng, Z., Law, H., Jiang, Y. 2010. Soil-Structure Interaction Analysis for Bridge Caisson Foundation. International Conferences on Recent Advances in Geotechnical Earthquake Engineering and Soil Dynamics. 48.

Chew, S.H., Karunaratne, G.P., Kuma, V.M., Lim, L.H., Toh, M.L., Hee, A.M., 2004. A field trial for soft clay consolidation using electric vertical drains. Geotext. Geomembr. 22: 17-35.

Chien, S. C., Ou, C. Y., Wang, M. K., 2009. Injection of saline solutions to improve the electroosmotic pressure and consolidation of foundation soil. Applied Clay Science, 44: 218-224.

Choa, V., Bo, M.W., Chu, J., 2001. Soil improvement works for Changi East reclamation project. Ground Improvement, 5(2): 141–153.

Chu, J., Yan, S. W., Yang, H., 2000. Soil improvement by the vacuum preloading method for an oil storage station. Ground and Soil Improvement. pp 21-28.

Chu, J., Bo, M.W., Choa, V., 2004. Practical considerations for using vertical drains in soil improvement projects. Geotextiles and Geomembranes, 22: 101-117.

Chu, J., Goi, M. H., and Lim, T. T., 2005. Consolidation of cement-treated sewage sludge using vertical drains. Canadian Geotechnical Journal, 42(2): 528-540.

Chu, J., Yan, S.W., 2005a. Estimation of degree of consolidation for vacuum preloading projects. International Journal of Geomechanics, ASCE 5(2): 158–165.

Chu, J., Yan, S.W., 2005b. Application of the vacuum preloading method in land reclamation and soil improvement projects. In Ground Improvement – Case Histories (Indraratna J and Chu J (eds)). Elsevier, Amsterdam, The Netherlands, Ch. 3: 91–118.

Chu, J., Bo, M. W., Choa, V., 2006. Improvement of ultra-soft soil using prefabricated vertical drains. Geotextiles and Geomembranes. 24(6): 339-348.

Chu, J., Yan, S. W., 2007. Ground improvement in disaster mitigation and rehabilitation works, Invited Special Lecture. In: Proceedings 16th Southeast Asian Geotechnical Conference, 8e11 May, Kuala Lumpur, pp 163-170.

Chu, J., Yan, S.W., Indraratna, B., 2008. Vacuum Preloading Techniques – Recent Developments and Applications. GeoCongress 2008, New Orleans, Geosustainability

and Geohazard Mitigation GPS 178, Reddy, KR, Khire, MV, Alshawabkeh, AN (eds), 586-595.

Chu, J., Varaksin, S., Klotz, U., Menge, P., 2009. Construction processes, State-of-the-art report, Proc. 17th International Conference on Soil mechanics and geotechnical Engineering, Alexandria, Egypt, 5-9 Oct, 4, 3006-3135.

Chu, J., Bo, M. W., Arulrajah, A., 2009a. Reclamation of a slurry pond in Singapore. Proceedings of the Institution of Civil Engineers - Geotechnical Engineering. 162(1): 13-20.

Chu, J., Bo, M. W., Arulrajah, A., 2009b. Soil improvement works for an offshore land reclamation. Proceedings of the Institution of Civil Engineers - Geotechnical Engineering. 162(1): 21-32.

Chu, J, Indraratna, B., Yan, S., Rujikiamjorn, C., 2012. Soft soil improvement through consolidation: An overview. Proceedings of the International Conference on Ground Improvement and Ground Control, Wollongong, Australia, pp. 251–280, state-of-the-art report.

Chu, J., Bergado, D. T., Shin, E. C., Chai, J., 2012a. Embankments on soft ground and ground improvement. 5th Asian Regional Conference on Geosynthetics Bangkok, Thailand, p. 3-24.

Chu, J., Yan, S., Lam, K. P., 2012b. Methods for improvement of clay slurry or sewage sludge. Proceedings of the Institution of Civil Engineers - Ground Improvement. 165(4): 187-199.

Chu, J., Raju, V.R., 2013. Prefabricated vertical drains. In Ground Improvement, Ch4, Eds Krich, K. and Bell, A.L., Taylor and Francis.

Chu, J., Guo, W., 2016. Land reclamation using clay slurry or in deep water: challenges and solutions. Japanese Geotechnical Society Special Publication. 2(51): 1790-1793.

Craig, R. F., 2004. Craig's Soil Mechanics, Seventh Edition. Taylor & Francis Ltd. London, United Kingdom.

Cognon J.M., 1991. Vaccum consolidation. Re´vue Francaise Ge´otechnique 57(3): 37–47.

Cooper, M.R., Rose, A.N., 1999. Stone column support for an embankment on deep alluvial soils. Proc. Inst. Civ. Eng. Geotech. Eng. 37(1): 15–25.

Deng, Y., Liu, G., Indraratna, B., Rujikiatkamjorn, C., and Xie, K., 2017. Model Test and Theoretical Analysis for Soft Soil Foundations Improved by Prefabricated Vertical Drains. International Journal of Geomechanics, 17(1).

de Lillis, Armando, Miliziano, Salvatore, Flora, Alessandro ad Fasano, Gianluca, 2017. Reclamation of a containment area: measurements and back analysis of the height of dredged mud. Conference: 19th International Conference on Soil Mechanics and Geotechnical Engineering, At Seoul.

Esrig, M.I., Gemeinhardt, J.P. 1967. Electrokinetic stabilization of illitic clay. Journal of the Soil Mechanics and Foundations Division,ASCE, 93(SM3): 109–128.

Esrig MI., 1968. Pore pressure, consolidation and electro-kinetics. Journal of the SMFD, American Society of Civil Engineers, 94(SM4): 899-921.

Fetzer, C., 1967. Electro-osmotic stabilization of west branch dam. Trans Am Soc Civ Eng 133: 540–563

Fitch, Bryant, 1983. Kynch Theory and Compression Zones. AIChE Journal. 29: 940 - 947.

Gibson, R.E., England, G.L., Hussey, M. J.L., 1967. The Theory of One-Dimensional Consolidation of Saturated Clays. Géotechnique, 17(3): 261-273

Gibson, R.E., Schiffman, R. L., Cargilt, K. W., 1981. The Theory of One-Dimensional Consolidation of Saturated Clays, II-Finite Non-Linear Consolidation of Thick Homogeneous Layers. Canadian Geotechnical Journal, 18: 280-293.

Guan, Y.F., Cao. Y.Y., 2018. Study on Penetration Resistance of Bucket Foundation Breakwater by Centrifuge Model Tests. Proceedings of China-Europe Conference on Geotechnical Engineering, SSGG, pp. 927–931.

Guan, Y.F., Cao. Y.Y., Tang, Y., Zhang, N., 2018. In-situ Tests on Behaviour of Breakwater with Bucket Foundation Under Wave Loading. Proceedings of GeoShanghai 2018 International Conference: Advances in Soil Dynamics and Foundation Engineering, pp. 819–828.

Giroud, J. P., Noirey, L, 1981. Geotextile-reinforced unpaved road design. Geotechnical Division, ASCE, 107: 1233-54.

Guo, W., Chu, J., Nie, W., 2014. Analysis of geosynthetic tubes inflated by liquid and consolidated soil. Geotextiles and Geomembranes, 42(4): 277-283,

Guo, W., 2009. Dike Construction Using Geotubes. 1st Year Progress Report. Nanyang Technological University, Singapore.

Hamir, R.B., Jones, C.J.F.P., Clarke, B.G., 2001. Electrically conductive geosynthetics for consolidation and reinforced soil. Geotext. Geomembranes, 19(8): 455-482.

Hansbo, S., 1979. Consolidation of clay by bandshaped prefabricated drains, Ground Engineering, 12(5): 16–25.

Hansbo, S., 1981. Consolidation of fine-grained soils by prefabricated drains, Proc. 10th International Conference Soil Mechanics and Foundation Engineering., Stockholm, 3, 677–682.

Hansbo, S., 2005. Experience of consolidation process from test areas with and without vertical drains. In B. Indraratna and J. Chu (Eds.), Chapter 1, Ground Improvement – Case Histories, Elsevier, 3–50.

Hansbo, S., 2008. Soil Improvement by Means of Electro-Osmosis. International Conference on Case Histories in Geotechnical Engineering.

He, J., Chu, J., Tan, S.K., Vu, T., 2016. Sedimentation Behaviour of Flocculant-Treated Soil Slurry. Marine Georesources & Geotechnology. 35.

Head, K.H., 2006. Manual of Soil Laboratory Testing: Hydraulic cell consolidation and permeability tests. 3rd edition. Whittles Publishing, UK.

Hird, C.C. Moseley, V.J., 2000. Model study of seepage in smear zones around vertical drains in layered soil. Geotechnique, 50(1): 89–97.

Holtz. R.D., 1975. Preloading by vacuum: current prospects. Transportation Research Record 48(5): 26–79.

Holtz, R.D., Jamiolkowski, M., Lancellotta, R. and Pedroni, R., 1991. Prefabricated Vertical Drains: Design and Performance, CIRIA Ground Engineering Report, Butterworth-Heinemann Ltd., London.

Imai, G., 1981. Experimental studies on sedimentation mechanism and sediment formation of clay materials. SOILS AND FOUNDATIONS. 21: 7-20.

Indraratna, B., Redana, I. W., 1997. Plane strain modelling of smear effects associated with vertical drains. Journal of Geotechnical and Geoenvironmental Engineering, ASCE 123(5): 474–478.

Indraratna, B., Redana, I. W., 1998. Laboratory determination of smear zone due to vertical drain installation. Journal of Geotechnical Engineering, ASCE 124(2): 180–184.

Indraratna, B., Sathananthan, I., Bamunawita, C., Balasubramaniam, A.S., 2005. Chapter 2 – Theoretical and numerical perspectives and field observations for the design and performance evaluation of embankments constructed on soft marine clay. Ground Improvement-Case Histories, Indraratna and Chu (ed.): 51–90.

Indraratna, B., Rujikiatkamjorn, C., Balasubramaniam, A., Wijeyakulasuriya, V., 2005a. Predictions and observations of soft clay foundations stabilised with geosynthetic drains and vacuum surcharge. In Ground Improvement – Case Histories (Indraratna B and Chu J (eds)). Elsevier, Amsterdam, The Netherlands, pp. 199–229.

Indraratna, B., Rujikiatkamjorn, C., Sathananthan, I., 2005b. Analytical and numerical solutions for a single vertical drain including the effects of vacuum preloading. Canadian Geotechnical Journal, 42(4): 994–1014.

Indraratna B, 2009. Recent Advances in the Application of Vertical Drains and Vacuum Preloading in Soft Soil Stabilization. Australian Geomechanics Society, Australia, E. H. Davis Lecture.

Indraratna, B., Rujikiatkamjorn, C., Kelly, R. Buys, H., 2010. Sustainable soil improvement via vacuum preloading. Proceedings of the Institution of Civil Engineers – Ground Improvement 163(1): 31–42.

Indraratna, B., Rujikiatkamjorn, C., Kelly, R., Buys, H., 2012. Soft soil foundation improved by vacuum and surcharge loading. Proc. of the ICE - Ground Improvement 165(2): 87–96.

Jeyakanthan, V., Gnanendran, C.T., Lo, S.C.R., 2011. Laboratory assessment of electro-osmotic stabilization of soft clay. Can Geotech J, 48(12):1788–1802.

Jones, C.J.F.P., 1996. Earth Structures and Soil Reinforcement. Thomas Telford, London, p. 379.

Jones, C.J.F.P., Fakher, A., Hamir, R., Nettleton, I.M., 1997. Geosynthetic materials with improved reinforcement capabilities. In: Ochiai, Otani, Yasufuku, Omine (Eds.), Earth Reinforcement, 2, pp. 865e887. Balkema.

Jones, C.J.F.P., 2001. Developments and innovations in reinforced soil technology. In: Ochiai, Otani, Yasufuku, Omine (Eds.), Landmarks in Earth Reinforcement, 1, pp. 1047-1061 (Swets and Zeittinger).

Jones, C.J.F.P., Pugh, R.C., 2001. A full-scale field trial of electrically enhanced cohesive reinforced soil using electrically conductive geosynthetics. In: Ochiai, Otani, Yasufuku, Omine (Eds.), Landmarks in Earth Reinforcement, 1, pp. 219-223 (Swets & Zeittinger).

Jones, C.J.F.P., Lamont-Black, J., Glendinning, S., Pugh, R.C., 2005. New applications for Smart geosynthetics. In: Rathje, E.M. (Ed.), Geo-Frontiers 2005. ASCE Special Publication, pp. 130-142

Jones, C.J.F.P., Lamont-Black, J., Glendinning, S., Bergado, D., Eng, T., Fourie, A., Liming, Hu, Pugh, R.C., Romantshuk, M., Simpanen, S., Zhuang, Yan-Feng, 2008. Recent research and applications in the use of electrokinetic geosynthetics. Key note paper. In: Dixon, N. (Ed.), 4th European Geosynthetics Conference eEuroGeo4. Edinburgh.

Jones, C.J.F.P., Lamont-Black, J., Glendinning, S., 2011. Electrokinetic geosynthetics in hydraulic applications. Geotext. Geomembr. 29: 381-390.

Jones, C., Lamont-Black, J., Huntley, D. Alder, D. Glendinning, S., 2017. Electrokinetic geosynthetics: From research to hype to practice. Proceedings of the Institution of Civil Engineers - Civil Engineering. 170: 1-8.

Jongeling, T.H.G., Rövekamp, N.H., 1999. Storm surge barrier Ramspol. Proceedings of xxviii IAHR Congress, 22-27 August, Graz, Austria.

Katagiri, M., Imai, G., 1994. A new in0laboratory method to make homogeneous clayey smaples and their mechnical properties. Soils and Foundation. 34(2): 87-93.

Kim, M., Freeman, M., FitzPatrick, B.T., Nevius, D.B., Plaut, R.H., Filz, G.M., 2004. Use of an apron to stabilize geomembrane tubes for fighting floods. Geotextiles and Geomembranes, 22(4), 239e254.

Kitazume, M., 2007. Design, execution and quality control of ground improvement in Landreclamation, Proc. of the 13th Asian Regional Conference on Soil Mechanics and Foundation Engineering, Keynote Lecture.

Kjellman, W., 1937. Redogbrelse for Statens geoteknisks instituts verksamhet under aran 1944-1948. Swedish Geot. Inst., Meddelande No, 2.

Kjellman, W., 1952. Consolidation of clayey soils by atmospheric pressure. Proceedings of a Conf. on Soil Stabilization, Massachusetts Institute of Technology, Boston, 258-263.

Koerner, G.R., Koerner, R.M., 2006. Geotextile tube assessment using a hanging bag test. Geotextiles and Geomembranes, 24(2): 129e137.

Lam, K.P., Wu, S.F., Chu, J., 2018. Field trial of a membraneless vacuum preloading system for soft soil improvement. Proceedings of the Institution of Civil Engineers - Ground Improvement. 1-30.

Lamont-Black, J., Jones, C.J.F.P., Fourie, A.B., Kruger, L., 2010. Electrokinetic belt press dewatering of kimberlite tailings e case study of a full scale field trial. In: Proceedings 13th International Seminar on Paste and Thickened Tailings, Nedland, WA, 1: 329-342.

Lamont-Black, J., Jones, C.J.F.P., 2015. Electrokintic geosynthetic (EKG) dewatering and treatment of waste sludge materials. Geosynthetic, 2015. IFAI, 96-100, Portland, Oregon.

Lamont-Black, J., Jones, C.J.F.P., White, C., 2015. Electrokinetic geosynthetic dewatering of nuclear contaminated waste. Geotext. Geomembr. 43(4): 359-362. Elsevier.

Lamont-Black, J., Jones, C. and Alder, D., 2016. Electrokinetic strengthening of slopes – Case history. Geotextiles and Geomembranes. 44: 319-331.

Lee, E.C., 2015. Chapter 15 - Electrokinetic Improvement of Soft Clay Using Electrical Vertical Drains, Editor(s): Buddhima Indraratna, Jian Chu, Cholachat Rujikiatkamjorn, Ground Improvement Case Histories, Butterworth-Heinemann. Pages 487-513.

Lee, K., Sills, G. C, 1981. The consolidation of a soil stratum, including self-weight effects and large strains. Int. J. Numer. Anal. Methods Geom, 5(4): 405–428.

Leung, C.F., Tan, S.A., Shen, R.F., 2005. Prediction versus performance of Land Reclamation Bund. Proceedings of the 16th International Conference on Soil Mechanics and Geotechnical Engineering.

Leshchinsky, D., Leshchinsky, O., Ling, H.I., and Gilbert, P.A. (1996), "Geosynthetic Tubes for Confining Pressurized Slurry: Some Design Aspects", J. Geotech. Eng., 122(8): 682-690.

Li, A.L., Rowe, R.K., 2001b. Combined effects of reinforcement and prefabricated vertical drains on embankment performance. Canadian Geotechnical Journal, 38(6): 1266–1282.

Li, Q., Tong J., and Huang Y., 2017. Physical Model Test on Long-term Performance of Prefabricated Vertical Drains in Soft Soil Improvement. Electronic Journal of Geotechnical Engineering, 22(11): 4471-4484.

Liu, H.L., Chu, J., 2009. A new type of prefabricated vertical drain with improved properties. Geotextiles and Geomembranes, 27(2): 152-155.

Liu, H., Cui, Y., Shen, Y., and Ding, X. 2014. A new method of combination of electroosmosis, vacuum and surcharge preloading for soft ground improvement. China Ocean Engineering, 28: 511–528.

Lo, K.Y., Inculet, I.I., Ho, K.S. 1991a. Electroosmotic strengthening of soft sensitive clays. Canadian Geotechnical Journal, 28(1): 62–73.

Lo, K.Y., Ho, K.S., Inculet, I.I. 1991b. Field test of electroosmotic strengthening of soft sensitive clay. Canadian Geotechnical Journal, 28(1): 74–83.

Lorenzo, G.A., Bergado, D.T., Bunthai, W., 2004. Innovations and performances of PVD and dual function geosynthetic applications. Geotext. Geomembranes, 22 (1 and 2): 1-25.

Madhav, M. R., Park, Y. M., Miura, N., 1993. Modelling and study of smear zones around band shaped drains. Soils and Foundations, 33(4): 135–147.

Miki, H., Yamada, T., Takahashi, I., Shinsha, H., Kushima, M., 1996. Application of geotextile tube dehydrated soil to form embankments. Proc. 2nd Int. Conf. on Environmental Geotechnics, Osaka, 5-8 Nov., 385-390.

Mitchell, J.K., 1993. Fundamentals of Soil Behavior, second ed. Wiley, New York.

Mitchell, J.K., Soga, K., 2005. Fundamentals of soil behavior, 3rd edn. Wiley, Hoboken

Moo-Young, H.K., Tucker, W.R., 2002. Evaluation of vacuum filtration testing for geotextile tubes. Geotextiles and Geomembranes, 20 (3): 191-212.

Mohamedelhassan, E., Shang, J. Q., 2003. Electrokinetics-generated pore fluid and ionic transport in an offshore calcareous soil. Canadian Geotechnical Journal, 40: 1185–1199.

Nettleton, I.M., Jones, C.J.F.P., Clarke, B.G., Hamir, R., 1998. Electrokinetic geosynthetics and their applications. In: Proceedings 6th International Conference on Geosynthetics, Atlanta, Georgia, USA, 2: 871-876.

Onoue, A., Ting, N., Germain, J., Whitman, R., 1991. Permeability of Disturbed Zone Around Vertical Drains. In Proceedings of American Society of Civil Engineering, Congress, Colorado, USA, pp. 879–890.

Pavlakis, J., Fourie, A.F., Jones, C.J.F.P., 2001. Stabilisation of mine tailings deposits using electrokinetic geotextiles. In: Proc. 4th Conf. on Environmental Engineering, Mulderschift, South Africa, September, pp. 12.

Pilarczyk, K.W., 2000. Geosynthetics and Geosystems in Hydraulic and Coastal Engineering. Balkema A. A, Rotterdam.

Plaxis 2D - Materal Models Manual 2018, https:/www.plaxis.com.

Pugh, R.C., 2002. The Application of Electrokinetic Geosynthetic Materials to Uses in the Construction Industry (PhD thesis). Newcastle University.

Pusch, R., 1976.Stabilisering av schakter I silt med hjälp av elektroosmos. Byggdokument 76-1601, Sverige.

Qian, J. H., Zhao, W. B., Cheung, Y. K., Lee, P. K. K., 1992. The theory and practice of vacuum preloading. Computers and Geotechnics, 13: 103-118.

Restall, S.J., Jackson, L.A., Heerten, G., Hornsey, W.P., 2002. Case studies showing the growth and development of geotextile sand containers: an Australian perspective. Geotextiles and Geomembranes, 20(5), 321-342.

Recio, J., Oumeraci, H., 2007. Effect of deformations on the hydraulic stability of coastal structures made of geotextile sand containers. Geotextiles and Geomembranes, 25 (4), 278-292.

Ritterong, A., Douglas, R.S., Shang, J.Q., Lee, E.C., 2008. Electrinetic improvement of soft clay using electrical vertical drains. Geosynth. Int., 15 (5): 369-381 (Thomas Telford).

Rujikiatkamjorn, C., Indraratna, B. N., Chu, J., 2008. 2D and 3D numerical modeling of combined surcharge and vacuum preloading with vertical drains. International Journal of Geomechanics, 8(2): 144–156.

Seah, T.H., 2006. Design and construction of ground improvement works at Suvarnabhumi Airport. Geotechnical Engineering Journal of Southeast Asian Geotechnical Society, 37, 171–188.

Segall, B.A., Bruell, C.J., 1992. Electro-osmotic contaminant removal process. J. Environ. Eng., 118: 84–100.

Schiffman, R. L., Cargill, K. W., 1981. Finite strain consolidation of sedimenting clay deposits. Proc. 10th Int. Conf. Soil Mech., 1: 239-242.

Shang, J.Q., Lo, K.Y., Huang, K.M. 1996. Effects of voltage gradient and polarity reversal on electro-osmotic consolidation. Proceedings, 2nd International Conference on Soft Soil Engineering, Nanjing, China, pp. 966-971.

Shang, J. Q., 1997. Electrokinetic dewatering of clay slurries as engineered soil covers. Canadian Geotechnical Journal, 34(1):78–86.

Shang, J.Q. 1998. Electroosmosis-enhanced preloading consolidation via vertical drains. Canadian Geotechnical Journal, 35(3): 491– 499.

Shang, J.Q., and Mohamedelhassan, E., 2001. Electrokinetic dewatering of Eneabba West Mine tailings: an experimental study. In Soft ground technology. Edited by J.L. Hanson and R.J. Termaat. ASCE Geotechnical Special Publication 112, ASCE Press, Reston, Va. pp. 346–357.

Shen, Y., Tao, M., Liu, H., Gao, Y., Cui, Y. 2012. The performance of super soft foundations under a modified vacuum preloading method. In Proceedings of the Sixth Congress on Forensic Engineering, San Francisco, Calif., 31 October – 3 November 2012. American Society of Civil Engineers, New York. pp. 708–715.

Shen, Y., Qiu, C., Li, Y., Shi, W., Rui, X., 2017. An analytical solution for two-dimensional vacuum preloading combined with electro-osmosis consolidation using EKG electrodes. PLOS ONE, 12(8).

Shin, E.C., Oh, Y.I., 2007a. Coastal erosion prevention by geotextile tube technology. Geotextiles and Geomembranes 25(4): 264-277.

Shin, E.C., Oh, Y.I., 2007b, Recent innovative applications of geosynthetics in geotechnical engineering. Proc. 13th Asia Regional Conf on Soil Mechanics and Geot Eng., 2: 207-221.

Shinsha H., Watari, Y. and Kurumada, Y., 1996. Improvement of Very Soft Ground by Vacuum Consolidation Using Horizontal Drains, Proc. of Int. Workshop on Technology Transfer for Vacuum Induced Consolidation: Engineering and Practice, Los Angeles, pp.113-118.

Shinsha, Hiroshi and Kumagai, Takahiro, 2014. Bulk Compression of Dredged Soils by Vacuum Consolidation Method Using Horizontal Drains. Geotechnical Engineering, 45: 78-85.

Silvester, R., Hsu, J.R.C. 1993. Costal Stabilization—Innovative Concepts: Prentice-Hall Inc.

Small, J., and Zhang, B., 1991. Consolidation of clays subjected to three dimensional embankment loadings. Int. J. Numer. Analyt. Meth. Geomech., 15(12): 857–870.

Sun, L., Meng, L., Guo, W., Feng, X., Nie, W., and Hou J., 2017. Pilot tests on methods to form working platform on dredged clay. Proceeding of ICE - Geotechnical Engineering, 170(5): 445-454

Su, J., Wang, Z., 2003. The two-dimensional consolidation theory of electro-osmosis. Geotechnique, 53(8):759-763.

Taku, Saitoh, 2013. Construction of a Perimeter Bund Using the Pre-Mixed (PM) -Clay Method. Terra et Aqua, No. 133.

Taylor, D.W., 1948. Fundamentals of Soil Mechanics, John Wiley & Sons, New York.

Tan, S., Tan, T. S., Ting, L. C., Yong, K. Y., Karunaratne, G. P., and Lee, S. L., 1988. Determination of Consolidation Properties for Very Soft Clay. Geotechnical Testing Journal ,11(4): 233-240

Tan, T.S., Yong, K.Y., Leong, E.C. and Lee, S. L., 1990. Sedimentation of Clayey Slurry. Journal of Geotechnical Engineering, 116(6).

TENCATE Geosynthetic. Installation guidelines: Alidrain® Prefabricated Vertical Drains for Consolidation Acceleration Applications. TENCATE Polyfelt. http://www.tencategeo.asia.

Toh, C.T., Chee, S.K., Lee, C.H., Wee, S.H., 1994. Geotextile-bamboo fascine mattress for filling over very soft soils in Malaysia. Geotextiles and Geomembranes 13(6–7), 357-369.

Yan S.W. and Chu J., 2003. Soil improvement for a road using the vacuum preloading method. Proceedings of the Institution of Civil Engineers – Ground Improvement, 7(4): 165–172.

Yan, S.W., and Chu, J., 2005. Soil improvement for a storage yard using the combined vacuum and fill preloading method. Canadian Geotechnical Journal. 42(4): 1094-1104.

Yan, H.S. and Cao, D.Z., 2005. Application of low-level vacuum preloading technique in offshore projects. Ocean and River Hydraulics, 3: 41-43.

Yan, S.W., Chu, J., Fan, Q.J. and Yan, Y., 2009. Construction of offshore breakwater on soft clay using prefabricated caissons. Geotechnical Engineering, Proceeding of ICE, London, 162(GE1): 3-12.

Yan, S.W., Chu, J., 2010. Construction of an offshore dike using slurry filled geotextile mats. Geotextiles and Geomembranes, 28 (5): 422-433.

Yeung, A., 2016. Geotechnical works of the Hong Kong-Zhuhai-Macao Bridge Project. Japanese Geotechnical Society Special Publication, 2: 109-121.

Yoshikuni, H., and Nakanodo, H., 1974. Consolidation of finegrained soils by drain wells with finite permeability. Soil Mechanics and Foundation Engineering, 14(2): 35–46.

Yoshimi, G. and Hiroshi, T.. (2000). A Reliability Design Method of Caisson Breakwaters with Optimal Wave Heights. Coastal engineering journal, 42(4).

Zeng, G., Xie, K., 1989. New development of the vertical drain theories. Proceedings of the 12th International Conference on Soil Mechanics and Foundation Engineering, Rotterdam, the Netherlands, 2: 1435–1438.

Zhang, N., Zhu, W., 2014. Study of Sedimentation and Consolidation of Soil Particles in Dredged Slurry. Geotechnical Special Publication, pp. 70-79.

Zhang, Nan, Zhu, Wei, He, Hongtao and Lv, Yiyan, 2017. Experimental study on sedimentation and consolidation of soil particles in dredged slurry. KSCE Journal of Civil Engineering. 21.

Zhaung, Y.F., Huang, Y., Lin, F., Zou, W., Li, Z., 2014. Case study of hydraulic reclaimed sludge consolidation using electrokinetic geosynthetics. In: 10th International Conference on Geosynthetics. Paper 35, Berlin.

Zhu, B., Zhang, W.L., Ying, P.P., Chen, Y.M., 2014. Deflection-Based Bearing Capacity of Suction Caisson Foundations of Offshore Wind Turbines. Journal of Geotechnical and Geoenvironmental Engineering, 140(5).

Zhaung, Y.F., 2015. Challenges of electro-osmotic consolidation in large scale application. Geosynthetics, pp. 447-449 (Porland, Oregon).

Varaksin, S., and Yee, K., 2007. Challenges in ground improvement techniques for extreme conditions: Concept and Performance, Proc. 16th Southeast Asian Geotechnical Conference, 8–11 May: Kuala Lumpur, pp. 101–115.

Walker, R., Indraratn, B., and Rujikiatkamjorn, C., 2012. Vertical drain consolidation with non-Darcian flow and void-ratiodependent compressibility and permeability. Geotechnique, 62(11): 985–997.

Wang, Y.Z., Zhong, X., 2008. stability analysis for bucket foundation breakwater with finite element method. Chinese-German Joint Symposium on Hydraulic and Ocean Engineering, August 24-30, 2008, Darmstadt.

Wang, B.. Vu, M. Q., 2010. Improvement of silty clay by vacuum preloading incorporated with electroosmotic method, J. Rock Mech. Geotech. Eng., 2(4): 365-372.

Wang, J., Ma, J., Liu, F., Mi, W., Cai, Y., Fu, H., and Wang, P. 2016. Experimental study on the improvement of marine clay slurry by electroosmosis-vacuum preloading. Geotextiles and Geomembranes, 44(4): 615–622

Wolfram Research, Inc., 2021. Mathematica, Version 13.0.0, Champaign, IL.

Wu, H., Hu, L., 2011. Theoretical analysis and numerical simulation of vacuum preloading in combination with electro-osmosis consolidation, in: Geo-Frontiers 2011: Advances in Geotechnical Engineering, ASCE, 605-615.